Identification of novel regulators of HIFs for use in anti-cancer target development

Paul David Grevitt

Thesis submitted in partial fulfilment of the requirements of the Degree of Doctor of Philosophy

September 2018
Centre for Molecular Oncology
Barts Cancer Institute
Barts and the London School of Medicine and Dentistry
Charterhouse Square
London
United Kingdom

Statement of originality:

I, Paul David Grevitt, confirm that the research included within this thesis is my own work or that where it has been carried out in collaboration with, or supported by others, that this is duly acknowledged below and my contribution indicated. Previously published material is also acknowledged below.

I attest that I have exercised reasonable care to ensure that the work is original, and does not to the best of my knowledge break any UK law, infringe any third party's copyright or other Intellectual Property Right, or contain any confidential material.

I accept that the College has the right to use plagiarism detection software to check the electronic version of the thesis.

I confirm that this thesis has not been previously submitted for the award of a degree by this or any other university.

Signature:

Date: 27/09/18

Publications:

Daniel E. Foxler, Katherine S. Bridge, John G. Foster, **Paul Grevitt**, Sean Curry, Kunal M. Shah, Kathryn M. Davidson, Ai Nagano, Emanuela Gadaleta. Hefin I. Rhys, Paul T. Kennedy, Miguel A. Hermida, Ting-Yu Chang. Peter E. Shaw, Louise E. Reynolds, Tristan R. McKay, Hsei-Wei Wang. Paulo S. Ribeiro, Michael J. Plevin, Dimitris Lagos, Nicholas R. Lemoine, Prabhakar Rajan. Trevor A. Graham, Claude Chelala, Kairbaan M. Hodivala-Dilke, Ian Spendlove. Tyson V. Sharp. **(2018**). *A HIF–LIMD1 negative feedback mechanism mitigates the pro-tumorigenic effects of hypoxia*. ***EMBO Mol. Med.*** **10(8): p. e8304**

Highlighted Abstracts:

September 2017 – Inaugural Crick Cancer symposium – Poster presentation from submitted abstracts
April 2018 – Keystone: Therapeutic targeting of hypoxic sensitive pathways – Oral presentation from submitted abstracts
April 2018 – International association for cellular coenzymes conference – Poster presentation from submitted abstracts
October 2018 – Crick Cancer symposium - Oral presentation from submitted abstracts

Awards:

Barts Cancer Institute PhD day - *Best poster prize*
IACC symposium – *Best poster prize*

Abstract:

Solid tumours display vast heterogeneity in oxygen tension as a consequence of poor vascularization and increased proliferation. Tumour hypoxia (low oxygen) is associated with poor prognosis as cells within this harsh microenvironment are viable and often resistant to chemotherapy and radiotherapy. The cellular response to hypoxia is regulated by transcription factors called hypoxia inducible factor (HIF). HIF is a heterodimeric protein consisting of an O_2-labile subunit (HIF-1α, HIF-2α and HIF-3α) and a beta subunit (HIF-1β). Expression of either HIF-1α or HIF-2α often correlates with poor prognosis. HIFα is degraded by a well characterized pathway, however numerous studies have shown multiple novel regulators that also effect HIF activity and stability. Such novel regulators could therefore represent new therapeutic targets for the development of novel anti-cancer therapies for those tumours with high levels of hypoxia.

In order to identify novel regulators of HIF, we undertook an unbiased approached and performed an RNAi kinome screen. Through this, we identified the bifunctional enzyme Coenzyme A synthase (CoAsy) as a novel negative regulator of HIF-1 transcriptional activity. Knockdown of CoAsy stabilizes both HIF-1α and HIF-2α in normoxia and hypoxia with no change in HIF-1β protein levels. Overexpression of PANK1, the rate limiting step in CoA biosynthesis, resulted in reduced HIFα expression thereby highlighting a role of Coenzyme A in regulating HIF stability. Analysis of breast cancer patients shows reduced *COASY* mRNA expression in the tumour compared to surrounding tissue and furthermore lower CoAsy expression is often found in triple negative breast cancer tumours compared to hormone sensitive tumours.

These data indicate that CoAsy is a novel negative regulator of HIFs and highlights a novel link between Coenzyme A biosynthesis and cellular hypoxic response.

Acknowledgements:

First and foremost I would like to thank Professor Tyson Sharp, for giving me the opportunity to work in his lab. Tyson has always been an endless supply of energy and enthusiasm. This project is very much a product of many 'What about this?!' and 'Have you thought about trying this?' moments, even though the project has nothing to do with LIMD1!

I would also like to thank the fantastic collaborators throughout this project. Professor Ivan Gout for providing key reagents and sharing his knowledge of CoA biology. To Dr. Ian Spendlove for aiding me in the IHC staining and analysing the samples and finally to Dr. Daniel Tennant, for his metabolomics expertise and valuable insight in hypoxic cell metabolism. Also Katiuscia, Gyorgy, Susana and everyone else who has helped throughout the project.

I would also like to thank all the 'Sharpies' that I have had the pleasure of sharing a bay with over the years. In particular the fantastic post-docs who have taught me so much over the years. Dan, who taught me almost every technique I know and use today. Katherine, who really taught me how to think like a scientist, and question data properly. Kunal, for his depth of knowledge in technical assays and for tolerating my 'jokes' so patiently for years. And finally John, who is always there when times are tough for a motivational pep talk over a beer or two. Also the PhD students; Katy, Yigen and Paul. We have shared many hours in the lab together, but they would have felt so much longer without the constant jokes and banter between us.

Finally to my family and friends, there are too many of you to mention by name, but your constant love and support has helped me throughout this project. For that I am, and always will be, eternally grateful.

Abbreviations

2-HG	2-hydroxygluturate
Ab	Antibody
a-KG	Alpha-ketogluturate
bHLH	Basic helix-loop-helix
ccRCC	Clear cell renal cell carcinoma
CDK	Cyclin-dependent kinase
cDNA	Complimentary deoxyribonucleic acid
CDS	Coding sequence
CoA	Coenzyme A
COASY	Coenzyme A Synthase
DCIS	Ductal Carcinoma *in situ*
DLL3	Delta like canonical notch ligand 3
DMEM	Dulbecco's modified eagle medium
DNA	Deoxyribonucleic acid
DPCK	Dephospho-CoA Kinase
E2F	Eukaroytic transcription factor
eGFP	Enhanced green fluorescent protein
EGFR	Epidermal growth factor receptor
EMT	Epithelial to mesenchymal transition
ER	Oestrogen receptor
FDA	Federal drug association
FIH	Factor-inhibiting HIF
FISH	Fluorescent *in situ* hybridisation
GFP	Green fluorescent protein
GST	Glutathione-S-transferase
HDAC	Histone deactylase
HER2	Human epidermal growth factor receptor 2
HIF	Hypoxia-inducible factor
HRE	Hypoxic responsive element
HSP70	Heat shock protein 70 kDa
IDH	Isocitrate dehydrogenase
kDa	Kilodalton
LATS1/2	Large tumour suppressor kinase 1/2
LIMD1	LIM-domains containing protein 1
MAPK	Mitogen activated protein kinase
mRNA	Messenger ribonucleic acid
MST1/2	Mammalian ste20-like protein kinase 1/2
mTOR	Mechanistic target of rapamycin
NSCLC	Non-small cell lung cancer
ODD/ODDD	Oxygen dependent degradation domain
OXPHOS	Oxidative phosphorylation
PANK	Pantothenate Kinase
PAS	Per-ARNT-Sim Domain
PCR	Polymerase chain reaction
PD-1	Programmed death receptor 1
PDGFB	Platelet derived growth factor B
PD-L1	Programmed death ligand 1
PHD	Prolyl-4-hydroxylase
PPAT	Phosphopantetheine adenyltransferase

PPP	Pentose phosphate pathway
PR	Progesterone receptor
pRB	Retinoblastoma protein
RCC	Renal cell carcinoma
RING	Really interesting new gene
RNA	Ribonucleic acid
RNAi	RNA interference
ROS	Reactive oxygen species
RPMI	Roswell park memorial institute medium
SCLC	Small cell lung cancer
shRNA	Short-hairpin RNA
siRNA	Short interfering RNA
SIRT1	Sirtuin 1
SLC2A1	Solute carrier family 2 member 1
TAD	Transactivation domain
TCGA	The cancer genome atlas
TetR	Tetracycline responsive element
TMA	Tissue microarray
TNBC	Triple negative breast cancer
TSS	Transcriptional start site
UTR	Untranslated region
VEGF	Vascular endothelial growth factor
VEGFR	Vascular endothelial growth factor receptor
VHL	Von Hippel-Lindau
WT	Wild-type

Table of Contents

Table of figures

Introduction

The role of hypoxia and HIF signaling in cancer

1. Introduction

1.1.1 The hallmarks of cancer

Cancer is one of the leading causes for death in the developed world. Recent statistics have shown that 1 in 2 people born after 1960 will be diagnosed with some form of cancer during their lifetime. In the UK there were over 350,000 new cases of cancer and over 160,000 deaths from cancer in 2016 [1]. Current survival rates are 50% for over 10 years, but this does not represent all cancers as almost half of all cancer deaths in 2016 were from cancers of the breast, prostate, bowel and lung. Globally, the cancer burden is estimated to be 9.6 million deaths in 2018 and 1 in 6 people dying of cancer [2]. This staggering disease burden has resulted in decades of research to further understand the pathogenesis, progression and ultimately treatment of disease.

Cancer is a heterogeneous disease, with each cancer type containing many other subgroups. Cancers cannot be defined by a singular source of rapidly proliferating cells; instead tumors are a complex tissue formed of multiple cell types and mutations resulting in a varied microenvironment. Despite this complexity a seminal paper by Hanahan and Weinberg defined common traits shared across all cancer types. These are referred to as the “Hallmarks of cancer.”[3, 4] The hallmarks describe cancer cell traits such as *sustained proliferative* signaling often arising from a gain in self-sufficiency of growth signaling pathways, such as activating mutations in epidermal growth factor receptor (EGFR) which results in sustained signaling without ligand induced stimulation [5]. Conversely, cancer cells display *insensitivity to anti-proliferative signals*, one such example is the well-characterized tumour suppressor protein

pRB, functional pRB binds to E2F and blocks transcriptional activity thereby blocking cells from progressing through G1 phase and continuation of cell cycle [6]. Furthermore for cancer cells to continue proliferative signaling, the mechanism of *programmed cell death (apoptosis) is inhibited*, this can be seen through upregulation of the oncogenes such as *BCL2 [7]*. To allow cells to maintain unrestrained replication telomerase activity is reactivated in cancer cells thereby *enabling replicative immortality [8]*. Cancer cells further alter the surrounding environment through *activation of angiogenesis*, the formation of new blood vessels through upregulation of activating factors such as VEGF-A [9]. Finally, cancer cells *invade and metastasise* to distal sites forming new colonies, this can occur by multiple processes, however one well established model is through epithelial-mesenchymal transition that is typified by altered cellular junctions such as loss of E-cadherin [10]. These six highlighted points are the initial hallmarks, the list was further expanded to include: deregulating cellular energetics, genome instability and mutation, avoiding immune destruction and tumour-promoting inflammation (**Fig. 1.1.1**) [4]. These hallmarks and emerging hallmarks give a simple overview to shared characteristics to the majority of human cancers, however cancer is a very heterogeneous disease with each type displaying a diverse set of molecular drivers.

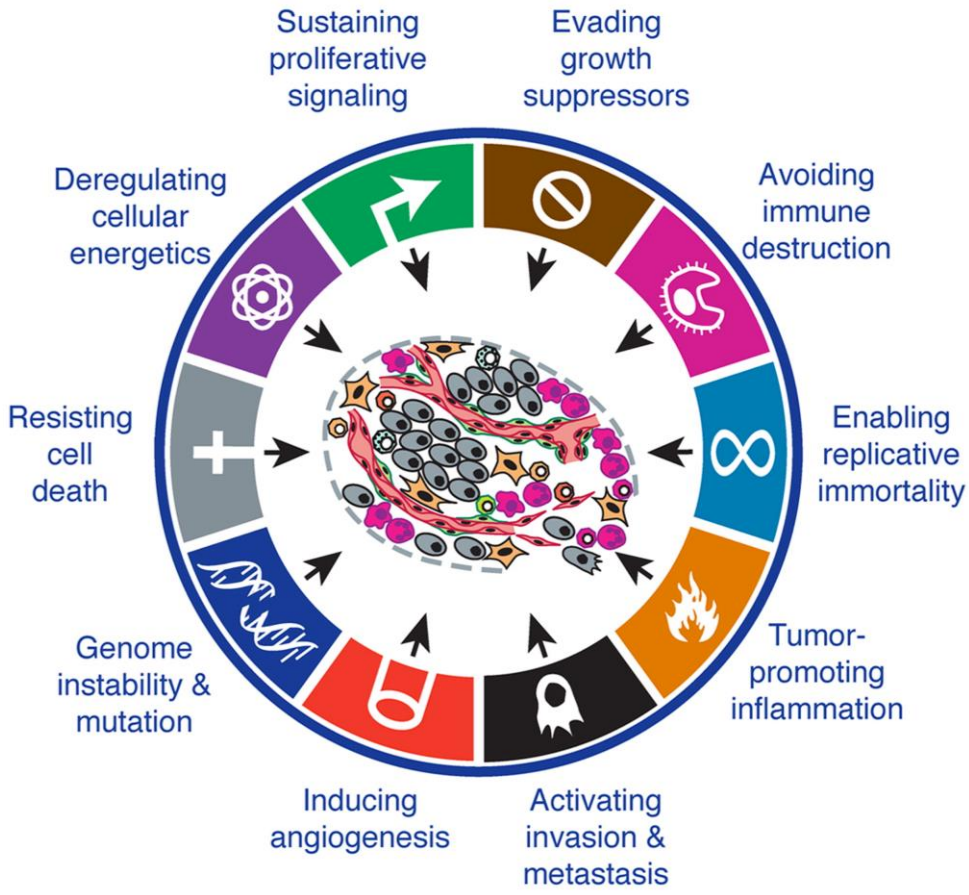

Figure 1.1.1: The hallmarks of cancer. The hallmarks of cancer and the next generation of hallmarks as termed by Hanahan and Weinberg, these are traits common to the majority of cancers [4]. Figure adapted from Hanahan and Weinberg

1.1.2 Lung Cancer

Lung cancer is currently the most common cancer worldwide and accountable for over 21% of UK cancer deaths in 2016 [11]. Patient survival has not seen much improvement in the last 40 years in the UK with only 5% of patients diagnosed live for ten years or more. These statistics represent a clear unmet medical need, therefore we utilized lung cancer as one of the disease models used throughout this project.

Lung cancer is broadly divided into two categories non-small cell lung cancers (NSCLC) that accounts for 85% of lung cancers, the remaining 15% of lung cancers are small-cell lung cancers (SCLC). NSCLC is broadly divided into three subtypes: adenocarcinoma, large cell carcinoma and squamous cell carcinoma. Even within these subtypes, there is great mutational diversity and further postulated subtypes, however for simplicity we will focus on the broader definitions [12]. Small-cell lung cancers are primarily found in heavy smokers, these tumours arise from pulmonary neuroendocrine cells [13]. Squamous cells primarily originate from the first four branchings of the bronchus and are thought to originate from the basal progenitor cells located here, however adenocarcinomas originate from alveolar type II cells; although this is still debated due to the plasticity observed between alveolar type I and type II cells [14]. Furthermore recent evidence has shown that tumour recurrence following EGFR inhibitor resistance appears as SCLC despite initial NSCLC tumours, the current theory behind this phenomenon is that alveolar type II cells can also give rise to SCLC [15].

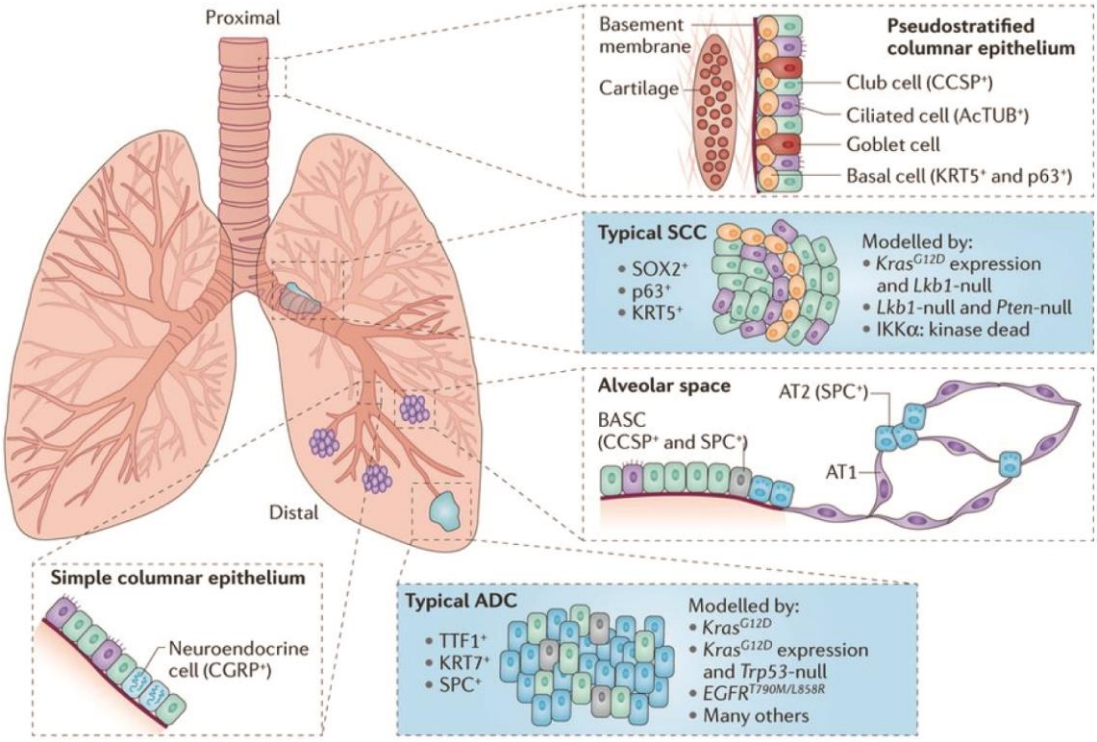

Figure 1.1.2.1: Cell type of origin for non-small cell lung cancer. Schematic diagram of cell type of origin in lung cancer. Image highlights squamous cell arising from the branching of the bronchus whereas adenocarcinoma develop from the alveolar cells, the cell type of origin is thought to be AT2 cells derived from Clara cells. Small-cell lung cancer, not pictured here, arises from neuroendocrine cells found in the columnar epithelium. Figure adapted from Chen *et al*., [16]

There are various genetic drivers of lung cancer; EGFR mutations are common in NSCLC and are predicted to be an early driver mutation, particularly in adenocarcinoma. Screening for EGFR mutations in a large cohort of lung cancer patients identified that they occurred in 16.6% of patients, particularly exon 19 deletions of L858R mutation, both resulting in constitutively active EGFR [17], however this figure is higher in Asia, however the reason for this is unclear [18]. EGFR inhibitors such as erlotinib and gerfitinib have shown some efficacy with partial responses in around 10% of NSCLC patients [12]. KRAS mutations are also prevalent in NSCLC, particularly in smokers. Often these mutations effect codons 12 or 13 and lead to a loss of Kras GTPase activity, thereby rendering a constitutively active Ras-Raf-Mek-Erk kinase pathway,

resulting in sustained cellular proliferation [19]. These are just some of the driver mutations associated with lung cancer, however as previously mentioned each subtype is largely heterogeneous and multiple other drivers have been identified, a summary of which can be found in **Fig 1.1.2.2**.

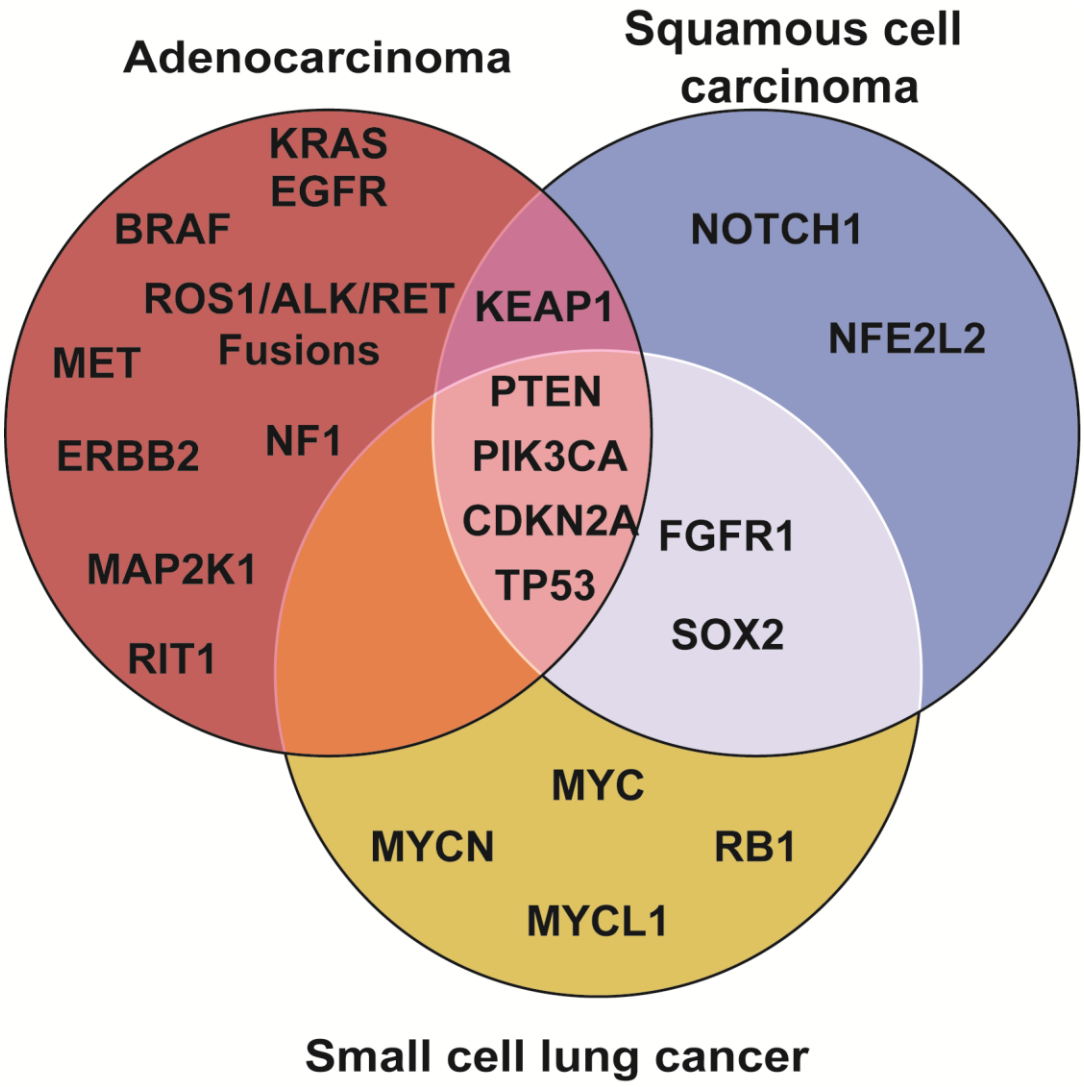

Figure 1.1.2.2: Driver mutations in Lung cancer. Known driver mutations in lung adenocarcinoma, squamous cell carcinoma and small-cell lung cancer. Driver mutations identified from [20-22].

Targeting these driver mutations is of significant clinical interest. Current therapies include targeting mutant EGFR using gerfitinib or erlotinib, due to the increased activity of EGFR, these patients show increased response to EGFR

therapy [13]. ALK and ROS1 fusions are another form of driver mutations that has been exploited for therapeutic targeting in adenocarcinoma, indeed the ALK-ROS1 fusion results in a pseudo-dimerization of each kinase resulting in hyperactive fusion enzymes. Phase III trials with the ALK-ROS fusion inhibitor, crizotinib, showed a significant increase in progression-free survival compared to chemotherapy as well as a greater improvement in quality of life [23]. The emerging role of immunotherapy in targeted therapies has transformed cancer research in recent years. Using inhibitors of immune checkpoint, the mechanism how cancer cells evade immune destruction, it is possible to re-sensitize tumour cells to immune destruction. Large scale trials targeting the PD-1/PD-L1 axis has resulted in successful trials showing increased patient survival both as first line treatment and with adjuvant chemotherapy [24-26].

In comparison to these successes in targeted therapies in NSCLC, there are currently no targeted therapies for patients with small cell lung cancer. Recent trials with a monoclonal antibody targeting DLL3, an oncoprotein that activates Notch signaling in small cell lung cancer, showed early response to reducing tumour burden however they failed to elicit significant changes in overall survival or progression free survival [27].

Whilst there have been great advances in development of targeted therapies of lung cancer, either through small molecule inhibitors or immunotherapy, it is still an area of clear unmet need as can be seen by the large disease burden. The plethora of molecular drivers results in a complex situation where it is unlikely that a single targeted therapy will be effective for all patients, therefore we

hypothesize through identification of novel drivers that may act as therapeutic targets, will help expand the current ‘toolbox’ of treatment options.

1.1.3 Breast cancer

In 2015 there were over 55,000 new cases of breast cancer in the UK, leading to over 11,500 deaths [28]. In fact, breast cancer remains the largest cause of cancer-related death in women world-wide [29].

Breast cancer has clearly defined subtypes depending on cell types of origin and expression of various molecular drivers. The majority of breast cancer cases arise from cells lining the milk ducts. Cancerous cells progress to form a pre-invasive lesion termed ductal carcinoma *in situ* (DCIS) before becoming invasive and finally presenting as metastatic disease [29].

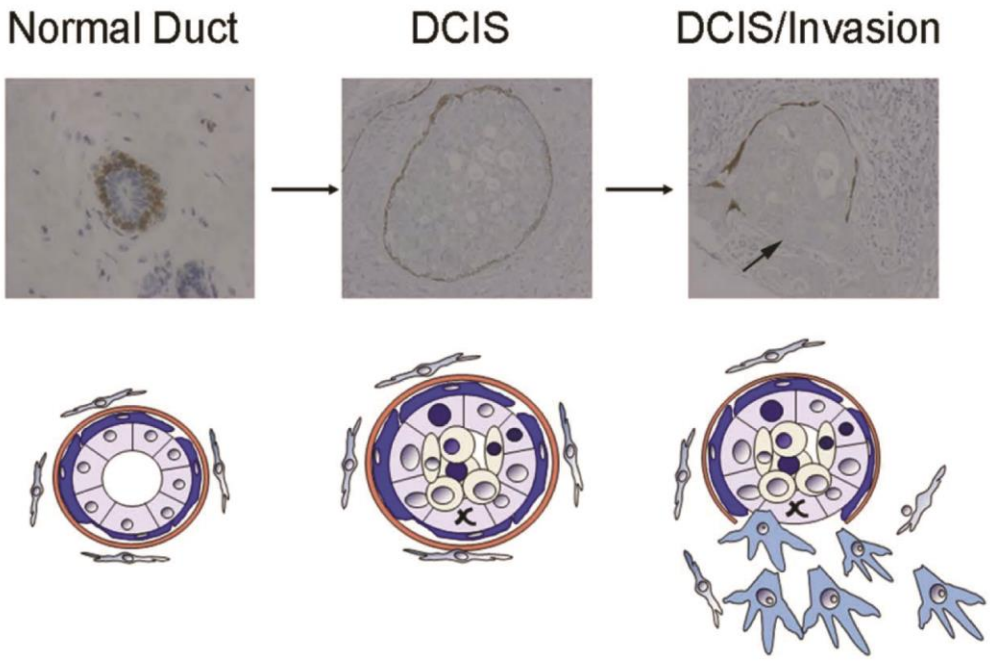

Figure 1.1.3: The progression of breast cancer from normal breast ducts to invasive carcinoma. Schematic diagrams and IHC from breast cancer patients showing pre-cancerous duct, which develops in to ductal carcinoma *in situ* before invading and presenting as metastatic disease. Staining in IHC is CK5/6, a marker of myoepithelial cells Figure adapted from Allen *et al*., [30]

Breast cancer is broadly separated in to four categories: luminal A, luminal B, HER2 positive and basal-like breast cancer [31]. Currently targeted therapy and treatment options is decided upon following analysis of molecular signatures and analysis of each subtype. Both Luminal A and Luminal B are hormone receptor positive, this means they are estrogen receptor (ER) and progesterone receptor positive (PR) therefore first line treatment is endocrine therapy for these patients [32]. Luminal A and B subtypes differ by Ki-67 expression, with luminal B patients expressing higher levels of Ki-67. Ki-67 is a well-established marker of cell proliferation therefore unsurprisingly luminal B tumours are known to grow faster and correlate with poor survival compared to luminal A [33]. HER2 positive cancers are so named due to high expression of the HER2 receptor, which is encoded by the *ERBB2* gene. This occurs primarily through

increased copy number with overexpressing cells expressing between 25-50 copies of the gene as identified through FISH [34]. This high level of HER2 expression makes these cells susceptible to treatment with Herceptin (trade-name: trastuzamab), due to increased dependence on HER2 signaling. The final group is triple-negative breast cancer/basal-like carcinoma, this group lacks expression of the aforementioned receptors which results in limited targeted therapeutic options. The basal-like carcinomas differ from triple-negative breast cancer (TNBC) tumours due to high expression of basal markers such as cytokeratin 5,6 and 17 [35, 36].

Like lung cancer, breast cancer is a highly heterogeneous disease, however there are strong familial links with germline mutations in *BRCA1* and/or *BRCA2* mutations. These mutations are well characterized and form screening practices employed today, however large scale analysis of 560 breast cancer patients identified that 90/560 contained these mutations, indicating that this risk factor only accounts for a small proportion of patients [37]. Instead, there are a number of lower penetrance mutations or molecular drivers that will account for the majority of breast cancer patients. Through identification of these alternative drivers it will allow for novel targeted therapies which are of particular clinical importance to the basal-like and TNBC patients.

1.2 Hypoxia in cancer

It has long been recognized that oxygen tensions vary greatly throughout solid tumours [38]. This phenomenon arises from rapid proliferation in growing tumors and aberrant vasculature resulting in an imbalance of oxygen supply and consumption. This imbalance leads to great O_2 heterogeneity with ranges in partial oxygen pressure (pO_2) from 40 mmHg (approximately 11% O_2) down to below 2.5 mmHg (below 1% O_2). These regions of sub 1% oxygen concentration are referred to as hypoxic [39]. Within these hypoxic regions, there is often substantial necrosis, uncontrolled cell death, but despite this harsh tumour microenvironment, a small subset of cancer and normal cells remains viable [40].

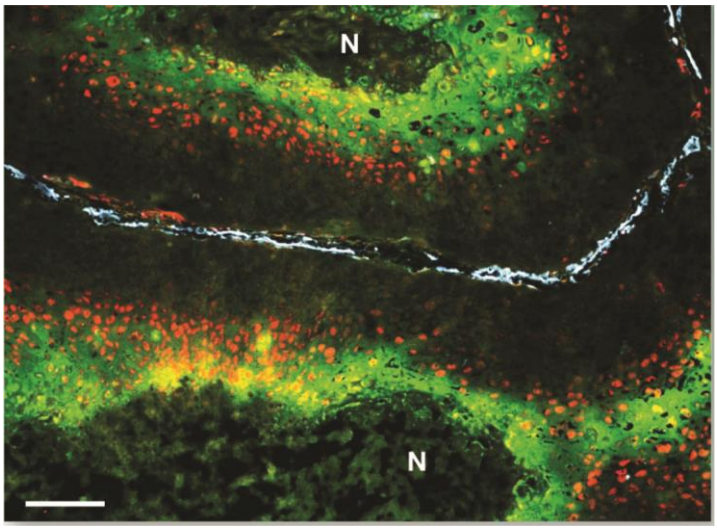

Figure 1.2: Imaging tumour hypoxia and necrosis in xenografts. Immunofluorescence of head and neck cancer xenograft stained for pimonidazole (green), HIF-1α (red) and blood vessels (blue). N indicates necrotic regions. This figure shows hypoxic regions stained in green, at the center of these regions there is an area of cell necrosis. This figure further shows the diffusion of tissue oxygenation away from blood vessels (blue). Figure adapted from Meijer *et al*.,

Early studies in head and neck tumors displayed that hypoxic in metastatic lesions correlated with poor survival following radiotherapy treatment [41]. This association of poor prognosis on disease-free and overall survival with tumor

hypoxia has also been reported in cervical cancer [42]. Tumour hypoxia still occurs in well oxygenated tissues such as the lungs, due to the poorly formed vascular surrounding tissues. Furthermore this tumour hypoxia correlates with poor patient survival; two studies with different imaging techniques to detect tumor hypoxia showed that hypoxia was a predictive indicator of tumor response to therapy and overall patient survival [43, 44].

1.3 Hypoxia inducible factors are responsible for cellular response to changes in O_2 tension

The cellular response to hypoxia is regulated by the hypoxia inducible factors (HIFs). HIFs are heterodimeric proteins consisting of an O_2 labile subunit (HIFα) and a beta subunit (HIF-1β). In low oxygen concentration, the subunits translocate to the nucleus, dimerize and initiate the transcription of target genes [45]. These target genes allow for response and adaptation to low oxygen tension, including those related to altering cellular metabolism, angiogenesis and cell cycle progression [46]. The general structure of HIFs (**Fig. 1.3.1**) consists of an N-terminal basic helix-loop-helix (bHLH) domain that facilitates DNA binding, a PER-ARNT-SIM (PAS) domain, that allows for dimerization and two transactivation domains (N-TAD and C-TAD) for transcriptional activity. In addition to these, the HIF alpha subunits contain an oxygen dependent degradation domain (ODD) that is essential for protein degradation in the presence of molecular oxygen.

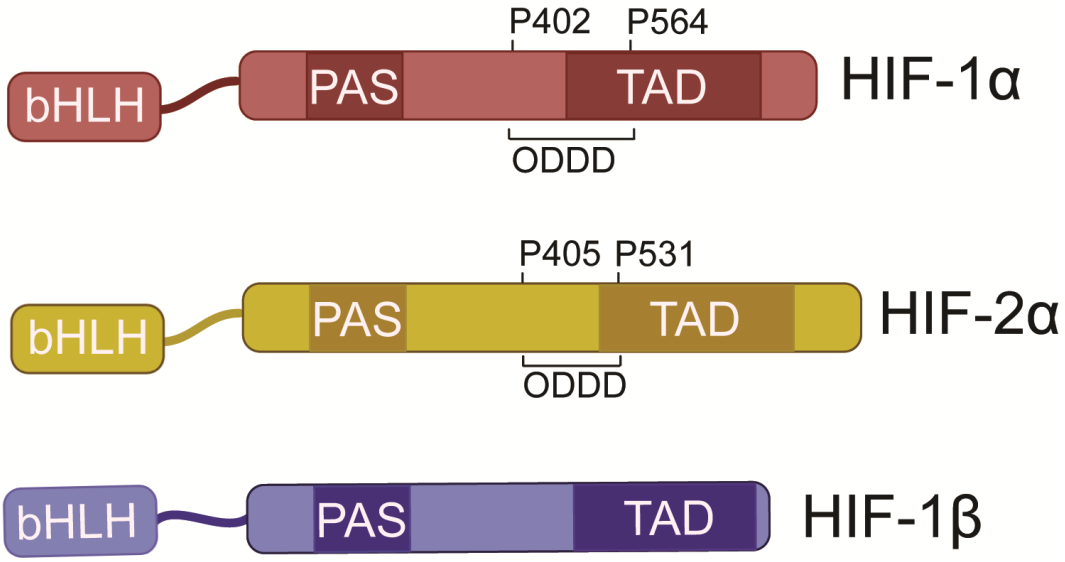

Figure 1.3.1: Structure of hypoxia inducible factors. Schematic of HIF isoform structures. Each subunit contains bHLH domains, PAS domains and two TAD domains. ODDD domains are only found in α subunits

There are three mammalian HIFα subunits; HIF-1α and HIF-2α are the two most well studied, less is known about the third subunit, HIF-3α, although this is a fast developing field. They each share the common motifs, such as the bHLH domain, PAS domain and TAD domain, but differ in sequence and length with approximately 48% amino-acid sequence homology [46]. Expression of HIF-1α is widespread and found in almost all tissue and cell types; initially it was thought that HIF-2α was exclusively found in the vasculature [47], until immunohistochemical analysis of mice following hypoxic exposure revealed HIF-2α expression in a variety of tissue types, although expression was still not ubiquitous as is observed with HIF-1α [48]. HIF-3α differs to HIF-1/2, as there are numerous splice variants that have been identified [49]. There are conflicting reports on the function of HIF-3α, it has been suggested that HIF-3α acts as a dominant-negative regulator of HIF-1/2 and has no activity as a transcriptional activator [50]. This does not hold true of all splice variants as Zhang et al., showed that human HIF-3α splice variants HIF-3α-1 and HIF-3α-

9 are able to upregulate target genes following identification of homologous splice variants in zebrafish [51]. Therefore, the biology and activity of HIF-3α largely depends on which splice variant is being expressed and the cellular context in which they are expressed, as these differences are not well characterized or fully understood we will focus on HIF-1α and HIF-2α

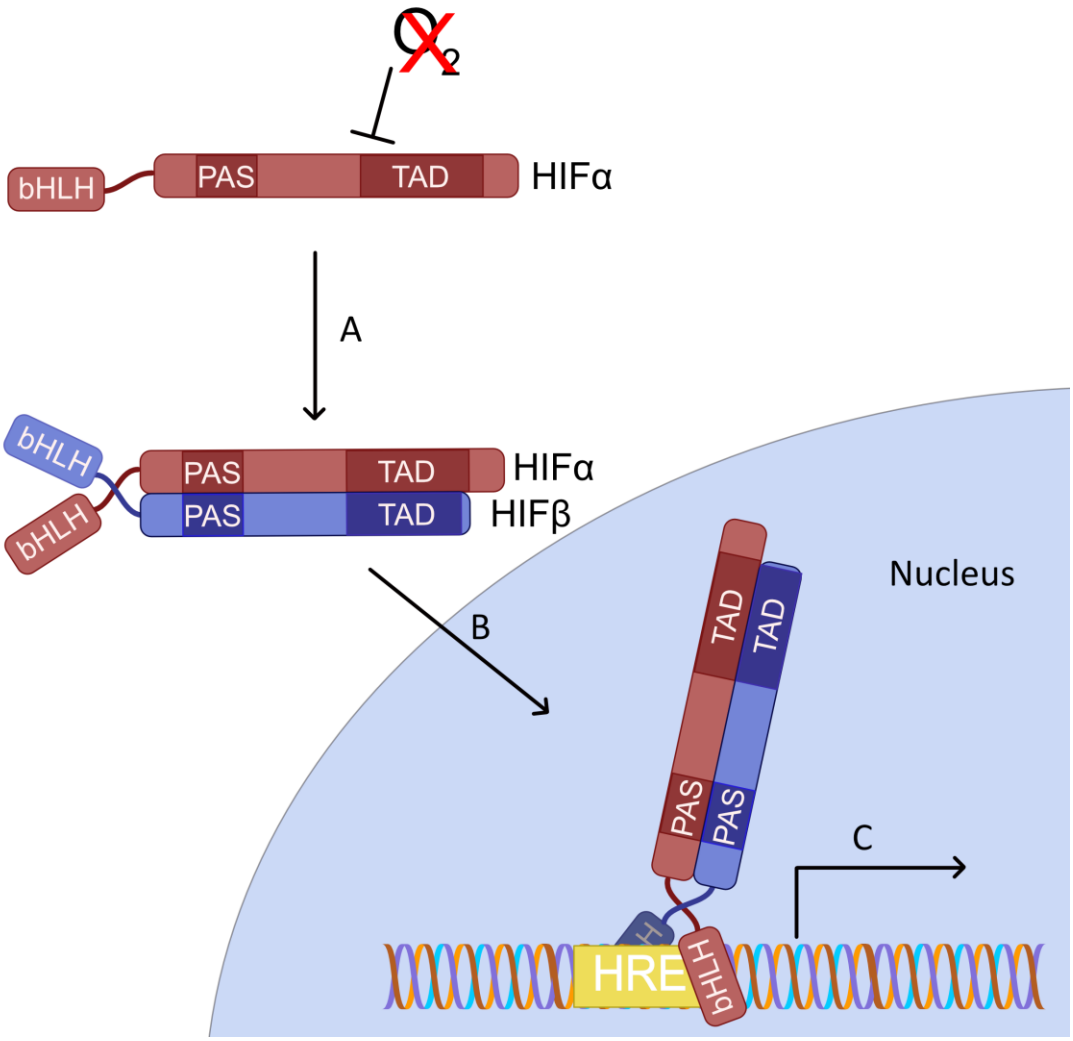

Figure 1.3.2: Mechanism of HIF transcriptional activity Schematic of HIF transcriptional activity. In low O_2 conditions the HIFα subunit is stabilised (**A**) and forms a heterodimer with the β subunit (**B**) before translocating to the nucleus and binding to hypoxic responsive elements and upregulating target genes.

HIF activity occurs when the alpha subunit becomes stabilized (**Fig. 1.3.2A**), binds to the constitutively expressed β-subunit (**Fig. 1.3.2B**) before translocating to the nucleus where it binds to consensus motifs (5'-RCGTG-3' [52]), termed hypoxic responsive elements (HREs) in DNA before initiating transcription (**Fig. 1.3.2C**). Despite numerous canonical HIF-binding motifs throughout the genome, not all of these are functional; ChIP-seq analysis in a breast cancer cell line (MCF-7), revealed over 500 HIF binding sites, with 400 for HIF-1α and 425 for HIF-2α (of which 356 and 301 overlapped with HIF-1β peaks for HIF-1α and HIF-2α respectively), whilst there was significant overlap in binding sites, others were distinct indicating different rolls for HIF subunit activity in response to hypoxia, furthermore this dataset showed that the HIF-1α binds more closely to transcriptional start sites (TSS) than HIF-2α with ~40% of HIF-1α binding sites within 2.5 kb from TSS compared to ~20% for HIF-2α [53]. This overlap of HIF-1α and HIF-2α target genes has also been noted in renal cell carcinoma [54, 55]. The specificity of HIFα subunit target genes has been mapped to the N-terminal transactivation domain, as overexpression experiments with mutant HIF-1α with the HIF-2α N-TAD was able to induce expression of HIF-2α specific target genes, and vice versa with mutant HIF-2α [54].

1.4 O_2 dependent regulation of HIFα protein stability and activity

1.4.1 Prolyl-hydroxylation of the ODDD in HIFα

How cells adapt to and sense changes in oxygen was unknown at the time HIF-1 was first discovered, instead it was just known that HIF-1 is stabilized in low oxygen tensions. A series of papers first identified the interaction between HIF-1α and pVHL (to be discussed later in **1.4.2**) required prolyl-hydroxylation at P565 residue, this hydroxylation event was further shown to be dependent of O_2, ascorbate, Fe^{2+} and 2-oxogluturate [56, 57]. Later, work in *C. Elegans* first identified the nematode homologue of HIFα before identifying Egl-9 as the hydroxylase that is functional. The human homologue was identified as a series of proteins now termed HIF-prolyl-4-hydroxylases (PHDs) [58]. Furthermore an additional hydroxylation site was further confirmed corresponding to P402 in HIF-1α, this was further shown to be critical for HIF-1α regulation both *in vitro* and *in cellulo* [59].

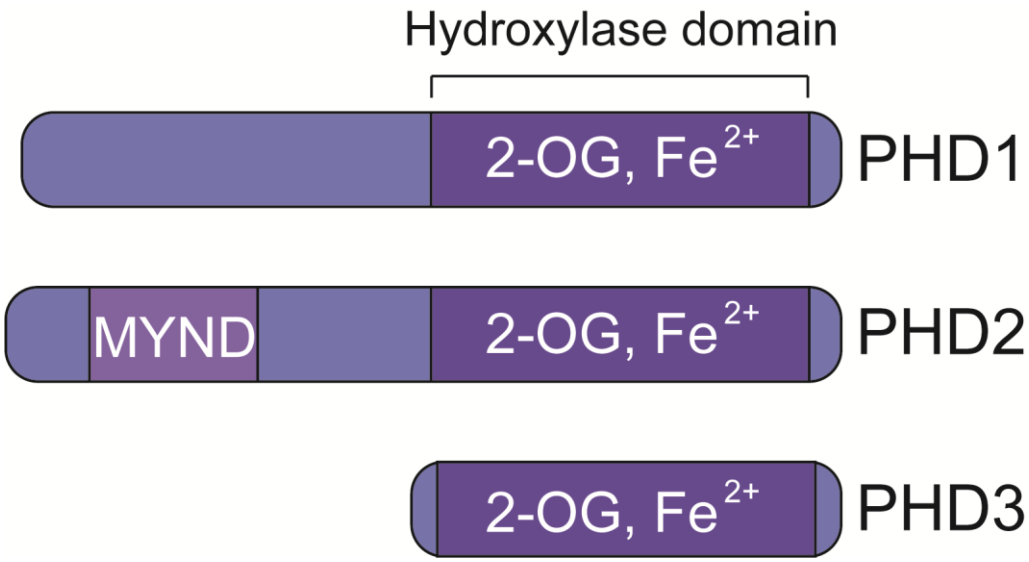

Figure 1.4.1: Schematic of Prolyl-4-hydroxylase structure. Schematic diagrams of prolyl-hydroxylase protein structures. Each isoform contains a C-terminal hydroxylase domain where the co-factors and active site are located. Between each isoform there is ~60% amino-acid sequence homology. PHD2 differs from the other isoforms as it contains an additional MYND domain.

There are 3 members of this family: PHD1, PHD2 and PHD3. Through siRNA mediated knockdown experiments it was shown that PHD2 is the isoform that is critical for HIF hydroxylation as knockdown of PHD1 or PHD3 had lesser effects on HIF stabilization in normoxia [60]. The PHD enzymes each contain a C-terminal hydroxylase domain that contains the catalytic residues and all required co-factor binding sites. PHD1 and PHD2 have extended N-terminal regions, the function of which is not known. Germline mutations in *EGLN1*, causing a D4E and C127S substitutions in mature protein, have been found in the Tibetan population and are associated with adaptation to high altitude, it has been further postulated this occurs through a reduction of binding from PHD2 and p23, a co-factor facilitating PHD2 and HIF interaction [61]. All three PHD isoforms are capable of hydroxylating HIF-1α with varying affinities [62, 63], however each enzyme displays a Km for O_2 at ranges above physiological

oxygen levels. As a result of this, the prolyl-4-hydroxylase enzymes are able to sense subtle changes in oxygen tension and hydroxylate HIF when O_2 concentrations are sufficient.

1.4.2 Regulation of HIF by the von Hippel-Lindau protein complex

In 1996, it was noted that a number of hypoxia-inducible genes were also negatively regulated by the tumour suppressor protein von Hippel-Lindau protein (pvHL), as renal carcinoma cells lacking wild-type pVHL expressed higher levels of *SLC2A1*, *VEGFA* and *PDGFB* mRNA irrespective of oxygen tension, which was reversed upon addition of reintroduction of wild-type pVHL [64]. It was later discovered that these cells display stabilized HIF-1α and HIF-2α and that pVHL co-immunoprecipitates with each HIFα subunit in an iron dependent manner. These findings in combination with those discussed in **1.4.1** highlighted an axis where HIFα is hydroxylated by the PHD enzymes which allows binding of pVHL and subsequent degradation. The degradation pathway was later characterized in 2000 by Cockman *et al*., who showed that the pVHL/HIFα interaction was required for HIF ubiquitylation and subsequent degradation via the proteasome [65].

pVHL exists in two isoforms, a 30 kDa isoform (p30) and 19 kDa isoform (p19), this second shorter isoform arises as a consequence of an internal translation start site resulting in a truncated product lacking the N-terminal sequence. Re-expression of the p19 isoform in renal cell carcinoma cell lines with mutated pVHL resulted in a reduction of HIF target gene expression and a reduction in tumour burden suggesting that the tumour suppressor properties of pVHL are

conferred by both isoforms [66]. pVHL forms part of a protein complex with Elongin B and Elongin C; the crystal structure of this complex has been resolved with a short fragment of hydroxylated HIF-1α, which shows how the binding pocket of pVHL contains multiple serine and histidine residues that interact with the hydroxylated proline residue and stabilise the protein-protein interaction, furthermore this binding pocket contains multiple frequently oncogenic mutated residues which destabilize this interaction [67, 68]. This pVHL-Enlongin B-Elongin C (VBC) complex acts as a recognition motif for Cul2, a scaffold protein that further recruits Rbx1, a RING structure that combined form a canonical Cullin-RING E3 ubiquitin ligase complex [69-71]. The E3-ubiquitin ligase complex polyubiquitinates HIFα, which signals HIFα for destruction via the 26S proteasome system [72].

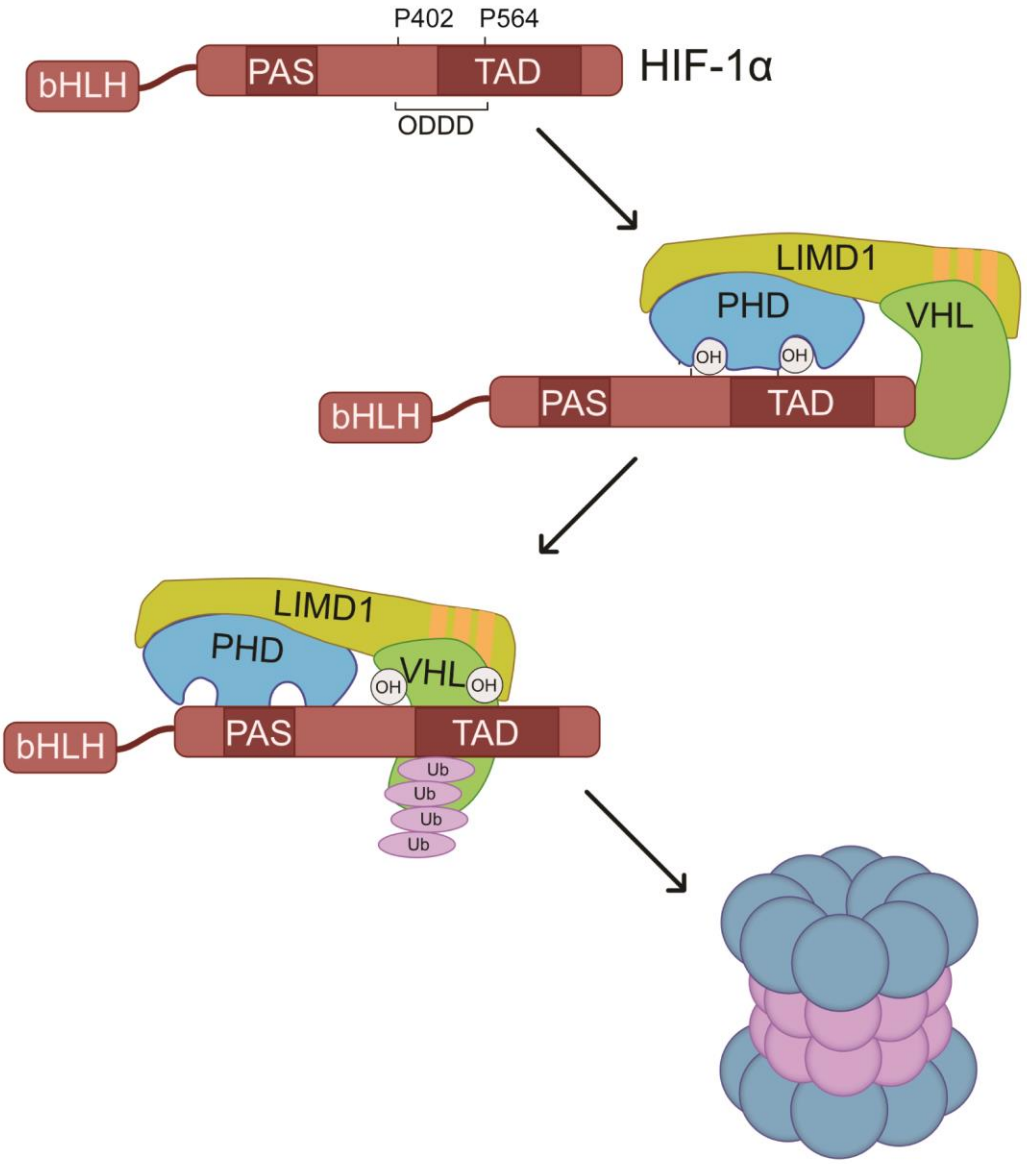

Figure 1.4.2.1: Oxygen dependent regulation of HIFα. O_2-dependent regulation of HIFα protein stability. PHD enzymes hydroxylate conserved proline residues in the ODDD that allows pVHL to bind. pVHL acts as a recognition sequence for E3-ubiquitin ligase complex (not pictured) that polyubiquitinates HIFα thus signaling it for degradation via the 26S proteasome. LIMD1 scaffolds this process, focusing enzymatic activity and enhancing degradation rate.

To summarise the oxygen dependent degradation of HIFα protein; the prolyl-hydroxylase enzymes hydroxylate proline residues in the oxygen dependent degradation domain of HIFα proteins in a reaction that requires O_2, Fe^{2+}, 2-oxogluturate and ascorbate. This hydroxylation event allows binding of pVHL in complex with Elongin B and C. pVHL acts as a recognition motif for the Cul2-

Rbx1 E3-ubiquitin ligase complex that polyubiquitinates HIF that signals the protein for degradation via the 26S proteasome. This process ensures that in cells with sufficient oxygenation, HIFα protein is rapidly degraded before eliciting a transcriptional response. The tumour suppressor protein LIM domains containing protein 1 (LIMD1) and related family members (Ajuba and WTIP) act as molecular scaffolds for PHDs and pVHL, thereby focusing enzymatic activity and increasing efficiency of HIF degradation [73] (**Fig. 1.4.2.1**). LIMD1 itself is a hypoxic responsive gene, like PHD2 and PHD3 [60, 74], ablation of the hypoxic response element in the promoter of LIMD1 alters the negative feedback loop of HIF regulation resulting in larger and more vascular tumour xenografts (**Fig.1.4.2.2**) [75]. This work highlights the biological significance of this degradation mechanism, as subtle changes in the efficiency of this process have profound implications on tumour progression.

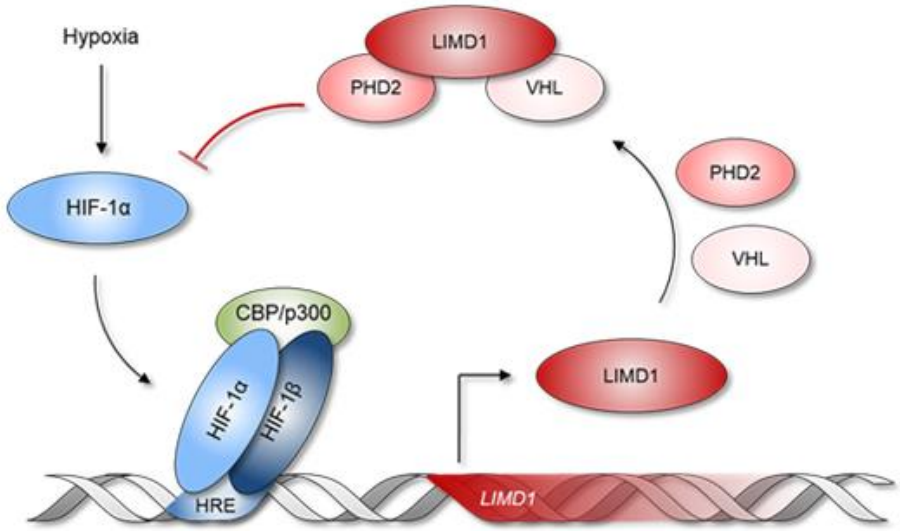

Figure 1.4.2.2: HIF-LIMD1 negative feedback loop. Schematic diagram representing negative feedback loop whereby HIF-1 promotes hypoxic expression of LIMD1, which in turn increases turnover of HIF-1α protein. Figure used with kind permission of Dr. Katherine Bridge.

1.4.3 Factor-inhibiting HIF negatively regulates HIF transcriptional activity

Factor inhibiting HIF (FIH-1) is another 2-oxogluturate dependent dioxygenase, that hydroxylates the C-terminus of HIF-1α and subsequently blocks transcriptional activity [76]. Unlike the PHD enzymes, FIH-1 hydroxylates HIF at an asparagine residue (asparagine 803 in HIF-1α) [77]. This hydroxylation event in the C-TAD blocks transcriptional activity through blocking the recruitment of transcriptional co-activators such as p300/CBP, this occurs due to disruption of hydrophobic interactions in the α-helix at the binding interface between HIFα and p300 [77-79]. It is important to note that unlike the previous mechanism of HIF regulation, this does not alter HIF protein stability instead blocks activity, as a consequence of this it means that just because HIF protein is present does not necessarily imply that there will be transcriptional activity. Analysis of the affinity of the PHD hydroxylases and FIH-1 for oxygen highlights a difference between the two groups, whilst the prolyl-hydroxylases display a higher Km for O_2 than FIH-1, this means FIH-1 will remain functional at lower oxygen tensions than the PHDs [80]. As a result of this there will be a window where HIF protein is stabilized due to lack of activities from PHDs but activity will be inhibited due to still functional FIH-1. As FIH-1 hydroxylation occurs at the C-TAD residual functionality is still maintained through activity through the N-TAD, however a different subset of genes will be activated. Through both overexpression and shRNA mediated knockdown of FIH these target genes were characterized in HeLa cells and separated in to ‘FIH-inhibited genes’ and ‘Non-FIH-inhibited genes’. Between these two groups, the FIH-inhibited genes displayed a significant increase in hypoxic induction when placed in 0.2% O_2

as opposed to 3% O_2 whereas the 'non-FIH-inhibted genes' had a lesser difference between the two oxygen tensions [81].

1.5 HIFs in cancer

1.5.1 Expression of HIFα often correlates with poor patient outcome

It has been observed that there is an increased expression of HIF-1α and HIF-2α across a variety of cancer types. Immunohistochemical analysis of patients with NSCLC showed that increased expression of either HIF-1α or HIF-2α correlated with decreased overall survival [82]. Overexpression of HIF-1α and HIF-2α has also been linked to poor patient outcome in prostate, ovarian and colorectal cancer as well as many others [83-85]. In breast cancer there are two reports that individually identify HIF-1α and HIF-2α expression as independent biomarkers of patient outcome [86, 87], recent work identified that of the breast cancer subtypes, there is an upregulated hypoxic signature observed with TNBC tumours compared to receptor positive tumours [88]. Mutations in *VHL* or loss of 3p and subsequent loss of *VHL* was the only truncal event found in large scale genetic analysis in clear cell renal cell carcinoma (ccRCC), indicating that this event happens early on in ccRCC development [89]. Unsurprisingly, as a consequence of loss of pVHL functionality, HIFα isoforms are often found upregulated in renal cell carcinoma. However in this cancer type there is isoform specificity in terms of tumorigenicity. Analysis of HIF-1α protein expression by western blot in 93 patients with RCC highlighted that high HIF-1α expression was favourable, and in contrary to other cancer types correlated with improved patient outcome [90]. However, IHC analysis of a larger TMA of 357 RCC patients indicated that HIF-1α in fact correlates with

poor patient outcome [91]. Overexpression of HIF-2α with mutated ODDD proline residues to ensure normoxic expression was sufficient to overcome VHL tumour suppression in ccRCC cell lines and xenografts [92], however a separate study demonstrated that no such effect was observed following normoxic expression of HIF-1α indicating that indeed HIF-2α is the isoform driving tumourigenesis in RCC [93]. Further studies identify that loss of 14q, the chromosome arm that contains *HIF1A* gene, occurs at high frequency in advanced kidney cancers, furthermore shRNA mediated knockdown of *HIF1A* resulted in larger tumour xenografts suggesting that HIF-1α inhibits cell proliferation [94]. The differential role of the HIF isoforms in renal cell carcinoma could be explained by work by Raval *et al*., which showed that protumorigenic genes were exclusively upregulated by HIF-2 in RCC and not HIF-1, furthermore that HIF-1α suppresses HIF-2α and vice-versa [95]. This highlights the context specificity behind HIF activity and function, however it can be said that in the majority of cases expression of HIFα is not favourable for patient outcome.

1.5.2 HIF target genes in cancer

HIFs upregulate a number of target genes in normal tissues as an acute response to fluctuations in oxygen homeostasis. However cancer cells hijack these mechanisms to promote tumorigenesis. Whilst HIF target genes vary between cell types, thus highlighting the importance of cell context when considering HIF signaling, a number of traits remain consistent when studied across cancer cells. A number of these pro-tumourigenic mechanisms will be

discussed below, with a particular focus of HIF signaling within cancer cells as opposed to peripheral cells in the surrounding microenvironment.

1.5.2.1 Angiogenesis

The formation of new blood vessels is a crucial event in tumour progression as after rapid expansion and proliferation the nutrient and oxygen demand of the proliferating cells exceeds the pre-existing vasculature. Furthermore angiogenesis serves as an avenue for cancer cells to invade and metastasize through thereby driving cancer progression [96]. Therefore significant research work has been performed to develop antiangiogenic therapies.

HIF drives angiogenesis through multiple mechanisms. The vascular endothelial growth factor (VEGF) family comprises 4 secreted ligands that bind to tyrosine kinase receptors on vascular endothelial cells, stimulating migration (VEGFR-1 and VEGFR-2). VEGF-A is the ligand that primarily drives the angiogenic switch [97, 98]. Early work displayed that *VEGFA* mRNA expression was induced by hypoxia and contains a canonical HIF-1 HRE sequence [98, 99], the secreted VEGF-A protein creates a gradient of expression around areas of low oxygen tension which endothelial tip cells grow towards from blood-vessel sprouts [100]. Angiopoieten-2 (Ang-2) is an antagonistic ligand for Tie2 receptor expressed on sprouting cells, which upon binding works to promote new vascularization to be formed [101]. Like *VEGFA*, the *ANGPT2* gene (that encodes Ang-2) also contains a functioning HRE and is a HIF responsive gene [102]. This result shows how HIF drives new blood vessel formation through the VEGF-Ang2 axis; a number of inhibitors have been

developed to target this axis. One such inhibitor is axitinib (related compounds include cabozantinib and pazopanib), a tyrosine-kinase inhibitor that targets multiple targets including VEGFR-1-3, which is currently approved for second line treatment of advanced renal cell carcinoma [103, 104].

HIFs further propagate angiogenesis through alteration of the platelet derived growth factor (PDGF) pathway. The endothelial cell receptor for this pathway activates the same kinase cascade as VEGFR-1 signaling following activation by PDGF ligand binding [105]. As with *VEGFA*, one of the PDGFR ligands, *PDGFB,* is a hypoxic responsive gene and contains a functional HRE in the 5' UTR [106]. In addition to this mechanism, the PDGFR-β receptor is hyper-phosphorylated in hypoxia in a HIF dependent manner. This hyper-phosphorylation indicates activity of the tyrosine kinase domain of PDGFR. This occurs through a HIF-dependent downregulation of a number of protein tyrosine phosphatases that dephosphorylate PDGFR [107]. This axis provides another mechanism how HIFs can regulate new blood vessel formation at both the receptor and ligand of the signaling pathway.

1.5.2.2 Hypoxia and HIFs in the development of resistance to radiotherapy and chemotherapy

Whilst we have primarily focused on targeted therapy through inhibition with small-molecules or monoclonal antibodies as a treatment strategy, radiotherapy remains a crucial tool in treating multiple cancer types. Tumour hypoxia has long been associated with radiotherapy resistance; this largely arises as a result of a HIF-independent mechanism termed 'the oxygen effect'.

Radiotherapy induces cell death through high-powered ionizing radiation inducing intracellular free radical formation and further radical propagation through ROS induction. These free radicals induce widespread DNA damage; the presence of molecular oxygen (O_2) 'fixes' the DNA maintains DNA in the damaged state thereby inducing cell death [108, 109].

HIF signaling can further induce radiotherapy resistance through modulation of cellular metabolism; further details on how HIF modulates cell metabolism will be discussed in more depth in **1.5.2.4.** Briefly, through HIF-dependent changes in metabolism, the antioxidant capacity of tumour cells is increased within the cancer cells as a result of increased flux through the pentose phosphate pathway that maintains glutathione in the reduced state [110]. Furthermore, lactate production has been linked to radioresistance through the ability of lactate to scavenge free radicals, this increased levels of lactate is a common hallmark of the glycolytic switch that occurs in hypoxic cancer cells as a consequence of increased HIF activity [111-114]. The role of HIF-1α in radiotherapy resistance was confirmed in a mouse model of soft tissue sarcoma with deleted *HIF1A*, where loss of *HIF1A* re-sensitised tumours to ionizing radiation. Levels of DNA damage repair and autophagy were similar between the *HIF1A* null and positive groups however there were significant mitochondrial defects, which possibly contributed to radiotherapy resistance [112].

Resistance to therapy is a major clinical problem with tumours either acquiring resistance as a result of treatment or presenting with innate resistance due to

the surrounding microenvironment. Through understanding these mechanisms there is the possibility to circumvent the problems and resensitise tumours to therapy. Early reports highlighted the importance of HIF-1α in promoting resistance to therapy as mouse embryonic fibroblasts knocked out for HIF-1α displayed increased sensitivity to treatment with carboplatin in both normoxia and hypoxia [115]. One mechanism behind HIF-mediated drug resistance is through increased expression of drug efflux pumps. Knockdown of HIF-1α in glioma cell lines reduced expression of multidrug resistance-associated protein 1 (MRP1) at both the protein and mRNA levels [116], this was later found to be due to a functional HRE that was found to be active in colorectal cancer lines [117]. Expression of this efflux pump increases export of drugs from the cell such that the concentration falls below sub-lethal levels [118]. P-glycoprotein (P-gp, also known as multidrug resistance protein 1, MDR1) is another HIF target gene that acts as a drug efflux pump, upregulation of P-gp has been reported in a number of cancer types such as breast cancer, gastric cancer and glioblastoma [119-121].

Recent work in pancreatic cancer cell lines and mouse models identified rewired glucose metabolism in gemcitabine resistant samples. Cell lines were cultured in increasing doses of gemcitabine to generate acquired resistance to gemcitabine (Gem-R). These lines have increased glucose uptake and displayed increased flux of glucose through non-oxidative pentose phosphate pathway compared to wild type cell lines. This increased flux through non-oxidative PPP resulted in increased pyrimidine biosynthesis, as gemcitabine is a nucleoside analog the efficacy of gemcitabine is inhibited upon increased *de*

novo nucleoside synthesis. This switch to increased glucose uptake and nucleoside synthesis is mediated through HIF-1α; pharmalogical inhibition of HIF-1α resulted in resensitisation to gemcitabine. This seminal work highlights how metabolic rewiring mediated by HIF-1α can confer acquired resistance to chemotherapy treatment [122].

1.5.2.3 HIF transcriptional activity drives EMT switch to promote metastasis

For the majority of cancer cases, the leading cause of death arises from metastasis. Therefore significant interest and research has gone in to further understanding the molecular drivers of metastasis. As previously mentioned in section **1.5.2.1** an early event in metastasis is the formation of vasculature to provide an avenue for cells to extrude through. Secondly, epithelial derived cancer cells undergo a process termed epithelial-to-mesenchymal transition (EMT). Through this process, cells lose E-cadherin which disrupts and cell-to-cell adhesion and acquire mesenchymal proteins such as vimentin which regulates cell shape and motility as well as multiple other changes [123]. The switch between these two cell states is driven by a number of transcription factors. TCF3, ZFHX1A and ZFHX1B are all transcription factors that repress expression of E-cadherin, each of these are HIF-1 target genes therefore active HIF-1 will drive expression of each and subsequently repress expression of E-cadherin [124]. TWIST1 is another transcription factor that mediates the EMT switch in cancer cells [125], the *TWIST1* gene is a hypoxic responsive gene that is activated in a HIF-2 dependent manner in HEK293T cells [126]. Further studies have shown that in some cellular contexts *TWIST1* is upregulated by

HIF-1, furthermore knockdown of *TWIST1* in HIF-1α overexpressing cells resulted in a reversal of the EMT/metastatic phenotype thereby indicating that the HIF-1 upregulation of TWIST1 is a key mediator of hypoxia induced metastasis [127].

Following EMT cancer cells invade surrounding tissues, in order to do so the cells need to degrade the extracellular matrix surrounding the tissue. This occurs through secretion of matrix metallo-proteases (MMPs) [128]. A number of these MMPs have been identified as HIF responsive genes [129-131], therefore as the cancer cells undergo EMT, HIF will continue to upregulate expression of MMPs thereby degrading extracellular matrix and allowing cancer cells to migrate through.

1.5.2.4 HIFs promote the glycolytic switch in cancer cells

In 1925, Otto Warburg first described the phenomena whereby the cellular metabolism in cancer increases glucose consumption and lactate secretion even with functioning mitochondria and sufficient oxygenation [132]. This was paradoxical at the time as lactate production is a product of anaerobic metabolism, therefore the term aerobic glycolysis was coined, and this refers to the shift from full oxidation of glucose through mitochondrial processes such as TCA cycle and subsequent oxidative phosphorylation (OXPHOS) to the cytoplasmic glycolytic pathway. Whilst this switch in metabolism appears to be an inefficient system for ATP production, it has been hypothesized that this occurs as a mechanism to sustain biosynthesis of other molecules such as nucleosides and lipids to maintain cell proliferation [133].

Hypoxia and HIFs regulates metabolism in a multitude of ways. O_2 acts as the terminal electron acceptor during OXPHOS, therefore the electron transport chain (ETC) ceases to function during hypoxia. HIF signaling directs glucose metabolism away from mitochondrial processes at multiple stages. One such example is the HIF-mediated upregulation of pyruvate dehydrogenase kinase 1 (*PDK1*). This enzyme phosphorylates the pyruvate dehydrogenase (PDH) complex at the PDH-E1α subunit, blocking the conversion of pyruvate to acetyl-CoA [134]. This reaction utilizes Coenzyme A as a substrate to transfer two carbons from pyruvate into the TCA cycle. Glucose metabolism is further altered through the HIF-dependent induction of *LDHA*, the gene that produces lactate dehydrogenase an enzyme that catalyzes the reversible formation of lactate from pyruvate [135]. Lactate is secreted from the cells through the MCT4 transporter, recent work in fasted mice has demonstrated that lung and pancreatic tumours can utilize circulating lactate to fuel the TCA cycle at higher rates than glucose [136].

Glutamine addiction is a term to describe how many cancer cells rely on glutamine as the predominant mitochondrial substrate to maintain cellular function [137]. Glutamine is converted to α-ketogluturate (α-KG) which can then participate in the forward TCA cycle to produce ATP, however in hypoxic cells this α-KG is reductively carboxylated by isocitrate dehydrogenase (either IDH1 or IDH2) to form citrate. Citrate is then used to maintain lipogenesis, which is required for cell proliferation and function [138-140]. This reductive carboxylation is HIF dependent as overexpression of HIF-1α in normoxia

diverts glutamine to citrate and the carboxylation is reduced following loss of HIF-1α. This result highlights the dependence of cancer cells to utilize glutamine as an alternative carbon source, this is of clinical importance as it has been shown that treating VHL-null RCC xenografts with glutaminase inhibits tumour growth [140].

This section shows how HIFs drive a shift in cancer cell metabolism that has been a defining characteristic of cellular transformation that was first noted almost a century ago. Furthermore that this switch also provides inherited vulnerabilities as a result of glutamine dependency.

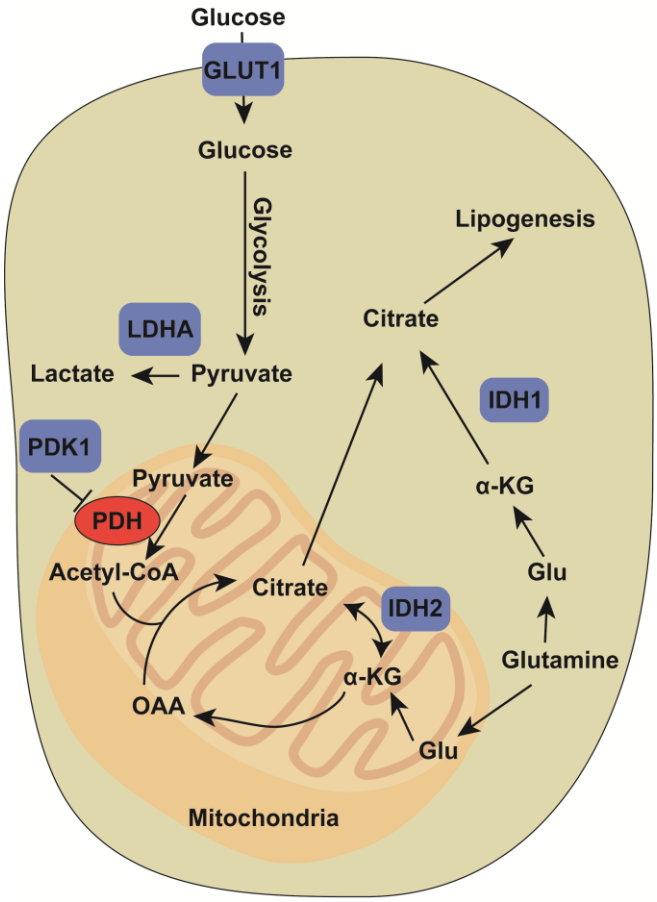

Figure 1.5.2.4: The HIF mediated metabolic switch in hypoxia. Schematic diagram showing how metabolism is altered during hypoxia summarizing section 1.5.2.4. Pyruvate dehydrogenase complex (red) is inhibited by phosphorylation by PDK1. Enzymes highlighted in blue are upregulated or increase in activity in low oxygen tensions.

1.6 Non-canonical regulation of HIFs

The O_2 dependent regulatory pathway maintains HIF homeostasis in normal cells, however multiple cancers upregulate HIF irrespective of oxygen tensions, this is exemplified by *VHL* deletions in ccRCC. There has been extensive research in identifying new regulators of HIFs that are often altered in cancer and drive tumorigenesis.

1.6.1 Differential regulation of HIF-1α and HIF-2α by mTOR

The mechanistic target of rapamycin (mTOR) is a kinase that is the core component of two complexes, mTOR complex 1 (mTORC1) and mTOR complex 2 (mTORC2) [141]. Reports have shown that HIF-1α protein expression and transcriptional activity is sensitive to treatment with rapamycin, but no changes in protein stability were observed suggesting that this is through the role of mTOR in regulating protein translation [142, 143]. Furthermore, in RCC cells HIF-1α and HIF-2α protein expression are both reduced following siRNA knockdown of *MTOR.* HIF-1α protein expression is dependent on both raptor (component of mTORC1) and rictor (component of mTORC2) indicating that both complexes regulate HIF-1α protein however only knockdown of rictor resulted in reduced HIF-2α protein [144].

1.6.2 Direct or indirect post-translational modifications that regulate HIFs

1.6.2.1 Ubiquitination and proteasomal degradation of HIF-1α

The canonical mechanism of PHD-VHL dependent ubiquitination of HIF-1α is a well characterized process, however a number of alternative ubiquitination pathways also serve to negatively regulate HIFα protein stability. One such

example is the HSP70-CHIP axis. Through LC-MS/MS analysis of HIF interacting proteins both heat shock protein 70 (HSP70) and carboxyl terminus of Hsc70 interacting protein (CHIP) were identified. CHIP is an E3 ubiquitin ligase that ubiuitates HIF-1α in chronic hypoxia in the presence of HSP70. Only HIF-1α was subject to ubiquitination through this axis and only in sustained hypoxia as part of a negative feedback loop, due to the differential target genes between the HIFα isoforms this may regulate differential transcriptome in acute and chronic hypoxia [145].

Parkin is an E3 ubiqutin ligase protein that displays reduced expression in breast cancer and inhibits breast cancer cell proliferation *in vitro* [146, 147]. Furthermore parkin was identified as a HIF-1α interacting protein capable of ubiquitinating HIF-1α at Lys477 in the ODDD, an alternative residue to pVHL mediated ubiquitination. Through this degradation axis, parkin inhibits cancer cell metastasis invasion in a HIF-dependent manner [148]. Both the HSP70-CHIP and Parkin axis show how HIF-1α is subject to further ubiquitination and proteasomal degradation beyond the canonical PHD-VHL axis, however Montagner *et al.* demonstrated that HIF-1α can be degraded by the proteasome in a ubiquitin-independent manner [149].

SHARP1 (also known as Dec2) is a basic-helix-loop-helix protein that is a transcriptional repressor playing a role in regulating the circadian rhythm [150]. Co-immunoprecipitation experiments showed that SHARP1 directly interacts with HIF-1α and promotes interaction with the proteasome in an oxygen and

VHL independent manner [149]. Furthermore loss of SHARP1 increases TNBC cell metastasis and invasion in a HIF dependent manner.

1.6.2.2 Regulation of HIF protein stability and activity by acetylation

Protein acetylation is a major post-translational modification prevalent across a wide variety of targets. Acetylation occurs through an enzymatic process, mediated by acetyltransferases, where the acetyl group from acetyl-CoA is transferred to the N-terminus of proteins or lysine residues [151]. P300/CBP-associated factor (PCAF) is a lysine acetyltransferase that acts a transcriptional cofactor for HIF-1α and p53 [152]. Furthermore PCAF acetylates HIF-1α at Lys674 that stabilizes the interaction with the transcriptional coactivator p300, deacetylation at this residue is catalyzed by sirtuin 1 (SIRT1) [153]. HIF-2α is not acetylated by PCAF, instead through CBP mediated acetylation exclusively from Acetyl CoA synthetase 2 (ACSS2) derived acetyl-CoA [154, 155]. SIRT1 is still the deacetylase active for HIF-2α, however increased SIRT1 expression promoted HIF-2 activity, thereby indicating differential roles of SIRT1 and acetylation in regulating HIF-1 or HIF-2 transcriptional activity independent of protein stability [156].

RNAi-mediated knockdown of the class II histone deactylases, HDAC4 and HDAC6, resulted in reduced HIF-1α protein levels and activity in a VHL-independent manner [157]. Acetylation of HIF-1α by HDAC4 occurs at a cluster of lysine residues at the N-terminus (Lys-10, 11, 12, 19 and 21) that serves to stabilize HIF-1α as evidenced through cyclohexamide chase assay [158] .

These two pathways show contrasting roles of protein acetylation on HIFs as one axis regulates protein activity in an isoform specific manner whereas the second pathway discussed regulates protein stability in addition to activity.

1.6.2.3 Kinase regulators of HIF

The role of protein phosphorylation in regulating HIF was established the same year that HIF was first characterized, as treating cells with protease inhibitors reduced both HIF-1α protein expression and DNA binding capability [159]. Since these early experiments a number of kinases that regulate HIF stability and activity have been identified. A number of reviews have compiled comprehensive lists of these kinases [160, 161], however for brevity, here a number of kinases will be discussed to cover different mechanisms that kinases regulate HIF activity.

Using an RNAi screen targeting the human kinome, Chen *et al.* assayed a HRE based reporter in HeLa cells. Through this approach they identified SMG-1 as a negative regulator of HIF-1 transcriptional activity, which acts through inhibition of MAPK [162]. Whilst the authors do not decipher how SMG-1 regulates MAPK, this work shows that unbiased RNAi screens are an effective way of identifying novel regulators of HIF activity.

Inhibitor of differentiation 2 (ID2) is a protein that regulates stem cell characteristics that is frequently upregulated in glioma, driving tumorigenesis and angiogenesis [163, 164]. Active ID2 binds to pVHL displacing cullin 2 and subsequently inhibiting HIF-2α proteasomal degradation. However the kinase

DYRK1 maintains ID2 in an inactive state through phosphorylation at Thr27, this phosphorylation event is oxygen dependent as DYRK1A and DYRK1B are direct targets of PHD1, PHD2 and PHD3 [165]. This work highlights a kinase that is required to maintain efficient HIF-2α turnover and presents a novel mechanism of destabilization of the pVHL-E3 ubiquitin ligase complex.

Cyclin-dependent kinase 1 (CDK1) plays a crucial role in regulating cell-cycle, however CDK1 was identified as a kinase that directly phosphorylate HIF-1α [166]. This phosphorylation event occurs at Ser668, the phosphorylation stabilizes HIF-1α protein and enhances cell migration and invasion *in vitro* and stimulates tumour growth *in vivo*. However, another paper proposed a different mechanism behind CDK1 mediated HIF-1α stabilisation. These findings confirmed that there was a direct interaction between CDK1 and HIF-1α, however treatment with the lysosome inhibitor bafilomycin A1 negated the effects of CDK1 overexpression [167]. It is unclear as to which mechanism is true, or if different cellular context accounts for these differences. Regardless these two papers show that direct interaction between an active kinase and HIF-1α is capable of stabilising HIF-1α.

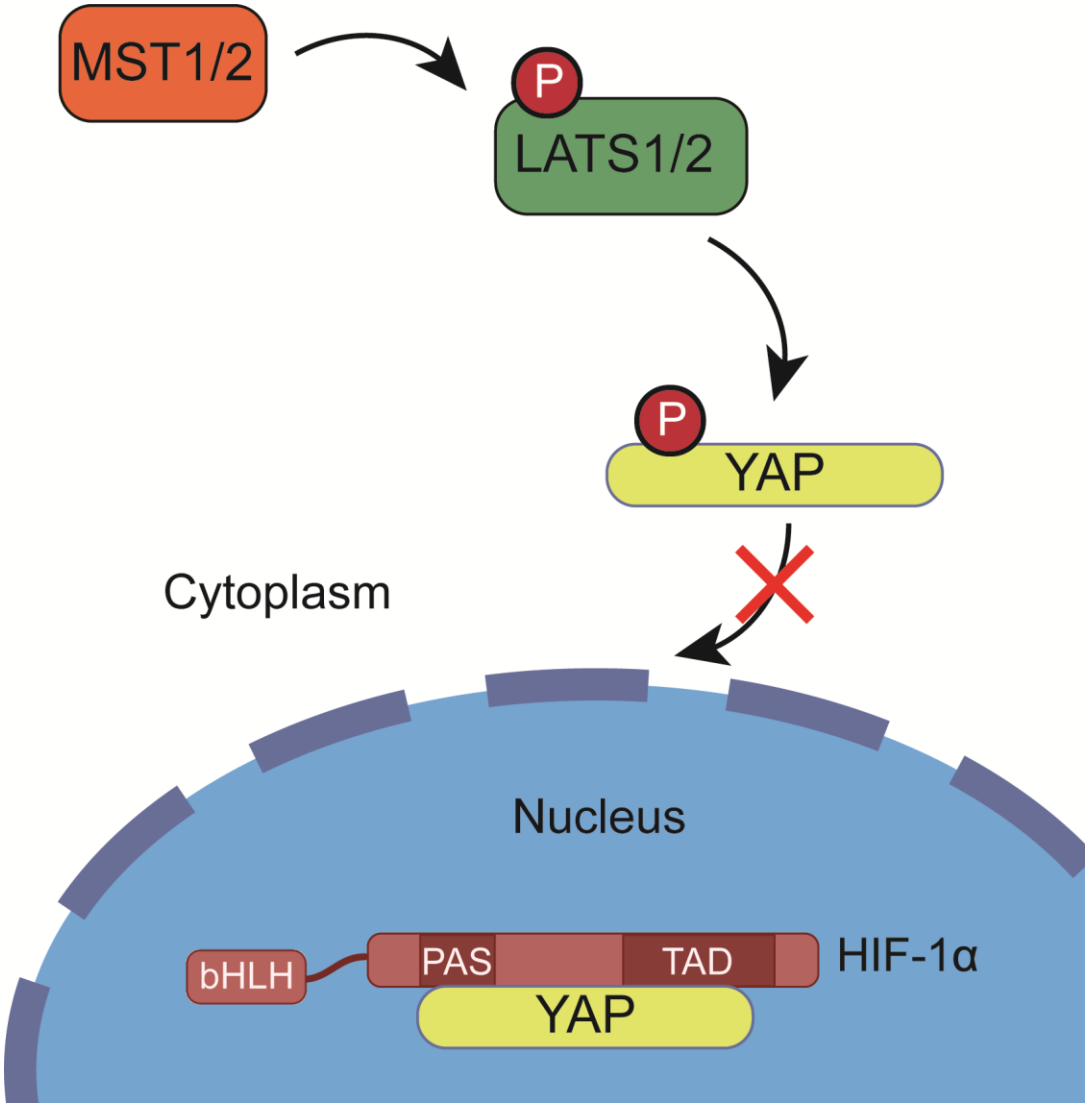

Figure 1.6.2.3: Hippo signaling regulates HIF-1α activity. Schematic diagram of HIF regulation through Hippo signaling pathway. MST1/2 phosphorylates and activates LATS1/2. Phosphorylated LATS then phosphorylates YAP, which blocks nuclear import. Upon dysregulation of this signaling cascade YAP accumulates in the nucleus whereby it binds to HIF-1α thus stabilizing protein and increasing transcriptional activity [169].

The hippo signaling pathway plays an important role in development and cancer [168], this pathway involves a kinase cascade where MST1/2 phosphorylates LATS1/2 which in turn results in the phosphorylation of YAP, a transcription factor that is retained in the cytoplasm upon phosphorylation [169, 170]. A non-transcriptional function of YAP in the nucleus is to directly bind to and stabilize HIF-1α [171], therefore deregulation of MST1/2 or LATS1/2 will

cause accumulation of nuclear YAP and subsequent stabilisation of HIF-1α. LATS2 mutations have not been identified in cancer, however the E3 ubiquitin ligase SIAH2 destabilises LATS2 and is found upregulated in breast cancer [171]. SIAH2 plays a further role in cancer as other ubiquitination and subsequent degradation targets of SIAH2 are the PHD1/3 proteins, therefore upregulation of SIAH2 will increase hypoxia signaling via multiple mechanisms [172].

1.6.3 Emerging role of metabolites as regulators of HIFs

1.6.3.1 Succinate and fumarate inhibit prolyl-hydroxylases

The TCA cycle is impaired in both hypoxia and pseudo-hypoxia through activation of HIFs, induction of PDK1 and phosphorylation of the pyruvate dehydrogenase complex as discussed in **1.5.2.4**. It has been shown that succinate accumulates in multiple hypoxic tissues suggesting that succinate acts as a 'dead-end' in TCA cycle flux in low O_2 conditions [173]. This accumulated succinate in the mitochondria diffuses in to the cytoplasm where it can inhibit PHDs thereby resulting in stabilised HIFα proteins [174, 175]. Loss-of-function mutations in succinate dehydrogenase complex enzymes are prevalent in multiple cancers including renal cell carcinoma and colorectal [176, 177].

Germline mutations in fumarate hydratase (FH) predispose patients to developing renal cell carcinoma [178, 179]. Addition of fumarate to cells or siRNA mediated knockdown of FH result in stabilised HIF-1α in normoxic as a consequence of PHD inhibition [180]. Despite both succinate and fumarate

being found in non-transformed cells and acting as intermediates in TCA cycle, they are still considered to be oncometabolites when accumulated at high levels [181], in part due to inhibition of PHDs and regulation of HIFs. These results highlight how perturbations in TCA cycle homeostasis can drive cancer progression.

1.6.3.2 Prolyl-hydroxylases sense intracellular changes in cysteine

After an initial observation that TNBC cells expressed stabilised HIF-1α in normoxic conditions, which is degraded following the addition of fresh culture medium, L-glutamine was identified as a secreted molecule that stabilizes HIF-1α through inhibition of prolyl-hydroxylase function [88]. L-glutamine was secreted through the xCT cystine-glutamine antiporter, which depletes intracellular cysteine. This depletion of intracellular cysteine is sufficient to inhibit prolyl-hydroxylase function and stabilise HIF-1α. This landmark paper provides insights in to how PHD enzymes are able to sense changes in cysteine as well as oxygen.

1.6.3.3 IDH1/2 mutations and the role of 2-HG as an oncometabolite

As previously discussed, cell metabolism is significantly altered in cancer. Rewiring of these metabolic pathways does not solely result in altered levels and fluxes of metabolites; certain mutations can result in formation of atypical metabolites, one such example of this is mutations in isocitrate dehydrogenase (IDH1 and IDH2). Mutations in IDH1 and IDH2 occur at high frequency in gliomablastoma patients with mutations always affecting the R132 codon; in a cohort of 445 CNS tumours over 70% of patients were positive for IDH1-R132

mutations [182]. Furthermore, IDH mutations have been identified, albeit less frequently (1.1% of NSCLC), in breast and lung cancer [183, 184]. Wild-type IDH catalyzes the decarboxylation of isocitrate to form α-ketogluturate (also known as 2-oxogluturate, αKG) in a reversible reaction that occurs both in the cytoplasm as well as in the mitochondria as part of the TCA cycle, however mutant IDH gains the ability to convert αKG into the (R)-enantiomer of 2-hydroxygluturate (2-HG) [185, 186]. The role of HIFs in brain tumours is different to other tumours as it has been reported that HIF-2α acts as a tumour suppressor in these cancers and that HIF-1α reduces tumour growth and brain penetrance in orthotopic tumour models [187, 188]. This is of importance as 2-HG accumulates in tumours with IDH mutations and acts as a substrate for PHD enzymes, thereby increasing turnover of HIF-1α protein. This increased degradation of HIF resulted in increased proliferation and anchorage independent growth of astrocytes [189]. Whilst the role of HIF is reversed in brain tumours compared to most solid tumours, these results highlight how oncogenic mutations resulting in the formation of novel metabolites can modulate HIF pathway activity that drives cancer progression. The converse of this has been observed in cancer-associated fibroblasts, which display a reduction in IDH3α (a related homolog of IDH1 and IDH2 but performs non-reversible reactions) following transformation from fibroblast to CAF. In these IDH3α deficient cells, prolyl-hydroxylase function is inhibited as a consequence of depleted levels of α-KG and subsequent accumulation of succinate and fumarate. This results in stabilised HIF-1α that helps promote pro-tumour functions of CAFs [190].

Through genetic screens in haploid cell lines, Burr *et al*. identified that loss of *OGDH* (the gene encoding a core component of the alpha ketogluturate dehydrogenase complex) and *LIAS* (Lipoic acid synthase, of note lipoate was further identified as an OGDHC inhibitor) resulted in stabilised HIF-1α in normoxic conditions. Disruption of this complex resulted in accumulation of L-2-HG, an enantiomer of R-2-HG that also inhibited PHD activity [191].

1.7 Aims

This work highlights the importance of HIF signaling in driving tumourigenesis in multiple cancer types. HIF target genes regulate many pro-tumourigenic functions such as inducing metastasis, increasing resistance to treatment and altering cellular energetics to sustain growth. Dysregulation of HIF occurs by multiple mechanisms resulting in a pseudo-hypoxic phenotype and a HIF driven cancer progression.

We aim to identify novel regulators of HIFs that may serve as therapeutic targets in breast and lung cancer.

To achieve this we aim to:

- Perform an unbiased screen of HIF-1 activity to identify novel regulators
- Validate hits and determine mechanism behind HIF regulation
- Determine the role of this novel regulator on cellular transformation
- Assess the expression of this regulator in patient data and determine suitability for targeted therapy
- Identify a small molecule to selectively target this novel regulator of HIFs in cancer cells

Materials and Methods

2.1 Buffers and materials

2.1.1 Materials and solutions for bacterial culture

1. ***Agar plates*** – 3.5% (w/v) LB-Agar was dissolved in distilled water and autoclaved and stored at room temperature until use. To prepare plates agar was boiled in microwave to before allowing to cool to ~40°C. Once cool, appropriate dilution of antibiotic was added and solution was poured into sterile plates and left to set at room temperature. Plates were stored at 4°C and used within 4 weeks.

2. ***Ampicillin*** – 100 $mg.mL^{-1}$ stock solutions were stored at -20°C in 1 mL aliquots. Working concentrations of 100 $\mu g.mL^{-1}$ were used throughout.

3. ***Kanamycin*** – 50 $mg.mL^{-1}$ stock solution of kanamycin was stored at 4°C. Agar plates were made at concentration of 50 $\mu g.mL^{-1}$ and liquid cultures were prepared at a concentration of 33 $\mu g.mL^{-1}$.

2.1.2 Solutions for DNA agarose electrophoresis

1. ***10X DNA loading solution*** – 30% glycerol and 0.25% (w/v) bromophenol blue were dissolved in MilliQ distilled water and stored at room temperature. Solution was diluted to 1X with sample prior to loading.

2. ***Tris-Borate EDTA buffer*** – 10X TBE buffer was diluted to 1X with distilled water to achieve final concentration of 40 mM Tris-Borate and 2 mM EDTA.

2.1.3 Cell lysis buffers

1. ***RIPA buffer*** – 150 mM NaCl, 0.5% (w/v) sodium deoxycholate, 0.1% (w/v) SDS, 1% (v/v) IGEPAL-630 and 50 mM Tris (ph 8.0) were dissolved in MilliQ distilled water and stored at 4°C.

2. ***Protease and phosphatase inhibitors*** – Pierce protease inhibitors and phosphatase inhibitor tablets (Thermofisher) were dissolved in 10 mL of RIPA buffer before storing solution in -20°C.

2.1.4 Solutions for SDS-Page and Western blotting

1. ***Phosphate buffered saline (PBS)*** – 10X PBS solutions were prepared by dissolving 1 sachet of PBS powder (Severn biotech) in 1 L of distilled water. 10X solution was further diluted to 1X with distilled water to achieve final concentration of 137 mM NaCl, 2.7 mM KCl, 4m3 mM Na_2HPO_4 and 1.47 mM KH_2PO_4.

2. ***PBS-T*** – 10X PBST solution was prepared by dissolving 1 sachet of PBS powder in 1 L of distilled water before adding 5 mL of Tween-20 (Sigma-aldrich). 10X solution was further diluted to 1X with distilled water to achieve a final concentration of 1X PBS with 0.05% tween.

3. ***Western blot blocking solution*** – 5% skimmed milk powder (w/v) (Sigma-Aldrich) or 5% Bovine serum albumin (w/v) (Sigma-Aldrich) were dissolved in 1X PBST and stored at 4°C and used within 4 days.

4. ***SDS-PAGE Gel casting solutions*** – Resolving gel: 30% Protogel Acrylamide, 4X Resolving buffer (BioRad) were made up to appropriate concentration in distilled water. Acrylamide was set with the addition of 1:100 of 10% Amino persulfate (Sigma-aldrich) and 1:1000 of N,N,N’,N’-

tetramethylethylenediamide (TEMED) (Sigma-aldrich). Stacking buffer was made as before but with 1:200 of 10% Amino persulfate and 4X stacking buffer (1.0M Tris pH 6.8, 10% (w/v) SDS).

5. ***SDS-PAGE Running buffer*** – 10X Tris glycine-SDS buffer was diluted to 1X with distilled water to achieve a final concentration of 25 mM Tris (ph 8.3), 0.2 M Glycine and 1% (w/v) SDS.

6. ***Transfer buffer*** – 10X Tris glycine buffer was diluted with distilled water and methanol added to make final solution of 1X tris-glycine with 20% methanol.

7. ***5X SDS-PAGE loading buffer*** – 250 mM Tris-HCl (ph 6.8), 50% (v/v) glycerol, 0.05% (w/v) Bromophenol blue and 5% (w/v) SDS were dissolved in distilled water. For reducing conditions 5% (v/v) β-mercaptoethanol was added to loading buffer. Buffer was stored in 1 mL aliquots at -20°C.

8. ***Coomassie Blue staining solution*** – 0.1% (w/v) Coomassie Brilliant Blue R was dissolved into a 40% Methanol, 10% acetic acid and 50% distilled water solution. Solution was stored at room temperature.

9. ***Coomassie Blue De-staining solution*** – 10% (v/v) and 10% (v/v) acetic acid were mixed with distilled water and stored at room temperature.

2.2 Bacterial culture

2.2.1 Transformation of chemically competent cells

DH5α chemically competent cells (New England biolabs) were removed from -80°C and thawed on ice for 10 minutes. 2 µL of ligated DNA or 1 uL of purified plasmid were added to 25 uL of competent cell suspension before incubating on ice for 30 minutes. The cells were then heat shocked in a water bath set to 42°C for 30 seconds before incubating on ice for a further 5 minutes. 500 µL of

Luria Broth (LB) was added to the cell suspension and resulting mix was incubated at 37°C for 1 hour with gentle agitation. 40-400 µL of the bacteria cell suspension was spread onto agar plates with appropriate antibiotic (Kanamycin at 50 µg.mL^{-1} and Ampicillin at 100 µg.mL^{-1}) and left overnight at 37°C. Positive colonies were picked with 200 µL pipette tip and inoculated overnight in 5 mL of LB containing appropriate antibiotic selection. The following day 800 µL of bacteria suspension was mixed with 200 µL of glycerol before immediately storing at -80°C. Remainder of bacteria suspension was used for downstream analysis.

2.2.2 Plasmid DNA extraction from bacteria cultures

2.2.2.1 Mini-prep DNA extraction

Mini-prep DNA extractions were performed using Monarch Plasmid miniprep kit (New England Biotech) as per manufacturers instructions. Briefly 5 mL of bacteria culture was inoculated overnight in LB containing appropriate antibiotic selection. 4 mL of the bacterial suspension was centrifuged at 5000 G to pellet bacteria prior to continuing the protocol. The protocol is based around the traditional alkaline lysis method with the RNAse added to the first suspension buffer to remove all bacterial RNA prior to continuing with the purification using a column based approach. Eluted plasmid DNA was analysed on Nanodrop to measure purity and concentration, 260:280 ratio of over 1.8 and 260:230 ratio of at least 1.9 was used as quality control of plasmid DNA.

2.2.2.2 Midi-prep and Maxi-prep DNA extraction

Both Midi-prep and Maxi-prep kits were performed using kits from Qiagen as per manufacturers instructions. Starting cultures of 50 mL (Midi-prep) and 200 mL (Maxi-prep) were used for plasmid isolation. Extractions were performed as in 2.2.2.1 but with larger reaction mixtures. The primary difference lies in an altered elution step that contains an additional isopropanol precipitation step. DNA pellets were washed 2 times with ice-cold 70% ethanol before dissolving in TE buffer. Quality and concentration of plasmid DNA was analysed using nanodrop spectrophotometer.

2.3 Nucleic acid techniques

2.3.1 Agarose gel electrophoresis of DNA

Agarose gels (0.8-3% agarose w/v) were prepared by melting the appropriate amount of agarose in 1X TBE (Tris-Borate EDTA) buffer depending on DNA size and required resolution. Warm agarose solution was allowed to cool before adding either GelRed or GelGreen (Biotium) and pouring into casting station with suitable comb. DNA size was estimated by running GeneRuler 1Kb plus DNA ladder (ThermoFisher). DNA electrophoresis was performed on horizontal gel electrophoresis equipment at a constant voltage of 80-100V. Bands were visualised under UV or blue light and imaged using Amersham Imaging ChemiDoc 600 (GE Healthcare) or G:BOX imaging system (Syngene) and GeneSnap software.

2.3.2 Extraction of DNA from agarose gels

DNA bands were visualised under blue light and excised from agarose using clean scalpel. The DNA was extracted using Monarch gel extraction kit (New England Biolabs) as per manufacturers instructions. DNA bands were weighed inside a sterile 1.5 mL eppendorf before dissolving band in 4 volumes of dissolving buffer at 55°C. Solutions were transferred to Monarch DNA cleanup columns before being washed two times with DNA wash buffer. DNA was eluted in elution buffer and quantified using Nanodrop.

2.3.3 Restriction enzyme digest of DNA

Restriction enzyme digest of DNA was performed with enzymes in their appropriate buffer (New England Biolabs). For each 1 µg of DNA to be digested, 10 units of enzyme and 1 µL of appropriate buffer was added to nuclease free water to a final reaction volume of 10 µL. Reactions were heated to 37°C using Verity thermocycler (Applied Biosystems). 10X DNA buffer was added to stop reaction before separating DNA fragments by agarose gel electrophoresis.

2.3.4 Ligation of digested DNA insert into linearised vector

All digestions were performed with sticky-ends created by two distinct restriction endonucleases such that vector and insert had complementary overhanging ends to ensure correct insert orientation. Prior to ligation vector and insert were both digested as described in 2.3.3 and DNA was purified as detailed in 2.3.2. Ligations were performed with an insert to vector molar ratio of 3:1. A total of 25 ng of vector and the appropriate amount of insert was made up to a final volume of 5 µL with nuclease free water. 5 µL of 2X Instant sticky-

end ligase master mix was added and mixed by gentle pipetting. Reactions were left for 5 minutes at room temperature before proceeding with bacteria transformation as described in 2.2.1. In parallel a second reaction was performed without insert to assess self-annealing of plasmid DNA.

2.3.5 DNA amplification by polymerase chain reaction (PCR)

For Amplification of DNA, the proofreading polymerase Phusion Hot Start Flex 2X master mix (New England biolabs) was used. Forward and reverse primers were used at a final concentration of 0.5 µM each. DMSO is also added to the reaction mixtures at a final concentration of 3%, DMSO binds to cytosine residues making the DNA more susceptible to heat denaturation and aids in the amplification of G-C rich regions. Template DNA was used at a concentration of 2-20 ng for plasmid DNA or at least 50 ng for genomic DNA.

Cycling conditions are displayed below:

Table 2.3.5: Cycling conditions used for PCR

Step	Temperature	Duration
Initial Denaturation	98°C	30 seconds
Cycles	98°C	5-10 seconds
	Annealing temperature 50-72°C	10-30 seconds
	72°C	20 seconds/kb
Final Extension	72°C	5 minutes
Hold	4°C	Indefinitely

Number of cycles varied depending on subsequent usage, for example site directed mutagenesis reactions were performed with 25 cycles however amplification from cDNA for ligations were performed with 40 cycles.

2.3.6 Site directed mutagenesis (SDM)

Primers were designed for SDM using the online tool nebbasechanger (New England Biolabs). PCR reactions were performed as described in section 2.3.5 prior to performing the KLD reaction as described by the manufacturer. The KLD reaction phosphorylates the PCR product to allow for the ligation prior to DpnI digest to degrade the template DNA (due to dam methylation which occurs in bacterial production of plasmid DNA). The resulting KLD mix is then transformed as described in section 2.2.1 before confirming successful mutagenesis by Sanger sequencing (Source bioscience).

2.3.7 Nucleic acid extraction from cultured cells

2.3.7.1 Genomic DNA extraction from cultured cells

Genomic DNA was extracted from cultured cells using QuickExtract DNA extraction solution (EpiBio) as per manufacturer's instructions. Briefly, cell pellets (~ $x10^4$ cells) were collected and washed with PBS before resuspending in 500 µL of extraction solution. Samples were vortexed before heating to 65°C for 6 minutes and then 98°C for 2 minutes. The resulting solution contains genomic DNA ready for PCR amplification. Samples were stored at -20°C.

2.3.7.2 mRNA extraction from cultured cells.

For RNA extractions the ReliaPREP RNA Miniprep system (Promega) was used. This is a column based assay kit that extracts mRNA from cultured cells. The column has binding capacity for mRNA and other lncRNA but does not capture small RNA such as miRNA. For mRNA extractions the protocol was followed as per manufacturer's instructions. Briefly, cell lysis is performed with a guanidine thiocyanate buffer supplemented with 1-thioglycerol to disrupt cell integrity whilst maintaining RNA integrity. After loading lysate on to the column and wash steps, the column is treated with DNAse I for 15 minutes to ensure RNA is pure following extraction. Following further washes the RNA is eluted in nuclease free water and concentration and purity is measured using Nanodrop spectrometer.

2.3.8 Real-time quantitative reverse transcription PCR (RT-qPCR)

qRT-PCR was performed using 1-Step qRT-PCR GoTaq system (Promega) as per manufacturer's instructions. Briefly, 35 ng of RNA was used in a 20 µL reaction with 50X RT and 2X Go-Taq master mixed diluted down to 1X with nuclease free water. For each primer pair two wells of no template controls were assayed to ensure no non-specific amplification arises from potential contaminations of stock solutions, to ensure amplification is from cDNA derived from initial RNA stock reaction mixtures lacking the 50X RT were also prepared for each sample. QuantStudio 5 (Applied Biosystems) was used for all qRT-PCR experiments using the in built QuantStudio software. Cycling conditions for qRT-PCR are listed below. Melt curve analysis was performed for each reaction mix to ensure only a single peak is present and amplification is specific,

any reactions where mixed peaks were present in sample were discarded from subsequent analysis.

Table 2.3.8: Cycle conditions used for all qRT-PCR reactions

Stage	Temperature	Time
Hold stage	37°C	15 minutes
	95°C	10 minutes
PCR Cycle	95°C	15 seconds
(40X cycles)	60°C	45 seconds
Melt Curve	95°C	15 seconds
	60°C	15 seconds
	95°C	1 second (0.15°C.s^{-1} ramp speed)

Prior to performing experiments, primers were optimised to achieve 100% efficiency. To achieve this, serial dilutions of RNA were prepared with a top RNA volume of 50 ng was assayed against a concentration range of primer concentration at a set annealing temperature of 60°C. Reaction efficiencies were calculated by plotting Log (RNA concentration) vs Average CT value, the gradient of this standard curve was used in the equation below:

$$Primer\ efficiency\ (\%) = 100 \times (10^{\frac{-1}{(Gradient-1)}})$$

Primer concentrations that yielded efficiencies between 95-105% were used for subsequent reactions. For each primer pair used the final concentration was 200 nM apart from *HIF1A* and *HIF2A* were concentrations of 250 nm were used.

For analysis of samples the standard curve was used to give relative mRNA concentrations that are then normalised to housekeeping genes such as *RPII*.

2.4 Cell culture

2.4.1 Culturing of cells in 2D monolayer

Adherent cells were cultured in media indicated in the **Table 2.4.1** and maintained in humidified incubator set to 37°C and 5% CO_2. Hypoxic incubations were performed by incubating cells in INVIVO$_2$ (Ruskinn) at 1% O_2, 5% CO_2 and 94% N_2 for specified time.

For plating of cells for downstream experiments or passaging of cells; cells were washed in sterile PBS to remove residual medium prior to detaching cells with Trypsin-EDTA at 37°C. Complete media was added to neutralize trypsin. Cell suspension was centrifuged for 3 minutes at 1,300 rpm to form a cell pellet, which was subsequently washed 1x with sterile PBS before re-suspending in complete media. Cells were counted using TC20^{TM} BioRad Cell Counter before plating at optimal cell density for each cell line and assay.

Table 2.4.1: Cell culture medium and additives used for culturing cell lines

Cell line	Basal Medium	Serum	Other Supplements
A549	DMEM	10% FBS	
HeLa	DMEM	10% FBS	
U2OS	DMEM	10% FBS	
HEK293T	DMEM	10% FBS	
SAEC	Small airway medium (Lonza)		Kit includes: hEGF, epinephrine, triiodothyronine, transferrin, BSA, retinoic acid, GA-1000, Hydrocortisone, Insulin and BPE
MCF10A	DMEM/F12 media	5% Horse serum	20 $ng.mL^{-1}$ EGF, 0.5 $mg.mL^{-1}$ hydrochortisone, 100 $ng.mL^{-1}$ Cholera toxin 10 $\mu g.mL^{-1}$ Insulin
T47D	RPMI	10% FBS	
ZR-751	RPMI	10% FBS	
SKBR3	McCoy's 5A media	10% FBS	
MDA MB231	RPMI	10% FBS	
MDA MB468	RPMI	10% FBS	
HCC1143	RPMI	10% FBS	
MCF7	RPMI	10% FBS	

2.4.2 Cell Freezing

Adherent cells were trypsinised and collected by centrifugation (Section **2.4.1**). The resulting cell pellets were washed with PBS to remove residual trypsin and media; cells were further pelleted by centrifugation (3 minutes at 1300 rpm) before removing supernatant. Freezing media (90% FBS (v/v) and 10% DMSO (v/v)) was used to resuspend cell pellet before aliquoting into 1 mL cryovials. Cells were immediately stored at -80°C overnight before transferring to liquid nitrogen for long-term storage.

2.5 Transfection of nucleic acids to 2D cultured cells

2.5.1 Transfection of plasmid DNA with ViaFect™

Cells were plated a day prior to transfection and left to adhere overnight. DNA transfections were performed using ViaFect™ transfection reagent as per manufacturer's instructions. ViaFect was added to Opti-MEM serum free medium to give a 3:1 ratio (µL of viafect to µg of plasmid DNA) and incubated for 5 minutes to allow lipid complexes to form. DNA is then added for a further 20 minutes to allow for DNA:lipid complexes to form before adding to cells in antibiotic free medium. The following day media was changed to fresh medium with antibiotics and cells are analysed 48 hours post transfection.

2.5.2 Transfection of siRNA with Dharmafect™

For forward transfections cells are plated a day prior to transfection at appropriate cell density; reverse transfections are performed by adding transfection mix directly to wells prior to adding cell suspension. Unless otherwise stated, siRNA transfections were performed with either Dharmafect

1 or Dharmafect 2 transfection reagents. Transfection reagent was added to Opti-MEM serum free medium at an equal volume to siRNA (diluted to 20 μM) and incubated for 5 minutes. siRNA was added directly to transfection mixture and mixed by gentle pipetting before adding to cells in antibiotic free medium. The following day media was changed to fresh DMEM containing antibiotics and cells are analysed 72 hours post transfection.

2.6 Lentirviral transduction to produce stable cell lines

To produce lentivirus, HEK293T cells were transfected with lentiviral vector and second-generation packaging plasmids pHR'-CMV-8.2ΔR (packaging) and pMDG.2 (VSV-G envelope plasmid) at a ratio of 15:6:11 respectively.

48 hours following transfection, viral media was harvested, centrifuged at 1500 rpm for 3 minutes to remove cell debris and passed through 0.22 μM sterile filter before mixing with complete medium (50% v/v) and adding to cells to be transduced. Transduced cells were maintained in antibiotic containing medium at appropriate concentration for at least 10 days to select for successful transgene incorporation. To determine appropriate dose of antibiotic for selection, kill curves were performed for each experiment. Cells were plated at an appropriate density to be 50-60% confluency the following day, cells were treated with a varying dose of antibiotics for 72 hours before determining minimum dose required to kill all cells.

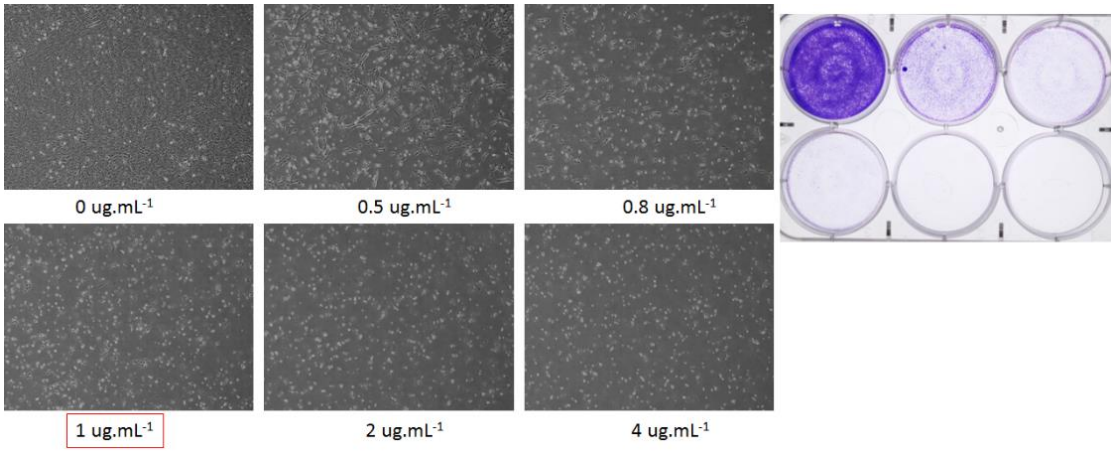

Figure 2.6: Puromycin kill curve. Representative image of puromycin kill curve. A549 cells were treated with puromycin for 48 hours before imaging cells by bright field microscopy. Cells were then fixed in methanol overnight before staining with crystal violet.

2.7.1 Analysis of cell proliferation using Incucyte

Cells were grown and pretreated with doxycycline (25 ng.mL^{-1}) in 2D monolayer and maintained in logarithmic growth phase prior to incucyte analysis. Cells were trypsinised and re-plated at 30,000 cells per well in 12-well plate. Once cells had adhered the plate was placed into incucyte with brightfield images taken every 6 hours for 7 days. Media was replaced with fresh complete media every 48 hours. Confluency masks were calculated for each well to account for plate surface coverage, results were presented as percentage confluency.

2.7.2 Analysis of cell proliferation using Countess II cell counter

A549-tet-shRNA lines were pretreated with doxycycline at 25 ng.mL^{-1} for 72 hours prior to plating. On day of plating cells were detached as described in **2.4.2** before being plated at a density of 30,000 cells per well in duplicate plates with one being placed immediately in 1% O_2 and the other maintained in atmospheric oxygen. On days 1, 3, 5 and 7 cells were detached and re-

suspended in a final volume of 1 mL of cell culture media. The resulting cell suspension was counted on Countess II cell counter.

2.7.3 Clonogenic assays

Inducible shRNA lines were treated with doxycycline at 25 ng.mL^{-1} for 72 hours before cells were detached from plate with trypsin and neutralising with complete medium. Cells were spun at 1300 rpm for 5 minutes before re-suspending in 1 mL of complete medium before counting using TC20^{TM} BioRad Cell Counter or Countess II (ThermoFisher) using Trypan blue to detect viable cells. Cells were plated at either 100 cells per well and immediately placed into hypoxia workstation or 21% O_2 incubator for 10 days with regular media changes every 2-3 days. After 10 days and visible cell colonies formed, cells were washed three times in PBS before fixing in 100% methanol overnight. Fixed cells were stained with crystal violet solution (aq, 0.05% w/v) for 40 minutes before being washed in distilled water. Colonies were counted manually on top of a white light box.

2.7.4 Wound healing assay

A549-tet-RNA cells were pre-treated with 25 ng.mL^{-1} for 72 hours prior to plating at a density to be a confluent monolayer the following day. Once cells had adhered and the cells reached a confluent monolayer wells were scratched with a P200 pipette to remove cells. Each well was washed three times with fresh complete DMEM with doxycycline to remove any floating cells. Scratches were imaged and photographed using a 4x objective, wound closure was measured 6 and 24 hours later. Wound closure was measured using the MRI

wound healing tool plug-in on ImageJ [192]. Wound closure percentage was calculated using formula below:

$$Percentage\ wound\ closure = 100 \times \left(\frac{(Start\ wound\ size - Closed\ wound\ size)}{Start\ wound\ size}\right)$$

2.8 Protein expression analysis

2.8.1 Sample collection and protein quantification

Cells were washed 3 times in ice cold PBS and lysed in RIPA buffer (150 mM NaCl, 1% (v/v) IGEPAL, 0.5% (w/v) Deoxycholic acid, 0.1% (w/v) SDS, 50 mM Tris) with added protease and phosphatase inhibitors (Roche). Cell lysate was scraped and transferred to a 1.5 mL Eppendorf tube before centrifugation at 14000 rpm for 10 minutes to clear insoluble cellular debris. Supernatant is collected and stored at -80°C. Protein concentration was quantified using Pierce BCA protein assay kit as per manufacturer's instructions (ThermoFisher). Samples were made up to the required concentration in sample buffer (250mM Tris-HCL ph 6.8, 50% (v/v) glycerol, 5% (v/v) SDS, 0.05% Bromophenol Blue and β-mercaptoethanol) and boiled for 5 minutes at 95°C to denature proteins.

2.8.2 Western blot

Samples were separated via electrophoresis on 6-12% gels (BioRad). Proteins were transferred onto PVDF membrane (activated with methanol and rehydrated with ddH_2O) using either semi-dry transfer method (Trans-Blot,

BioRad) or wet transfer (Criterion, BioRad). Membranes were blocked in 5% skimmed milk solution (Sigma) in PBS-T (0.05% Tween-20) or 5% BSA solution (Sigma) in TBS-T (0.1% Tween-20). Membranes were incubated in primary antibody at 4°C overnight (see **Table 2.8.2** for concentrations). The following day membranes were washed three times in PBS-T and incubated in secondary antibody for 1 hour at room temperature. Protein expression was detected using either Immobilon chemiluminescent HRP western blotting substrate (Millipore) or Pierce Enhanced chemiluminescence (ECL) western blotting substrate (Thermo Fisher) and developed onto chemiluminescent detection film or using Amersham Imaging ChemiDoc 600 (GE Healthcare). Band densitometry was calculated using either ImageJ software.

Table 2.8.2: Antibodies used throughout the thesis and dilutions required for western blotting.

Target	Supplier	Dilution	Target	Supplier	Dilution
HIF-1α	BD Trasnduction	1:500	**ACSS1**	Proteintech	1:1000
HIF-2α	Novus	1:500	**ACSS2**	Proteintech	1:1000
HIF-1β	Cell Signalling	1:500	**OGDH**	Proteintech	1:1000
CoAsy (mAb)	Abcam	1:1000	**PDHA1**	Abcam	1:1000
CoAsy (pAb)	Abcam	1:1000	**LIMD1**	Homemade	1:1500
β-actin	Sigma-aldrich	1:25,000	**GST**	Cell Signalling	1:1000
PHD2	Abcam	1:2000	**GFP**	Roche	1:2000
PD-L1	Cell signalling	1:1000	**HA**	Cell Signalling	1:1000
VHL	BD Transduction	1:1000	**CoA**	Homemade (Prof. Ivan Gout)	1:6000

2.8.3 Immunoprecipitation assays

Immunoprecipiration experiments were performed with the ImmunoCruz Optima IP Matrix system (Santa-Cruz biotech). IP matrix species was selected to correspond to the antibody used in IP. Tubes containing matrix were vortexed gently until homogenous bead slurry is formed before aliquoting 35 µL per reaction. Beads were re-suspended in a 500 µL of 2% BSA and 2 µg of primary antibody and left overnight at 4°C with gentle agitation. The following day beads were pelleted by centrifugation before being washed with RIPA lysis buffer. Input samples were taken from cleared lysate before adding the rest to IP

matrix. IP mixtures were incubated for 1 hour at room temperature with gentle agitation. Bead-IP-Protein complexes were pelleted by centrifugation before being washed 3x with RIPA lysis buffer. Complexes were eluted by boiling IP matrix in 35 µL of 5x protein sample buffer. Samples were analysed by western blot.

2.8.4 Immunohistochemistry

Staining of TMA was performed using Leica autostainer system and Novolink detection kit (Leica). Slides were heated to 60°C for 10 minutes to aid in section attachment to the slides before dewaxing and rehydrating on Leica autostainer (2 washes with Xylene, 3 washes with industrial methylated spirits and a final wash in water). Antigen was performed by boiling slides in citrate buffer (pH 6.0) for 15 minutes in microwave. Slides were blocked using peroxidase block and protein block as per manufacturers instructions before being stained with α-CoAsy pAb (ab155551) at a concentration of 1:75 for 1 hour at room temperature. Post primary, polymer, haematoxylin and DAB solutions were added as per manufacturers instructures before dehydrating and clearing slides using Leica autostainer. Slides were mounted on to coverslips with DPX before leaving to dry overnight prior to downstream analysis.

2.9 siKinome Screen

2.9.1 siKinome library

The screening library was the siGENOME protein kinases set from Dharmacon. This library includes 720 SMARTpool siRNA (4 siRNA sequences per target gene) targeting all known kinases, pseudokinases and proteins with predicted kinase activity. The library is supplied as 5 µL aliquots of 2 µM stock in the inner wells of a 96 well plate. The edge wells were filled with 5 µL of 2 µM siRNA targeting *HIF1A, HIF2A, PHD2* and scrambled control.

2.9.2 siKinome screen protocol

A549 HRE reporter cells were plated in an optimized cell density. After 24 hours cells were transfected with siRNA library in duplicate using INTERFERin (Polyplus) transfection reagent and optiMEM (Thermo Fisher) reduced serum media to a final concentration of 50 nM. The following day, siRNA-containing media was replaced with fresh complete media. One set of library-transfected cells was placed into hypoxia 48 hours after transfection. 18 hours later cells were removed from hypoxia and resazurin solution was added to a final concentration of 0.4 $mg.mL^{-1}$ to all transfected cells before incubating for 3 hours at 37°C and cell viability was assessed by measuring fluorescence using Wallac 1420 Multilabel counter plate reader at 560Ex/590Em. Cells were subsequently washed 3x with PBS prior to lysing in 25 µL passive lysis buffer (PLB, Promega), before freezing at -80°C. Luciferase activity was measured using Luciferase assay substrate (Promega) as per manufacturers instructions.

2.9.3 siKinome screen analysis

Luminescence values from luciferase activity were normalized to resazurin fluorescence values. Z-scores were calculated for each kinase, representing standard deviations from the mean, negative values represent knockdown of a positive regulator of HIF-activity or positive values represent knockdown of a negative regulator of HIF-activity. Z scores of ±2 were considered to be 'hits'.

2.10 Labelled glucose metabolomics sample preparation

For labelled glucose experiments, A549 cells were treated with siRNA at 40 nM with 5 technical replicates in duplicate plates. 24 hours later the media was replaced with fresh DMEM and one plate placed into hypoxia. The following day media was changed to 'heavy' glucose media (1X DMEM with 10 mM ^{13}C-Glucose (Cambridge isotopes) and 2 mM Glutamax). 24 hours following cells were washed with 0.9% NaCl before being place immediately on to dry ice to halt metabolism. Cells were scraped into 50:50 mix of 0.05% beta-hydroxytoluene (in methanol) and 1 µg.mL^{-1} d6-glutaric acid (in MilliQ filtered water). Samples were snap frozen and stored at -80°C prior to

2.11 FDA approved drug library screen

Prior to drug screen, tet-shRNA cells were treated with doxycycline at 25 ng.mL^{-1}. On day 0 cells were plated at optimum density before being left overnight to attach. The library contains 14 plates of drugs arrayed so that each well contains 2 µL of 10 mM solution in DMSO, this solution was dissolved in complete DMEM to achieve a final concentration of 200 µM. Control wells of DMSO alone and media alone were added to the surrounding wells on the

plate. On day 1 and 3, the culture medium on cells was moved and replaced with 95 µL of fresh medium (with doxycycline) before adding 5 µL of drug aliquot. On day 5 cell viability was measured using resazurin viability reagent as described previously. Fluorescence values were used to calculate modified Z-scores using the formula below:

$$Z\ score = X - \frac{Median\ (sample)}{MAD\ (sample)}$$

$$MAD\ (sample) = \ median_{\mathrm{i}}(|X_{\mathrm{i}} - median_{\mathrm{i}}(X_{\mathrm{i}})|)$$

Results Chapter One:

RNAi kinome screen identifies Coenzyme A synthase as a negative regulator of HIFs

3.1 Chapter aims

HIF transcriptional activity has been reported as a driver of tumourigenicity across multiple cancer types. Furthermore multiple regulators of HIFs have been identified that are mutated or deregulated in cancer, thereby driving tumour progression in a HIF dependent manner. We aim to identify novel regulators of HIF activity. We achieved this through development a reporter system that was screened with a library targeting the entire human kinome, followed by subsequent validation.

To summarise we sought to:

- ***Develop stable HIF-1 reporter cell line and validate isoform specificity***
- ***Optimise siRNA screen protocol to ensure result validity***
- ***Perform siRNA screen using siKinome library***
- ***Validate significant hits***

3.1.1 Generation of a stable HIF reporter cell line

In order to develop a robust screening platform, lung adenocarcinoma A549 cells were lentivirally transduced to stably express a construct expressing a synthetic HRE sequence (containing three canonical hypoxic responsive element motifs), promoting expression of a *firefly* luciferase and EGFP separated by a 2A cleavage site (**Fig 3.1.1**). The 2A cleavage site is a short peptide isolated from foot and mouth virus that allows for equimolar expression of two proteins from one promoter with minimal effect on protein function [193]. The construct was a kind gift from Dr. Tristan McKay, however Dr. Daniel Foxler added the Zeocin resistance gene to the vector by PCR amplifying the ZeoR gene from pcDNA4.1 vector with MluI restriction sites flanking gene promoter

and PolyA tail, before digesting and ligating into the vector. This vector allows for HIF activity to be measured, as upon HIF DNA binding to the HRE sequences this will initiate transcription and subsequent translation of *firefly* luciferase (that can be measured through addition of appropriate luciferin substrate) and enhanced green fluorescent protein (eGFP) (**Fig 3.1.1.1**).

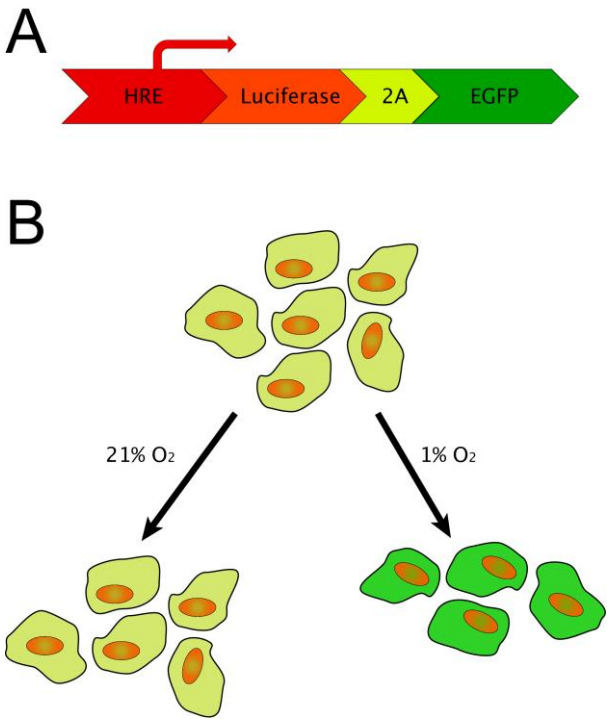

Figure 3.1.1.1: Hypoxic responsive element driven *firefly* luciferase reporter. **A**) Schematic of reporter construct with synthetic HRE driving expression of firefly luciferase and eGFP separated by 2A motif. **B**) Diagram of transduced cells upon hypoxic activation of HIFs. Cells will produce eGFP and firefly luciferase as a surrogate marker of HIF activity.

Following lentiviral transduction and selection for successful transgene incorporation with Zeocin, A549-HRE reporter cells were exposed to hypoxia across a time course before lysing, measuring luciferase activity and HIF-1α protein levels by western blot.

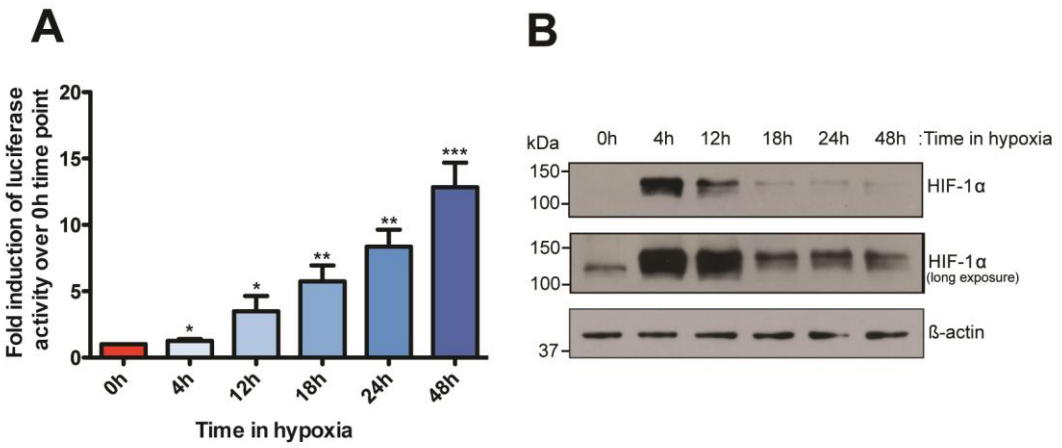

Figure 3.1.1.2: Hypoxic induction of A549-HRE cells. **A**) A549-HRE reporter cells were exposed to hypoxia before measuring firefly luciferase values. Results displayed are shown as fold induction over normoxia (n=3). **B**) Western blot analysis of HIF-1α protein in A549-HRE reporter cells over a hypoxic time course (representative image of n=3). Statistical analyses presented are student T-tests of indicated bar compared to 0 hour time point. * $p<0.05$, ** $p<0.01$, *** $p<0.001$

Figure 3.1.1.2 shows A549-HRE cells following hypoxic exposure (1% O_2) over a time course ending at 48 hours. HIF-1α transcriptional activity was measured using luciferase assay substrate (**Fig. 3.1.1.2A**) and normalized to total protein as measured by BCA assay; results are displayed as fold induction over cells at atmospheric oxygen (21%). HIF-1α protein levels were determined by western blot (**Fig. 3.1.1.2B**). This figure shows a steady increase of HIF-1α transcriptional activity over 48 hours and a clear hypoxic induction of *firefly* luciferase activity. One key observation is that the protein levels do not reflect transcriptional activity. HIF-1α protein is stabilized after 4 hours of hypoxia, whereas *firefly* luciferase activity remains low, it is unclear whether this is due to a delay in translation of *firefly* luciferase mRNA into protein or if further post-translational modifications of HIF are required for activity. Furthermore the luciferase will accumulate overtime resulting in larger activity at later time points. In order to determine a suitable time frame for performing the RNAi screen, it is important to consider a window where both positive and negative

regulators of HIF activity in hypoxia can be clearly identified. To this end, 18 hours was selected as an appropriate time point as there is a significant increase in luciferase activity over normoxic levels (5.7 fold increase) but not as high as 48 hours which could lead to false negatives.

In order to determine the HIFα isoform specificity, siRNA knockdown experiments were performed to determine which has an effect in reducing luciferase activity.

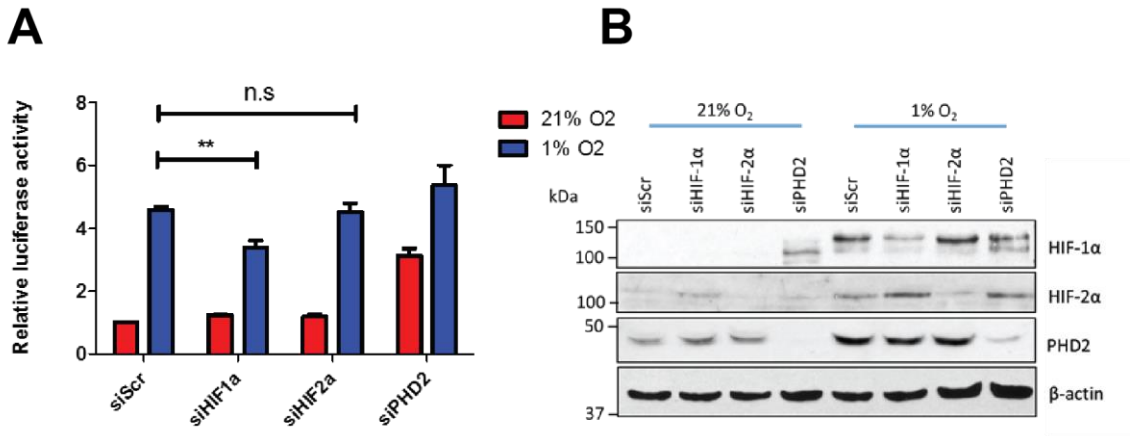

Figure 3.1.1.3: HIF isoform specificity of hypoxic responsive element. A) A549-HRE reporter cells were transfected with siRNA targeting HIF1A, HIF2A, PHD2 and Scrambled control at a concentration of 50 nM. Cells were exposed to hypoxia for 18 hours before lysis and downstream analysis. **B**) Western blot to confirm knockdown efficiency in A549-HRE cells. N=3 * p<0.05, ** p<0.01, *** p<0.001

Figure 3.1.1.3 shows that following partial knockdown of HIF-1α, there is a significant reduction in luciferase activity in hypoxia. However after treatment with siRNA against HIF-2α, there was no change in luciferase activity indicating that in A549 cells and at this time point. In normoxia there was no significant change in luciferase activity with siRNA against either *HIF1A* or *HIF2A*, this is to be expected, as HIFs will show minimal activity in normoxia. *PHD2* siRNA was included as a positive control; as expected, knockdown of PHD2 resulted

in a large increase in luciferase activity in normoxia that coincides with stabilization of HIF-1α protein. Taken together this data suggests that this is indeed a HIF-1α specific reporter and is sensitive to siRNA-induced changes in protein expression in both normoxia and hypoxia.

3.1.2 Optimisation of arrayed RNAi kinome screen

3.1.2.1 Optimisation of transfection reagent

Before performing RNAi screens it is important to select an appropriate transfection reagent, which is both effective and relatively non-toxic. To test this, Interferin and lipofectamine RNAi-Max transfection reagents were used to transfect water (mock transfection), non-targeting control siRNA and HIF-1α siRNA. Both transfection reagents showed reduction in luciferase activity following HIF-1α knockdown, but there was more cell death observed with cells transfected with lipofectamine, therefore interferin was used for RNAi screens.

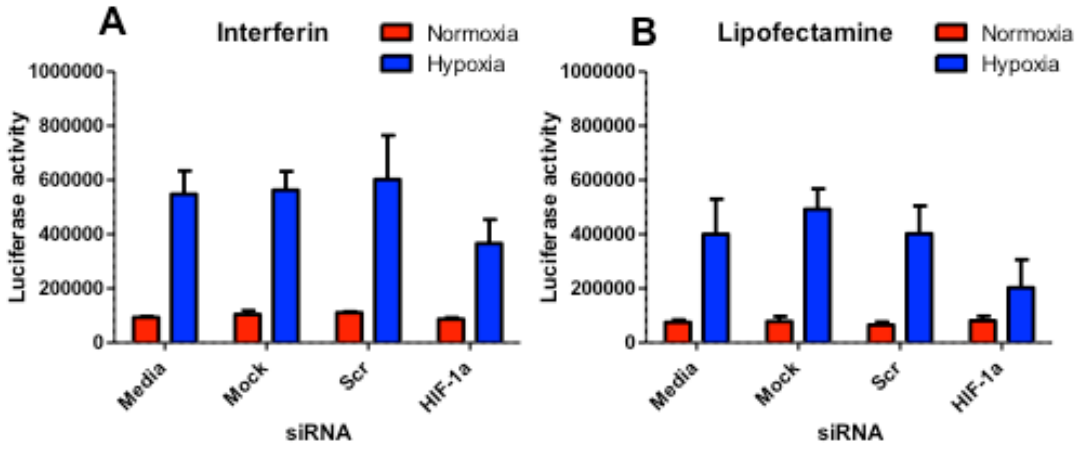

Figure 3.1.2.1: Optimisation of siRNA transfection reagent. Transfection reagent optimization. A549-HRE reporter cells were transfected with mock transfection (water), non-targeting siRNA, siRNA targeting HIF1A and media only with either interferin (**A**) or lipofectamine (**B**).

3.1.2.2 Optimisation of cell viability reagent

As the screening platform is based around a stable reporter cell line, it is crucial to normalize *firefly* luciferase activity to a certain parameter. False positives may arise from RNAi knock down of essential kinases, as cell death would also result in a reduction of luciferase activity. In order to differentiate true results from these false positives, *firefly* luciferase activity was normalized to cell viability. Cell viability was measured using resazurin solution. Resazurin is the active compound in commercially available methods of measuring cell viability, such as Alamar Blue. Resazurin is a weakly fluorescent blue dye that is irreversibly reduced by viable cells to form a highly fluorescent compound called resorufin. In order to determine the correct concentration of resazurin to use, a titration of cell number was prepared and treated with two doses. Both doses showed strong positive linear correlations (**Fig. 3.1.2.2A**), but treatment of cells with 0.4 $mg.mL^{-1}$ displayed a stronger correlation (R^2 = 0.9918) than that observed with 1.0 $mg.mL^{-1}$ treated cells (R^2 = 0.9724). This method was compared with the commercially available alternative, Cell-titer Fluor (**Fig. 3.1.2.2B**). Once again, resazurin showed a strong positive correlation (R^2 = 0.9803) as did Cell-titer Fluor (R^2 = 0.9735); however in this assay, resazurin displayed a larger range of activity compared to cell-titer fluor (125,000 cells per well compared to 62,500 cells per well respectively). These results indicate that resazurin solution is a suitable method of determining cell viability.

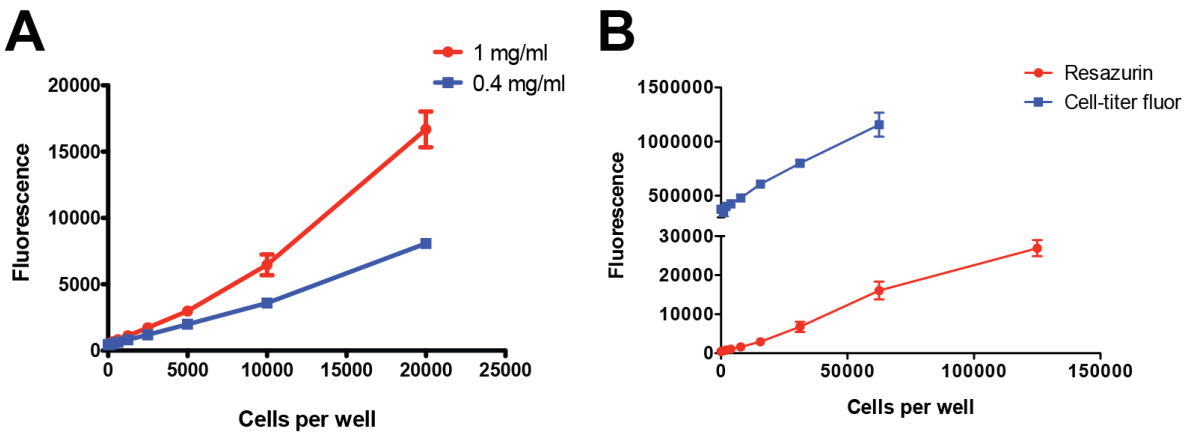

Figure 3.1.2.2: Optimization of cell viability reagent. Optimization of Resazurin solution as a measure of cell viability. **A**) A549 reporter cells were plated out across a wide range of cell densities before incubating with Resazurin solution at either 1 mg/mL or 0.4 mg/mL and incubating for 3 hours at 37°C and measuring fluorescence. **B**) Resazurin solution was compared with Cell-titer Fluor cell viability reagent.

3.1.3 Primary siRNA kinome screen

The A549-HRE reporter cell line was for regulators of HIF1 transcriptional activity with an arrayed siRNA library targeting all known kinases, pseudo-kinases and proteins with predicted kinase activity. The library used was the siGENOME library from Dharmacon, which contains SMARTpool siRNA (4 distinct sequences per kinase mixed in a single well). The edge wells of the plate were lined with siRNA against *HIF1A*, *HIF2A*, *PHD2* and a scrambled control to act as positive and negative controls for the reporter construct. Z-scores were calculated for each well and hits were identified by selecting those with Z-scores ± 2.

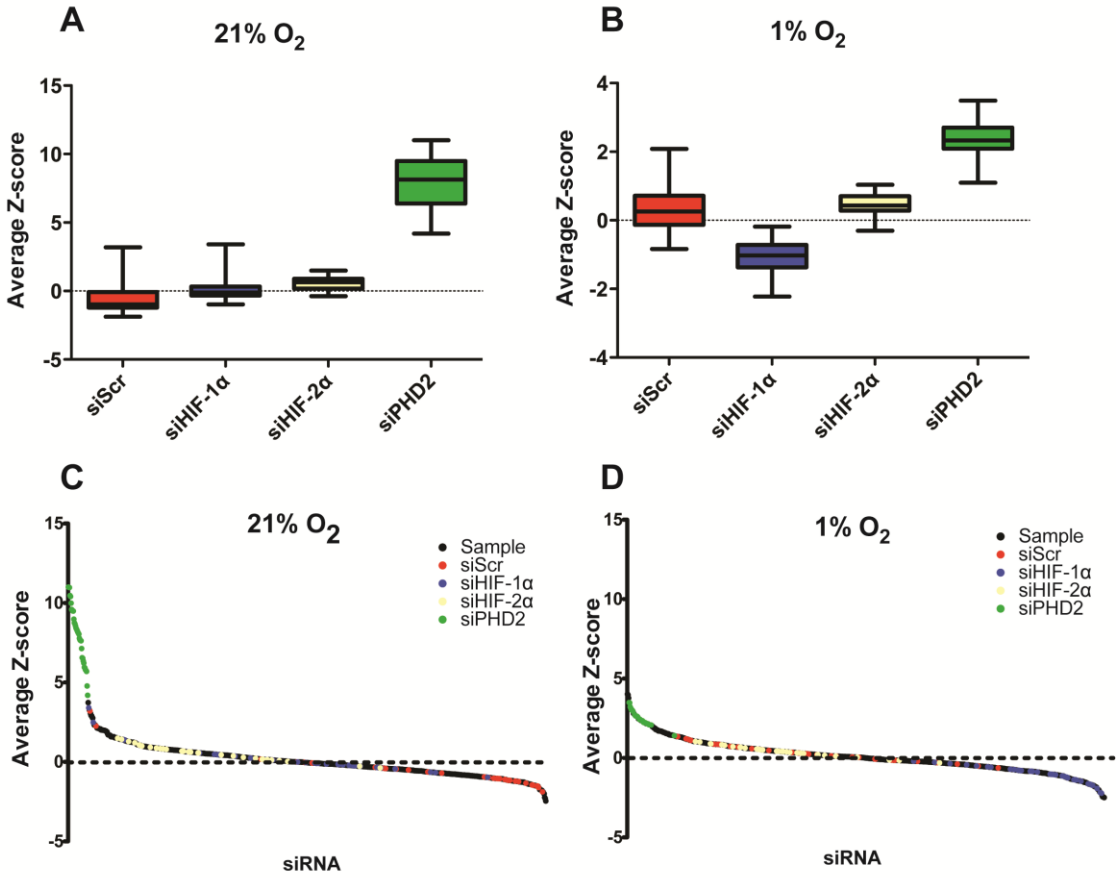

Figure 3.1.3.1: Primary siKinome screen for HIF transcriptional activity. A-B) The control siRNA added to each plate for the hypoxia screen in both normoxia (**A**) and hypoxia (**B**). **C-D**) Waterfall plots of siRNA kinome screen in both normoxia (**C**) and hypoxia (**D**), each dot represents an individual kinase. Cells were tranfected with siRNA at a final concentration of 50 nM n=2.

The controls from the screen show an increase in HIF transcriptional activity following knockdown of PHD2 compared to non-targeting control in normoxia, this is likely due to stabilization of HIFα protein (**Fig. 3.1.3.1A**). In hypoxia, transfection of HIF1A siRNA decreased HIF transcriptional activity compared to non-targeting control; this reduction was not observed following HIF2A (**Fig. 3.1.3.1B**). The controls match previous results, thereby suggesting that the screen results can be considered valid and robust. Z-scores of ± 2 were selected as a cut off point to identify hits from the primary screen, with Z-scores over 2 representing a potential negative regulator of HIF activity and below 2

as a potential positive regulator of HIF activity. In total the screen identified a total of 45 hits, with 34 potential negative regulators of HIF activity and 11 potential positive regulators of HIF activity (**Fig. 3.1.3.1C-D**). Of these hits a few previously identified regulators of HIFs were identified such as CDK1 and LATS2 [166, 171], this further suggests that the screen is valid. In order to determine if any kinase pathways were identified in the screen, STRING analysis was performed [194]. Through this analysis a few common pathways were identified, including the TGF-β pathway (*ACVR2A, ACVR2B* and *TGFBR3*) (**Fig. 3.1.3.2**).

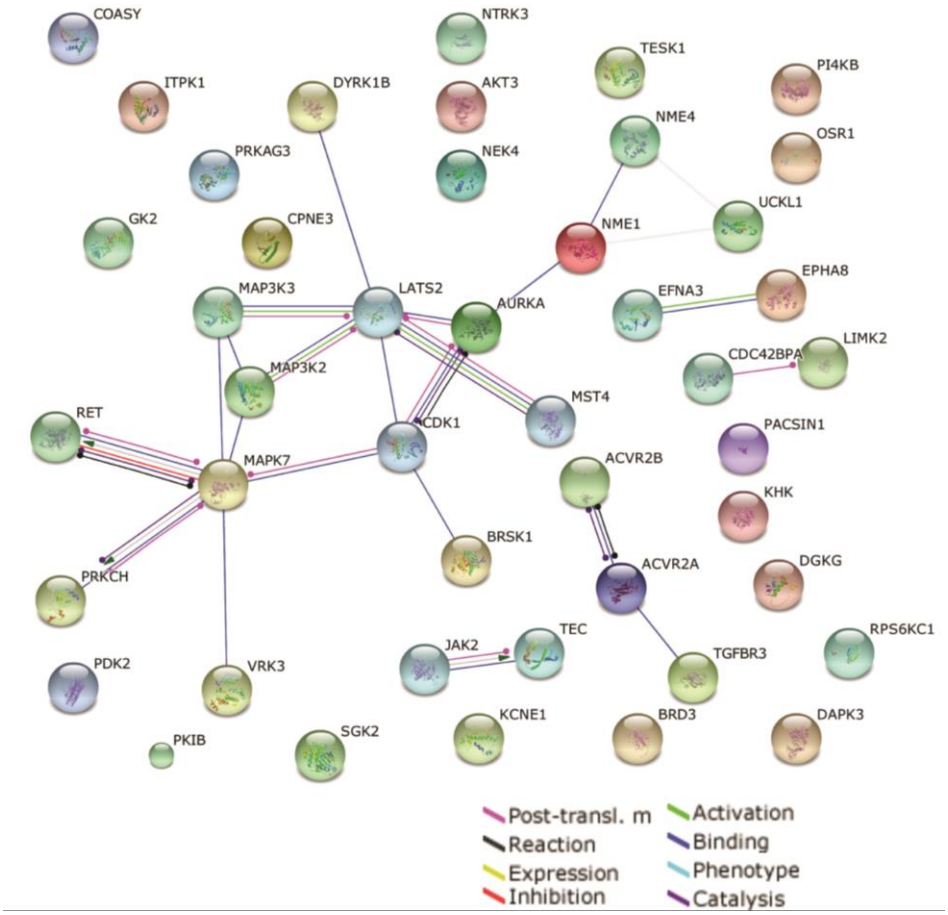

Figure 3.1.3.2: String network of all the hits from primary siKinome screen.
String analysis shows interaction of proteins based upon published literature, type of interaction highlighted in legend below.

3.1.4 Secondary validation siRNA screen

A secondary validation screen was performed, targeting the 45 hits identified in the primary screen. The secondary screen was performed using an arrayed siRNA plate from Dharmacon (ON-TARGETplus cherry picked library) with SMARTpool siRNA as used in the primary screen. The screen was performed in both normoxia (21% O_2) and hypoxia (1% O_2); firefly luciferase activity was normalized to cell viability as before. Results are displayed as fold change over non-targeting control siRNA.

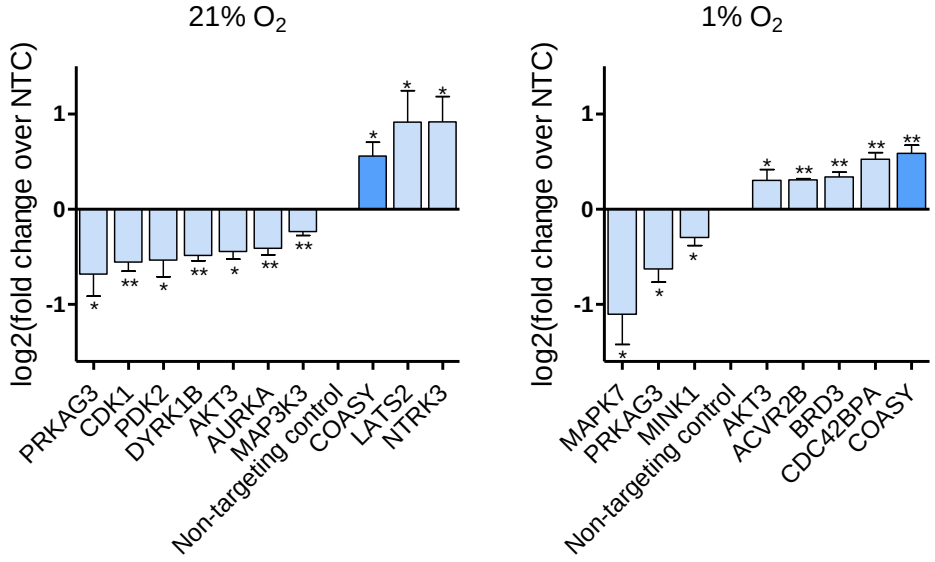

Figure 3.1.4: Significant hits from secondary screen. A549 reporter cells were transfected with siRNA targeting all previous hits from primary screen at final concentration of 50 nM. 48 hours later cells were either left in normoxia (A) or placed in hypoxia (B) for 18 hours. Only hits that were statistically significantly different from non-targeting control siRNA were included. Statistical analyses presented are student T-tests of indicated bar Non-targeting control siRNA. N=3. * $p<0.05$, ** $p<0.01$, *** $p<0.001$

The results indicate that of these 45 hits, 9 kinases significantly influenced HIF1 transcriptional activity in normoxia and 8 influenced transcriptional activity in hypoxia (**Fig. 3.1.4**). Of the previously reported hits identified in the primary

screen, knockdown of MAPK7 and CDK1 still showed significant reduction of HIF transcriptional activity in the secondary screen, which suggests that the screen is valid. Amongst these hits, some are regulators in both normoxia and hypoxia, such as COASY. COASY was identified as a negative regulator of HIF transcriptional activity and MAP3K3 and PRKAG3 as positive regulators. Many of the hits were novel and had not previously been reported as a regulator of HIF activity. One such hit/protein was CoAsy, which negatively regulates HIF activity in both normoxia and hypoxia. Due to no previous publications linking CoAsy and HIF signalling, and the fact that loss of CoAsy increased HIF-1 activity irrespective of oxygen tension, it was decided to further investigate how CoAsy may regulate HIF.

3.1.5 Coenzyme A synthase (CoAsy)

Coenzyme A synthase (CoAsy) is a bifunctional enzyme that catalyzes the final two steps of Coenzyme A (CoA) biosynthesis from pantothenate (Vitamin B5) [195]. CoAsy contains two functional domains, dephospho-CoA Kinase domain (DPCK) and phosphopantetheine adenyltransferase domain (PPAT). The PPAT domain transfers an AMP moiety to 4'phosphopantetheine prior to phosphorylation at the 3'hydroxyl position on dephospho-CoA yielding mature CoA. This pathway is conserved from prokaryotes through to humans, however in prokaryotes the PPAT and DPCK enzymes are separate, in addition to this the PPAT domain in CoAsy does not have significant sequence homology with the prokaryote counterpart, which makes it an interesting anti-bacterial drug target. Coenzyme A itself is not membrane permeable, however intermediates in the pathway are, such as 4'phosphopantetheine [196]. Germline mutations

in *COASY* have been associated with a form neurodegeneration with brain iron accumulation (NBIA) called CoPan [197], other NBIA diseases have been associated with mutations in the CoA biosynthetic pathway such as PKAN (mutations in *PANK2* gene) [198]. CoAsy is found anchored into the outer mitochondrial membrane facing into the cytoplasm; deletion of the amino acid residues 1-29 in CoAsy removes the mitochondrial localization and distributes CoAsy throughout the cytoplasm [199].

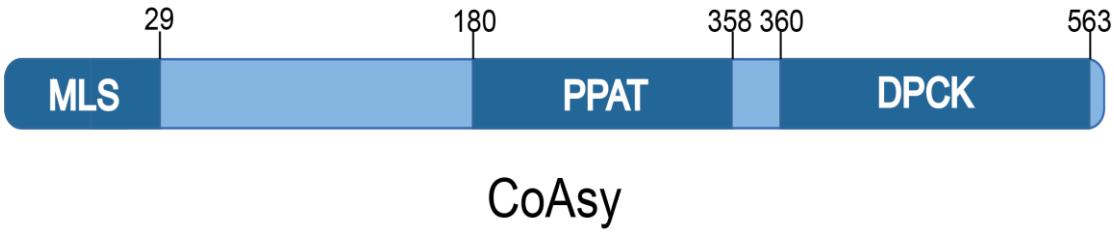

Figure 3.1.5: Schematic of CoAsy protein. Schematic of CoAsy protein with the functional domains highlighted. MLS = Mitochondria localization sequence, PPAT = phosphopantetheine adenyltransferase and DPCK = Dephospho-CoA kinase

3.1.6 Validation of CoAsy as a novel regulator of HIFs

3.1.6.1 siRNA knockdown of CoAsy

The previous screens have all been performed with SMARTpool siRNA, this contains 4 distinct sequences targeting each gene that ensures efficient knockdown, making it very effective for screening purposes, however there is an increased risk of off target effects and results could potentially be due to off target effects. To address this, knockdown experiments were performed with a different siRNA from a different supplier and a distinct sequence to those used in the SMARTpool siRNA (**Table 3.1.6.1**).

Table 3.1.6.1: siRNA sequences against CoAsy

siRNA	Supplier	Sequence
siGenome_CoAsy1	Dharmacon	GAACAGAUAUUCUCCAUAA
siGenome_CoAsy2	Dharmacon	GGCAGAACCUGGUCCAUGA
siGenome_CoAsy3	Dharmacon	GGCAGCAGCUUGUGGAACA
siGenome_CoAsy4	Dharmacon	AGAAGCAGCUGAAGAUACU
Mission siRNA CoAsy	Sigma-Aldrich	UGGAGUCUGUAUGUCUCUUAC

Knockdown experiments were performed in a number of cell lines (A549, U2OS, HEK293T and T47D). As a positive control, siPHD2 was included in experiments, as loss of PHD2 will result in decreased HIF degradation and stabilised protein. For these experiments cells were placed into hypoxia for 4 or 8 hours or cultured at atmospheric oxygen.

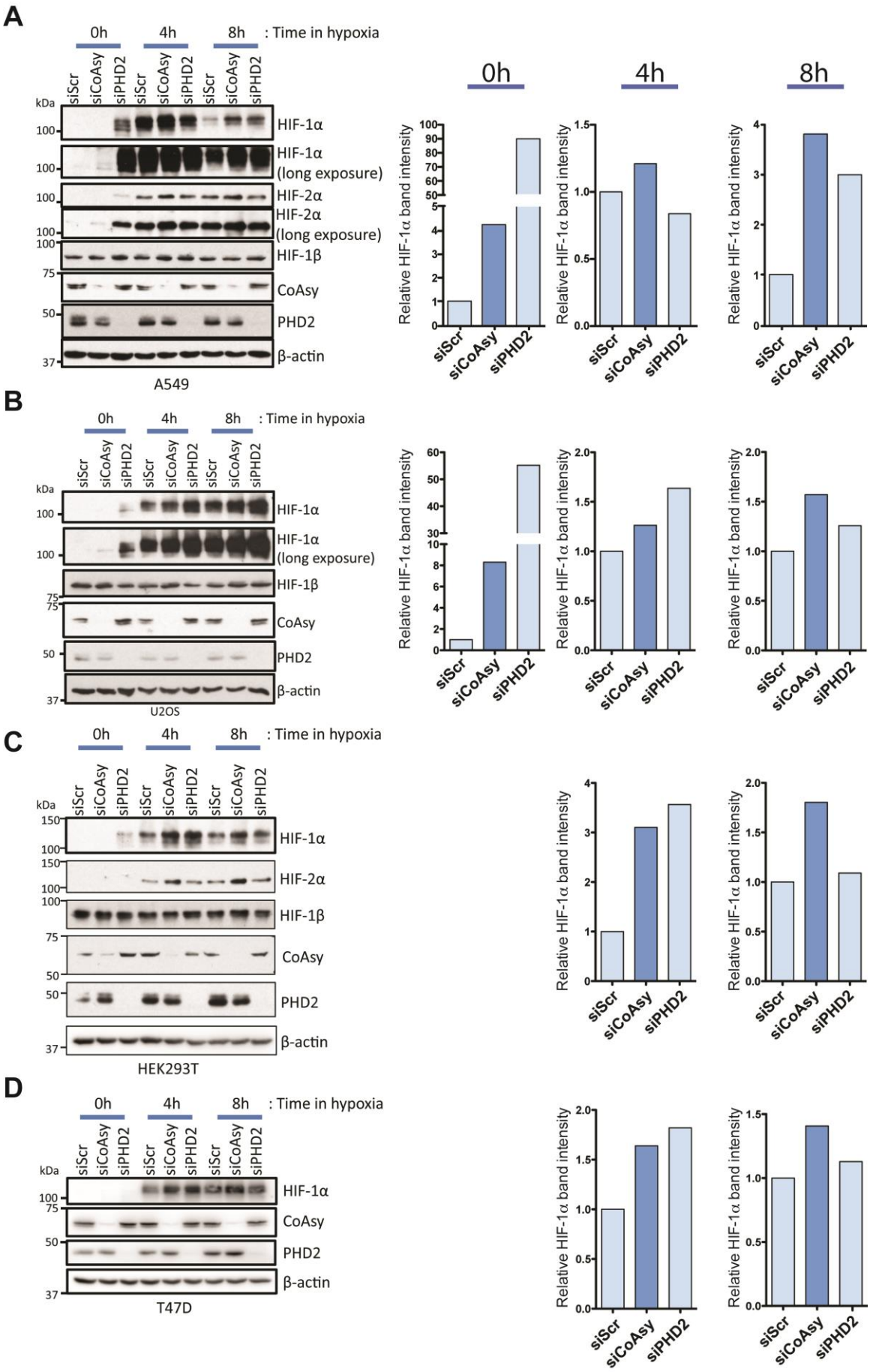
A
0h
4h
8h
: Time in hypoxia
siScr
siCoAsy
siPHD2
kDa
HIF-1α
HIF-1α (long exposure)
HIF-2α
HIF-2α (long exposure)
HIF-1β
CoAsy
PHD2
β-actin
A549
Relative HIF-1α band intensity
B
U2OS
C
HEK293T
D
T47D

Figure 3.1.6.1: Knockdown of CoAsy results in stabilized HIFα protein. Knockdown of CoAsy results in stabilized HIFα in multiple cell types. A549 (**A**), U2OS (**B**), HEK293T (**C**) and T47D (**D**) were treated with siRNA against *COASY*, *PHD2* and non-targeting control at 40 nM for 72 hours. Cells were exposed to 1% O_2 for 0, 4 or 8 hours before lysis and analysis by western blot. Relative HIF-1α band densitometry of indicated blot was calculated and plotted on bar chart. A549 n=4, U2OS n=3, HEK293T n=3 and T47D n = 2.

Figure **3.1.6.1** shows that A549, U2OS, HEK293T and T47D cells each show an increase in HIF-1α protein levels following siRNA mediated knockdown of CoAsy. In A549 and U2OS, longer exposures of the membrane stained with anti-HIF-1α antibody shows an increase in HIF-1α protein in normoxia as well as after 4 hours and 8 hours of 1% O_2. Whilst there is an increase in HIF-1α in normoxia, it is not as large as observed following knockdown of PHD2. HEK293T and A549 lysates were probed for HIF-2α protein. In these lysates there was an increase in HIF-2α protein following knockdown of CoAsy at both 4 hours and 8 hours of hypoxia. In A549 cells we also observed an increase in HIF-2α protein in normoxia, whereas HEK293T no HIF-2α was observed in normoxia, even following knockdown of PHD2. In T47D cells, there was no HIF-1α protein detected in normoxia, apart from a feint band following loss of PHD2, it is unclear why this is occurring in this cell line however it suggests that the O_2 dependent turnover of HIF-1α is highly efficient in this cell line and less dependent on PHD2 as other cell line such as A549. As there is an increase in HIFα protein across a number of different cell types (A549 are lung adenocarcinoma, U2OS are osteosarcoma, T47D are Luminal A breast cancer and HEK293T are transformed embryonic kidney cells) it suggests that this mechanism is not restricted to only lung adenocarcinoma and instead, a fundamental mechanism across transformed cell types. It is important to note

that there was no significant change in HIF-1β expression following loss of CoAsy in any of the cell lines tested, suggesting that this effect is HIFα specific.

3.1.6.2 Cloning of pLKO-tet-shRNA vector to target CoAsy

In order to perform further knockdown experiments targeting CoAsy, the pLKO-tet-Puro vector (Addgene number = 21915) was purchased and sequences yielding shRNA hairpins targeting CoAsy or a non-targeting control were inserted, such that shRNA hairpins were expressed upon tetracycline treatment. To identify suitable sequences for the constructs, sequences from MISSION shRNA (Sigma Aldrich) were used, specifically a shRNA sequence targeting the 5' UTR of CoAsy mRNA was selected as this will allow future re-expression experiments with CoAsy cDNA constructs (**Fig. 3.1.6.2**), furthermore this siRNA sequence was distinct from those found in the SmartPOOL siRNA or individual mission siRNA.

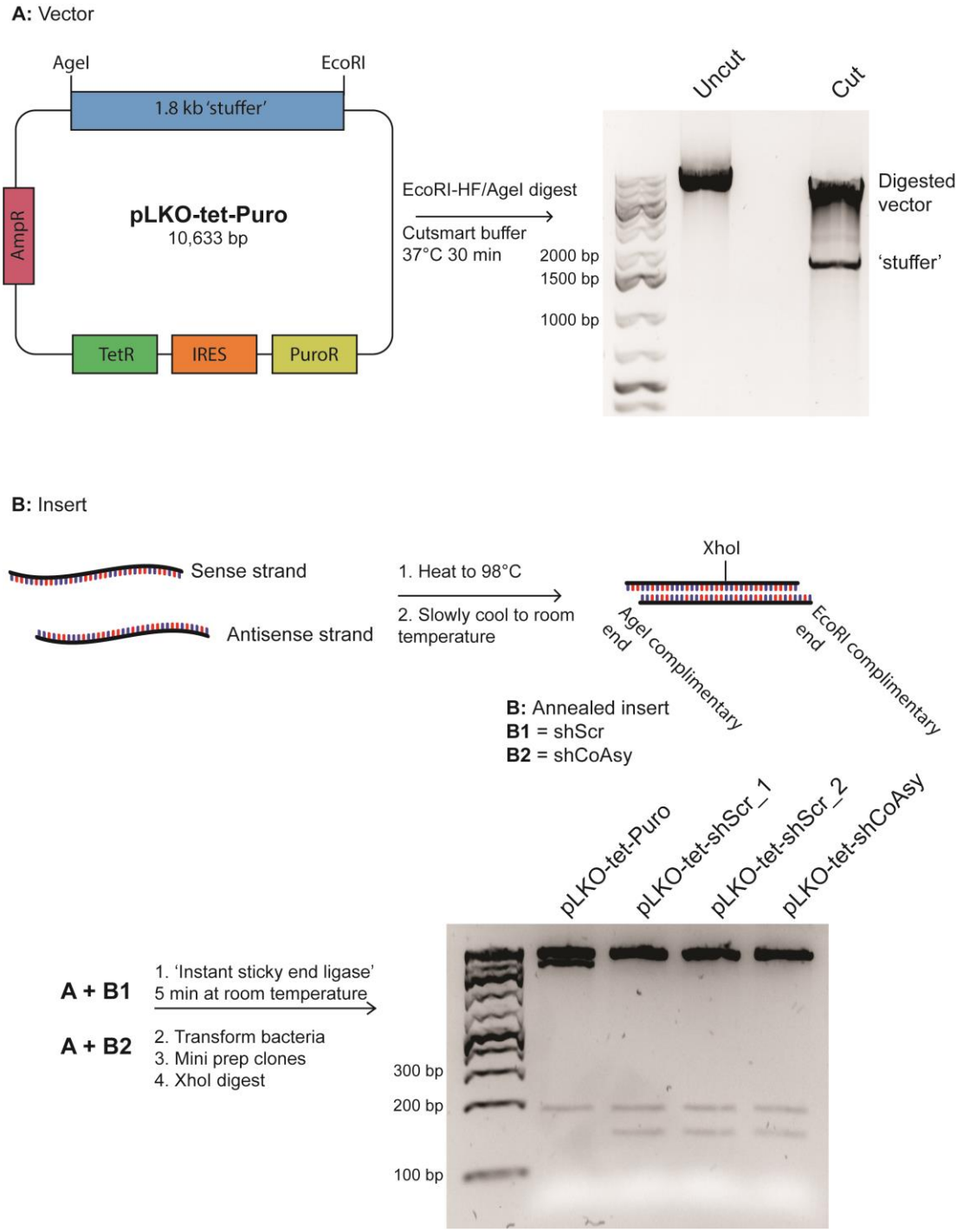

Figure 3.1.6.2: Cloning of inducbile shRNA vector. The pLKO-tet-Puro was digested with AgeI and EcoRI-HF prior to ligating with annealed shRNA insert strands. Ligation was confirmed with XhoI digest and sequence verified by Sanger sequencing (Source Bioscience).

3.1.6.3 Validation and optimisation of tetracycline inducible shRNA knockdown of CoAsy

In order to activate the TetR transgene and shRNA expression, Doxycycline was used instead of tetracycline due to increased stability in cell culture medium. Prior to performing experiments with doxycycline inducible shRNA lines it is important to determine an appropriate concentration to use to ensure that a suitable degree of mRNA knockdown is achieved with the minimal amount of doxycycline, this is crucial as excess doxycycline has been reported to induce changes in cellular metabolism and proliferation and may lead to incorrect interpretation of results [200].

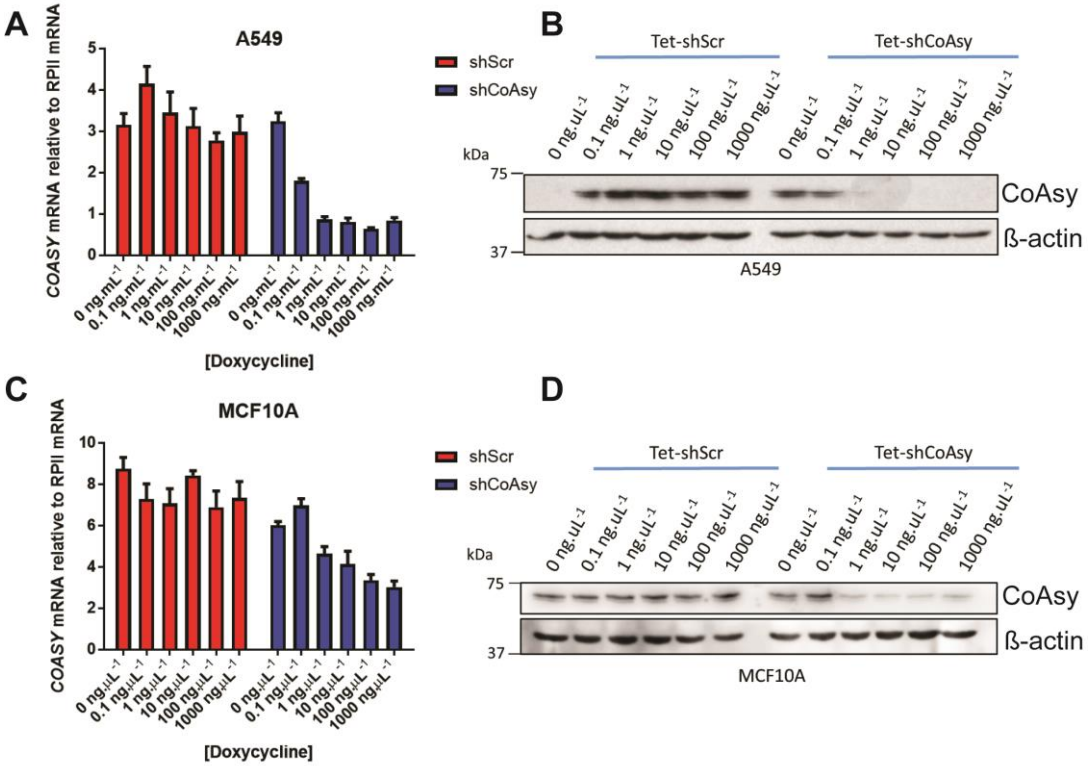

Figure 3.1.6.3: Validation of tet-shRNA system. Validation of inducible shRNA system in A549 (**A-B**) and MCF10A (**C-D**) cell lines. Inducible shRNA lines were treated with doxycycline or vehicle only for 48 hours prior to lysis and analysis by qRT-PCR (**A-C**) and western blot (**B-D**). n=1.

A549, T47D and the normal breast cell line MCF10A were transduced with lentivirus containing constructs made in **3.1.6.2** as described in **section 2.6**. In order to determine the correct concentration of doxycycline to use cells were treated with a serial dilution of doxycycline (ranging from 0.1-1000 $ng.mL^{-1}$) for 48 hours prior to cell lysis and analysis by western blot and qRT-PCR. For each cell line addition of doxycycline had no strong effect on CoAsy protein or RNA expression in the shScr line. In the shCoAsy lines addition of doxycycline induced knockdown of CoAsy RNA and protein across a broad range of doses. Western blot analysis shows that protein knockdown is achieved at concentrations at the bottom dose of 0.1 $ng.mL^{-1}$ in A549 cell line and 1 $ng.mL^{-1}$ in MCF10A cell line; however both cell lines showed maximum protein knockdown at this dose of 1 $ng.mL^{-1}$. CoAsy mRNA expression matched protein expression as 0.1 $ng.mL^{-1}$ of doxycycline decreased CoAsy expression by 44% in the A549 cells. Treatment with doses of 1 $ng.mL^{-1}$ or higher achieved a maximum decrease in CoAsy mRNA of 73%. Future experiments were performed at a concentration of 25 $ng.mL^{-1}$; this concentration was selected as it will achieve a high degree of knockdown and is below doses that have been previously reported to alter cellular metabolism and proliferation [200].

3.1.6.4 shRNA mediated knockdown of CoAsy stabilizes HIFα protein

To test whether CoAsy knockdown had the same effect of stabilising HIF-1α protein the A549 and T47D tet-shRNA lines were pretreated with doxycycline (25 $ng.mL^{-1}$) to induce gene silencing before being exposed to hypoxia for 4 and 8 hours. As the inducible shRNA system uses siRNA sequences distinct

from the mission siRNA, it will further support that the stabilization of HIF-1α is an on-target effect of CoAsy knockdown instead of an off target effect.

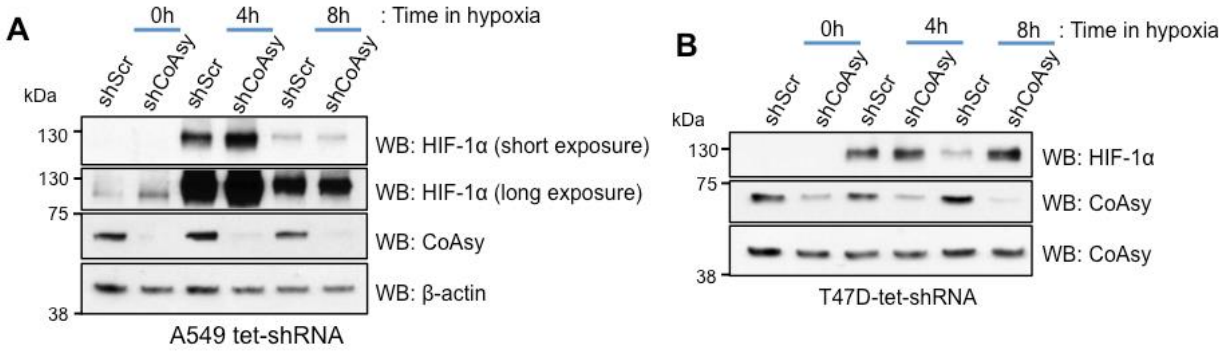

Figure 3.1.6.4: shRNA mediated knockdown of CoAsy results in stabilized HIF-1α. Knockdown of CoAsy using inducible shRNA system in A549 (**A**) and T47D (**B**) cells. Tet-shRNA inducible lines were plated before being treated with 25 $ng.mL^{-1}$ doxycycline for 72 hours. Cells were exposed to hypoxia for 0, 4 or 8 hours hypoxia before cell lysis and analysis by western blot. Representative blot from A549 (n = 3) and T47D (n = 2).

Knockdown of CoAsy in A549 cells resulted in stabilized HIF-1α at both 21% O_2 and following 4 hours of 1% O_2 (**Fig. 3.1.6.4A**). Interestingly no stabilization was observed at 8 hours of hypoxia, however this result was inconsistent as other biological replicates showed a degree of stabilization at this time point (See appendix). There was a large decrease in HIF-1α protein expression between 4 and 8 hours of hypoxia for the A549 cell line, this is likely due to the adaptive response that occurs following exposure to hypoxia, where a negative feedback loop induces expression of proteins such as PHD2 and LIMD1 that negatively regulate HIF-1α expression. For the T47D cell line (**Fig. 3.1.6.4B**) there was no HIF-1α protein observed even after long exposures for the western blot. However at 8 hours there was a clear stabilization of HIF-1α following loss of CoAsy.

3.1.6.5 Loss of CoAsy does not alter *HIF1A* or *HIF2A* mRNA expression but upregulates a subset of HIF target genes

So far results have indicated that loss of CoAsy upregulates HIF-1 activity in both normoxia and hypoxia using a synthetic reporter system and that loss of CoAsy results in increased protein levels in multiple cell lines. However it is important to test whether this increased HIF is active across a number of HIF target genes. HIF activity requires a number of co-activators that help dictate function such as CBP/P300. Furthermore HIF activity is further regulated by FIH mediated hydroxylation, as this hydroxylation event occurs at the C-terminus there are a number of target genes that are affected by this and a subset that are insensitive to FIH inhibition. As it is unclear how CoAsy regulates HIF, analysis of target genes may provide clues as to FIH functionality. In addition to HIF target genes, analysis of *HIF1A* and *HIF2A* mRNA can determine whether loss of CoAsy is upregulating HIF protein at the transcriptional stage or whether this is occurring post-transcriptionally. This is an important clue in determining how CoAsy regulates HIF and can help dictate future experiments. In order to address these points, A549 tet-shRNA lines were treated with doxycycline for 72 hours before exposing to hypoxia for 0, 4 and 8 hours prior to cell lysis, RNA extraction and analysis by qRT-PCR.

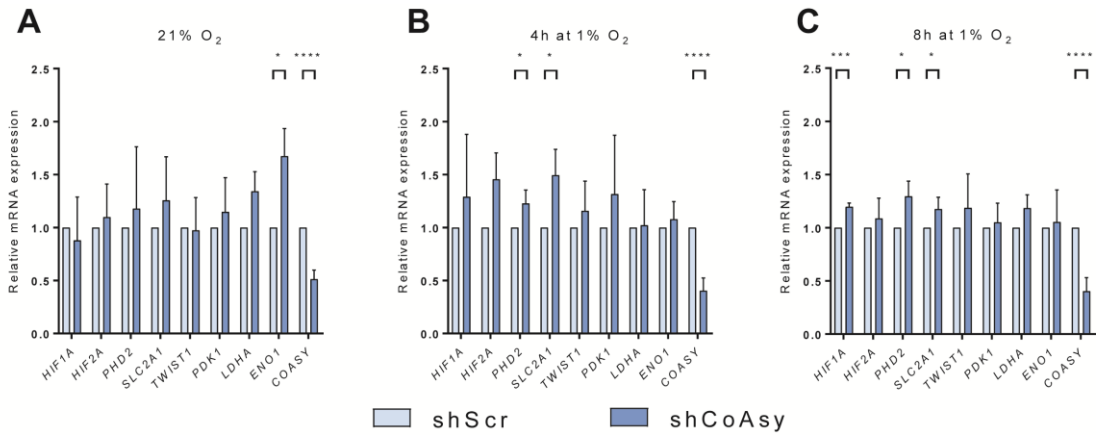

Figure 3.1.6.5: Analysis of HIF target gene expression in A549-tet-shRNA cell lines. qRT-PCR analysis of HIF target genes and *HIF1A* and *HIF2A* mRNA levels. A549 cells were treated with doxycycline (25 ng.mL-1) for 72 hours before being placed in hypoxia for 0 (**A**), 4 (**B**) or 8 (**C**) hours before cell lysis and analysis by qRT-PCR. Results are mean ± SD. n=4. Statistical tests are multiple T-tests with Holm-Sidak method. * $p < 0.05$, ** $p < 0.01$, *** $p < 0.001$, **** $p < 0.0001$

Figure 3.1.6.5 shows the qRT-PCR data from the knockdown experiments in the A549-tet-shRNA lines. Across each time point there was a significant reduction of *COASY* mRNA, indicating the shRNA system was working and achieving high levels of knockdown. At 0 and 4 hours of hypoxia there was no significant difference in either *HIF1A* or *HIF2A* mRNA. After 8 hours of hypoxia there was a significant increase in *HIF1A* mRNA but not *HIF2A* mRNA. As only the 8 hour time point displayed a significant increase in *HIF1A* mRNA level, it is unlikely that the increase in HIF-1α protein is a direct result of increased mRNA expression, especially as increased HIF protein expression is observed at 0 and 4 hours of hypoxia (section **3.1.6.4**). Furthermore knockdown experiments with mission siRNA have shown that HIF-2α protein also increases and there was no significant increase in *HIF2A* mRNA, therefore this suggests that the stabilization of protein observed is occurring post-transcriptionally. The increase in *HIF1A* mRNA could be explained by positive feedback mechanisms, such as through NFκB p65 [201]. In normoxia (21% O_2, **Fig.**

3.1.6.5A) the only HIF target gene that was statistically different following loss of CoAsy is *ENO1*. Other target genes did show increase in expression, however due to large variations in biological replicates there was no statistical significance (see appendix for alternative graphical representation). Following exposure to hypoxia, *ENO1* no longer showed a significant increase in expression following loss of CoAsy. However both *PHD2* and *SLC2A1* did show a significant increase (**Fig. 3.1.6.5B-C**). Once again other target genes also showed increased expression, however due to large variations between the biological replicates, were not statistically significant. This datum shows that there is a small increase in HIF target gene expression, however due to large variations in results it is unclear as to the extent and biological significance of these differences.

3.1.7 Summary

This chapter sought to identify novel regulators of HIF transcriptional activity. Through a siRNA screen targeting the human kinome and secondary validation screen, the Coenzyme A biosynthesis enzyme CoAsy was highlighted as a novel negative regulator of HIF transcriptional activity. Knockdown experiments with siRNA and shRNA, each with distinct target sequences to those used in the primary screen, showed that knockdown of CoAsy resulted in increased HIF-1α and HIF-2α protein expression with no change in HIF-1β. Analysis of *HIF1A* and *HIF2A* mRNA showed there was no increase in expression suggesting that this change is due to post-transcriptional events occurring following loss of CoAsy. In the A549 inducible shRNA cell line there was a significant increase in a small subset of the HIF target genes tested, however

further experiments are required to confirm to what extent HIF activity is affected and additional cell lines should be tested.

Results Chapter Two:

Elucidating the mechanism and functionality of CoAsy-mediated HIF regulation

4.1 Chapter aims

In the previous chapter we identified Coenzyme A synthase (CoAsy) as a novel negative regulator of HIF-1 transcriptional activity and a negative regulator of both HIF-1α and HIF-2α protein levels, but had no effect on *HIF1A* or *HIF2A* mRNA expression. However it was unclear as to the mechanism behind this stabilization, addressing this is the first aim of this chapter. Secondly, we will determine the consequences of loss of CoAsy in cellular transformation. The role of HIFs in driving cancer has been characterized in multiple cancer types; therefore it stands to reason that the upregulation of HIF following loss of CoAsy may increase cellular transformation and aggressiveness.

To summarise, we aim to:

- ***Determine the mechanism behind the upregulation of HIF protein following loss of CoAsy***
- ***Assess changes in cellular transformation in vitro following loss of CoAsy***

4.2.1 Cloning of CoAsy-EGFP

The previous chapter identified CoAsy as a negative regulator of HIFs through a siRNA screen. Subsequent validation experiments were performed also with RNAi techniques for knockdown of mRNA and consequently protein. We therefore asked if the converse may also be true, if CoAsy is overexpressed then HIFα protein levels may decrease as our hypothesis would predict. To test this an overexpression vector with fluorescently tagged CoAsy was made.

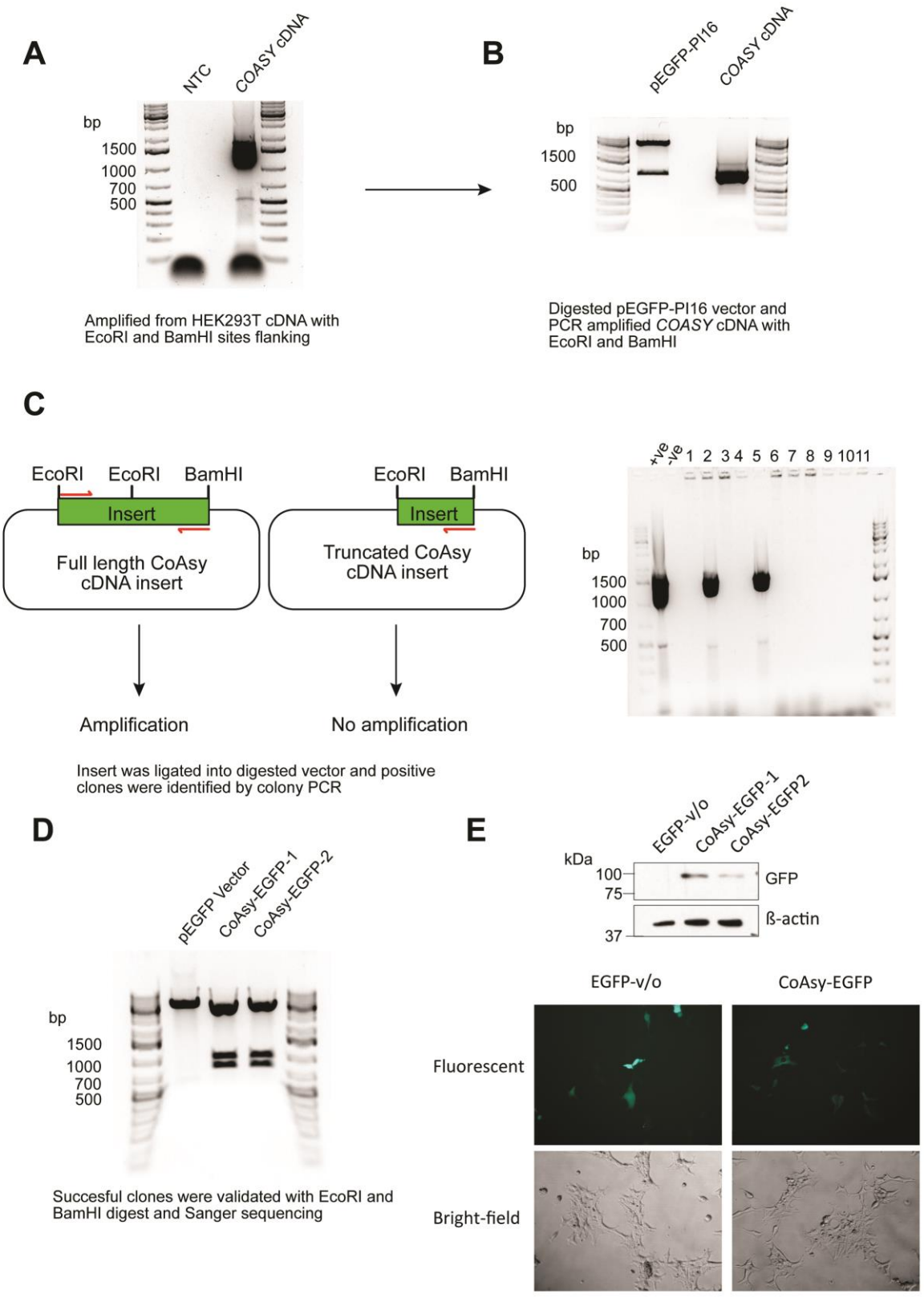

Figure 4.2.1: Cloning of CoAsy-EGFP. Cloning strategy to make CoAsy-EGFP over expression vector. CoAsy CDS was amplified from HEK293T cDNA (**A**) with the introduction of EcoRI and BamHI restriction sites and ligated into pEGFP-C1 vector (**B**). Successful cloning was confirmed by colony PCR (**C**) restriction digest (**D**), Sanger sequencing, western blotting and fluorescent microscopy (**E**).

To construct the CoAsy expression vector, the coding sequence of *COASY* was amplified from HEK293T cDNA with primers designed to add EcoRI and BamHI restriction sites to the 5' and 3' ends respectively (**Fig. 4.2.1A**). Both the PCR product and vector containing PI16-EGFP (an unrelated protein that was cloned in using the same restriction sites) were digested with EcoRI and BamHI before performing ligation (**Fig. 4.2.1B**). As the CDS for *COASY* contains an internal EcoRI site there are two potential products from the ligation. Either the full length CoAsy CDS insert or a truncated form, lacking the 5' half of the insert. To screen for successful insertion of the full length CoAsy cDNA, a colony PCR was performed. This technique utilizes PCR to selectively amplify only the full-length insert with no amplification observed in clones featuring the truncated insertion; the full length PCR product was used as a positive control for the reaction (**Fig. 4.2.1C**). Through this approach two positive clones were identified. Successful ligation was confirmed through EcoRI and BamHI digest and Sanger sequencing (**Fig. 4.2.1D**). HEK293T cells were transfected with plasmid and protein expression was confirmed by western blot and fluorescent microscopy (**Fig. 4.2.1E**).

4.2.2 Overexpression of CoAsy-EGFP does not affect HIF-1α protein levels but overexpression of Pank1β negatively regulates HIFα protein levels

To assess if overexpression of CoAsy can reduce HIFα protein levels as our hypothesis would predict, HEK293T cells were transfected with EGFP-vector only and CoAsy-EGFP before being exposed to 1% O_2 for 0, 4 and 8 hours prior to cell lysis and analysis of protein expression by western blot.

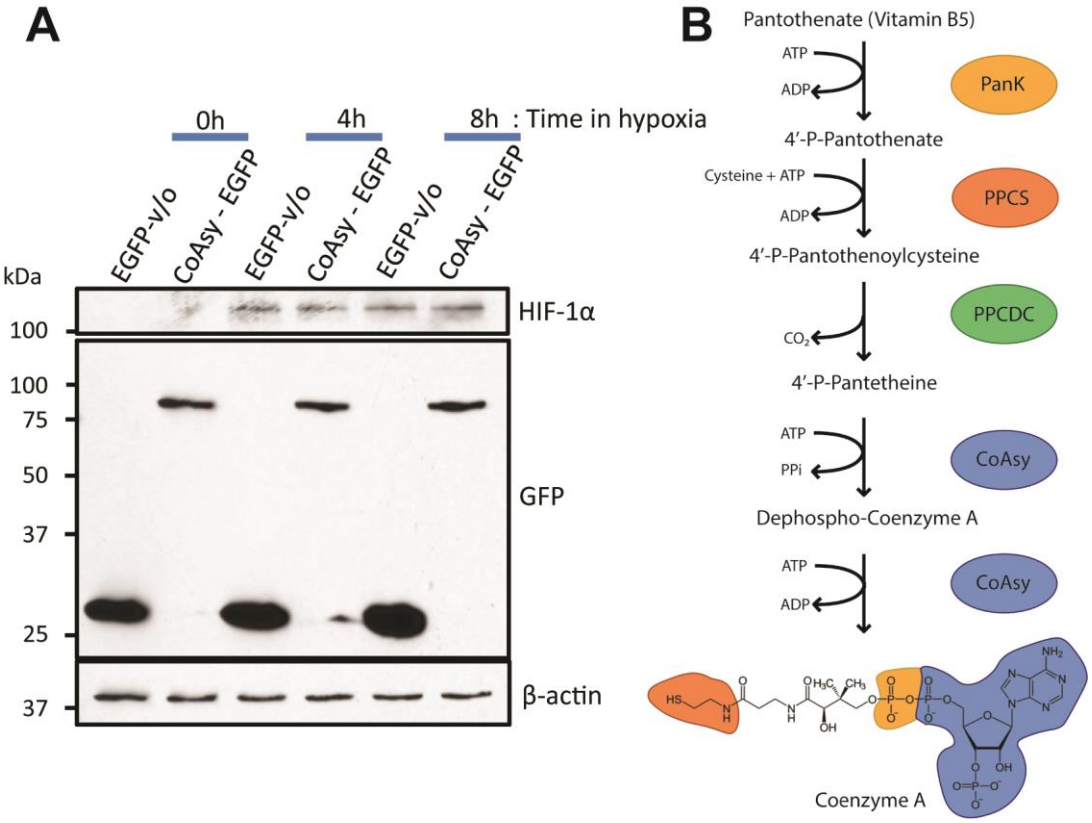

Figure 4.2.2.1: Overexpression of CoAsy does not alter HIF-1α expression. Overexpression of CoAsy-EGFP does not change HIF-1α protein levels. **A**) HEK293T cells were transfected with EGFP or CoAsy-EGFP for 48 hours before being exposed to hypoxia (1% O_2) for 0, 4 or 8 hours. Protein expression was analysed by western blot. **B**) Schematic of the Coenzyme A biosynthesis pathway.

As can be seen in figure 4.2.2.1, overexpression of CoAsy does not change HIF-1α protein levels after 4 or 8 hours of hypoxia. The overexpression of CoAsy was confirmed by fluorescent microscopy and by western blot analysis (**Fig. 4.2.2.1A**). One possible explanation for this result is that overexpression of a kinase does not necessarily mean that there is increased activity as substrate or cofactor availability may be rate limiting in this case. Indeed analysis of the literature highlighted a crucial role of pantothenate kinase (PanK) in regulating the levels of intracellular Coenzyme A (**Fig. 4.2.2.1B**) [202].

To test if overexpression of PanK can regulate protein levels of HIFα, HEK293T cells stably expressing Pank1β, a splice variant of one of the three PanK isoforms, were exposed to hypoxia as well as wild-type (WT) HEK293T cell lines. The HEK293-Pank1β cells were a kind gift from Prof. Ivan Gout. Metabolomics experiments have shown that these cells display ~6x higher levels of Coenzyme A compared to wild type cells as well as significantly elevated levels of Coenzyme A derivatives such as acetyl-CoA and malonyl-CoA (unpublished data from Prof. Ivan Gout).

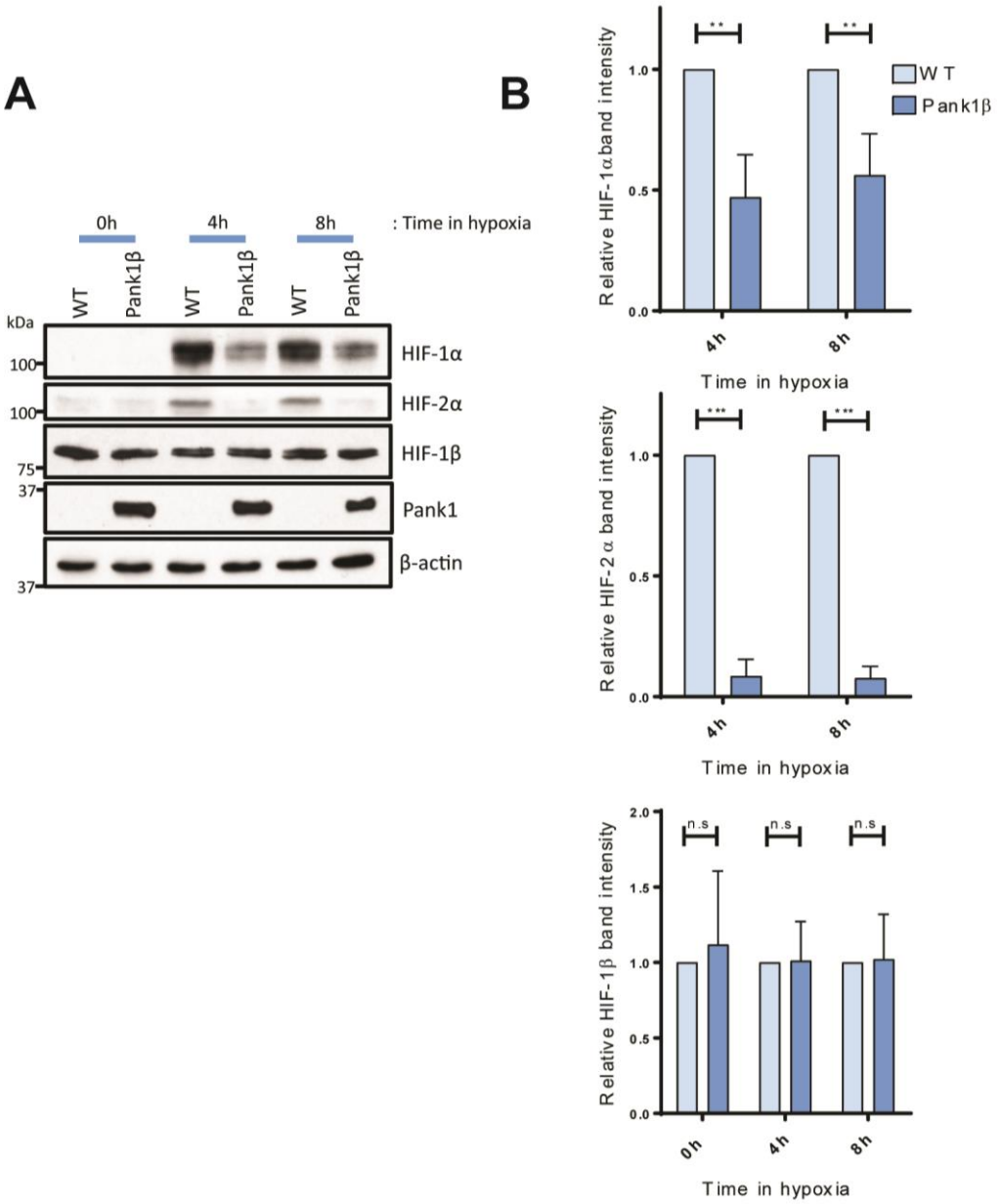

Figure 4.2.2.2: Overexpression of Pank1β reduces HIFα protein expression. A) HEK293T and HEK293-Pank1β cells were plated and exposed to 1% O_2 for 0, 4 and 8 hours before cell lysis and western blot analysis. **B**) Relative HIF-1α, HIF-2α and HIF-1β band densitometry is shown. Statistical analysis is Two-way ANOVA with Sidak's *post hoc* tests. Bar charts are represented as mean ± SD N=3. * $p < 0.05$, ** $p<0.01$, *** $p<0.001$.

As can be seen in figure 4.2.2.2, the HEK293T cells with overexpressed Pank1β display significantly less HIF-1α and HIF-2α protein levels in both 4 and 8 hours of hypoxia. Two-way ANOVA analysis shows that the difference in protein expression for HIF-1α and HIF-2α is clearly significant in hypoxia (HIF-

1α p values are 4h = 0.0015, 8h = 0.0047, HIF-2α p values are p <0.0001 for 4 and 8 hours) however there was no change observed in HIF-1β protein. No signal was observed for either HIF-1α or HIF-2α at atmospheric oxygen therefore it is unclear whether overexpression of Pank1β only regulates HIF expression in hypoxia and further experiments are required to confirm this. To assess the degree of *PANK1* overexpression qRT-PCR analysis was performed. In addition to Pank1, two HIF target genes were also analyzed to give an indication whether this reduction of HIFα proteins results in reduced HIF-1/2 transcriptional activity.

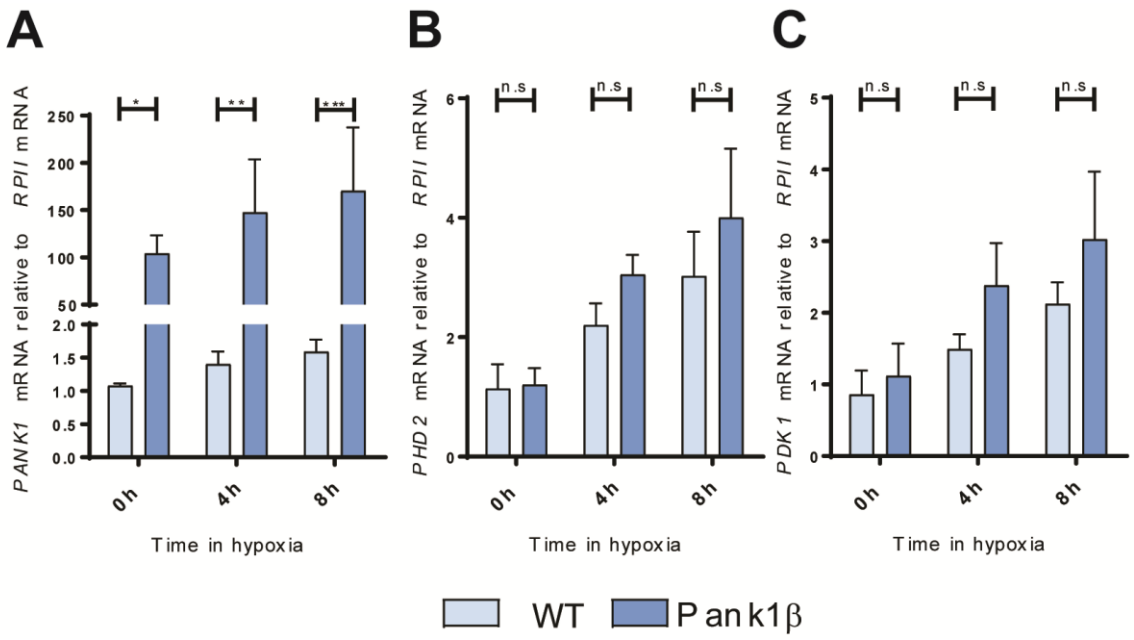

Figure 4.2.2.3: qRT-PCR analysis of HEK293-Pank1β cells and HEK293T WT. HEK293T and HEK293-Pank1β cells were plated and exposed to 1% O_2 for 0, 4 and 8 hours before cell lysis and qRT-PCR analysis of *PANK1, PHD2* and *PDK1*. Statistical analysis is Two-way ANOVA with Sidak's *post hoc* tests. Bar charts are represented as mean ± SD. N=3. * p < 0.05, ** p<0.01, *** p<0.001.

The *PANK1* overexpression in these cell lines is significantly higher than that observed in the WT HEK293T cells with ~100x higher expression observed in normoxia and hypoxia (**Fig. 4.2.2.3A**). There was a small increase of *PANK1* expression in hypoxia, which was observed in both the WT and Pank1β

overexpressing line. This suggests that HIF or an alternative HIF target gene may potentially transcriptionally regulate *PANK1* mRNA expression; however further experiments are required to confirm this. The two HIF target genes assayed here (*PHD2* and *PDK1*) did not show a significant difference between the lines (**Fig. 4.2.2.3B-C**). It is unclear why there is no reduction in expression of these target genes with the reduction in HIFα protein levels. One possible explanation is that following the reduction of HIFα; alternative transcriptional regulators of these proteins may be increased. An alternative explanation is that the increased levels of acetyl-CoA will increase the level of acetylation of HIF-2α resulting in increased affinity with HIF-1β and subsequent increase in activity [203]. Further experiments are required to fully determine why target gene expression is unaffected and additional target genes should also be tested to determine if this is a *PHD2* or *PDK1* specific effect.

This data suggests that Pank1β overexpression reduces HIF protein, however the wild-type cell line used is not the most appropriate control as it is not the matched vector only control and has not been lentivirally transduced. To address this point and directly address if PanK1 regulates HIF protein levels, siRNA knockdown experiments were performed in both the WT and Pank1β expressing cell lines were performed. This allows for comparison of HIF expression following loss of Pank1 compared to the scrambled siRNA control.

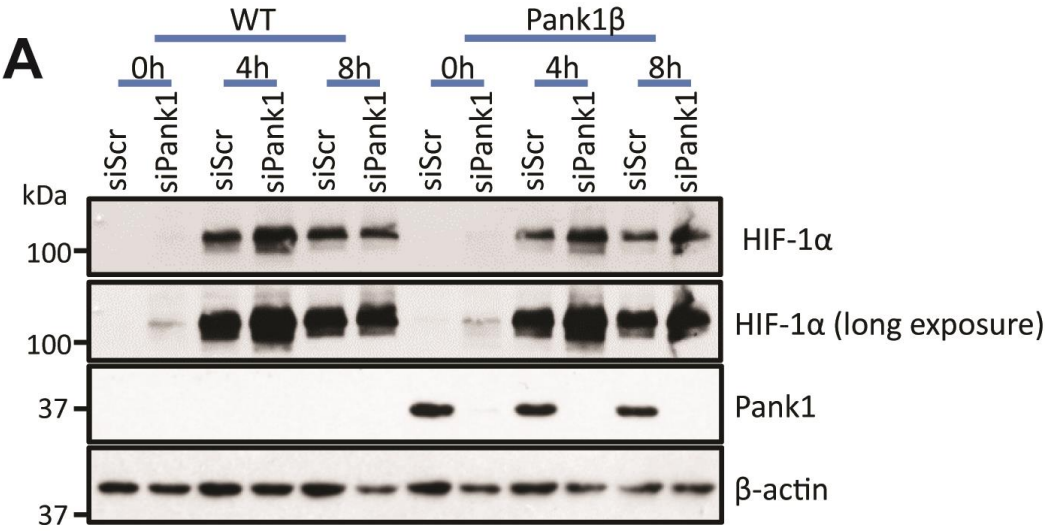

Figure 4.2.2.4: siRNA knockdown of *PANK1* stabilises HIF-1α. HEK293T and HEK293-Pank1β cells were treated with siRNA against *PANK1* or scrambled control at 40 nM. 72 hours post transfection cells were exposed to hypoxia (1% O_2) for 0, 4 or 8 hours before cell lysis and analysis by western blot. n=3.

Figure 4.2.2.4 shows that in both the WT and Pank1β overexpressing cell lines, knockdown of Pank1 with siRNA increases HIF-1α protein in normoxia as well as after 4 and 8 hours of hypoxia. As observed in figure 4.2.2.4, there was reduced expression of HIF-1α protein in the Pank1β cell lines compared to the WT HEK293T cells when treated with scrambled siRNA control. The primary antibody against Pank1 was not able to detect endogenous levels of Pank1 in the WT cell line, possibly due to low expression of the protein. The antibody did detect overexpressed Pank1 in the HEK293T-Pank1β cells and the siRNA knockdown was visible in these cells.

To summarise this section, overexpression of CoAsy had no affect on HIF-1α protein levels however overexpression of Pank1β did significantly reduce both HIF-1α and HIF-2α. Knockdown of Pank1 resulted in stabilized HIF-1α as was observed following loss of CoAsy. Taken together this data suggests that the Coenzyme A biosynthesis pathway plays a role in regulating HIFα protein in a

post transcriptional manner. Potentially implicating Coenzyme A or a Coenzyme A derivative in negatively regulating HIF protein expression.

4.2.3 Knockdown of enzymes that utilize CoA as a substrate

Previous results indicate a role of the CoA biosynthesis pathway in regulating HIFα protein stability. However it is unclear whether this is as a result of CoA or a related CoA derivative, this is of important to note as the Pank1β cells express higher levels of CoA and derivatives such as acetyl-CoA (unpublished data from Prof. Ivan Gout). Furthermore, published work has shown that siRNA mediated knockdown of CoAsy resulted in significant reduction of CoA and acetyl-CoA to the same extent thereby suggesting the close relationship between CoA and derivatives [204]. There are a number of different pathways in which CoA is used however many metabolites such as malonyl-CoA and acyl-CoA utilize acetyl-CoA as a precursor instead of CoA. In an attempt to determine which CoA function negatively regulates HIF we next examined suitable targets to address this line of investigation.

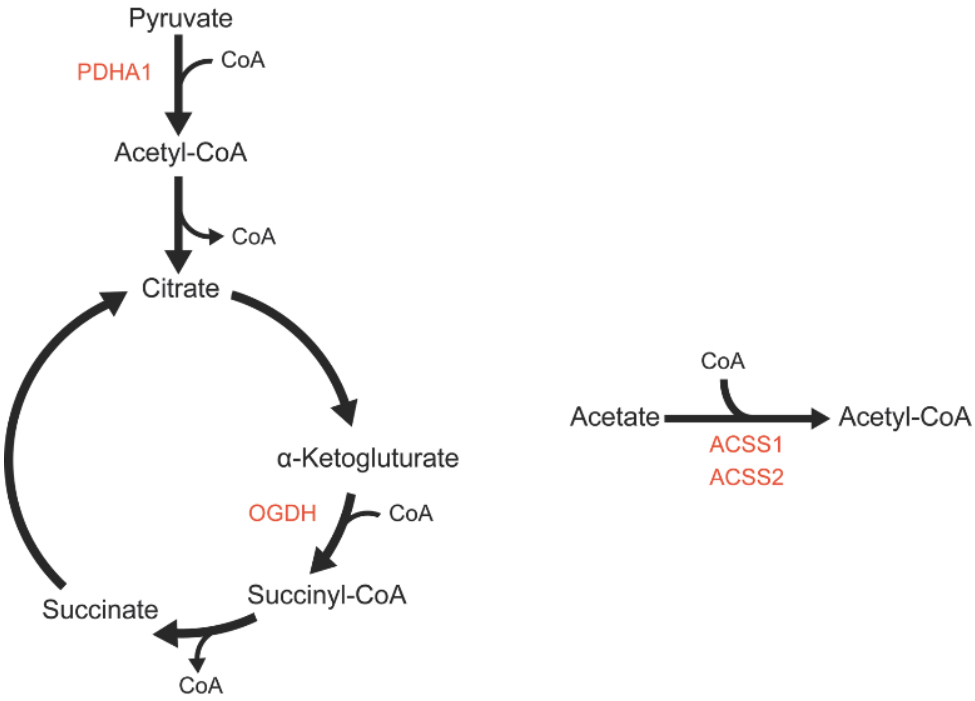

Figure 4.2.3.1: Schematic of enzymatic processes involving CoA. Schematic diagram of enzymes that require Coenzyme A as a substrate. CoA is utilized in the TCA cycle where pyruvate dehydrogenase complex and α-ketogluturate dehydrogenase complex both require CoA as a substrate. Acetyl-CoA is produced from acetate and CoA in by ACSS1 and ACSS2 in the mitochondria and cytoplasm respectively.

CoA is highly prevalent in the TCA cycle as the pyruvate dehydrogenase complex utilizes CoA to form acetyl-CoA that acts in 2-carbon metabolism. Another utilization of CoA in the TCA cycle is in the α-ketogluturate (αKG) dehydrogenase complex where αKG is converted to succinyl-CoA before being reduced to form succinate and thereby recycling CoA. To inhibit these steps smart pool siRNA targeting PDHA1 (pyruvate dehydrogenase complex subunit E1α) and OGDH (oxogluturate dehydrogenase complex E1) were purchased. The conversion of acetate to acetyl-CoA is compartmentalized due to the highly labile nature of the acetyl group and the membrane impermeability of acetyl-CoA [205], in the mitochondria acetyl-CoA is produced via ACSS1 whereas in the cytoplasm this reaction is catalyzed by ACSS2. It is important to note that

following changes in oxygen tension, ACSS2 relocates to the nucleus to maintain histone acetylation [206]. Targeting these key enzymes may elucidate which CoA derivative regulates HIF protein stability.

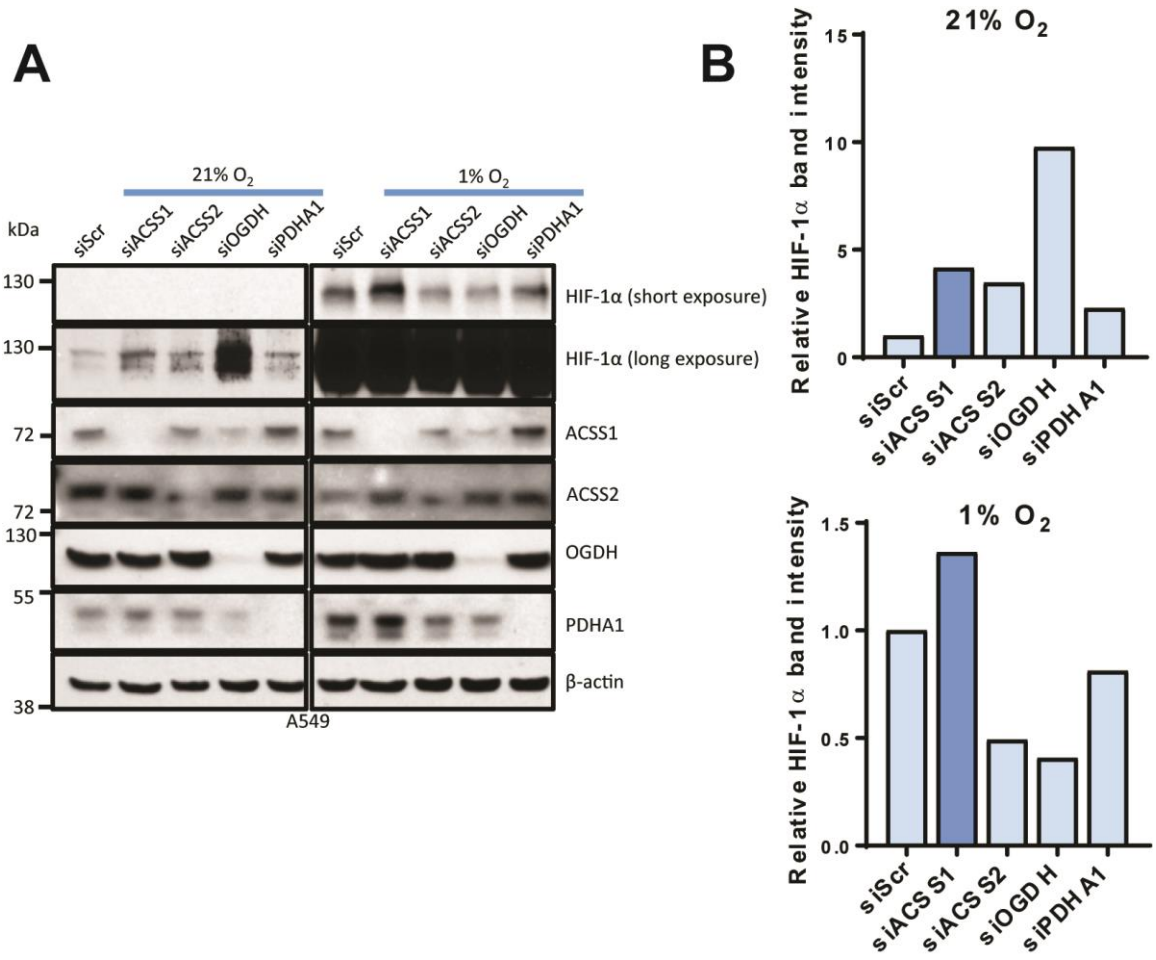

Figure 4.2.3.2: Knockdown of enzymes that utilize CoA in A549 cells. A549 cells were treated with siRNA against *ACSS1*, *ACSS2*, *OGDH* and *PDHA1* at 40 nM. 72 hours post transfection cells were placed into hypoxia (1% O_2) for 4 hours or cultured at 21% O_2 before cell lysis and analysis by western blot (**A**) densitometry was calculated for displayed western (**B**). Representative blot from n = 4.

Wild-type A549 cells were treated with siRNA against *ACSS1*, *ACSS2*, *OGDH* and *PDHA1* and analysed by western blot in Figure 4.2.3.2. In each case the western blot indicates that the proteins have been successfully knocked down by the siRNA. Knockdown of *ACSS1* resulted in stabilized HIF-1α in both normoxia and hypoxia. ACSS1 produces acetyl-CoA from acetate and CoA

inside the mitochondria matrix, however it is unclear how this may regulate HIF-1α stability. As HIF stabilization occurs in both normoxia and hypoxia as is observed following loss of CoAsy, they could potentially be occurring through a similar mechanism. Loss of ACSS2 resulted in stabilized HIF-1α in normoxia, however there was once again a decrease in protein levels in hypoxia; previous results indicate that ACSS2 is required for HIF-2 signaling, however little is known on the role of ACSS2 on HIF-1α stability. Knockdown of *OGDH* resulted in stabilized HIF-1α, which matches the literature that states loss of OGDH causes loss of prolyl-hydroxylase activity and subsequent stabilization of HIF-1α. Interestingly the same stabilization was not observed in hypoxia instead there was a slight decrease in HIF-1α levels. The mechanism for this is unclear. Knockdown of *PDHA1* resulted in an increase of HIF-1α in normoxia however this was not observed in hypoxia; as loss of CoAsy results in stabilized HIF-1α in both normoxia and hypoxia, we hypothesized that CoAsy may be regulating HIF through an alternative mechanism.

The previous figure showed that knockdown of ACSS1 resulted in stabilized HIF-1α, however it is unclear if this is occurring by the same mechanism as CoAsy. To address this the same knockdown was performed in A549-tet-shRNA lines, with the hypothesis being that if knockdown of ACSS1 regulation of HIF occurs through the same mechanism as CoAsy then there will only be a stabilization of HIF-1α in the shScr line and not in the shCoAsy line.

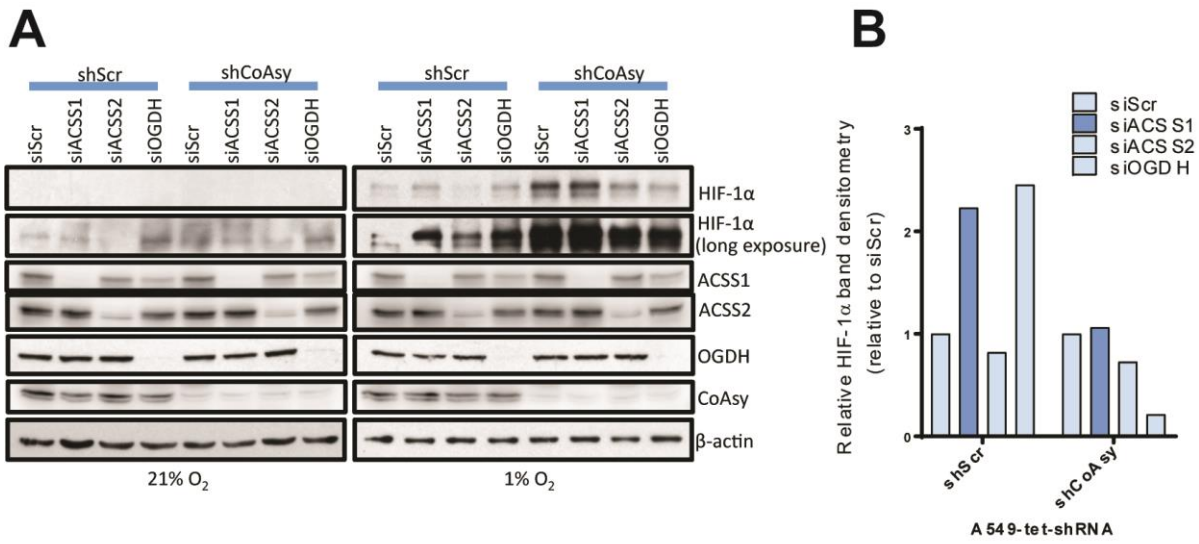

Figure 4.2.3.3 Knockdown of enzymes that utilize CoA in A549-tet-shRNA cells: A549-tet-shRNA cells were treated with doxycycline at 25 ng.mL-1 before treating with siRNA against *ACSS1*, *ACSS2*, *OGDH* and scrambled control. 72 hours after transfection cells were placed into hypoxia for 8 hours before lysis and analysis by western blot. Relative densitometry of HIF-1α band intensity of 1% O_2 was calculated normalized to siScr for each line. n=3.

Figure 4.2.3.3 shows that knockdown of ACSS1 results in an increase of HIF-1α protein in the shScr lines in hypoxia but not in the shCoAsy lines. The bar chart (**Fig. 4.2.3.3B**) shows relative HIF-1α band intensity normalized to the siScr control; in the shScr line there is a 2-fold increase in HIF-1α protein compared to scrambled control whereas there is no increase in the shCoAsy line. Between the lines there was a large increase in HIF-1α protein as has been previously shown following loss of CoAsy. ACSS2 was included as a related negative control; once again there was a slight decrease in HIF-1α protein levels following siACSS2 compared to siScr. Knockdown of OGDH resulted in stabilized HIF-1α in the shScr line, this result matches previous reports in the literature, however in the shCoAsy line there was a reduction of HIF-1α protein. It is unclear why there is this opposing effect. It has been reported that OGDH knockdown results in inhibition of prolyl-hydroxylase function through L-2HG production (an enantiomer of α-ketogluturate) however

it is unclear how CoAsy or CoA may be affecting L-2HG production or indeed how active prolyl-hydroxylase enzymes are following loss of CoAsy [191].

This data suggests that mitochondrial acetyl-CoA may be the CoA derivative responsible for negatively regulating HIFα, however these experiments have so far only assessed HIF-1α protein levels. It is important also to investigate HIF-1 activity through the use of reporter assays; this is of particular importance as it has previously been reported that ACSS2 is required for acetylation of HIF-2α thereby increasing transcriptional activity without altering protein stability but there have been no studies on the role of ACSS1 in regulating HIF activity.

4.3 CoAsy negatively regulates HIF-1α post-transcriptionally at the 30-389 and 390-462 amino acid domains.

Taking an alternative and complimentary approach to identifying the mechanism as to how CoAsy regulates HIFα protein, a series of HA-tagged domains from HIF-1α were overexpressed in A549 cell lines knocked down for *COASY* and *PHD2*. These constructs each contain the same CMV promoter sequence and the same 3' UTR each distinct from that of the *HIF1A* gene thereby negating any transcriptional or miRNA differences of expression, instead only differences in protein stability or translation will be observed. This is of interest as no changes in *HIF1A* or *HIF2A* mRNA were observed following loss of CoAsy in normoxic conditions where HIF-1α and HIF-2α protein levels are both stabilized. This suggests that CoAsy does not affect *HIF1A* or *HIF2A* gene transcription.

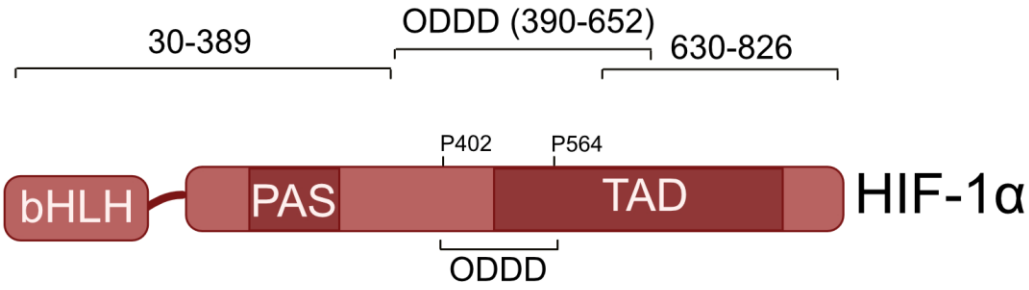

Figure 4.3.1: Schematic of HA-EGFP tagged domains of HIF-1α. Schematic of the HIF segments used for overexpression experiments. 30-389 domain encompasses the bHLH domain and PAS domains, the ODDDD contains N-TAD as well as proline residues and lysine residue required for O_2 dependent degradation of this subunit and the 630-826 contains C-TAD domain.

These constructs were transfected in to A549 cells that had been previously treated with siRNA against *COASY* and *PHD2*. si*PHD2* was included as a positive control as it has been well reported that loss of PHD2 would result in stabilized ODDD due to reduced prolyl-hydroxylation and inhibition of subsequent ubiquitination and degradation of ODDD domain via the proteasome. Through this approach it was confirmed that CoAsy regulates HIF post-transcriptionally and which domain or domains of HIF does CoAsy negatively regulate.

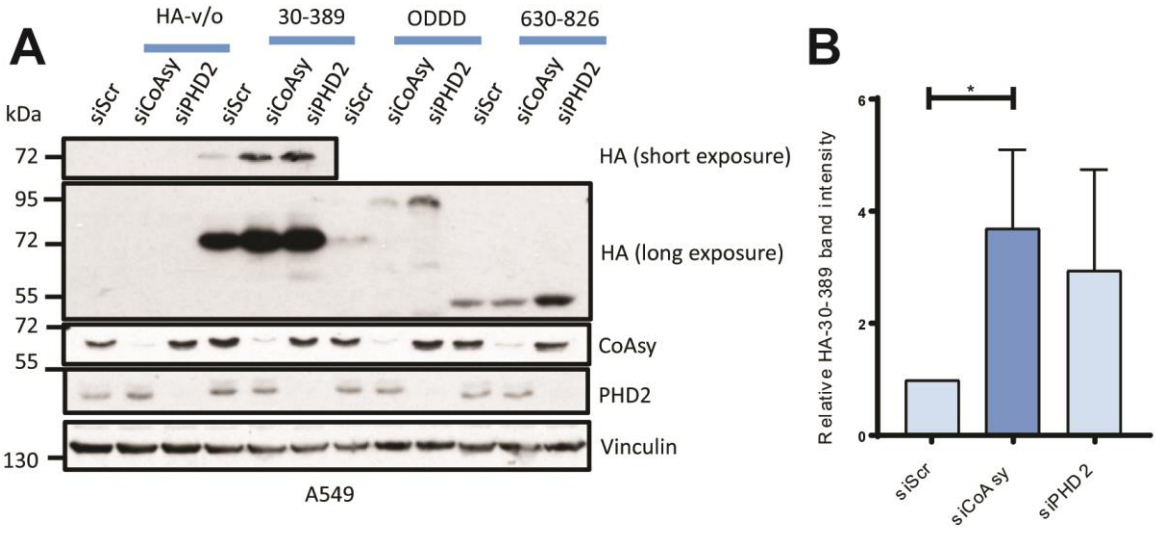

Figure 4.3.2: CoAsy negatively regulates 30-389 and the ODDD of HIF-1α. A549 cells were treated with siRNA against *COASY*, *PHD2* and scrambled control. The following day cells were transfected with HIF domains detailed in **Fig. 4.3.1**. 48 hours following transfection cells were lysed and analysed by western blot (**B**). Relative HA band densitometry of 30-389 domain was calculated for 3 biological replicates. Bar chart shows mean ± SD. Statistical analysis was Mann-Whitney U test. * $p < 0.05$. n=3.

A549 cells were treated with siRNA against *COASY, PHD2* and non-targeting control. Knockdown efficiency was confirmed by western blot and in each case the siRNA achieved high levels of protein knockdown. The 30-389 and ODDD domains both increase in expression following loss of CoAsy compared to scrambled siRNA control, this effect is specific for these domains as there was no change in the 630-826 domain thus suggesting that this effect is unlikely to be due to changes in transfection efficiency or translation efficiency. The ODDD domain was rapidly degraded in A549 cells treated with non-targeting siRNA however following loss of CoAsy this protein was stabilized and a faint band appears in the western blot; this increase is not as stark as that following loss of PHD2 which is a well-established regulator of the ODDD [60]. Loss of CoAsy also regulates the 30-389 domain of HIF-1α, calculating the changes in band densitometry reveals a significant difference between the siScr and siCoAsy treated samples ($p = 0.031$, **Fig. 4.3.2B**). The majority of the literature has

reported post-translational modifications at the ODDD or in the TAD of HIF-1α. To identify reported modifications of this domain the online server phosphosite was consulted [207]. This contains a database of reported post-translational modifications from high-throughput experiments, such as large-scale mass spectrometry of phosphorylated proteins, as well as papers with more focused approach and subsequent validation.

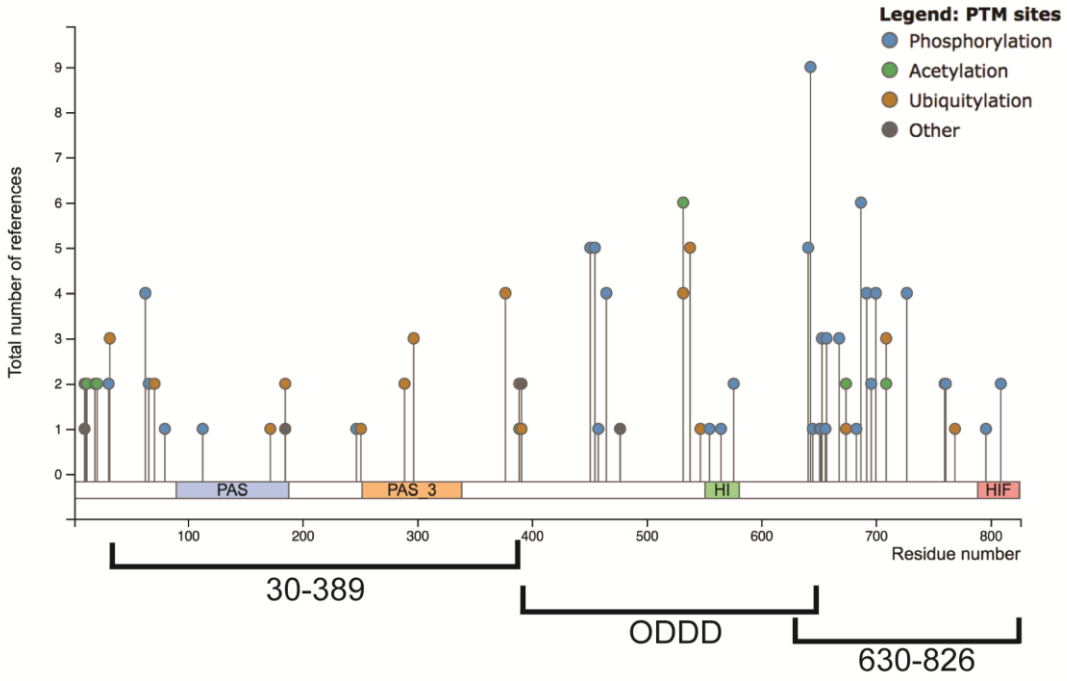

Figure 4.3.3: Identified post translational modifications in HIF-1α. Schematic of reported post-translational modifications of HIF-1α. Figure is taken from phosphosite online server [207].

As can be seen in figure 4.3.3 the majority of reported post-modifications cluster towards the N-terminus (first 100 amino acids) and C-terminus (post residue 450), however a number of post-translational modifications have been reported between the 30-389 region. The majority of these are ubiquitination events identified through mass-spectrometry experiments and were not subsequently validated. Of the reported post-translational modifications within this 30-389 domain, two had been experimentally validated. One such event was the

phosphorylation of HIF-1α at Ser247 by casein kinase 1 [208], however this phosphorylation did not affect protein stability instead it inhibited interaction with HIF-1β and subsequent transcriptional activity. The second post-translational modification was protein kinase A (PKA) mediated phosphorylation of HIF-1α at Thr63 [209]. This phosphorylation event increases HIF-1α protein stability. Therefore it could be that loss of CoAsy may in some way alter PKA activity, however PKA also phosphorylates HIF-1α at Ser692 that also results in stabilization of HIF-1α independent of Thr63 phosphorylation. As loss of CoAsy does not affect stability of the 630-826 amino acid domain (which encompasses the Ser692 phosphosite) it is unlikely that this is the mechanism behind HIF stabilization following loss of CoAsy.

To summarize this section, loss of CoAsy regulates HIF-1α at the post-translational stage. This occurs at both the 30-389 and ODDD domains but not at the 630-826 domain. A number of post-translational modifications have been reported in the 30-389 domain however further experimental validation is required to determine how these are effected following loss of CoAsy (see future work).

4.4 Protein CoAlation

Protein CoAlation is a recently identified protein modification that occurs in both prokaryotic and eukaryotic cells [210, 211]. This modification occurs at exposed cysteine residues as the free thiol of CoA forms a disulphide bond in a manner analogous to glutathionylation (**Fig. 4.4**). This protein modification is reversible and increased upon cellular stress. It was hypothesized that this protein modification may potentially play a role in regulating HIF; therefore when CoAsy is lost, CoA levels are reduced and subsequently CoAlation is diminished.

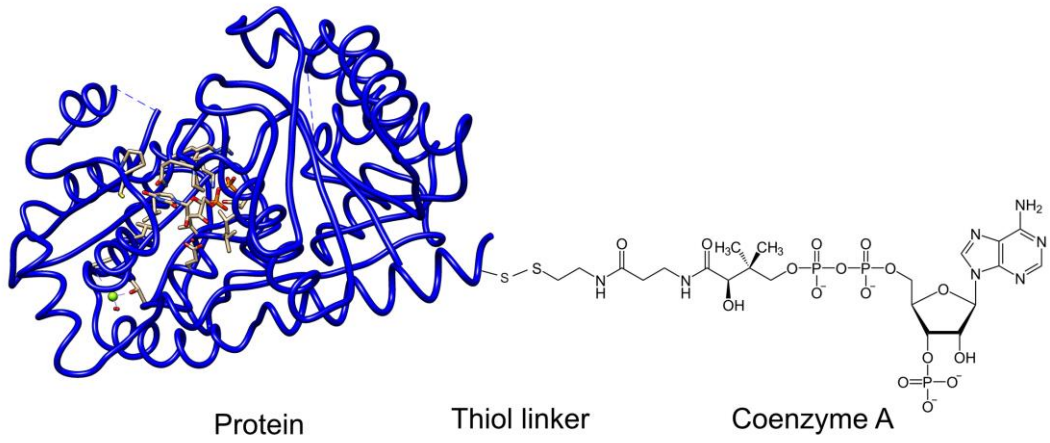

Figure 4.4: Protein CoAlation. Schematic of protein CoAlation. The thiol group in Coenzyme A forms a disulphide bond with free cysteine residues in proteins.

To assay the levels of protein CoAlation, a monoclonal antibody raised against CoA was prepared by Prof Ivan Gout. This mAb specifically detects CoA but not the biosynthetic precursors such as 3'-dephospho-CoA or 4'phosphopantetheine [212]. Using this tool, Tsuchiya *et al.* identified extensive protein CoAlation both *in cellulo* and *in vitro* (H_2O_2 perfused rat hearts and the liver of starved rats) [210].

4.4.1 Protein CoAlation in hypoxia

The role of protein CoAlation in hypoxia has not been studied. This is of particular interest as reactive oxygen species induces protein CoAlation in a dose dependent manner. It has been extensively reported that, rather paradoxically, ROS increases in hypoxia as a consequence of deficient electron transport train and aberrant functioning of complex III [213], therefore it could be assumed that CoAlation may increase in hypoxia as a result of elevated levels of ROS. However as mentioned previously, CoAlation occurs at free thiol groups however the hypoxic marker pimonidazole also works by binding to free thiol groups. If the ROS induced CoAlation is increased in hypoxia then it is possible that the free pimonidazole may not bind, thus CoAlation may not occur in low oxygen tensions. To address this, HEK293-Pank1β cells were exposed to 1% O_2 for varying time points before being treated with the menadione or vehicle only to test the propensity for CoAlation to occur in hypoxia.

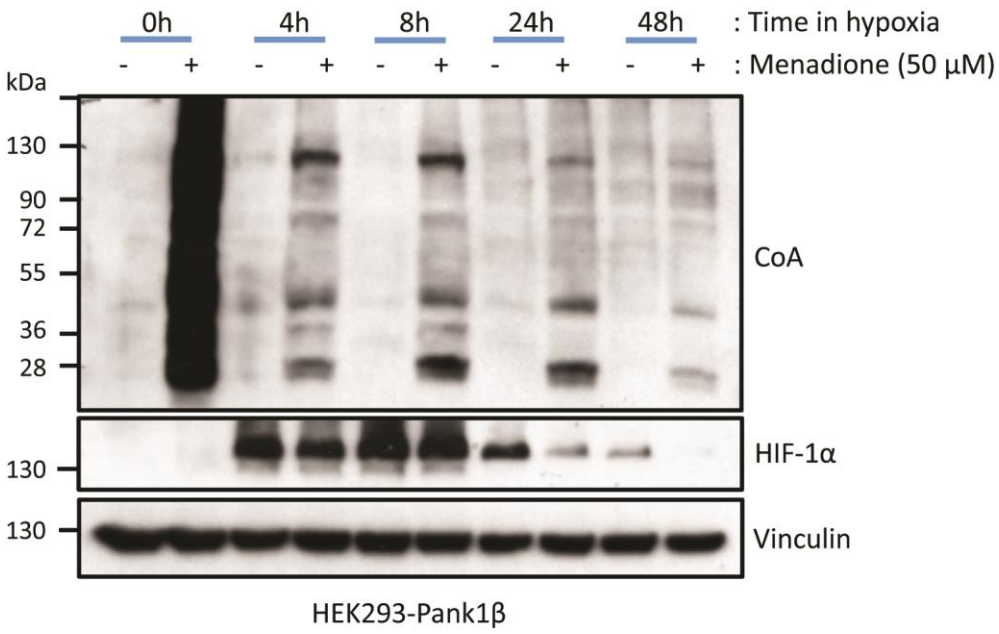

Figure 4.4.1: Menadione induced CoAlation in HEK293-Pank1β cells. Non-reducing western blot analysis of Protein CoAlation in hypoxia following menadione treatment. HEK293-Pank1β cells were exposed to 1% O_2 for varying time points before treating with 50 µM menadione for 30 minutes or DMSO for 30 minutes prior to cell lysis. n=3.

Figure 4.4.1 shows large changes in protein CoAlation across the conditions tested. In the cells cultured at 21% O_2 there was a large increase in CoAlation observed following treatment with 50 µM menadione. Interestingly, the cells cultured in hypoxia showed a large reduction in the menadione induced CoAlation even at the shortest time point of 4 hours. In contrast to the menadione induced CoAlation, endogenous CoAlation increases after 24 and 48 hours of low oxygen tension. HIF-1α protein expression was further affected by the addition of menadione, this effect was more pronounced at later time points of hypoxic incubation (24 and 48 hours) at which point the adaptive response to hypoxia would be triggered. Together this shows that hypoxia changes the ability of menadione to induce CoAlation however endogenous CoAlation actually increases after longer time periods of reduced oxygen availability.

It is unclear as to why HIF-1α expression was reduced following menadione treatment, as menadione will not just effect CoAlation; instead a plethora of other cellular functions will be altered by increased ROS. Furthermore the decrease of CoAlation in hypoxia could potentially be a menadione specific effect; menadione induces ROS through redox cycling, which requires NAD(P)H-quinone oxidoreductase (NQOR) activity to produce ROS this in turn alters NADPH/NADP+ ratio that may also have an effect on CoAlation [214]. To remove potential non-ROS related effects from menadione treatment, H_2O_2 was used as an alternative treatment to increase cellular ROS.

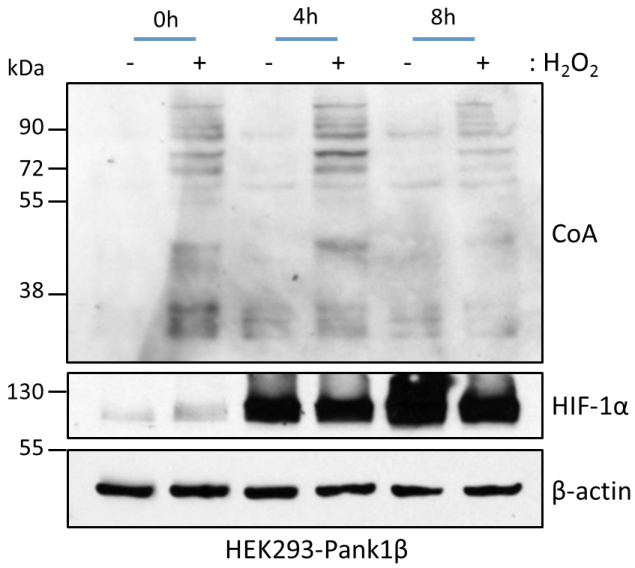

Figure 4.4.2: H_2O_2 induced CoAlation in HEK293-Pank1β cells: Non-reducing western blot analysis of Protein CoAlation in hypoxia following H_2O_2 treatment. HEK293-Pank1β cells were cultured in 1% O_2 for 0, 4 and 8 hours before treating with 500 µM of H_2O_2 for the final 30 minutes of incubation before cell lysis. n=3.

The western blot in figure 4.4.2 once again shows an increase in protein CoAlation following addition of ROS inducing agent. In hypoxia the degree of H_2O_2-induced CoAlation is similar to that observed in normoxia, this result is in contrast to that observed following menadione treatment. There was a decrease in HIF-1α levels following treatment with H_2O_2 in hypoxic cells (see

appendix for other biological replicates), however in normoxia, treatment with H_2O_2 increased HIF-1α levels, this could potentially be due to oxidative dimerization of PHD2 [215]. It is difficult to draw comparisons between the two treatment methods, as the degree of ROS induction was not measured for either treatment and the samples were run on separate western blots. However these two figures do show that endogenous protein CoAlation is increased after 24 hours of hypoxia and that ROS-inducing agents induce protein CoAlation and negatively regulate HIF-1α protein in hypoxia.

4.4.2 Direct protein CoAlation of HIF-1α

Due to the previously mentioned links between CoAlation, ROS and hypoxia, taking Occam's razor approach it was hypothesized that HIF-1α may potentially be subject to CoAlation and this may negatively regulate protein stability. Hence in cells with deficient in CoA biosynthesis this will result in stabilized HIF-1α protein levels.

4.4.3 Preparation of recombinant HIF-1α for *in vitro* CoAlation assays

One method to test if proteins are directly CoAlated is through the use of *in vitro* CoAlation assays. These assays were used extensively by Tschuyia *et al.* to validate whether proteins are directly CoAlated in a system without other proteins or other potential interactors that may yield false positive results. Dr. Thomas Webb (previous member of Professor Tyson Sharp's lab) subcloned *HIF1A* CDS into GST-tagged bacterial overexpression vector. In total, 4 positive clones were generated and tested for expression levels.

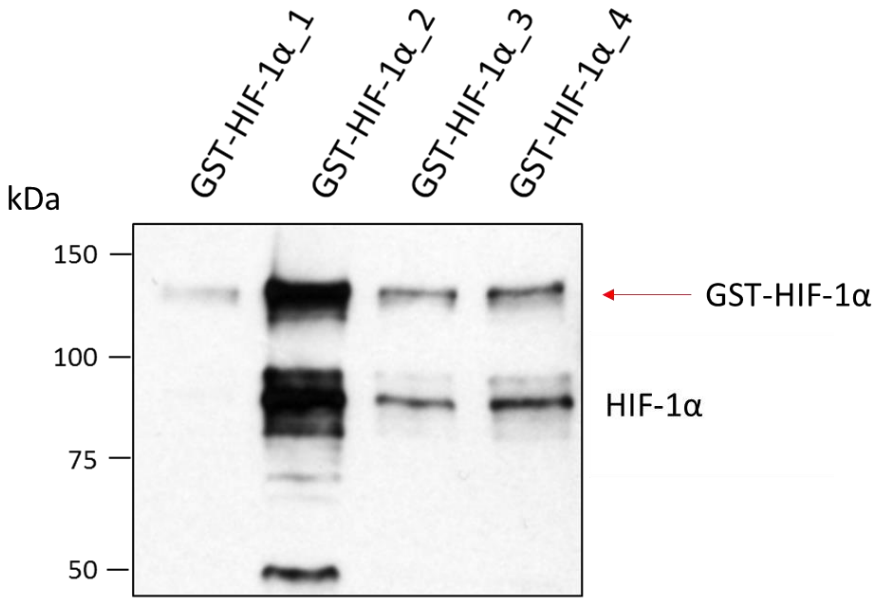

Figure 4.4.3.1: Recombinant expression of GST-HIF-1α fusion from multiple DNA plasmid clones. Protein expression of GST-HIF-1α bacterial expression plasmids. DH5α competent cells were transformed with each GST-HIF-1α construct before inducing with IPTG to promote protein expression. Expression was measured by western blot.

Each of the plasmid controls expressed HIF-1α, albeit to varying degrees. The western blot shows that clone 1 expressed a small amount of HIF-1α, as there was a band visible on the western blot corresponding to the correct size for GST-tagged HIF-1α (~140 kDa). Clone 2 showed the highest expression of GST-HIF-1α and was therefore used for subsequent expression studies. To express larger quantities of protein, the construct was retransformed in to Rosetta D3 cells. 3 colonies were picked, expanded to larger cultures and induced with IPTG.

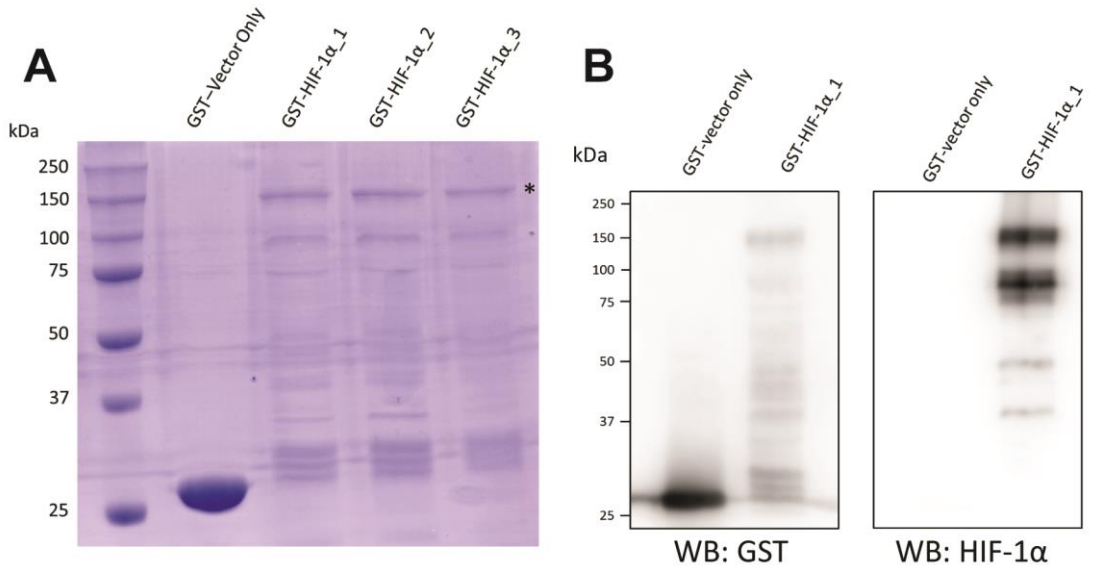

Figure 4.4.3.2: Bacterial expression of recombinant HIF-1α GST fusion protein for in vitro CoAlation analysis. Protein expression was confirmed by SDS-PAGE and coomassie Blue staining, full-length fusion protein is marked with an asterisk (**A**) and by western blot (**B**) with α-GST and α-HIF-1α antibodies.

Figure 4.4.3.2 shows that each of the colonies picked produced full length GST-HIF-1α (**Fig. 4.4.3.2A**) with the band on coomassie gel corresponding to full-length fusion protein marked with an asterisk. This band was confirmed to be the correct band by blotting with both α-GST and α-HIF-1α antibody (**Fig. 4.4.3.2B**). The coomassie stained gel clearly shows multiple degradation products from the production of the fusion protein, which can be further visualized in both GST and HIF-1α western blot. Therefore when considering *in vitro* CoAlation assays only the band corresponding to full-length fusion protein (~140 kDa) should be focused on as a true readout of protein CoAlation. These samples were stored at -80°C before being given to Prof. Ivan Gout for *in vitro* CoAlation analysis.

4.4.4 Preparation of endogenous IP of HIF-1α for CoAlation analysis

In addition to *in vitro* CoAlation assays, samples of endogenous HIF-1α immunoprecipitated (IP) from cell lysates were also prepared. This is an important condition to consider, because if protein CoAlation causes destabilization of HIF-1α protein and is responsible for the stabilization observed following loss of CoAsy then there must be sufficient basal levels of CoAlation prevalent in wild type cells without stimulation. IP conditions need to be adjusted for measuring CoAlation, as lysis buffer requires addition of n-ethylmaleimide (NEM) to bind to free thiol groups to avoid non-specific CoAlation and proteins need to be eluted from beads in sample buffer without reducing agents to preserve the disulphide thiol linker.

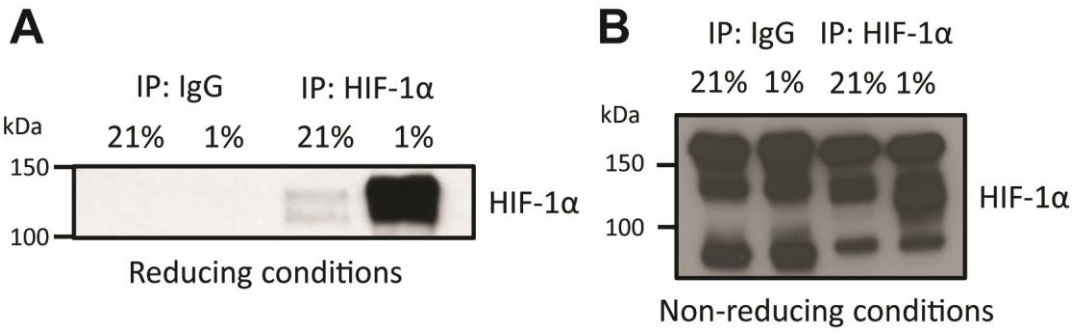

Figure 4.4.4.1: Optimisation of HIF-1α IP from HEK293T cells. HIF-1α was immunoprecipitated from HEK293T cells cultured in normoxia and hypoxia; IP was performed in both reducing (**A**) and non-reducing conditions (**B**).

The IP from HEK293T in reducing conditions shows clear pull down of HIF-1α from lysates cultured in both 21% and 1% oxygen. This IP was specific for the HIF-1α antibody as the species matched IgG did not show any HIF-1α coming down (**Fig. 4.4.4.1A**). However following the addition of NEM in the lysis buffer and eluting in non-reducing sample buffer a number of non-specific bands appeared in both IgG IP as well as HIF-1α IP (**Fig. 4.4.4.1B**). It is unclear if the

non-specific bands are degradation of the IgG, this will run differently in non-reducing conditions compared to reducing conditions. Instead of separating into light and heavy chains (bands running at ~50 kDa and ~25 kDa), the disulphide bonds will remain intact and appear at a higher molecular weight. To reduce non-specific bands the IP was repeated as before but with increased wash steps.

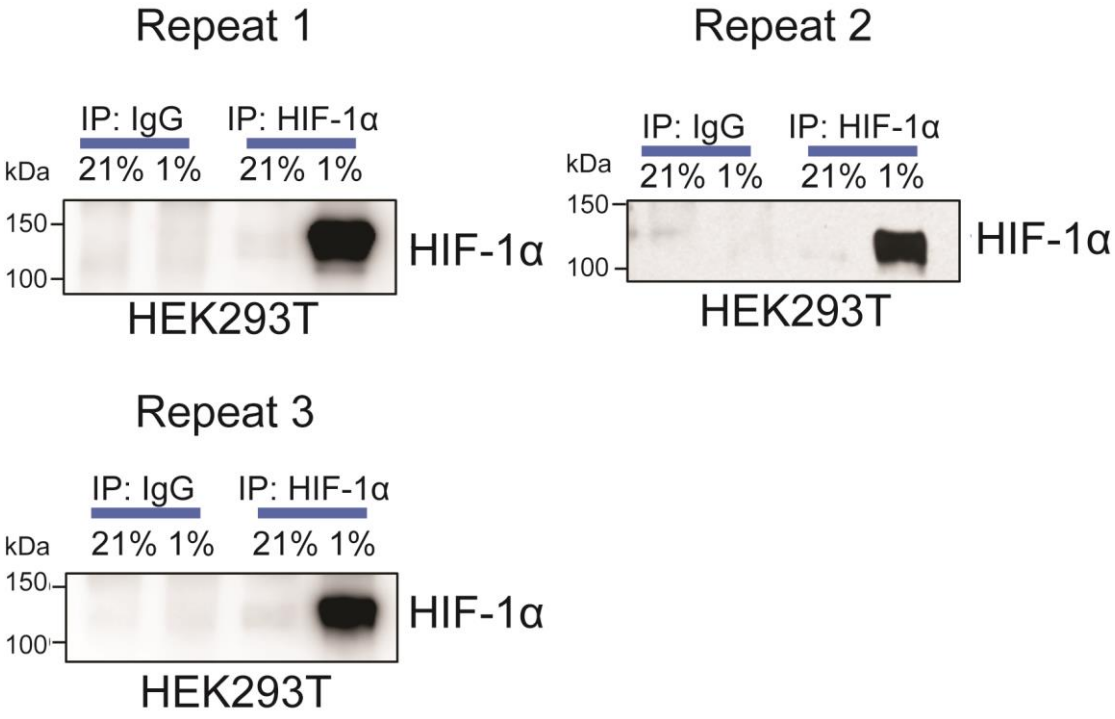

Figure 4.4.4.2: Immunoprecipitation of HIF-1α from HEK293T cells. Three biological replicates of HIF-1α IP from HEK293T cells cultured in normoxia and hypoxia, protein was eluted and SDS-PAGE was performed in non-reducing conditions.

The extra wash steps in the IP reduced the non-specific bands in the western blot. For each IP there is a specific pull down of HIF-1α protein in the cell lysate from hypoxic cells, however there is only a faint band observed in the normoxic lysate. Only a small proportion of the IP eluate was run on western blot, with the rest saved for assessing CoAlation, therefore loading more would show a

more intense band in the normoxic IP. The three repeats were submitted to Prof. Ivan Gout for CoAlation analysis.

4.4.5 Analysis of potential CoAlation on HIF-1α

The three clones of recombinant GST-HIF-1α and GST tag only along with three biological replicates of endogenous HIF-1α immunoprecipitated from HEK293T cells were submitted for *in vitro* CoAlation experiments and western blot analysis of endogenous CoAlation by Prof. Ivan Gout and his lab. These experiments will show if HIF-1α has the biophysical properties that allow for CoAlation as well as if this CoAlation occurs without stimulation in HEK293T cells.

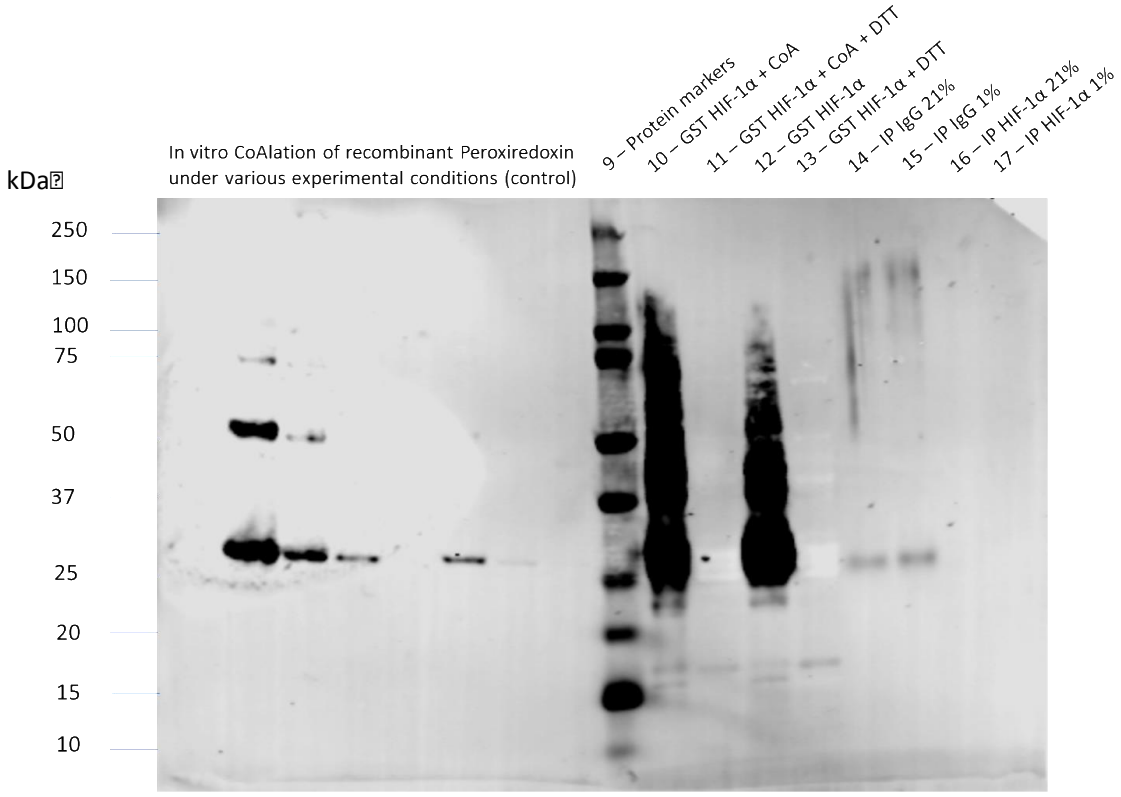

Figure 4.4.5: CoAlation analysis of HIF-1α samples. Results from *in vitro* CoAlation assay of GST-HIF-1α and endogenous IP of HIF-1α, *in vitro* CoAlation of peroxiredoxin was used as positive control. Figure used with kind permission of Prof. Ivan Gout.

The endogenous IP of HIF-1α showed no signal in either sample (IP from either normoxic or hypoxic cell lysates, lane 16 and 17 respectively), whereas the IgG control did show an unidentified CoAlated protein at ~150 kDa that is not specific for HIF-1α IP. Multiple conditions were tested for *in vitro* CoAlation of GST-HIF-1α; lane 10 is the *in vitro* CoAlation assay, with HIF-1α combined with CoA and producing a large smear on the western blot. No clear band is present at the correct size of ~150 kDa, however the western pattern appears to be specific for CoAlation as treatment with the reducing agent DTT completely reduces the signal observed (lane 11). Lane 12 is the reaction with GST-HIF-1α and no CoA added, this control is included to ensure the CoAlation observed is due to the *in vitro* CoAlation and not from any CoAlation arising from the bacterial protein expression. Lane 10 and 12 display similar band profiles with neither showing a clear band at the predicted size for full-length GST-HIF-1α fusion protein. Taken together, this data suggests that HIF-1α is not CoAlated *in cellulo* or *in vitro*. The signal observed in the GST-HIF-1α samples could result from CoAlation of the GST tag, as CoA is a common molecule to both eukaryotes and prokaryotes there is potential for the GST tag to become CoAlated during bacterial protein production, analysis of the GST only recombinant protein would have determined if this is the case.

4.4.6 CoAlation of members of the canonical pathway of HIF regulation

The previous results indicated that HIF-1α is not directly CoAlated, however this is not to say that CoAlation does not play a role in regulating HIF-1α expression, as there are multiple regulators of HIF that may be subject to CoAlation. To test this multiple targets of the O_2-dependent pathway of HIF

regulation (PHD, pVHL and LIMD1) were immunoprecipitated from HEK293-Pank1β cell lysate cultured in atmospheric oxygen.

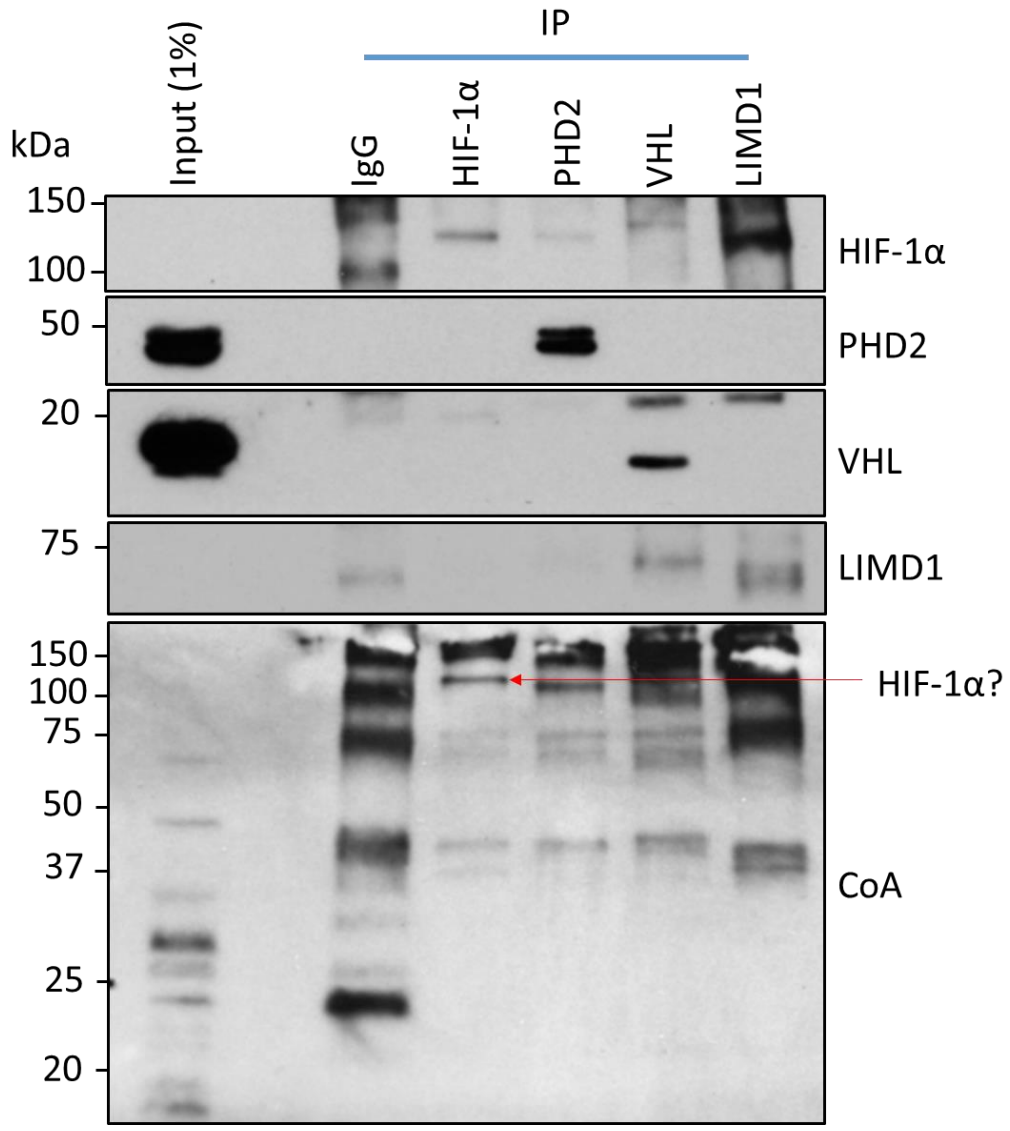

Figure 4.4.6: IP to assess CoAlation of HIF-1α and O_2-depdenedent regulators of HIF-1α: Immunoprecipitation of HIF-1α, PHD2, pVHL and LIMD1 from HEK293-Pank1β cell lysate. IP and CoAlation was determined by western blot. n=2.

Figure 4.4.6 shows successful IP of each target proteins. Despite this IP being performed in atmospheric oxygen conditions there was a clear band observed in the HIF-1α IP, the same band was also observed, albeit faintly in the PHD2 Co-IP but no band of the same size in the IgG IP indicating that this interaction is specific, which is in concordance with the literature. IP of PHD2 revealed a

specific band with no band observed in Co-IP of other proteins. In this HEK293-Pank1β cell line only the p19 isoform of pVHL was observed in either the input or IP. In the CoA western blot there is a degree of basal CoAlation observed in the input sample. The IgG control shows a number of strong non-specific bands thus making analysis of specific CoAlation difficult, for example the LIMD1 IP shows a strong band at ~75 kDa which may potentially indicate CoAlation of LIMD1 however due to the non-specific band in the IgG lane it remains inconclusive. No specific signal was observed at the correct size for pVHL or PHD2 IP. In the HIF-1α IP there was a band observed at the correct size as HIF-1α in the CoA blot indicating that contrary to previous results, HIF-1α may indeed be directly CoAlated. This band was not the same size as non-specifics in the IgG IP.

It remains inconclusive as to whether HIF-1α is directly CoAlated or not. The *in vitro* assay and initial HIF-1α IP from HEK293T suggests that CoAlation does not occur, however subsequent IP from HEK293-Pank1β cells indicates a degree of CoAlation may occur. It is unclear why there is such discrepancy between results, one possible explanation may be as simple as sample storage in the initial analysis, as it is not known how stable the CoAlation modification is and may become cleaved in long term storage or subsequent freeze thaws. An alternative explanation is that the level of basal CoAlation in HEK293T cells may be so low that HIF-1α may not be CoAlated without overexpression of Pank1β and increased CoA levels, which casts doubts over the biological relevance of CoAlation in regulating HIF-1α in cancer. However, further studies

with appropriate controls are required to validate whether HIF-1α is CoAlated or not.

4.5 Analysis of cell transformation following loss of CoAsy

The second aim of this chapter was to determine the cellular consequences of losing CoAsy. Irrespective of how loss of CoAsy increases HIF-1 activity and stability, there will be multiple HIF dependent changes that can alter cell proliferation, motility and metabolism. However, CoA is crucial for many cellular processes such as TCA cycle therefore loss of CoAsy may impart proliferative defects to the cell. Therefore it is important to determine these cellular changes *in vitro* as it may highlight any pro-tumourigenic changes following loss of CoAsy.

4.5.1 Loss of CoAsy does not change cell proliferation in A549 cells

The first parameter tested was cell proliferation. Cancer is frequently considered a disease of uncontrolled cellular proliferation, thus it is an important consideration when looking at potential tumour suppressor genes. To determine cell proliferation rates, A549-tet-shRNA cells were pretreated with doxycycline before plating at low density. Cells were cultured at 21% O_2 or 1% O_2 for 7 days, proliferation was measured by counting cells at indicated timepoints.

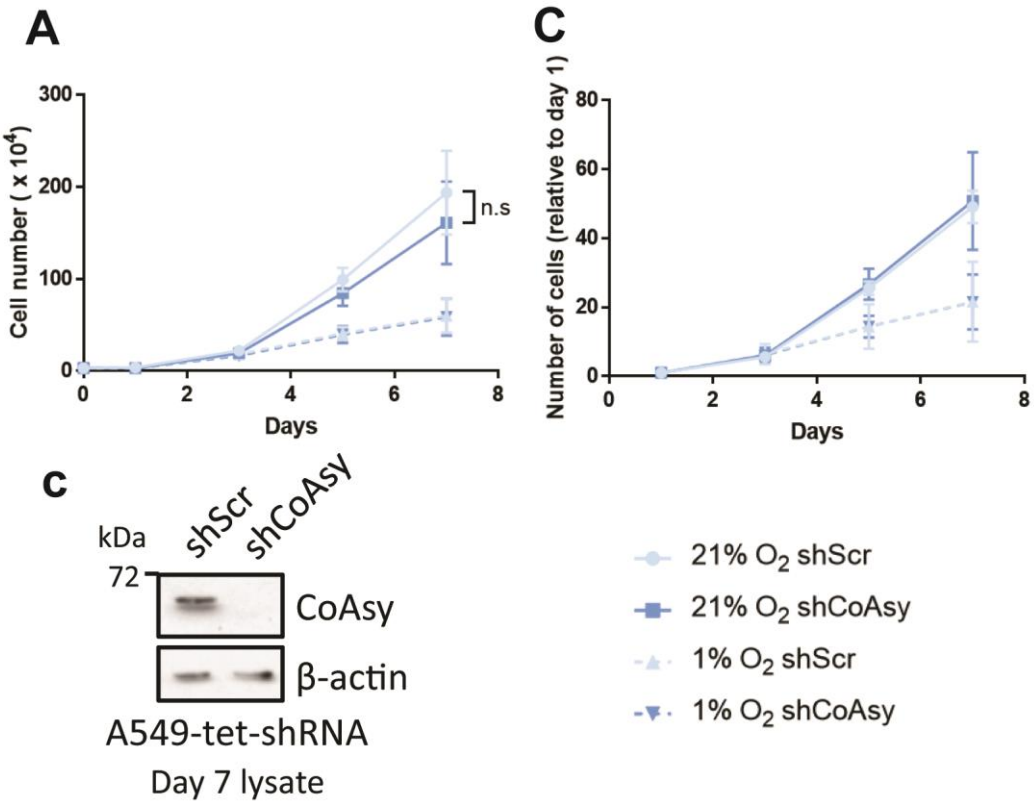

Figure 4.5.1.1: Loss of Coasy does not alter cell proliferation in A549 cells. Growth curve of A549-tet-shRNA cell lines. Lines were pretreated with doxycycline to activate shRNA knockdown before plating on day 0 and placing into normoxia (21% O_2) or hypoxia (1% O_2). Cells were counted on day 1, 3, 5 and 7. Cell counts were presented as average cell counts (**A**) or normalized to day 1 (**B**). CoAsy knockdown was confirmed by western blot (**C**). Results are shown as SD. n=3.

The plots in figure 4.5.1.1 indicate that there is no significant difference in cell proliferation following loss of CoAsy in A549 cells. When comparing average cell counts (**Fig. Figure 4.5.1.1A**) it appears in normoxia that there is a slight decrease in cell proliferation in 21% O_2 following loss of CoAsy however this result is not statistically significant, instead this difference likely arises from plating errors at day 0 as normalizing results to day 1 accounts for this error

and the proliferation rates are equal between groups (**Fig. Figure 4.5.1.1B**). Proliferation was significantly reduced in hypoxia for the shScr and shCoAsy cell lines and there was no difference observed between the groups.

There were no differences observed in cell proliferation between the A549 shRNA lines whilst manually counting the cells. As an alternative readout of cell proliferation the Incucyte live cell analysis was used. This machine takes bright field images of live cells and measures percentage confluency, by tracking changes of percentage confluency across a time course it is possible to measure cell growth. The A549-tet-shRNA cells were pretreated with doxycycline before plating and being placed into incucyte.

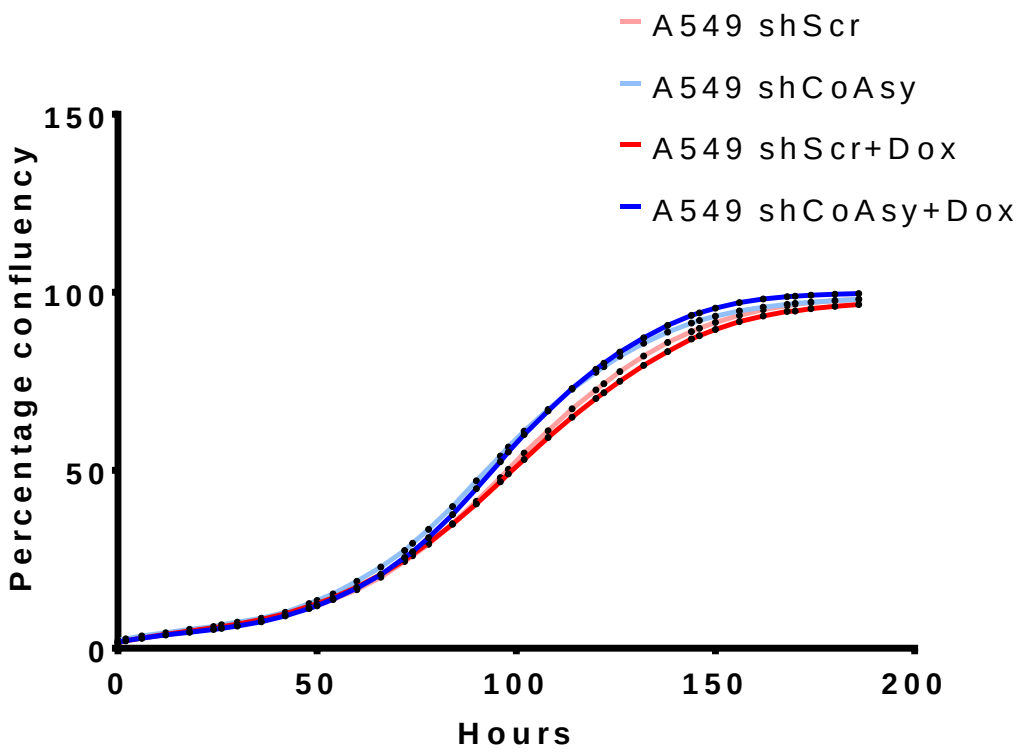

Figure 4.5.1.2: Analysis of cell proliferation of A549-tet-shRNA cells using incucyte: Growth curve of A549-tet-shRNA. Line represents average percentage confluency at time point indicated. A549 cells were pretreated with doxycycline (dark blue or red lines) or grown in media without doxycycline (pink or pale blue lines) before being replated and placed in the incucyte for analysis. n=1.

The incucyte data once again shows that there is no difference in proliferation following loss of CoAsy in these cell lines. The lines were cultured in the presence or absence of doxycycline, for both the shScr and shCoAsy lines there is no difference between the doxycycline treatment and media alone. This confirms that the dose of doxycycline used in the experiments is not sufficient to cause changes in cell proliferation. Furthermore this result shows that activation of the shRNA system does not further effect cell proliferation. As both the incucyte analysis and manual cell counts data shows no differences between the two lines it can be said that loss of CoAsy has no effect on cell proliferation in A549 cells.

4.5.3 Loss of CoAsy does not affect wound closure in A549 cells

In vitro wound healing assays are a well-established technique for measuring 2D migration of cancer cells. This technique involves growing cells to a complete monolayer before ‘scratching’ the plates to remove cells. The cells are then allowed to migrate and proliferate towards the free space provided by the scratch. A549-tet-shRNA cells were pretreated with doxycycline before plating and performing wound healing assay.

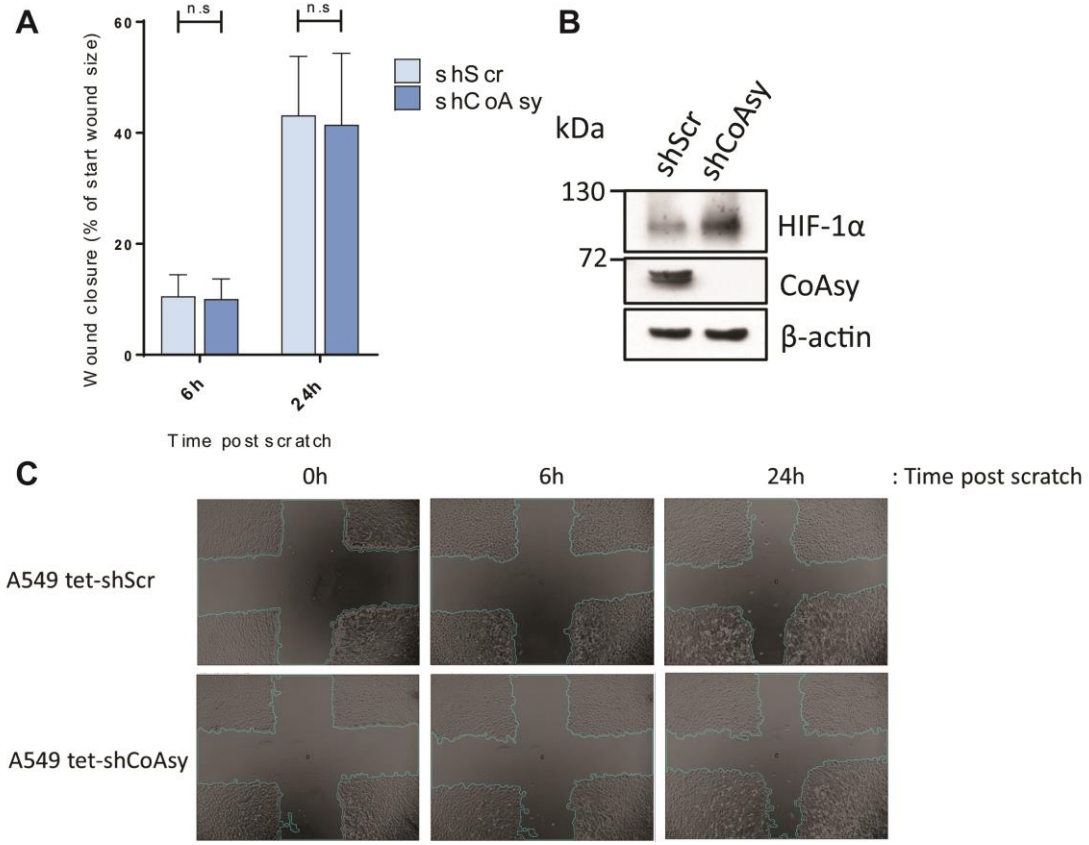

Figure 4.5.3: Loss of CoAsy does not affect wound healing in A549 cells. Wound healing assay in A549-tet-shRNA cells. A549 cells were pre-treated with doxycycline before replating in triplicate. Cells were left to adhere prior to scratching plates to remove cells. Wound closure was measured 6 and 24 hours later. N=3.

This wound closure assay shows that loss of CoAsy does not affect wound closure. As this assay was not performed in serum free media or after inhibition of cell proliferation, this assay does not solely measure changes in migration instead changes in proliferation will have an effect. However due to the previous observation that cell growth is not affected it is unlikely to alter the results in this assay. As the bar chart shows (**Fig. 4.5.3A**) there was no difference in wound closure between the cell lines after 6 hours or 24 hours of wound closure. Successful knockdown was confirmed by western blot (**Fig. 4.5.3B**), the western blot was also probed for HIF-1α, in concordance with previous results, there was increased HIF-1α expression. This data suggests that the elevated

HIF-1α following loss of CoAsy is not sufficient to increase cell migration in this cell type.

4.5.4 Loss of CoAsy does not affect clonogenic potential of A549 cells

Clonogenic assays are another well-established *in vitro* technique that assays the ability of a cell to survive and grow from a single cell, which acts as a marker for increased cell survival and proliferation. Cells are plated at an equal number and left to grow, before fixing, staining and counting the colonies. Increased colony number is associated with increased tumourigenicity. A549-tet-shRNA cells were pretreated with doxycycline to induce knockdown before plating at 100 cells and culturing for 10 days either in 21% O_2 or 1% O_2.

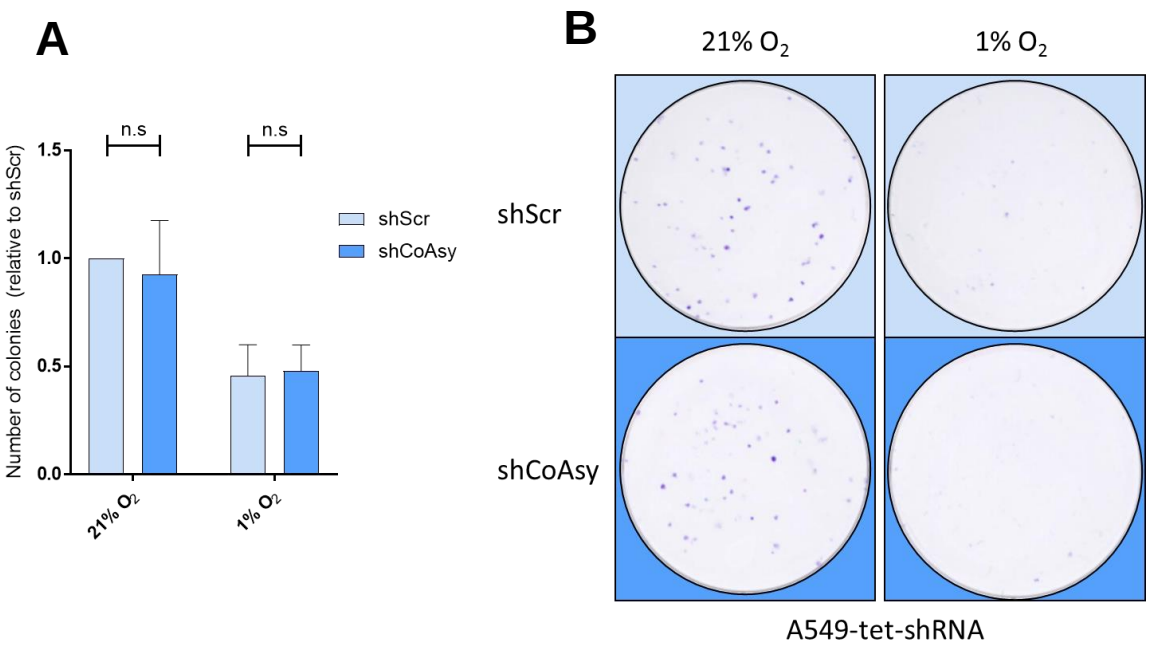

Figure 4.5.4: CoAsy does not alter clonogenic potential of A549 cells. Colony assay of A549-tet-shRNA cell lines. A549-tet-shRNA cells were pretreated with doxycycline before replating at 100 cells per well in 6 well plates before culturing for 10 days in 21% O_2 or 1% O_2. Colonies were fixed stained and counted. **A**) Bar chart of relative number of colonies, normalized to 21% O_2 shScr. **B**) Representative image of colonies. Statistical analysis performed is two-way ANOVA with Sidak's *Post Hoc* test. n=3.

Figure 4.5.1 shows that loss of CoAsy does not affect colony number in A549 cells. For both cells cultured at 21% O_2 and 1% O_2 there was no significant difference in number of colonies between shScr and shCoAsy cell lines. Two-way ANOVA indicates that there was a significant decrease in number of colonies between normoxic and hypoxic cells ($p<0.0001$, **Fig. 4.5.1A**) in addition to reduced number the colonies were also smaller in size as they contained fewer cells (**Fig. 4.5.4B**). This result is in keeping with earlier results indicating that in A549 cells there is no change in cell proliferation or fitness following loss of CoAsy.

4.5.5 Loss of CoAsy increases clonogenic potential of T47D cells

As there were no changes in cell proliferation, wound closure or clonogenic potential in A549 cells lacking CoAsy other lines were tested to ensure that this isn't specific to A549 cells. Therefore the clonogenic assays were repeated with T47D-tet-shRNA lines.

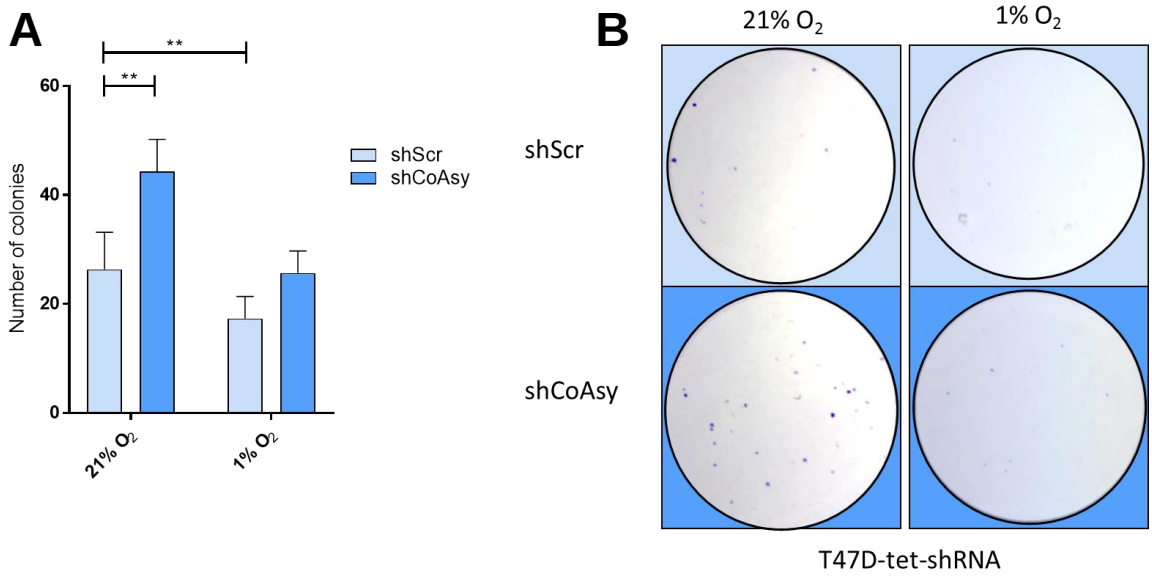

Figure 4.5.5: Loss of CoAsy increases clonogenic potential of T47D cells: Colony assay of T47D-tet-shRNA cell lines. T47D-tet-shRNA cells were pretreated with doxycycline before replating at 100 cells per well in 6 well plates before culturing for 10 days in 21% O_2 or 1% O_2. Colonies were fixed stained and counted. **A**) Representative bar chart of number of colonies. **B**) Representative image of colonies. Bar charts from other two biological replicates can be found in appendix. Statistical analysis performed is two-way ANOVA with Sidak's Post Hoc test. n=3.

The clonogenic assay in T47D shows a stark difference to that in A549 cells, as loss of CoAsy shows a significant increase in number of colonies in cells grown at 21% O_2 ($p = 0.0065$). Cells cultured in hypoxia showed a slight increase in colony number however this result was not statistically significant ($p = 0.175$). As in A549 cells there is a significant decrease in colony number in the cells cultured in hypoxia compared to normoxia. This increase in clonogenic potential suggests that loss of CoAsy in T47D cells may confer a

fitness advantage that allows cells to grow from a single cell. Furthermore this highlights a difference between the role of CoAsy loss between A549 and T47D cells.

4.6 Summary

This chapter sought to identify how loss of CoAsy drives HIFα expression. Whilst the mechanism is still unclear, the data suggests that CoA or a CoA derivative negatively regulates HIFα. The data further points to HIFα being regulated at the post-translational stage, with both the 30-389 and ODDD amino acid domains of HIF-1α being affected. Finally the chapter showed that in A549 cells there was no difference in proliferation, wound closure or clonogenic potential however there was an increase in clonogenic potential in the luminal A breast cancer cell line T47D. The biological consequences of this are unclear and further lines will need to be tested, however this may highlight a difference in the role of CoAsy as a tumour suppressor in lung and breast cancer.

Results Chapter Three:

Analysis of CoAsy expression in lung and breast cancer

5.1 CoAsy expression in non-small cell lung cancer (NSCLC)

5.1.1 Analysis of CoAsy copy number from TCGA data

The previous results chapters have shown that CoAsy is a novel negative regulator of HIF transcriptional activity and protein stability in a number of cell types *in vitro*. However it is important to confirm that this regulation is relevant in patients; specifically, We hypothesise that CoAsy may be lost in lung cancer and ask the whether CoAsy expression can predict patient morbidity. As the siKinome screen and subsequent validation was performed in lung adenocarcinoma cells (A549), CoAsy expression in non-small cell lung cancer was investigated.

To first investigate *COASY* expression, gene copy number analysis data from TCGA was analysed using the open source platform cbioportal. This platform allows analysis of a wide variety of datasets including TCGA provisional datasets.

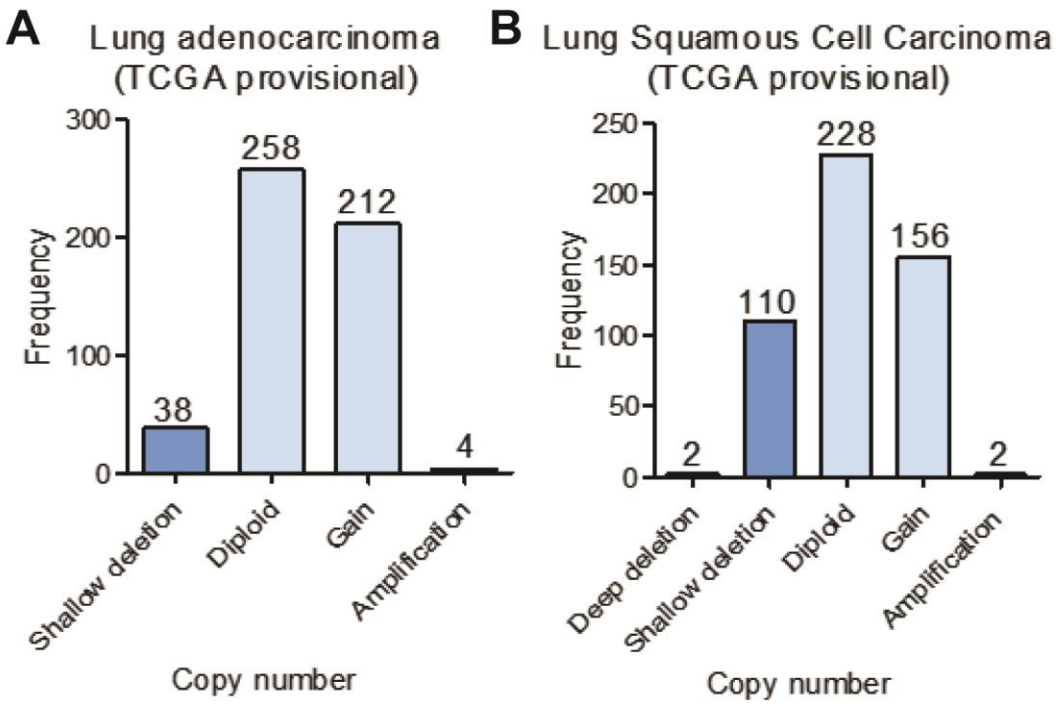

Figure 5.1.1.1: Copy number analysis of *COASY* in lung cancer: Copy number analysis of *COASY* in Lung adenocarcinoma (TCGA provisional) and lung squamous cell carcinoma (TCGA provisional). Plots show frequency of copy number status.

Copy number analysis of *COASY* in lung cancer TCGA data reveals distinct trends between adenocarcinoma and squamous cell carcinoma. This is likely due to the differing cell types of origin for these cancers. In the lung adenocarcinoma patient cohort (**Fig 5.1.1.1A**), no patients had deep deletion of the *COASY* gene and only 7.4% had shallow deletion. Over half the patients were diploid for *COASY* and a further 212 (41.4%) had a gain in copy number. In the lung squamous cell carcinoma cohort, deep deletions and amplifications were rare occurring in 2 patients each. However shallow deletions were more frequent than observed in the adenocarcinoma cohort (22% of patients). Most patients were diploid for *COASY* and there was still a large amount of patients with gain in copy number for *COASY*. In addition to the copy number analysis for this cohort, mRNA-seq data has been performed quantifying *COASY*

expression, plotting this against copy number shows that the copy number analysis correlates with mRNA expression thereby allowing conclusions on gene expression to be drawn from the copy number analysis data. Taken together this data suggests that a degree of CoAsy loss does occur in lung cancer, however this is not in the majority of cases and appears to be more frequent in squamous cell carcinoma.

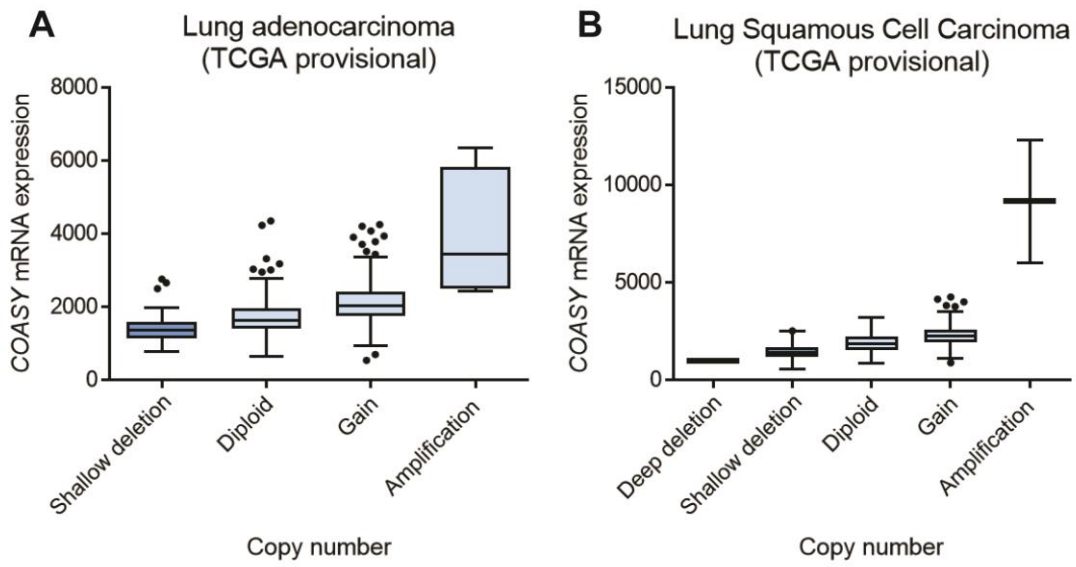

Figure 5.1.1.2: *COASY* copy number correlates with mRNA expression: Box and whiskers plot (Tukey) of *COASY* copy number analysis plotted against CoAsy mRNA expression measured by RNA-seq (RNA-seq V2 RSEM). Data is from TCGA provisional datasets obtained from cbioportal server.

5.1.2 Analysis of CoAsy mRNA expression as a prognostic marker in NSCLC

In addition to determining the extent of CoAsy loss in lung cancer, the effect of CoAsy expression on survival was also investigated. To this end, Dr. Jun Wang performed univariate analysis of CoAsy expression from TCGA data correlating with overall survival.

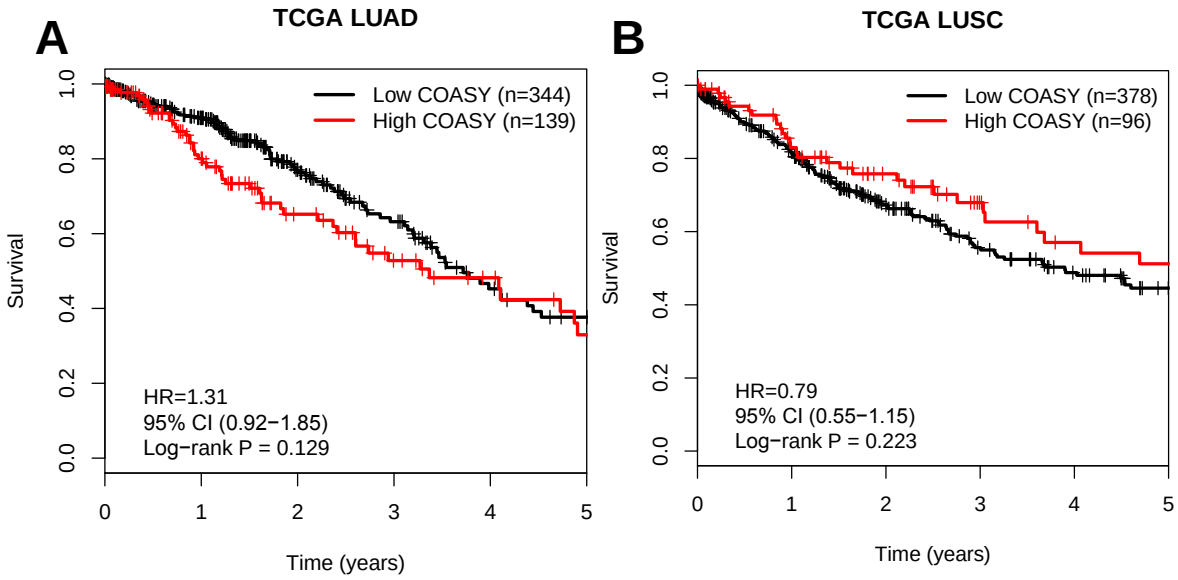

Figure 5.1.2: *COASY* expression does not correlate with patient survival in lung TCGA datasets. Kaplan-Meier plots of patient overall survival stratified by *COASY* expression for both lung adenocarcinoma (**A**) and squamous cell carcinoma (**B**). Graphs were prepared by Dr. Jun Wang and the data is from the provisional TCGA dataset. Results show that *COASY* expression is not an independent predictor of patient outcome for either squamous cell carcinoma or adenocarcinoma

Figure 5.1.2 shows that CoAsy expression data from TCGA does not serve as a significant prognostic marker for either lung adenocarcinoma or squamous cell carcinoma. In lung adenocarcinoma the hazard ratio (HR) is 1.31 indicating that higher CoAsy mRNA expression indicates a less favourable patient outcome and reduced survival, however this is not statistically significant as the P-value is 0.129. Conversely, the HR in lung squamous cell carcinoma data set is 0.79 suggesting that low CoAsy confers poor patient outcome however once again this is not significant (p = 0.223). As neither LUAD nor LUSC datasets show a significant correlation with patient outcome it can be said that CoAsy mRNA expression is not an independent indicator of patient outcome. However further multivariate analysis with other patient stratification such as patient age, stage or even co-expression with other hypoxic markers may reveal statistically significant trends in patient outcome. Despite neither dataset revealing

significant correlation, the difference in hazard ratios between the lung adenocarcinoma and squamous cell carcinoma is interesting nonetheless.

5.1.3 Analysis of CoAsy mRNA expression as a prognostic marker using KMplot server

KMplot [216] is an online portal that contains relapse free and overall survival data from a curated database of samples from TCGA, EGA and GEO sources. This allows the user to split patient samples into two groups based upon expression of biomarker of interest. This was performed twice for *COASY,* once with the cut off point adjusted to achieve maximum significance and again with patients separated by median *COASY* expression.

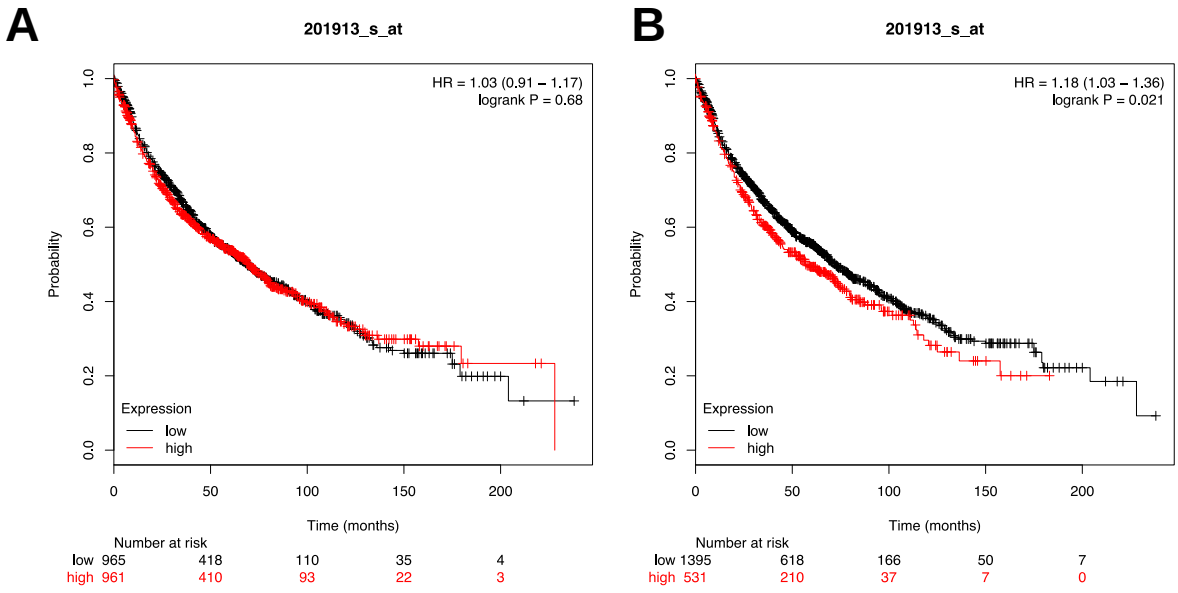

Figure 5.1.3: High *COASY* expression correlates with poor patient outcome in lung cancer. Kaplan-Meier plots of lung cancer patient overall survival stratified by *COASY* expression. Patients were either stratified by median (**A**) or by a margin to create optimal statistical significance (**B**).

For the probe used in the analysis (Affymetrix probe = 201913_s_at) there was a total of 1926 patients. When separating patients by the median *COASY*

expression there was no significant difference in patient prognosis with a HR of 1.03 and a logRank P value of 0.68. With the option to stratify patients in such a way to maximize the statistical significance, there is a significant difference in patient prognosis with high *COASY* expression correlating with poor outcome. The HR is 1.18 and the logRank P value is 0.021 suggesting a small difference similar to that that observed in the adenocarcinoma TCGA data. This dataset contains a mixture of both adenocarcinoma and squamous cell carcinoma patients as well as other undefined lung cancer patients.

Considering survival data from both TCGA and the larger cohort of lung cancer patients on the KMplot server, it can be said that in lung cancer *COASY* mRNA expression does not act as an independent prognostic marker.

5.1.4 Optimisation of antibody to detect CoAsy in formalin fixed paraffin embedded tissue microarrays.

As the lung data for *COASY* mRNA data did not show statistically significant results, it does not mean that CoAsy protein expression is not relevant in cancer. There are numerous reports highlighting the poor correlation between mRNA expression and protein expression, this is also true in hypoxia with alternative translation machinery resulting in reduced correlation between mRNA expression and the resulting protein. Thereby suggesting that mRNA is a poor indicator of protein expression in cancer. To measure CoAsy protein in lung cancer, a TMA containing a mixture of adenocarcinoma and squamous cell carcinoma patients was stained for CoAsy protein expression. However prior to staining and analysis the antibody requires optimization to minimize

background staining. One commercially available antibody has previously been optimized for immunohistochemistry with antigen retrieval techniques optimized therefore this was used for staining. To identify an appropriate concentration of primary antibody for staining, multiple dilutions were used.

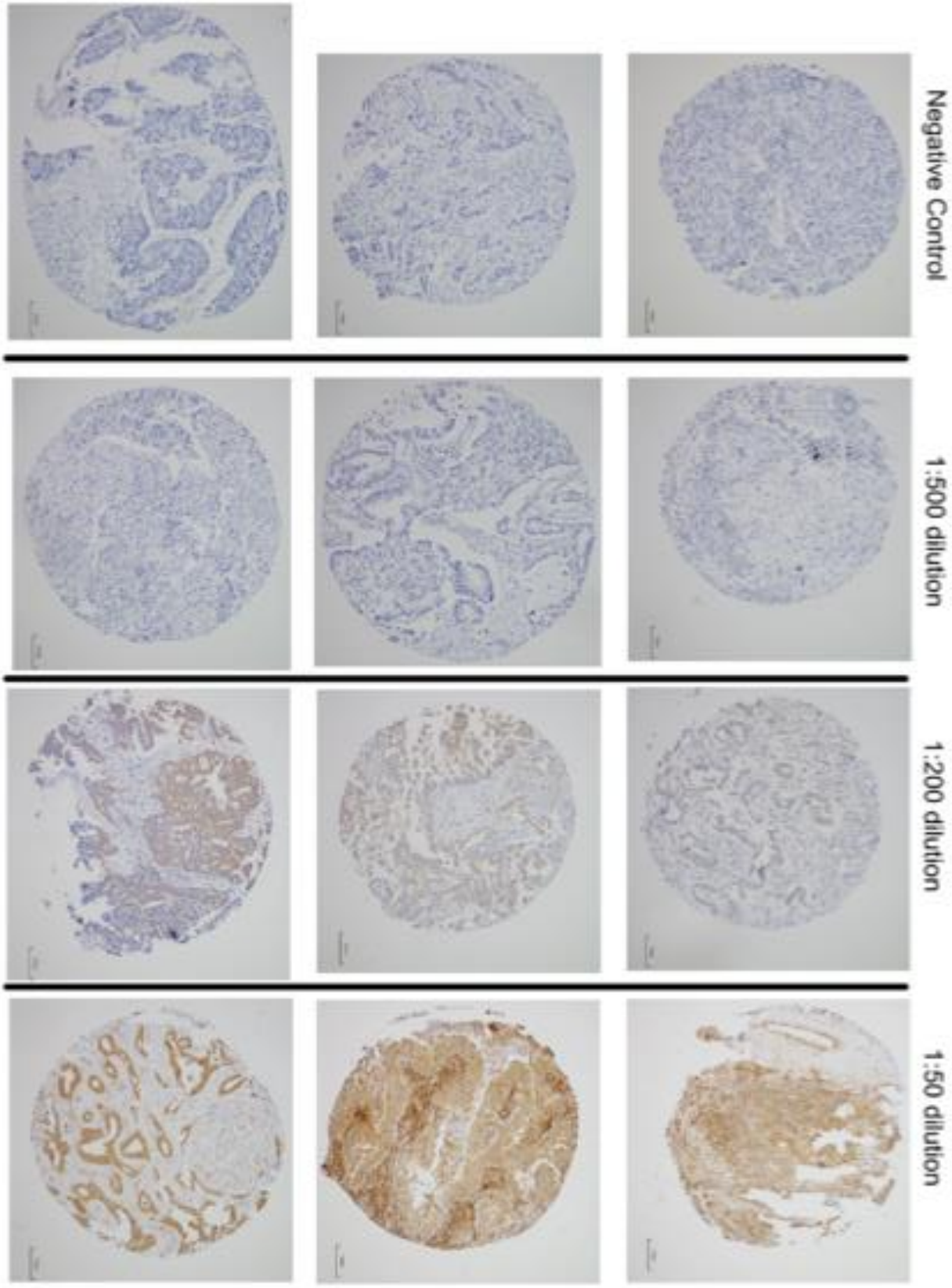

Figure 5.1.4: Optimisation of anti-CoAsy antibody for IHC. The rabbit polyclonal anti-CoAsy (ab155551) was used at 1:50, 1:200 and 1:500 on a test lung TMA to determine appropriate dilution for subsequent staining.

Across the dilutions used there was a wide variety of staining intensity observed. The negative control, staining without primary antibody, showed no staining at all indicating any colour from the DAB detection agent is as a result of reactivity with the primary antibody. To ensure scoring is accurate and robust, the primary antibody concentration should be adjusted such that the range in staining intensities is as broad as possible. Primary antibody dilution of 1:500 resulted in no visible staining at all. Dilutions of 1:200 showed a degree of staining however across the slide there was not a large range in staining intensities. The staining observed with primary antibody at 1:50 resulted in intense staining as well as some regions of no visible staining and no visible staining in the surrounding stromal tissue. However the majority of cores across the TMA had high levels of staining making it difficult to differentiate between high and middle levels of CoAsy expression. Therefore the staining of the TMA was performed with primary antibody at 1:75.

5.1.5 High CoAsy expression in lung cancer results in poor patient prognosis and correlates with high HIF expression and VEGF expression.

Following staining of the lung TMA, cores were scored by Dr. Ian Spendlove (University of Nottingham). The scoring analysis used was H-score analysis, this is performed by defining staining intensities as high, medium and low which are given a numerical value (+3, +2 and +1 respectively). H-score is calculated by multiplying the percentage of cells that fit into each category for each core. This results in a number between 0-300. Frequency of H-score is plotted to check for normal distribution and discriminatory cut off is determined to determine which samples are ‘CoAsy High’ or ‘CoAsy Low’.

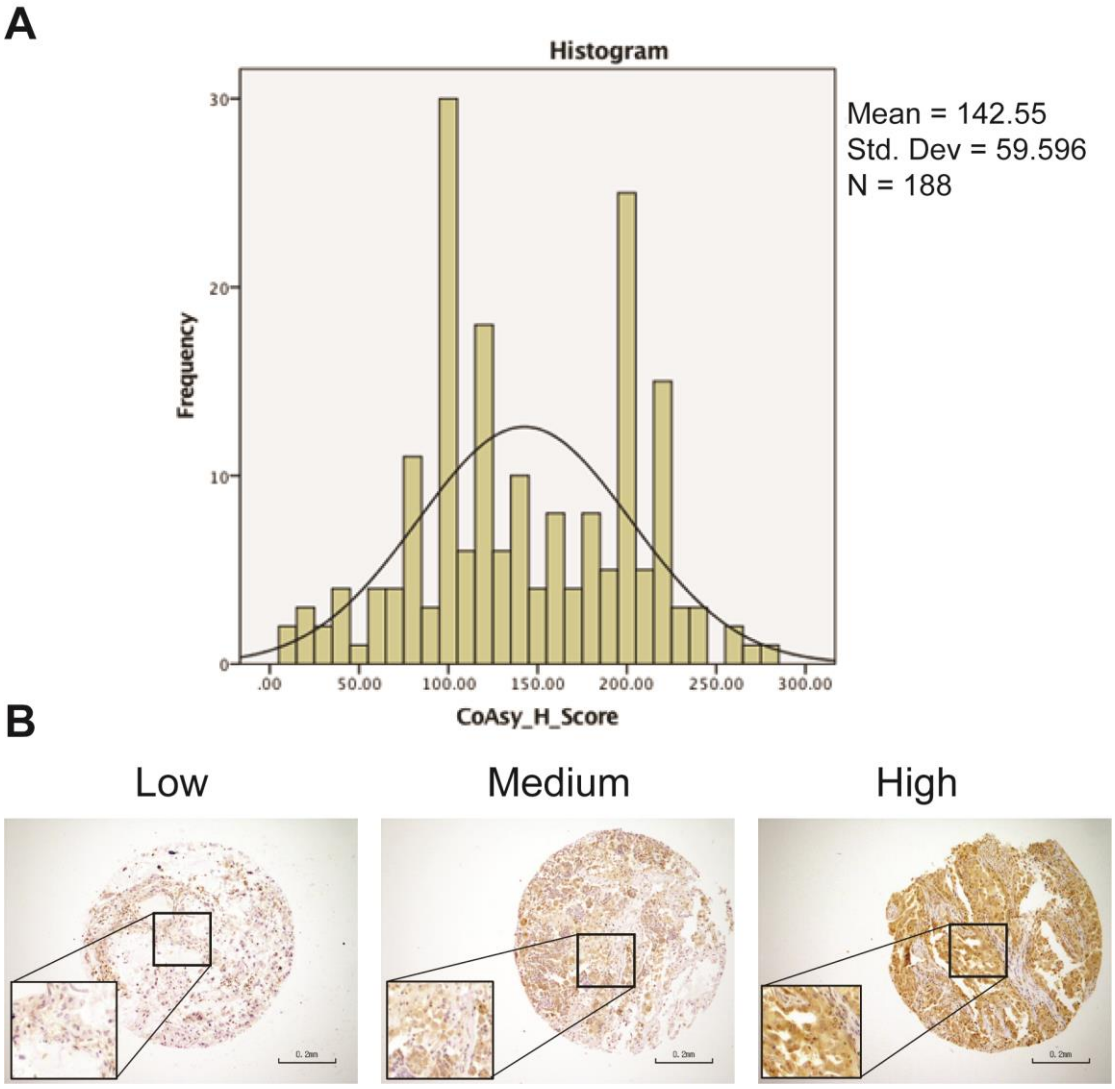

Figure 5.1.5.1: H-scores from CoAsy stained lung TMA: A) Scores plot of H-score scoring of CoAsy staining in the lung cancer TMA, the plot shows a bimodal distribution with two peaks at 100 and 200. **B)** Representative cores for low, medium and high intensity staining intensity used for scoring TMA.

Figure 5.1.5.1 shows representative cores of staining intensities. The staining observed was cytoplasmic with no nuclear staining observed. This matches the literature as CoAsy is found anchored in the mitochondrial membrane facing into the cytoplasm. One interesting feature observed was intense staining in infiltrating lymphocytes when present in the cores; the biological consequence of this is unclear at this date. The plot of scores forms a bimodal distribution

with two peaks at 100 and 200. A cut off point of 142 was used to define CoAsy high or low patients. Dr. Ian Spendlove performed statistical analysis on this cohort.

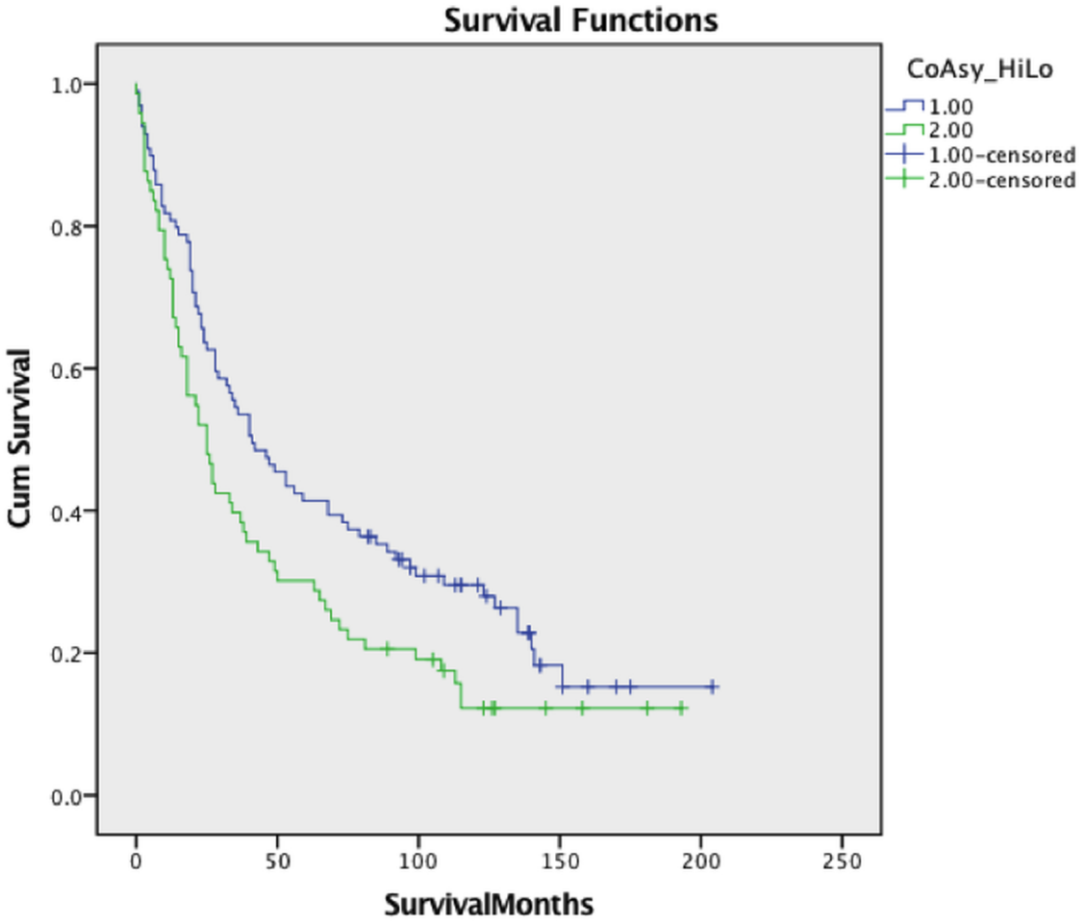

Test	Chi-square	Degrees of freedom	Significance (p value)
Log Rank (Mantel-Cox)	5.082	1	0.024

Figure 5.1.5.2: Kaplan-Meier plot of lung cancer patient survival stratified by CoAsy protein expression. Patients with low CoAsy expression are in blue whereas patients with high CoAsy expression are in green. Results show that patients with high CoAsy expression have a significantly poorer outcome than low expression (p = 0.024).

Figure 5.1.5.2 shows the resulting Kaplan-Meier plot from the lung TMA stained for CoAsy expression. The line in blue represents low CoAsy expression and the line in green is high CoAsy expression. The graph shows that patients with

high CoAsy expression have a poorer prognosis compared to those with low CoAsy expression. The Log Rank (Mantel-Cox) confirms that the difference between the groups is statistically significant (p=0.024). This result is surprising as the *in vitro* work suggests that loss of CoAsy upregulates the known oncoproteins HIF-1α and HIF-2α, which would suggest that loss of CoAsy would result in poor patient outcome as tumours with high HIFα in general have a poorer outcome. This TMA has also previously been stained for HIF-1α expression and the HIF target gene, VEGF. With these additional datasets it is possible to determine if there is a correlation between CoAsy expression and HIF-1α and VEGF. HIF-1α and VEGF staining and statistical analysis was performed by Dr. Ian Spendlove.

CoAsy HiLo vs HIF1α _two_cats Crosstabulation

Count

		HIF1A_two_cats		Total
		low	high	
CoAsy_HiLo	1=low	78	9	87
	= hi	53	17	70
Total		131	26	157

Table 5.1.5.1: Counts of intact cores from both CoAsy and HIF-1α staining

Table 5.1.5.1 shows the number of intact cores common across for each stained TMA. During the process of sectioning slides from the block, cores may become damaged or lost. Furthermore during the staining process and subsequent washes others may fall off therefore subsequent correlation analysis can only consider cores common between both datasets.

Chi-Square Tests

	Value	df	Asymp. Sig. (2-sided)	Exact Sig. (2-sided)	Exact Sig. (1-sided)
Pearson Chi-Square	5.456[a]	1	.020		
Continuity Correction[b]	4.493	1	.034		
Likelihood Ratio	5.458	1	.019		
Fisher's Exact Test				**.030**	**.017**
Linear-by-Linear Association	5.421	1	.020		
N of Valid Cases	157				

a. 0 cells (0.0%) have expected count less than 5. The minimum expected count is 11.59.

b. Computed only for a 2x2 table

Table 5.1.5.2: Chi-square tests of table above comparing likelihood of CoAsy expression to be related to HIF-1α expression

Table 5.1.5.2 shows the Chi-square tests for this dataset, this statistical test measures the 'goodness of fit' for a dataset therefore acts as a readout for correlation between two variables. Table 5.1.5.2 shows an exact significance (2-sided) of p = 0.030 which shows that there is a statistically significant relationship between the two datasets. Comparing the groups in first table it indicates that the correlation is a positive relationship suggesting that in his the cohort the patients with high CoAsy expression are more likely to have high HIF-1α expression.

CoAsy_HiLo * vegf_two_cats Crosstabulation

Count

		vegf_two_cats		Total
		low	high	
CoAsy_HiLo	1=low	25	64	89
	= hi	8	63	71
Total		33	127	160

Table 5.1.5.3: Counts of intact cores from both CoAsy and VEGF staining

Chi-Square Tests

	Value	df	Asymp. Sig. (2-sided)	Exact Sig. (2-sided)	Exact Sig. (1-sided)
Pearson Chi-Square	6.827[a]	1	.009		
Continuity Correction[b]	5.838	1	.016		
Likelihood Ratio	7.172	1	.007		
Fisher's Exact Test				**.010**	**.007**
Linear-by-Linear Association	6.784	1	.009		
N of Valid Cases	160				

a. 0 cells (0.0%) have expected count less than 5. The minimum expected count is 14.64.

b. Computed only for a 2x2 table

Table 5.1.5.4: Chi-square tests of table above comparing likelihood of CoAsy expression to be related to VEGF expression

The analysis was repeated as before with VEGF staining, in this cohort once again the Pearson's Chi-square test shows that the relationship between CoAsy and VEGF is significant and therefore did not happen by chance. Once again this is a positive relationship suggesting that in this cohort patients with low CoAsy expression are more likely to have low VEGF expression and vice versa.

5.1.6 Summary

Taken together this data shows that there is a small proportion of patients with reduced *COASY* mRNA expression and loss of copy number in both adenocarcinoma and squamous cell carcinoma. However when looking at survival analysis of TCGA data there was no significant difference. Analysis of a small lung TMA showed that high CoAsy expression correlated with poor patient outcome. Interestingly there was also a positive correlation with CoAsy and both HIF-1α and the target gene VEGF. This result is in contrast to the *in vitro* data where high HIF-1α was observed with low levels of CoAsy, which may suggest why the trend observed with CoAsy expression and overall survival did not match the original hypothesis in this cohort.

5.2 CoAsy expression in breast cancer

In addition to analysing CoAsy expression in lung cancer, we further examined CoAsy expression in breast cancer. This was important as the *in vitro* data showed that loss of CoAsy resulted in stabilized HIF-1α and HIF-2α in T47D cells, which are luminal A breast cancer cells.

5.2.1 Analysis of *COASY* and *PANK1* in an in-house dataset of breast cancer patients

COASY expression was analysed in an in-house cohort of breast cancer patients, in addition to CoAsy, *PANK1* expression was also assessed, as there may be other defects across the CoA biosynthesis pathway. The in-house cohort is a small well annotated cohort (n = 19) with proteomics, phospho-proteomics and RNA-seq data from each sample. In addition to the RNA-seq data, tissue sections also collected and patients have been stratified by receptor status. Each patient is still alive therefore no survival data can be collected. However serial samples were collected from tumour, adjacent tissue (2.5 cm^2 from primary tumour) and surrounding tissue (between 5-10 cm^2 from primary tumour), this data allows comparisons to be made in gene expression in tumour compared to matched adjacent normal tissue.

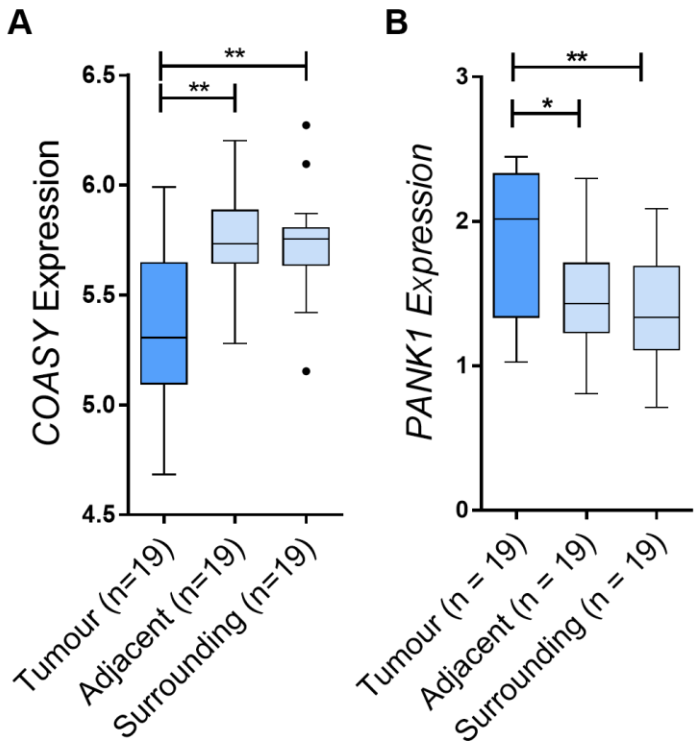

Figure 5.2.1.1: RNA-seq data of *COASY* and *PANK1* : RNA-seq data showing expression of *COASY* (**A**) and *PANK1* (**B**) in the in-house cohort of breast cancer. Samples were taken from primary tumour or adjacent (2.5 cm from primary tumour) and surrounding tissue (over 5 cm from primary tumour). Statistical analysis is two tailed paired T-tests.

The RNA-seq data from the in-house cohort shows a significant reduction in *COASY* expression in tumour compared to the adjacent and surrounding tissue ($p = 0.00160$ and $p = 0.00217$ respectively). In contrast to this, one of the enzymes catalyzing the first step in CoA biosynthesis, PANK1 shows the opposite result with increased expression in tumour compared to the surrounding tissue ($p = 0.0381$ and $p = 0.00681$ respectively). The biological consequence of this is not entirely clear, as expression of PanK isoforms generally dictates the amount of CoA. However reduced expression of CoAsy could also reduce flux through the pathway and thereby inhibit CoA production. In order to best test this direct metabolomics should be performed to measure CoA and levels of intermediates in the CoA pathway (such as

4’phosphopantetheine, the substrate for CoAsy). This cohort has also been stained for the three important receptors in breast cancer (ER, HER2 and PR) that allows for further analysis and stratification of patients by receptor status.

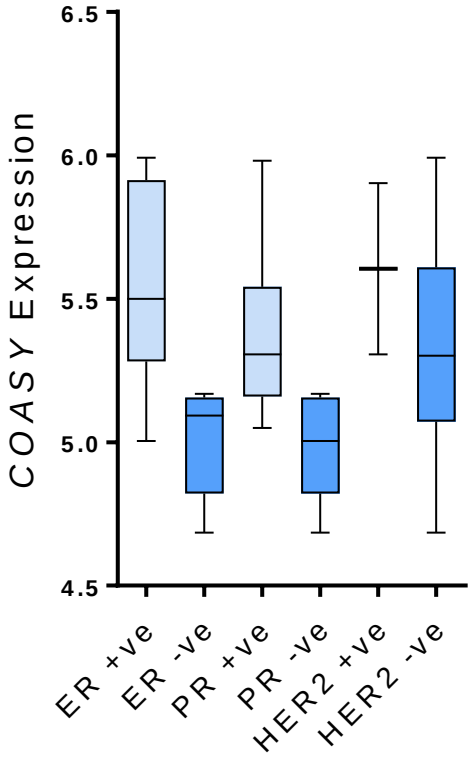

Figure 5.2.1.2: *COASY* expression from in-house cohort stratified by receptor status. RNA-seq data showing expression of *COASY* in the in-house cohort. Patients were stratified by receptor status (ER, PR and HER2) as determined by IHC.

As can be seen in figure 5.2.1.2, low *COASY* mRNA expression was observed in ER and PR negative patients. There appears to be a trend towards lower expression in HER2 negative patients, however due to the small sample size (2 patients with HER2 positive), it is not possible to perform statistical analysis on this dataset. The reduced *COASY* expression in the receptor negative patients is of particular interest as triple negative breast cancer (patients lacking all three receptors) remains an area of unmet clinical need and lacks efficient targeted therapies. Following on from this result, further investigation was

performed in to the correlation between CoAsy expression and receptor status in breast cancer.

5.2.2 CPTAC proteomics database reveals low CoAsy protein expression in ER and PR negative tumours

Due to the small sample size in the in house cohort and thus limited, larger datasets were analyzed to test the correlation between low CoAsy expression and lack of ER and PR receptors in breast cancer. To this end, data from the national cancer institute's Clinical Proteomic Tumour Analysis Consortium (CPTAC) was used. This dataset contains integrated proteomics and complimentary genomics/RNA-seq data that is all made publically available and added to the TCGA (provisional) dataset. Using the online portal, cbioportal, CoAsy protein levels were correlated against both ER and PR receptor status.

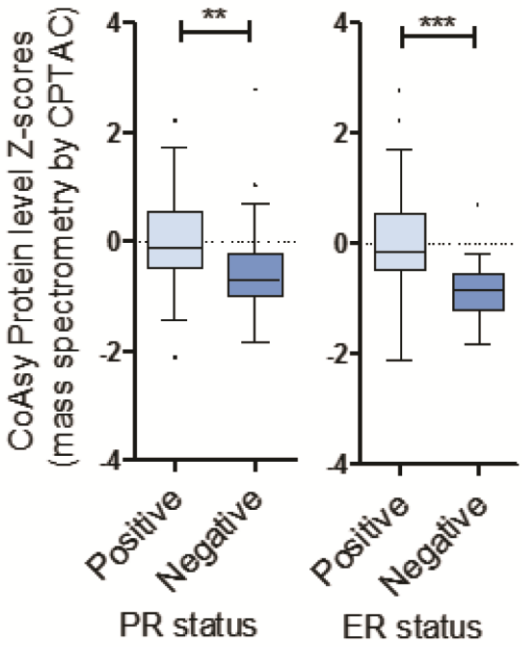

Figure 5.2.2: CoAsy protein expression from CPTAC data stratified by ER and PR status: Tukey plot of CoAsy protein expression (from CPTAC database) in breast cancer patients stratified by PR and ER status. Data was obtained from cbioportal. Statistical test performed was unpaired two tailed T-test.

The data from CPTAC confirms the findings observed in Figure 5.2.1.2 and further suggests that low CoAsy expression is observed in patients lacking ER and PR receptor possibly implicating CoAsy protein level as a biomarker for patients with triple negative breast cancer. There were numerous metrics for HER2 expression within this dataset, however due to the poor consensus between different methods of measuring HER2 and lack of binary system as employed in figure 5.2.1.2, this data has not been included.

5.2.3 Triple negative breast cancer cell lines express low levels of CoAsy protein

A panel of breast cell lines were analysed for CoAsy protein expression as well as HIF-1α. In addition to this RNA was also collected and *COASY* mRNA was measured by qRT-PCR. The panel included 3 ER positive cell lines, a HER2 positive and three triple negative breast cancer cell lines.

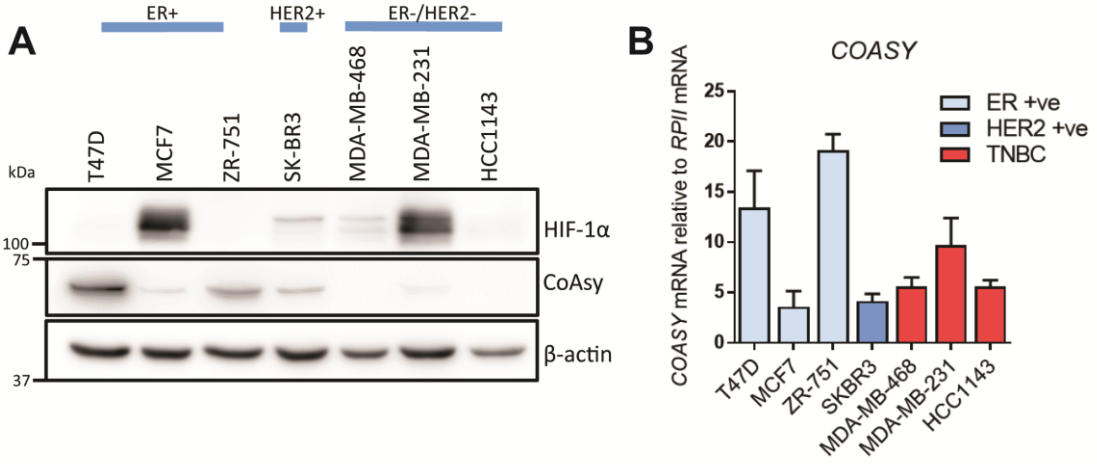

Figure 5.2.3: CoAsy protein and mRNA expression in breast cancer cell lines. CoAsy protein (**A**) and mRNA (**B**) expression in a panel of breast cancer cell lines. Western blot is representative image from n = 3 biological replicates. qRT-PCR of *COASY* mRNA is 3 biological replicates ± SD.

Western blot analysis (**Fig. 5.2.3**) shows a correlation between CoAsy expression and HIF-1α protein levels in the three ER positive samples tested, with the MCF7 cells showing the lowest CoAsy expression and stabilized HIF-1α even though samples were cultured at 21% O_2. The triple negative cell lines (MDA-MB468, MDA-MB231 and HCC1143) show reduced CoAsy expression compared to the receptor positive lines. The qPCR data shows the T47D and ZR-751 expressing high levels of *COASY* mRNA reflecting the high protein levels observed in the western blot. Interestingly the mRNA levels observed in triple negative patients were not lower than the HER2 positive or MCF7 cells which is contrast to the protein levels. This highlights that in cancer mRNA levels do not always reflect protein expression [217]. Considering the in-house cohort, proteomics data and the results from the cell lines, it can be said that CoAsy is lost in breast cancer patients compared to surrounding tissue and loss of CoAsy is more frequently observed in triple negative breast cancer patients.

5.2.4 Correlation of *COASY* mRNA and HIF target genes from TCGA data

The *in vitro* data showed that loss of CoAsy resulted in increased HIFα protein levels and activity observed with both synthetic reporters as well as endogenous target genes. Whilst causality cannot be determined in patient datasets, correlation and trends in HIF target genes can be measured. To this end *COASY* mRNA was correlated with mRNA expression of HIF target genes. Target genes were selected from Dayan *et al.,* 2006 and Briggs *et al.,* 2016 [81, 88]. These lists were selected due to encompass both FIH-dependent and independent targets (from Dayan *et al.*) and Briggs *et al.* identified a signature

of hypoxic responsive genes that were upregulated in triple-negative breast cancer.

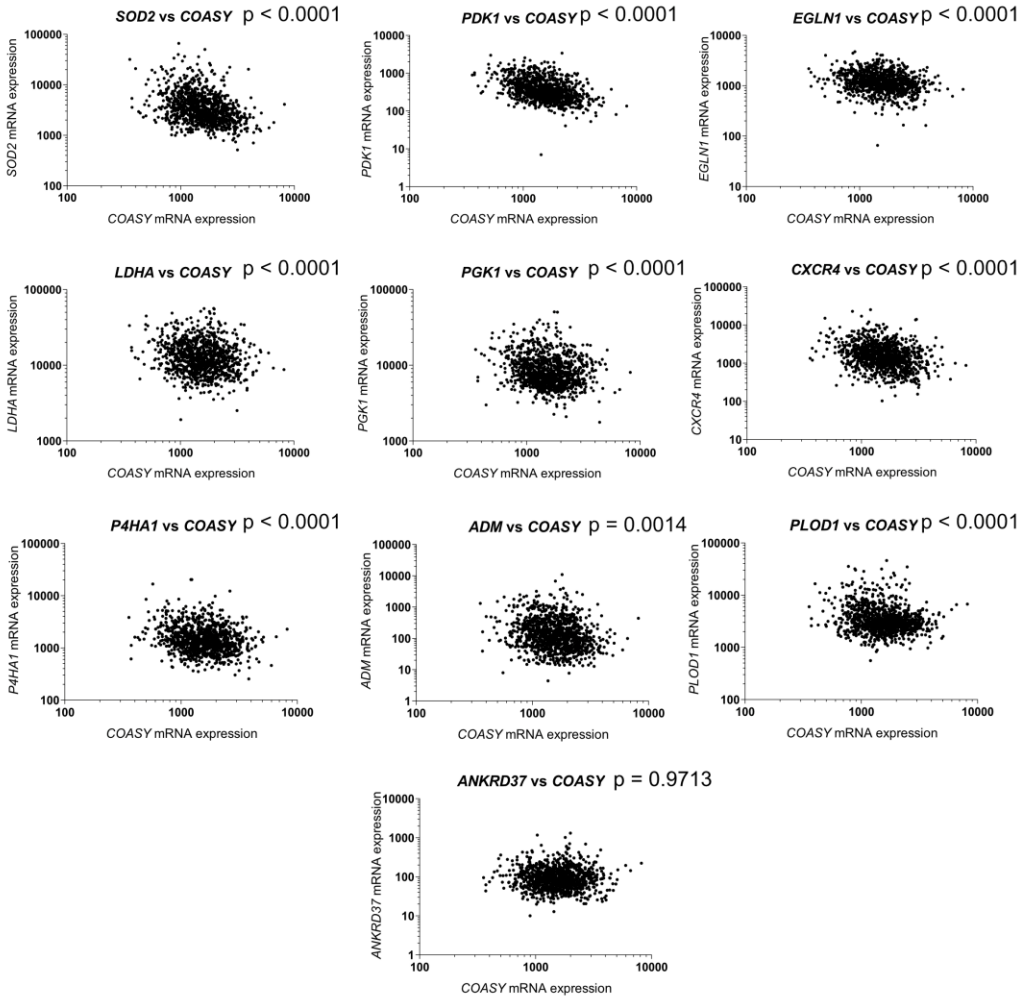

Figure 5.2.4: Correlation of *COASY* mRNA expression and HIF target genes. Scatter plots showing correlation of HIF target genes with *COASY* expression in breast cancer patients. Data was taken from TCGA (provisional) accessed on cbioportal.

Gene Correlated with *COASY*	Pearson's Correlation Coefficient	Spearman's Correlation Coefficient	P-value
PDK1	-0.3246	-0.4347	<0.0001
SOD2	-0.2266	-0.3535	<0.0001
EGLN1	-0.1925	-0.2129	<0.0001
LDHA	-0.1259	-0.1576	<0.0001
PGK1	-0.1393	-0.1827	<0.0001
CXCR4	-0.2016	-0.3055	<0.0001
P4HA1	-0.1438	-0.1947	<0.0001
ANKRD3	-0.001088	-0.01743	0.9713 (P) 0.5636 (S)
ADM	-0.09646	-0.2262	0.0014 (P) <0.0001 (S)
PLOD1	-0.129	-0.1667	<0.0001

Table 5.2.4: Correlation coefficients and significance from TCGA (provisional) RNA-seq data of *COASY* and a number of HIF-target genes. Correlation analysis was performed using Graphpad Prism 7.

Across a number of HIF target genes (9/10 analysed) there was a statistically significant negative correlation between *COASY* expression and HIF target gene. The P-value was $p < 0.0001$ for the majority of targets analysed indicating these results were highly significant. However this is likely due to the large sample number present ($n = 1100$). It is important to consider the correlation coefficient. Negative values represent a negative correlation and higher negative values, up to -1, indicates a stronger negative correlation. For HIF target genes such as *PDK1* and *SOD2* the Spearman's correlation coefficient was below -0.3 indicating that this is a strong correlation however other genes such as *LDHA* are less strongly correlated. Interestingly *ANKRD3* expression did not correlate with *COASY* expression, as Spearman's correlation coefficient was -0.01743 and p value was 0.5636. This suggests that not all HIF target

genes are affected by *COASY* expression and this may be a tissue or tumour type specific effect. There was no clear trend when comparing HIF target genes that have been reported to be FIH sensitive or insensitive. *LDHA* has been reported to be a gene that is inhibited by FIH whereas *PGK1* has been reported to be insensitive to FIH activity, these two genes express similar correlation coefficients when compared to *COASY* expression in this dataset. The biological significance of both FIH dependent and independent targets is unclear as each could be derived from different regions across the tumour and oxygen tensions will vary greatly, therefore it is unclear whether FIH will be active in the tumours from which the samples were derived. Taken together these data shows that in patient RNA-seq data there is a small but consistent negative correlation between *COASY* expression and a number of target genes, which strongly supports the *in vitro* data presented earlier where loss of CoAsy resulted in increased HIFα, although it is important to note that this datum is a correlation and cannot determine causality.

5.2.5 *COASY* expression is an independent prognostic biomarker in breast cancer

The previous results have shown that there is a loss of *COASY* expression in breast cancer and this correlates with both the triple negative breast cancer subtype and high expression of HIF target genes. As triple negative breast cancer patients often have poor prognosis compared to receptor positive patients and high HIF expression has been associated with poor prognosis we hypothesized that *COASY* might act as an independent marker for patient

outcome. To this end *COASY* expression was used to stratify patients on the KMplot server.

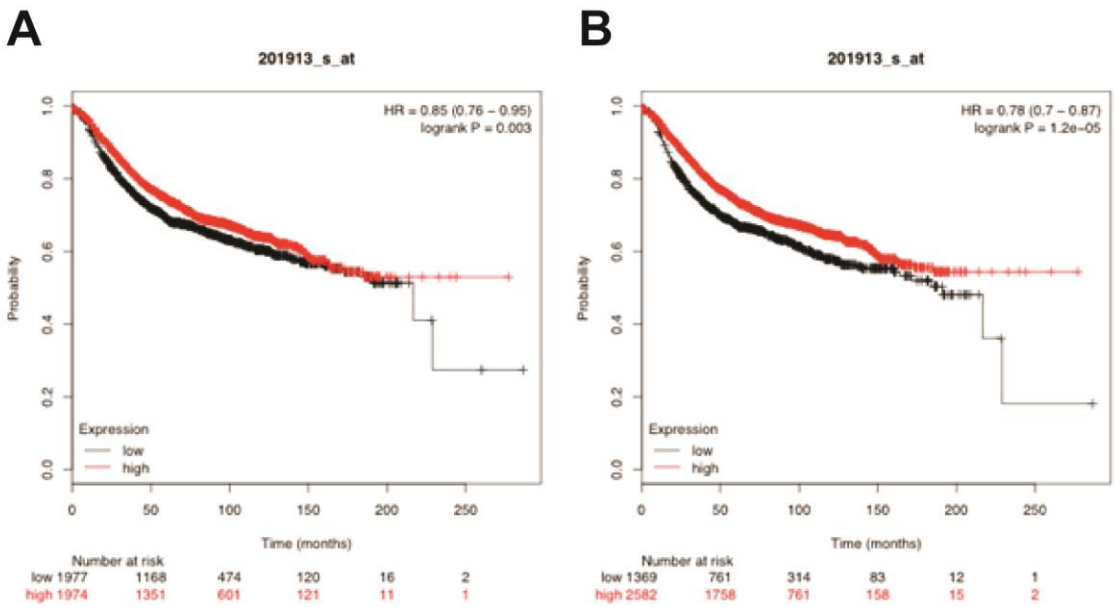

Figure 5.2.5: *COASY* mRNA expression correlates with poor patient outcome. Kaplan-Meier plots generated on KMplot server showing overall survival with patients stratified by *COASY* expression. Patients were stratified by median *COASY* expression (**A**) or with a cut off designed to achieve maximum significance (**B**).

The Kaplan-Meier plots were prepared with varying methods for stratifying patients. The first plot (**Fig. 5.2.5A**) was prepared by separating the two patient groups by *COASY* expression by the median with the second plot (**Fig. 5.2.5B**) prepared to select the cut-off point to achieve maximum significance between the two patient groups. Both methods result in a statistically significant difference in patient survival based upon *COASY* expression with low *COASY* expression resulting in poor patient outcome. Separating the patients by median results in a subtle difference between the two populations as can be seen on the graph with the lines on the Kaplan-Meier plot close resulting in a hazard ratio of 0.85. However when separating the patients to achieve maximum significance the lines separate slightly which results in a lower hazard

ratio of 0.78 and increased significance. Taken together these results indicate that in breast cancer *COASY* acts as a prognostic biomarker and may implicate CoAsy as a novel tumour suppressor in breast cancer.

5.2.6 Investigating the mechanism of *COASY* loss in breast cancer

Previous results have shown that *COASY* is lost in breast cancer, but quite how this occurs is not clear. Previous data shows that there was a reduction in *COASY* mRNA expression in the tumour compared to surrounding tissue, however this can occur by multiple different means. This section will interrogate copy number loss and promoter methylation as two potential mechanisms.

5.2.6.1 Analysis of *COASY* copy number in TCGA provisional dataset

Genetic alterations are frequent in cancers with wide range of aneuploidy observed in every cancer type. Further rearrangements also occur as a consequence of chromosomal instability in a wide variety of cancer types. To investigate the copy number variations of *COASY*, TCGA breast (provisional) data was analysed on the cbioportal server. Prior to drawing any conclusions from this dataset it is important to establish if the copy number reflects mRNA expression. This is crucial as for genes that are tightly regulated by a specific transcription factor, gene copy number will be a less important indicator of expression than this hypothetical transcription factor activity. To address this copy number was plotted against mRNA expression for matched samples taken from this cohort.

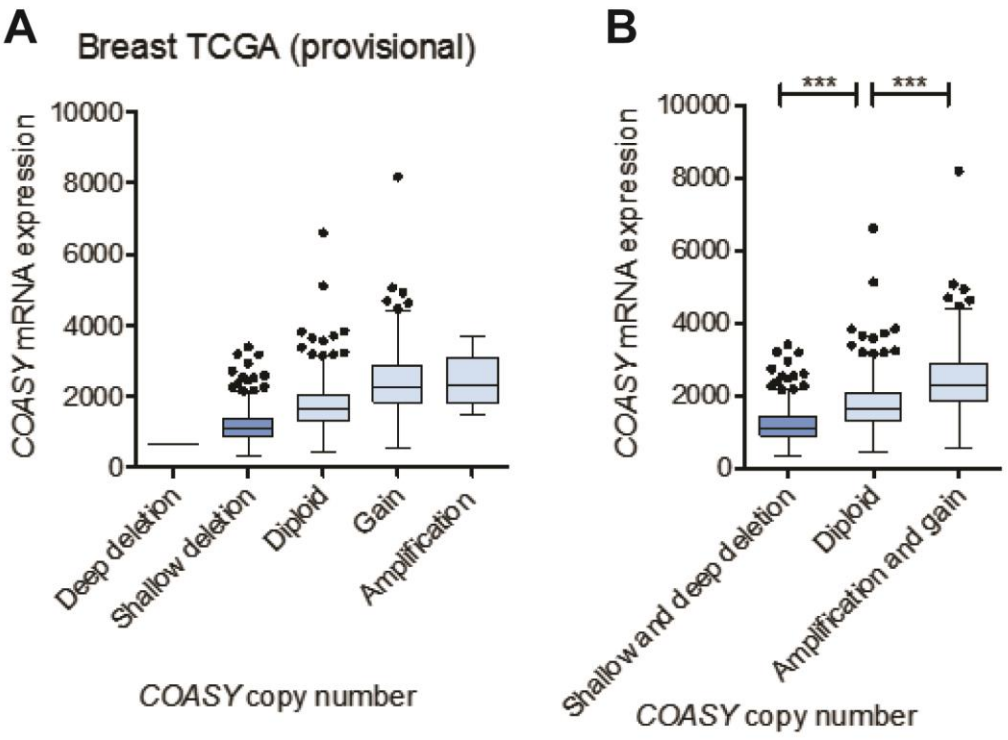

Figure 5.2.6.1.1: *COASY* copy number correlates with mRNA expression: A) Tukey plot showing *COASY* mRNA expression against gene copy number annotation. **B**) Collated data showing *COASY* mRNA expression against pooled data from patients with increased or decreased *COASY* copy number. Data is from TCGA (provisional) accessed on cbioportal. Statistical tests performed are Mann-Whitney T-tests.

The Tukey plot in figure 5.2.6.1.1 shows that *COASY* copy number is an indicator of mRNA expression. Separating patients into copy number analysis shows that patients with loss of *COASY* (deep and shallow deletions) have reduced *COASY* expression compared to diploid patients (**Fig. 5.2.6.1.1A**). Within this dataset there was a subset of patients that had gain and amplification of *COASY* gene. These patients had an increased level of *COASY* mRNA compared to diploid patients; this is confirmed statistically when pooling together these patients as Mann-Whitney T-tests shows each group had significantly different levels of *COASY* mRNA expression compared to the

diploid patients. Therefore subsequent tests can assume that *COASY* copy number is an indicator of expression in this dataset.

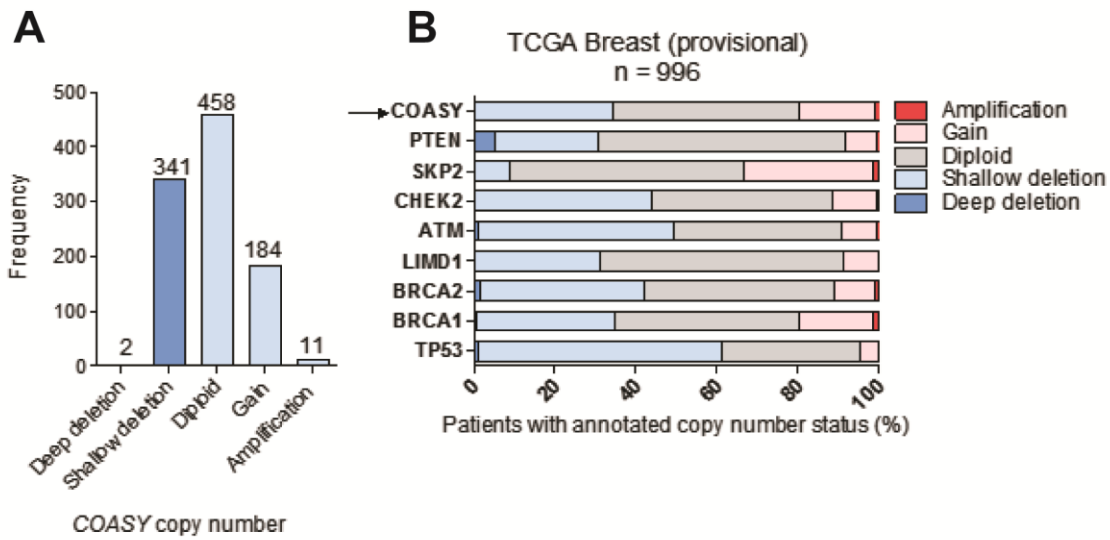

Figure 5.2.6.1.2: *COASY is* deleted in over 33% of breast cancer patients. A) Frequency of *COASY* copy number alterations in breast cancer. Data taken from TCGA (provisional) accessed on cbioportal. **B)** Percentage of copy number alterations for *COASY* and another of reported tumour suppressor genes in breast cancer.

This large patient cohort allows us to determine how frequent loss of *COASY* is in breast cancer patients. Of the total 996 patients, 2 showed deep deletion of *COASY* with 341 patients with shallow deletion. In total this group represents over a third of breast cancer patients (34.4% of total) with loss of *COASY*. Less than 20% of patients had gain or amplifications in *COASY* copy number (19.5%) indicating that loss of *COASY* is a more frequent event. In addition to *COASY* copy number, a number of other reported tumour suppressors were analysed (**Fig. 5.2.6.1.2B**). The figure shows that across the tumour suppressors analysed, deep deletions are not frequent events with the highest observed for *PTEN*. The gene with the highest frequency of loss is *TP53*, a well-established tumour suppressor gene in multiple cancer types. It is clear that the copy number profile for *COASY* is comparable to that of the other classical breast

cancer tumour suppressors such as *BRCA1* and *CHEK2*. Interestingly there was a higher degree of loss in *COASY* than observed with *PTEN* in this cohort. Taken together this data suggests that *COASY* copy number is an indicator of mRNA expression and that over a third of patients have loss of *COASY* which is in line with other classical breast cancer tumour suppressors such as *CHEK2*.

5.2.6.2 Promoter methylation as an alternative mechanism for loss of gene expression

An alternative mechanism for regulating gene expression is through DNA methylation. The majority of DNA methylation occurs at regions of DNA termed CpG islands, named as they contain multiple CG bases linked with the phosphodiester bond. The general consensus is that promoter methylation in these CpG islands corresponds with inhibited gene transcription and therefore reduced expression. To investigate the potential for *COASY* expression to be diminished by promoter methylation, the online server MethHC was utilized [218]. This server contains gene expression and methylation data from the TCGA. Analysis was also performed on *TWIST1*, a gene that has previously been reported to be hypermethylated in breast cancer [219].

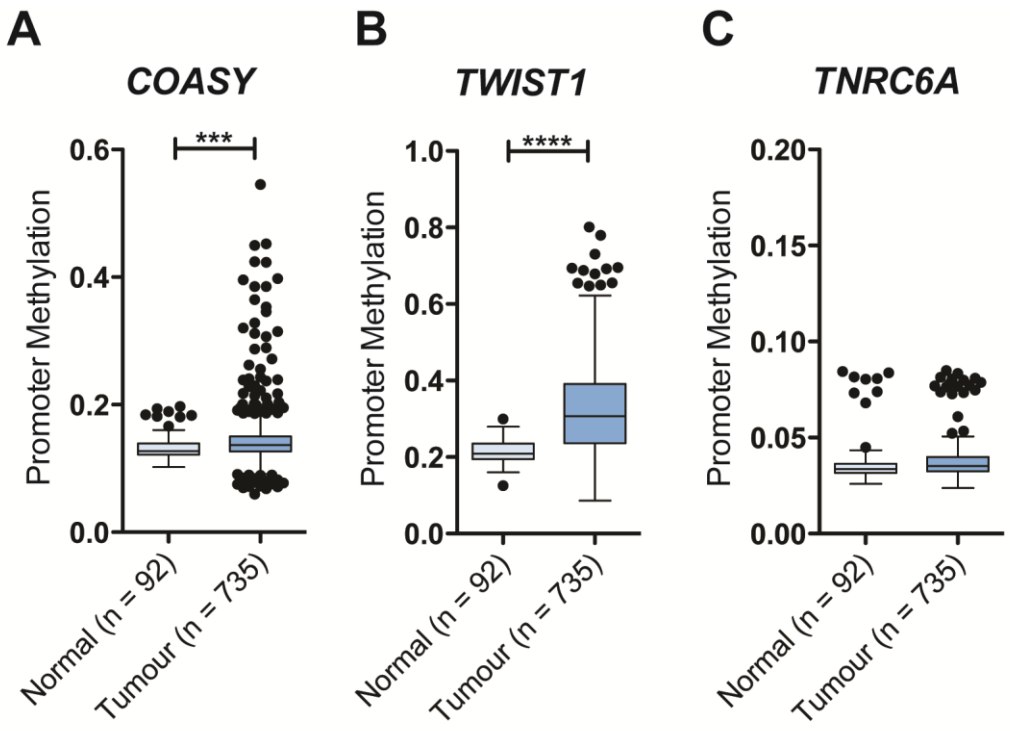

Figure 5.2.6.2: The promoter of *COASY* gene is hypermethylated in cancer. Promoter methylation status for *COASY* (**A**) and *TWIST1* (**B**) and *TNRC6A* (**C**). Data is TCGA data accessed on MethHC online server. Results show a significant increase in promoter methylation in tumour samples compared to normal tissue in both *COASY* and *TWIST1*. Statistical test performed was Mann-Whitney T-test

The Tukey plot in figure 5.2.6.2 shows a significant increase in *COASY* promoter methylation from tumour samples compared to that observed in normal healthy tissue ($p = 0.0001$). In the same dataset, the *TWIST1* promoter also showed a significant increase in promoter methylation for the tumour samples compared to the normal ($p < 0.0001$). *TNRC6A* was included as a negative control, and no significant difference in methylation was observed between normal and tumour samples, furthermore the levels of methylation were all below 0.1 for each sample indicating that the promoter is not heavily methylated. Between the normal and tumour *COASY* promoter methylation datasets there is a small difference in the median values (0.1272 for normal and 0.1367 for tumour) that implies there is not a large difference between the two groups, however there are a large number of outliers with increased

methylation, which is why the difference between the groups is statistically significant. In contrast there is a large shift in median for the *TWIST1* promoter (0.2091 and 0.3069 for normal and tumour respectively). The difference in normal and tumour promoter methylation is clear for both genes however this does not mean there is any biological significance, instead correlation between gene expression and promoter methylation needs to be compared. This dataset also contains RNA-seq gene expression data for matched methylation data, therefore to assess if the promoter methylation inhibits gene transcription this data was plotted in a scatter plot.

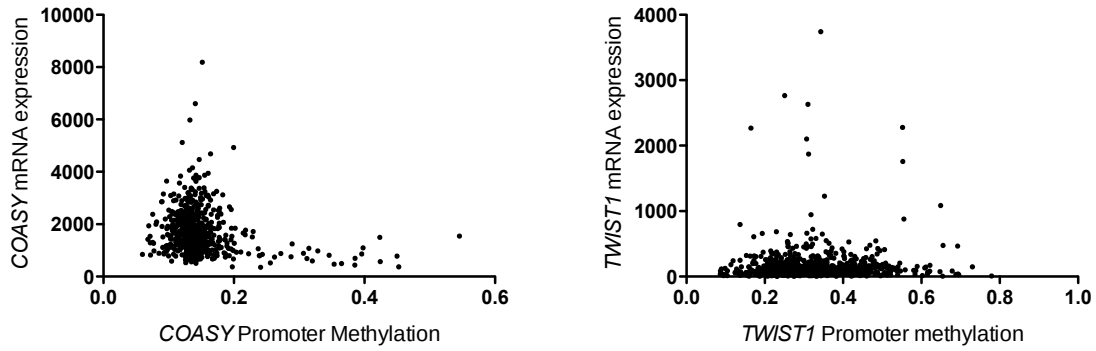

Figure 5.2.6.3: *COASY* mRNA expression correlates with promoter methylation. Scatter plots showing gene expression plotted against promoter methylation for *COASY* (**A**) and *TWIST1* (**B**). Pearson's correlation coefficient shows a significant correlation between *COASY* promoter methylation and mRNA expression. No significant correlation was observed for *TWIST1.*

The scatter plots in figure 5.2.6.3 show two distinct patterns between promoter methylation and gene mRNA expression. Pearson's correlation analysis reveals no significant correlation between *TWIST1* methylation and mRNA expression ($p = 0.3004$, Pearson's correlation coefficient = 0.03883), this is in concordance with the literature as it has previously been shown that *TWIST1* CpG island methylation levels do not correlate with RNA or protein expression [220]. In this cohort there was a statistically significant correlation between

COASY mRNA expression and promoter methylation ($p < 0.0001$, Pearson coefficient = -0.1830). Whilst the correlation is not strong it is highly significant, likely as a consequence of the large cohort size. Examining the scatter plot it is clear that no samples with methylation over 0.2 had high *COASY* expression thereby suggesting that promoter methylation may have an effect on *COASY* mRNA expression however further functional validation studies are required.

In order to test if promoter methylation regulates *COASY* expression *in vitro,* a pair of triple negative breast cancer cell lines with low *COASY* expression were treated with the DNMT1 inhibitor 5'aza-2'-deoxycytidine. DNMT1 is the enzyme responsible for maintaining methylation patterns following cell division; therefor inhibiting this enzyme will block global DNA methylation as cells proliferate.

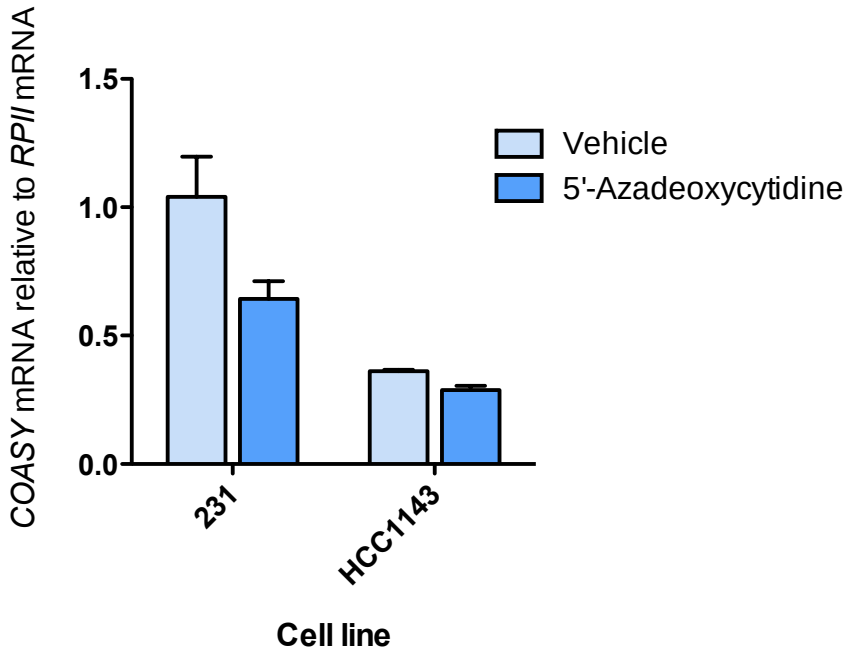

Figure 5.2.6.4: 5'-Azadeoxycytidine reduces *COASY* expression in MDA-MB231 and HCC1143 cells: Bar chart showing *COASY* mRNA expression in two triple negative breast cancer cell liens following treatment with demethylating agent 5'-azadeoxycytidine for 48 hours. Bar chart is representative image from n=2.

Figure 5.2.6.4 shows MDA-MB231 and HCC1143 cells treated with 5'-azadeoxycytidine for 48 hours before collecting RNA and analyzing *COASY* expression by qPCR. As can be seen in the bar graph treatment with 5'-azadeoxycytidine reduces *COASY* mRNA expression in MDA-MB231 cells (~40% reduction compared to vehicle only) whereas the HCC1143 cells displayed ~25% reduction in expression compared to vehicle. These results are in contrast to the initial hypothesis that demethylating agents will increase *COASY* expression. One important caveat from this experiment is that 5'-Azadeoxycytidine acts as a global demethylating agent therefore other transcription factors or potential transcriptional repressors may also be affected. Another important point to consider is the basal levels of methylation in these cell lines, to address this the CCLE database was consulted. This database contains gene expression and methylation data for a wide array of cell lines. A number of breast cancer cell lines were taken from this database and plotted in a scatter plot to assess the degree of *COASY* promoter methylation in the cell lines used for the demethylation experiments.

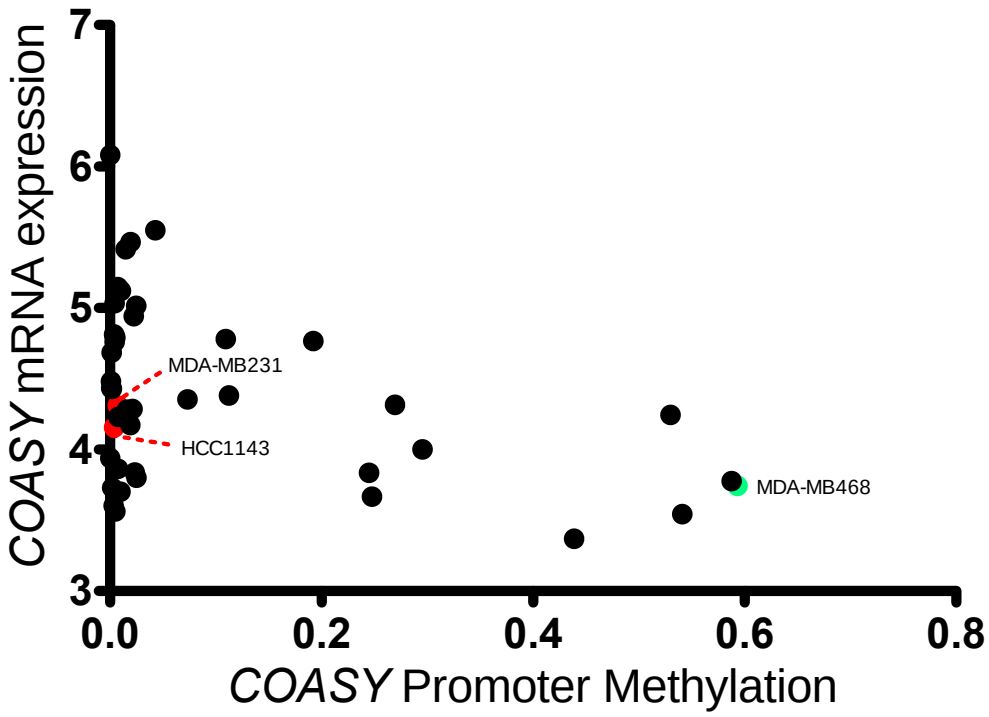

Figure 5.2.6.5: *COASY* promoter methylation in breast cancer cell lines. Scatter plot of *COASY* mRNA expression plotted against promoter methylation from a number of breast cancer cell lines. Data obtained from CCLE database. Datapoints highlighted in red are the two cell lines used for 5'-azadeoxycytidine treatments

The scatter plot in figure 5.2.6.5 shows that the methylation of *COASY* promoter is low in the two cell lines used in the *in vitro* experiments with MDA-MB231 showing methylation status of 0.0074 and HCC1143 with 0.0037. This low level of methylation may explain why no increase in *COASY* expression was observed following treatment with 5'-azadeoxycytidine, instead alternative cell lines such as MDA-MB468 (in green) would be more appropriate to use due to the high methylation status observed in this cell line. Taken together, this data suggests that methylation is increased in tumour samples compared to normal tissue and correlates with *COASY* expression however further studies are required to define the causality between promoter methylation and *COASY* expression.

5.3 Conclusion

This chapter sought to determine the expression levels of CoAsy protein and mRNA in breast and lung cancer patients and to further determine if this correlates with patient survival. In large datasets of lung cancer (both squamous and adenocarcinoma), a small proportion of patients displayed loss of copy number however in the same datasets there was no significant correlation with patient survival for either adenocarcinoma or squamous cell carcinoma. In a small lung cancer TMA CoAsy protein expression was analysed, in this TMA high CoAsy expression was associated with poor patient outcome and there was a positive correlation observed with HIF-1α and the target gene VEGF. This is in contrast to the *in vitro* data observed in the lung adenocarcinoma cell line A549 where knockdown of CoAsy resulted in stabilized HIF-1α.

In contrast to the lung data, there was a larger proportion of copy number loss (over 34%) in breast cancer patients. In a small cohort of breast cancer tumours with matched adjacent tissue there was a significant reduction of *COASY* expression in the primary tumour compared to adjacent suggesting that *COASY* is lost in breast cancer. Further stratifying patients by receptor status shows that reduced CoAsy expression is correlated with lack of hormone receptors, this trend was further observed in larger cohorts (proteomic analysis) and in cultured cell lines. Further bioinformatics analysis shows that low *COASY* expression is associated with poor outcome. It is currently unclear as to the mechanism behind loss of CoAsy in breast cancer, however promoter methylation may play a role. Taken together it can be said that CoAsy is lost in

breast cancer and may potentially act as a tumour suppressor gene, particularly in triple negative breast cancer.

Results Chapter Four:

Exploiting the concept synethic lethality to target CoAsy deficient cells

6.1 Chapter aims

Previous chapters have identified CoAsy as a novel negative regulator of HIF transcriptional activity and protein stability. Further analysis has shown that CoAsy is lost in over 34% of breast cancer patients and is correlated with poor patient prognosis. Due to this clear loss of CoAsy in breast cancer we sought to identify a targeted therapy against CoAsy negative cancers. To identify such an inhibitor, the concept of synthetic lethality was be exploited whereby a drug will selectively kill cells lacking in CoAsy but will spare healthy cells with normal levels of CoAsy expression (**Fig. 6.1**).

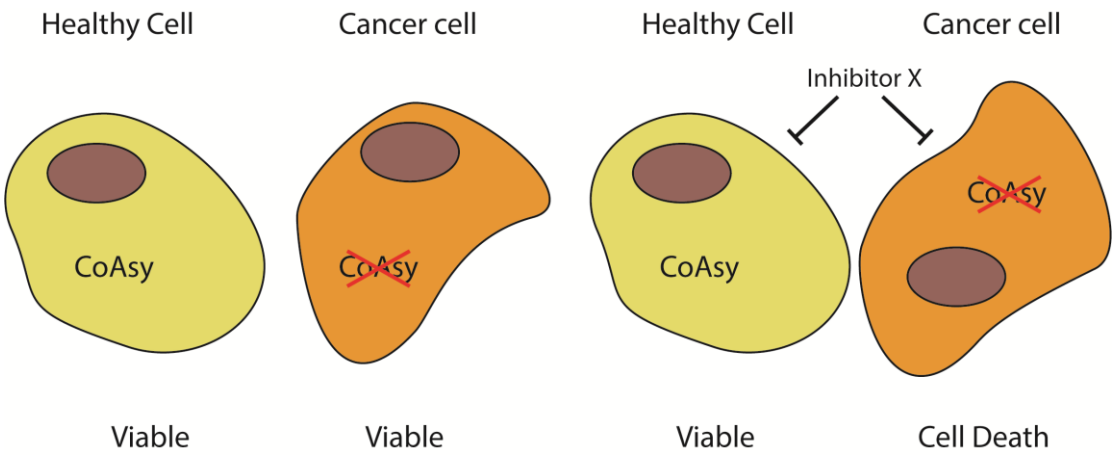

Figure 6.1: Synthetic lethality: Schematic diagram showing the concept of synthetic lethality

To summarise the aims for this chapter:

- ***To screen a library of compounds in inducible shRNA lines to identify a compound that selectively kills CoAsy knockdown cells***
- ***To validate identified hits across a dose response to determine change in Sf_{50}***

6.1.1 Optimisation of cell viability reagent

For the arrayed drug library screen, the final readout for the assay is cell viability. Previous drug screens performed by collaborators with the same library used Cell Titer-Glo (Promega) as a viability reagent, however previous experiments in this project utilized the resazurin for cell viability. In order to determine the differences between the two reagents dose response curves were generated and treated with both reagents. As resazurin is a non-lytic reagent it is possible to perform the experiments in tandem on the same sample to allow for direct comparison.

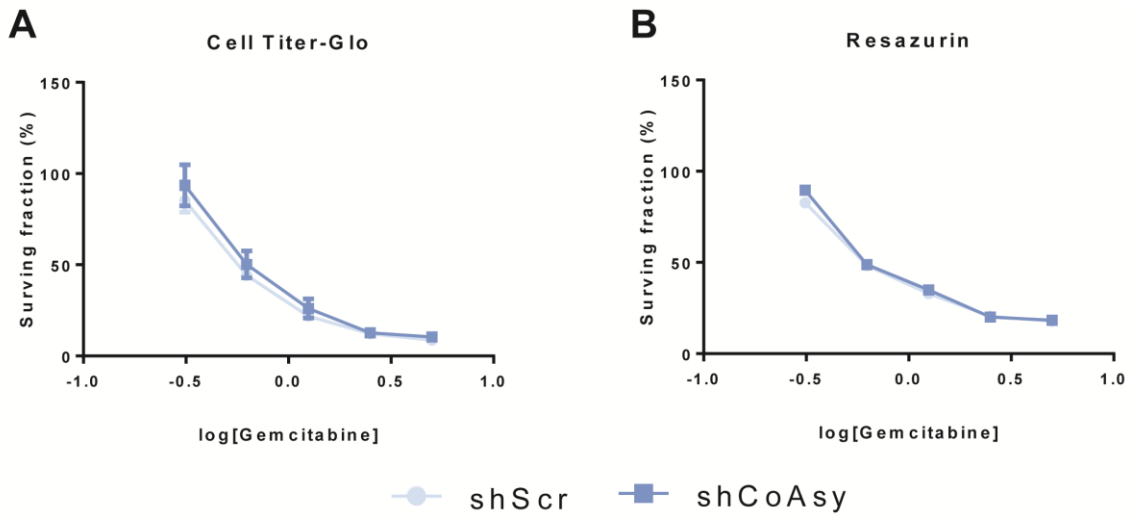

Figure 6.1.1: Optimisation of cell viability reagent for drug screen. T47D-tet-shRNA cells were treated with doxycycline (25 ng.mL^{-1}) for 72 hours prior to plating and treating with gemcitabine across a wide dose range. Cells were dosed on day 1 and 3 of assay before reading cell viability with Cell Titer-Glo (**A**) and resazurin (**B**). n=1.

T47D tet-shRNA cells were pretreated with doxycycline for 3 days prior to plating and treated with a dose range of gemcitabine. Gemcitabine was arbitrarily picked as an agent to induce cell death to test validity of viability reagents. Both shScr and shCoAsy cell lines were tested with viability agents as these have differing mechanisms of actions (Cell Titer-Glo measures cellular

ATP whereas resazurin requires functioning mitochondrial NADPH dehydrogenase) that may be altered by loss of CoAsy. As can be seen by the dose response curves there is no significant difference between the two viability reagents. There was a slight increase in variability with the luminescence readings from Cell Titer-Glo compared to the fluorescent readout from resazurin, however error bars are small for each viability reagent. This assay also shows that loss of CoAsy does not alter sensitivity to gemcitabine in T47D cells.

6.1.2 FDA library drug screen in inducible shRNA cell lines

To identify an inhibitor that selectively targets CoAsy deficient cells, three pairs of inducible shRNA lines were used (A549, MCF10A and T47D). These lines were selected as HIF stabilization following loss of CoAsy has been observed in both the A549 and T47D cell lines. The MCF10A-tet-shRNA pair were also included as these represent a 'normal' cell type, however it is important to note that these cells are naturally immortalized and had undergone EMT prior to lentiviral transduction, therefore a degree of cellular transformation has already occurred and cannot be considered a true primary cell line. Nevertheless the MCF10A pair still represents an isogenic pair of breast cells with or without CoAsy.

The drug library used was an arrayed library containing 1177 FDA approved compounds; this library encompasses a wide range of inhibitors with chemotherapy agents, hypertensive agents and other compounds such as Talc included in the library. The advantage of this FDA approved library is that

significant pre and post clinical work has been performed on the compounds, with drug pharmacokinetics and mechanism of action (including off-target effects) being well established for the majority of compounds. The drug screen was performed at a dose of 10 µM per compound with two doses performed per replicate; a schematic of the drug protocol is below:

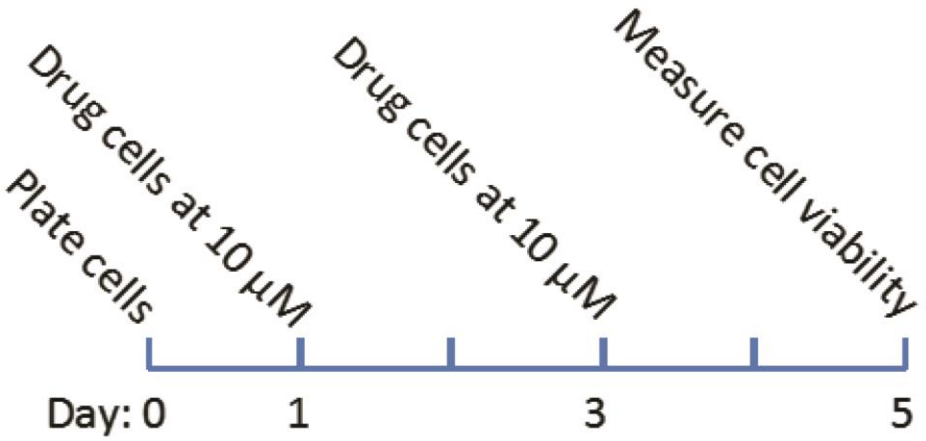

Figure 6.1.2.1: protocol for FDA-approved library screen. Schematic of drug screen dose schedule. Cells were pretreated with doxycycline (25 ng.mL^{-1}) for 72 prior to plating on day 0. Cells were treated with library at 10 µM at day 1 and day 3 with fresh doxycycline media added each time. Cell viability was measured at the end point of day 5 with resazurin viability reagent.

Drug screen was performed as described above in the A549-tet-shRNA pair (2 biological replicates), T47D-tet-shRNA pair (2 biological replicates) and in the MCF10A-tet-shRNA pair (1 biological replicate). After measuring cell viability the modified Z-score was used to determine statistical outliers, each representing a ‘hit’ from the screen.

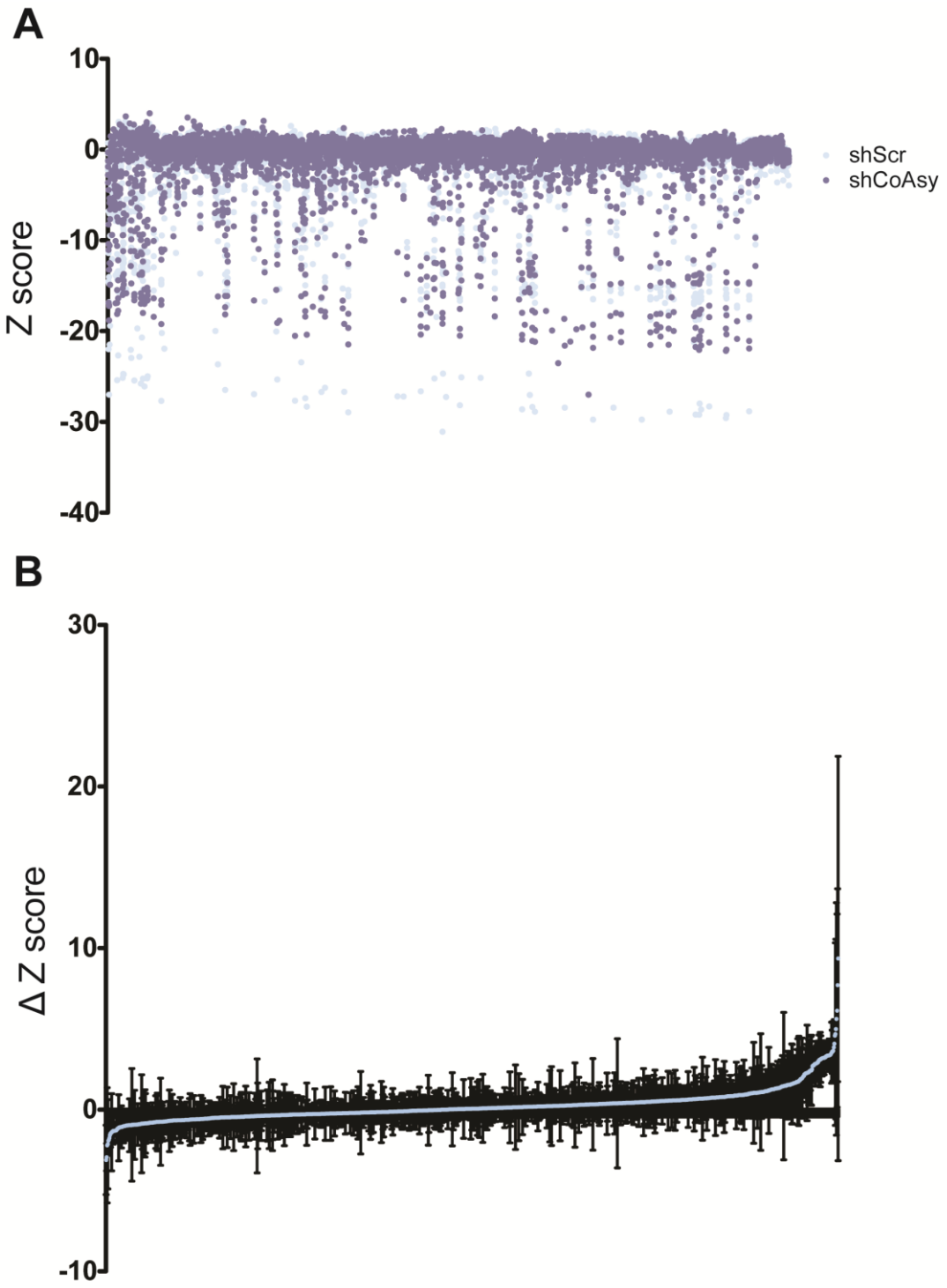

Figure 6.1.2.2: Drug screen of FDA approved compounds. A) Scatter plot of 5 biological replicates in the primary drug screen. T47D (n = 2), A549 (n = 2) and MCF10A (n = 1) tet-shRNA lines were screened with FDA approved library as described in **Fig 6.1.2.1**. **B**) Δ-Z scores were calculated from two biological replicates of the T47D shRNA screen and plotted in increasing Z-score. Results are presented as mean ± SD.

The scatter plot in figure 6.1.2.1A displays a broad distribution of Z-scores for the tested compounds, this shows that there is a wide range of effects from drug treatment with some inhibitors being very toxic. However, examining the spread of data in figure 6.1.2.1A shows the majority of the compounds did not greatly alter cell viability; this is important as it allows the Z-score statistical approach to be valid, as it is a measure to determine outliers, the assumption is based on the majority of results having no effect. Figure 6.1.2B shows a plot of Δ Z-score, which represents the change in viability between shCoAsy and shScr cell lines. Therefore the negative values on the screen means the inhibitor selectively targets CoAsy deficient cells whereas the positive suggest that loss of CoAsy confers some resistance to this drug. The error bars in this figure are large across the entire dataset; this could be a result of the degradation of the drug stock or through pipetting errors. The large error bars means that simply analyzing the average ΔZ-score will be an inefficient way of identifying hits as there will likely be a large number of false positive and negative hits and other more systematic approaches will be more applicable.

6.2 Validation of hits from drug screen

6.2.1 Quarternary ammonium compounds

To identify hits the first approach was to look at each cell line individually and compare the hits with the largest differences between shScr and shCoAsy lines. The first line tested was the MCF10A-tet-shRNA pair.

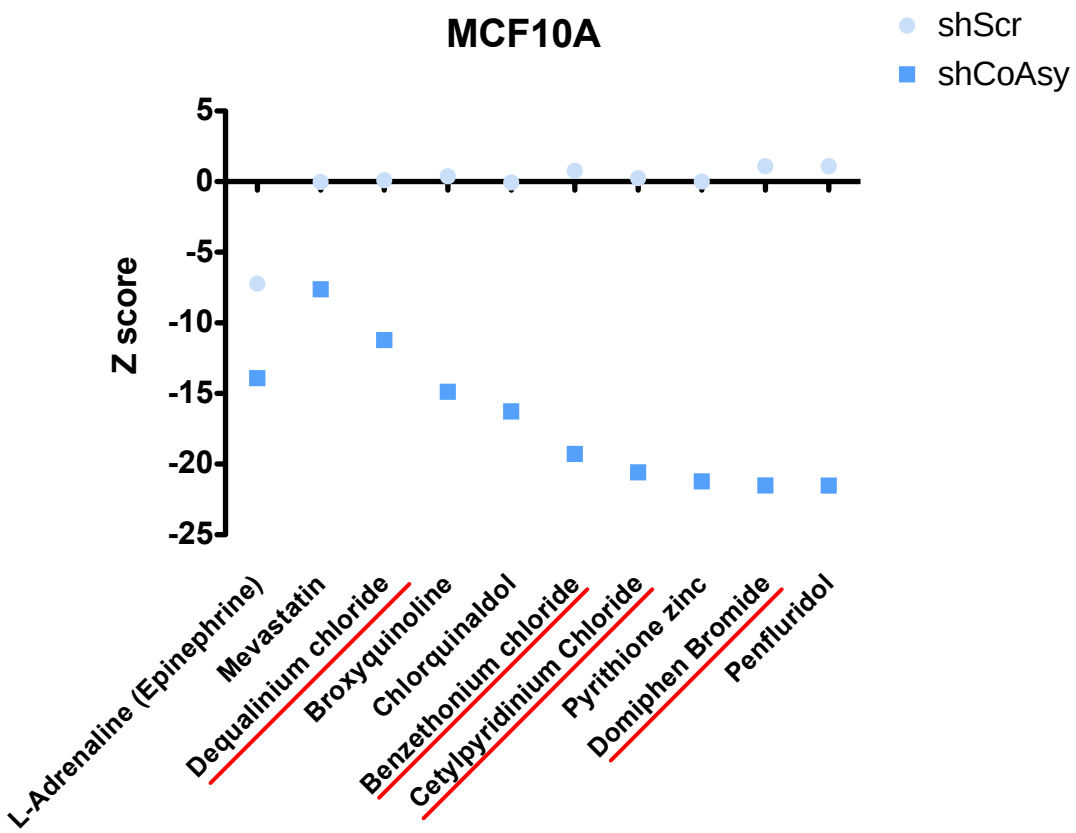

Figure 6.2.1: Top 10 hits from drug screen in MCF10A-tet-shRNA cells. Drugs underlined in red represent drugs from the quaternary ammonium class of antimicrobial agents.

Analysis of the top hits of this screen revealed a number of molecules that belong to the same class with each containing a quaternary ammonium cation. These compounds are all broad-spectrum microbiocidal compounds that are used in many antiseptics [221]. It is important to note that each of these compounds were across different plates and different locations across plates,

therefore it is unlikely that the effect observed in the screen occurred due to technical errors during manual pipetting.

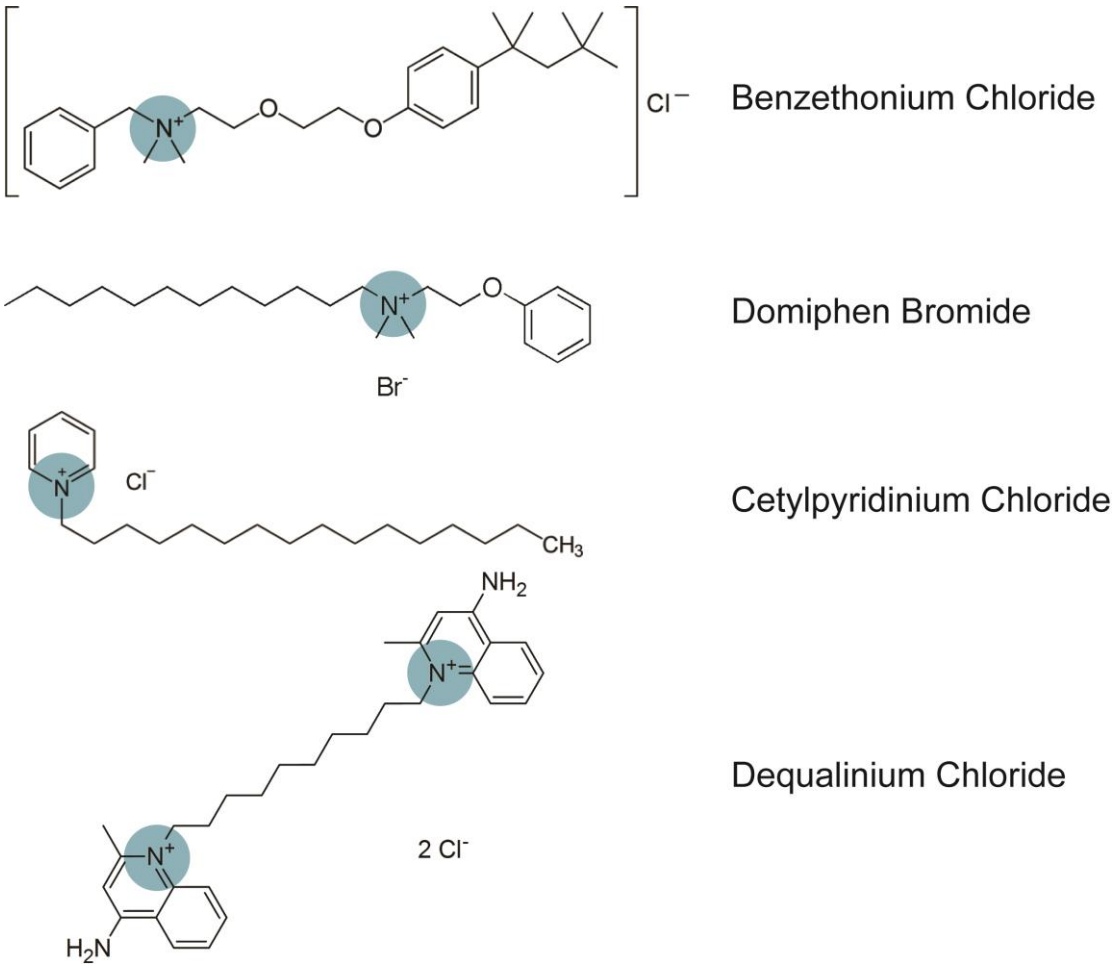

Figure 6.2.2: Quaternary ammonium compounds. Structures of the quaternary ammonium compounds identified during the drug screen. Each compound contains the positive nitrogen cation that is covalently bonded to 4 alkyl side groups (or double bonds as part of an aromatic ring) highlighted here in blue.

Two of these quaternary ammonium compounds were purchased and the A549, T47D and MCF10A tet-shRNA cell lines were treated using the same protocol as that from the primary screen across a wider dose range. The two selected were benzothenium chloride and domiphen bromide. Domiphen bromide was selected as in the drug screen it showed the highest degree of selectivity whereas benzothenium chloride was selected as it is a related

compound, however is formulated with a different salt anion. Therefore testing this compound will help determine if the salt anion is important for activity.

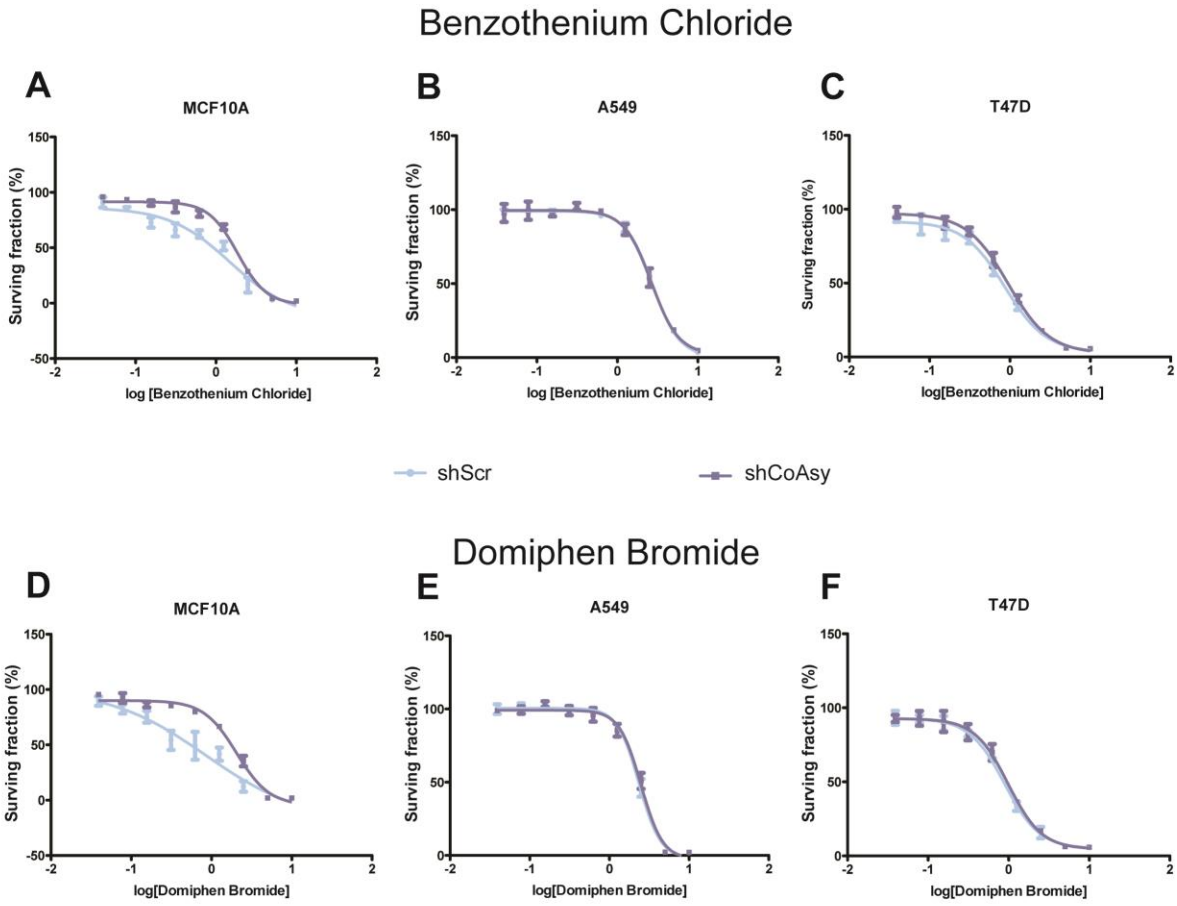

Figure 6.2.3: Dose response curves for quarternary ammonium compounds in inducible shRNA lines. A-C) Dose response of Benzothenium chloride in MCF10A (**A**), A549 (**B**) and T47D (**C**). **D-E**) Dose response of Benzothenium chloride in MCF10A (**D**), A549 (**E**) and T47D (**F**). Experiments were performed using the same protocol as initial drug screen. N=1

The dose response curves in figure 6.2.3 show that in A549 and T47D there is no difference in selectivity between the shScr and the shCoAsy for either domiphen bromide or benzothenium chloride. This is to be expected as neither hit showed significant selectivity in these lines in the initial drug screen. In the MCF10A lines there was a slight degree of selectivity in for each drug as Sf_{50}

values were shScr = 1.507 µM and shCoAsy 1.865 µM for benzothenium chloride and shScr = 0.845 µM and shCoAsy = 2.05 µM for domiphen bromide, this selectivity is different to that observed in the screen where treating MCF10A inducible lines with 10 µM of each drug resulted in selectivity for the CoAsy deficient cell line. It is unclear as to why this class appeared to be selective in the primary screen but failed to reproduce across a dose range. Therefore these drugs were not taken forward for further experiments.

6.3 Nicardipine HCl

Taking an alternative approach to identify hits, the screen was re-analysed to select compounds that showed a degree of selectivity in each cell line tested. Furthermore the hits with very large Z-scores were excluded from analysis as these results often skew the analysis and results in increased false positives. Through this approach nicardipine HCl was identified. Nicardipine HCl is a potent calcium channel blocker that is used in the treatment of hypertension [222].

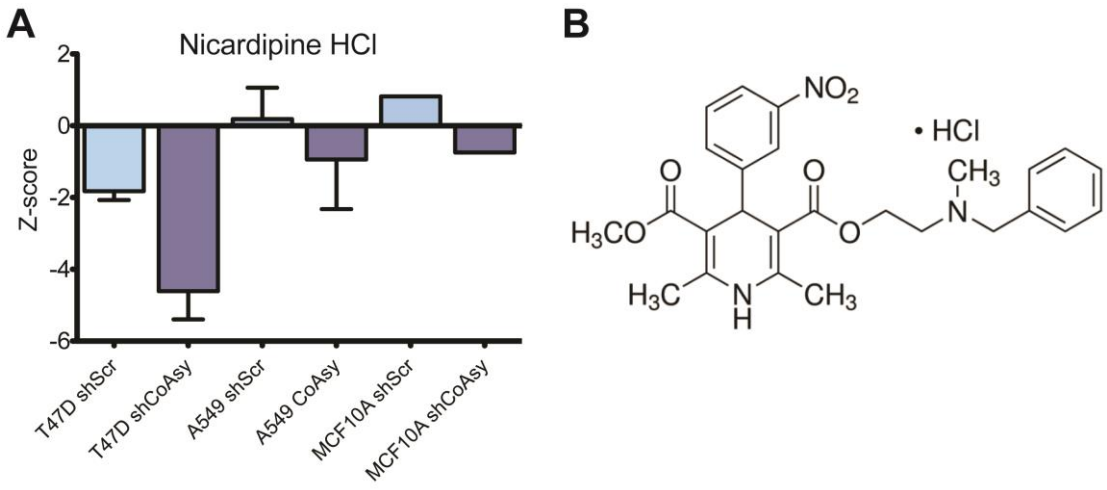

Figure 6.3.1: Nicardipine HCl was selective for CoAsy deficient cells in primary screen. A) Bar chart showing the Z-scores for T47D, A549 and MCF10A inducible shRNA lines treated with 10 µM nicardipine HCl in primary screen. **B**) Chemical structure of nicardipine HCl.

As can be seen in figure 6.3, nicardipine HCl appears to be selective against CoAsy deficient cells in T47D and MCF10A at a dose of 10 µM, the error bars are large for the A549 experiments therefore it is hard to determine if there is any selectivity in this cell line. The drug is toxic in T47D cells as there is a large amount of cell death in both the shScr and shCoAsy cell lines, this is in contrast to the A549 and MCF10A cells where no significant cell death was observed in

the shScr cell lines. To further validate nicardipine, A549-tet-shRNA cells were treated with nicardipine across a wide dose range.

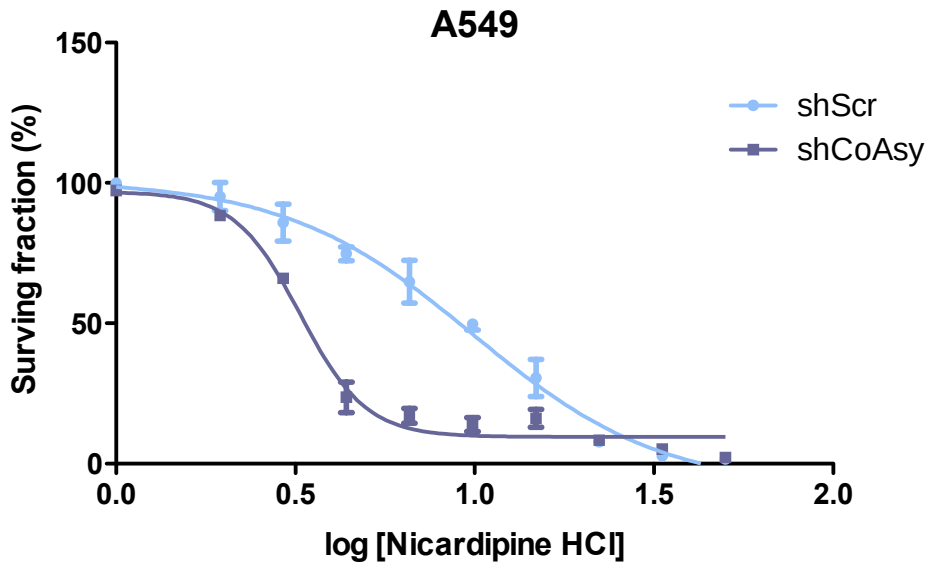

Figure 6.3.2: Loss of CoAsy sensitizes A549 cells to Nicardipine HCl. A549-tet-shRNA cells were pretreated with doxycycline for 72 hours before plating and treated with nicardipine HCl across a dose range. Cells were treated as in the primary drug screen. N=1.

The initial validation of nicardipine HCl in the A549 cell line showed promising results, as loss of CoAsy sensitized the cells to treatment with nicardipine HCl. The Sf_{50} values were shScr = 9.89 µM and shCoAsy = 3.26 µM, indicating a threefold reduction in drug required to kill half of the cells. Subsequent repeats were performed to confirm this result in the A549-tet-shRNA cell lines.

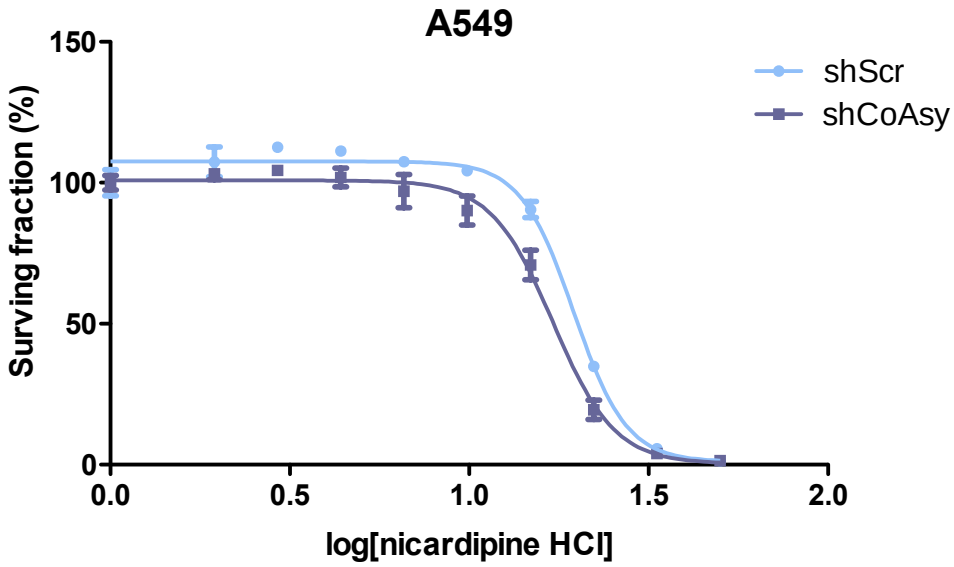

Figure 6.3.3: Nicardipine HCl treatment of A549-tet-shRNA cells. A549-tet-shRNA cells were pretreated with doxycycline for 72 hours before plating and treated with nicardipine HCl across a dose range. Cells were treated as in the primary drug screen. N=2.

As can be seen in figure 6.3.3 the further repeats of nicardipine HCl treatment differed greatly to the first repeat. There is still a degree of selectivity for the CoAsy deficient cells with a reduction in Sf50 of 2.μM, however it is to a lesser extent as seen in figure 6.3.2. In both the shScr and shCoAsy lines there is an increase in Sf_{50} values (shScr = 19.5 μM and shCoAsy = 17.1 μM) compared to figure 6.3.2 and a decreased sensitivity for Nicardipine in these lines. This decrease in drug efficacy led to the hypothesis that there has been degradation of the drug after multiple freeze-thaw cycles. To negate this effect fresh drug was purchased from multiple suppliers and the experiments were repeated again.

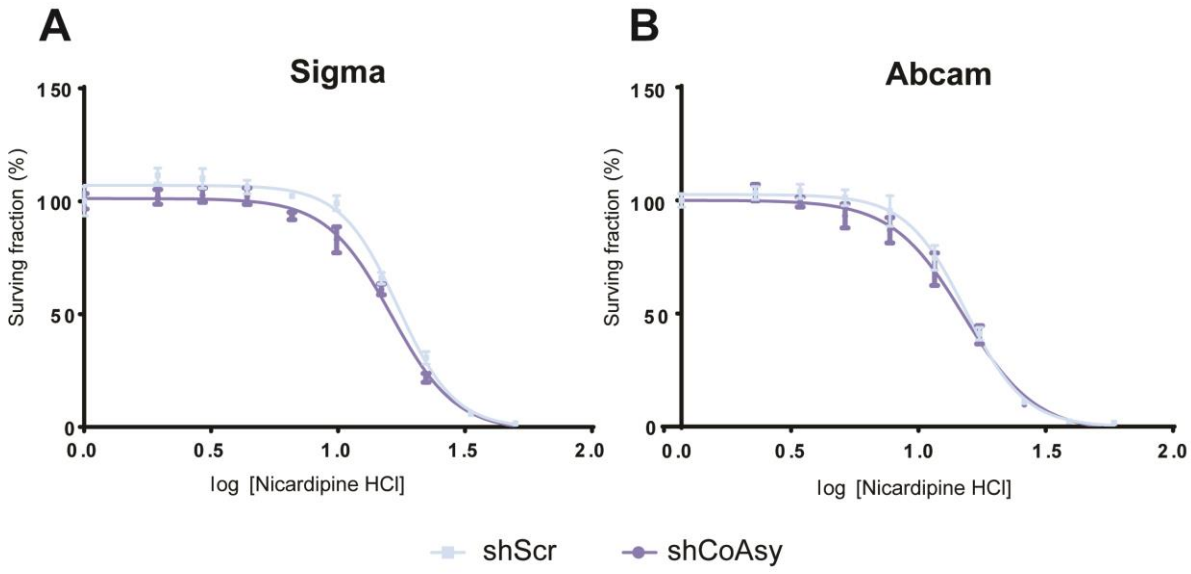

Figure 6.3.4: Treatment of A549-tet-shRNA cells with Nicardipine HCl from two different suppliers. A549-tet-shRNA cells were pretreated with doxycycline for 72 hours before plating and treated with nicardipine HCl purchased from Sigma-Aldrich (**A**) and Abcam (**B**). Cells were treated as in primary drug screen. n=2.

Treatment of A549 tet-shRNA lines with fresh aliquots of nicardipine HCl from either supplier failed to display the selectivity observed in Figure 6.3.4. The Sf_{50} values were shScr = 17.21 μM and shCoAsy = 16.17 μM for the drug purchased from Sigma-Aldrich and shScr = 13.08 μM and shCoAsy 12.88 μM. As there was no observed selectivity for either batch of drug it was decided to not continue any further experiments with nicardipine HCl and the initial repeat with the observed selectivity was dismissed as a false positive.

6.4 Future drug validation experiments

Due to the previous inhibitors not validating, an alternative approach to identify hits to validate was performed. The previous chapter identified loss of CoAsy in breast cancer that correlated with poor prognosis, whereas in lung cancer low CoAsy correlated with better patient prognosis, therefore the lung

adenocarcinoma cell line (A549 tet-shRNA pair) was discounted from the screen. Furthermore to simplify analysis of hits, the MCF10A inducible shRNA pair were discounted from analysis, as these are untransformed cells (albeit having undergone EMT prior to lentiviral transduction) they will be significantly different from the transformed cell line T47D. Therefore the top hits from T47D were compiled as potential candidates.

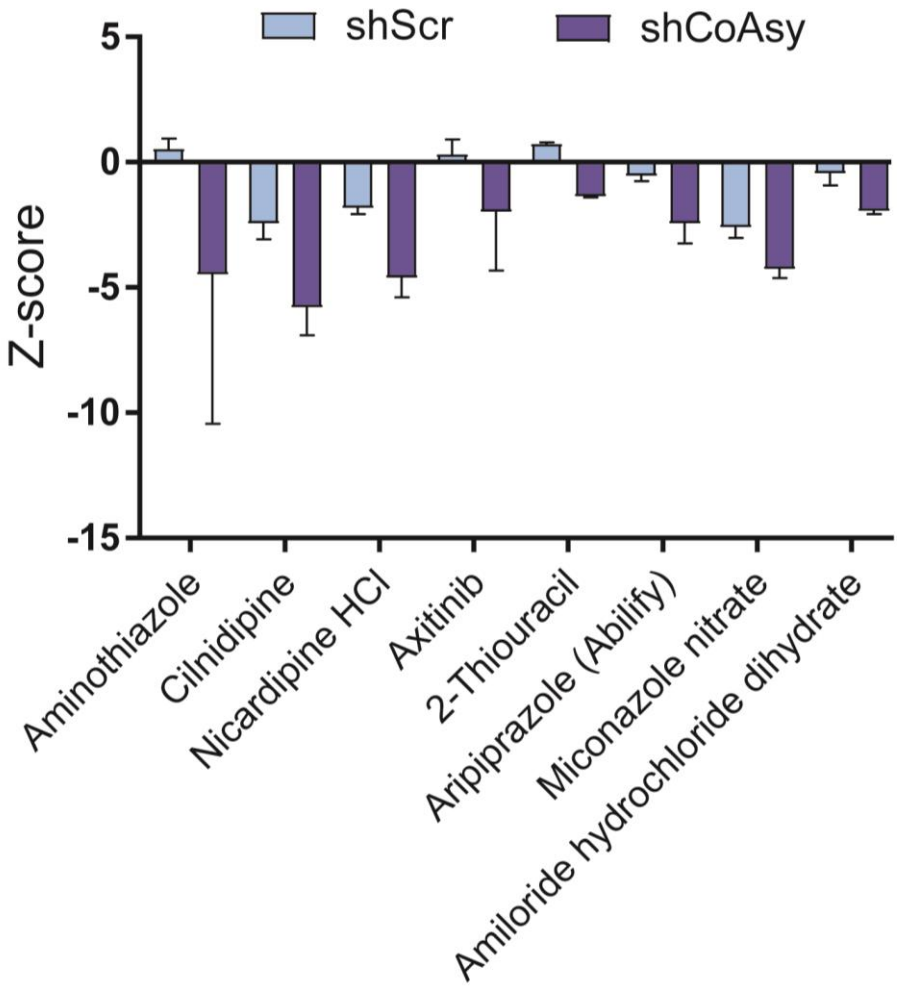

Figure 6.4: Top hits from T47D screen. The Z-scores from the two biological replicates were manually screened to identify an inhibitor with increased cell death in the shCoAsy line compared to the shScr. Bar chart shows Z-scores from the top hits. Bars are average ± SD. N=2.

From these compiled hits from the screen in T47D-tet-shRNA lines, two inhibitors shared a mechanism of action, as both 2-thiouracil and aminothiazole

are used in the treatment of hyperthyroidism through inhibition of thyroid peroxidase [223]. Axitinib is a tyrosine kinase inhibitor that targets VEGFR, c-KIT and PDGFR, which in turn, inhibits angiogenesis [105]. Currently there is market authorization for treatment of renal cell carcinoma with axitinib. Future experiments will test these inhibitors across a wide dose range to determine if these compounds are truly selective against CoAsy deficient cells.

6.5 Summary

In this chapter we sought to identify an inhibitor that selectively targets CoAsy deficient cells. To achieve this A549, T47D and MCF10A inducible shRNA cell lines were screened against a library of 1177 FDA approved compounds and cell viability was measured. Attempts to validate some of the inhibitors are thus far unsuccessful, however there are a number of promising candidates that still require validation. Whilst the screen has highlighted a number of inhibitors with common mechanisms, it is unclear whether there are any pathways that are altered through loss of CoAsy. This is in part due to the high concentration of inhibitor used during the primary screen, which increases the likelihood of off-target drug effects from occurring. Once a hit from the screen has been validated, this opens up the exciting prospect of preclinical studies for a novel targeted therapy against CoAsy deficient cancers.

Discussion and future work

7.1 CoAsy is a negative regulator of HIF-1 transcriptional activity

The initial aim of the project was to identify novel regulators of HIFs. Taking an unbiased approach, an arrayed library of siRNA targeting all known human kinases, pseudo-kinases and proteins with predicted kinase activity was screened against A549 cells stably expressing HIF-1 HRE driven *firefly* luciferase. Through this primary screen and secondary validation screen, the Coenzyme A biosynthesis enzyme, CoAsy, was identified as a negative regulator of HIF-1 transcriptional activity in both normoxia and hypoxia. siRNA mediated knockdown experiments in multiple transformed cell lines indicated that loss of CoAsy results in stabilised HIF-1α and HIF-2α protein levels. This was an unexpected finding as there have been no previous reports linking the CoA biosynthesis pathway to HIF signaling.

A number of non-canonical functions of CoAsy have been reported, as it has been shown that CoAsy binds to the P-body component EDC4 and ribosomal protein S6 kinase 1 (S6K1) [224, 225]. It has been shown that the EDC4:CoAsy interaction results in reduced CoAsy kinase activity however it is not known what function this interaction has in regulating EDC4 mRNA decapping ability, furthermore whether this interaction can have an effect on HIF signaling. Inhibition of S6K1 results in reduced rates of HIF-1α protein as a consequence of reduces *HIF1A* mRNA translation rates. However, the CoAsy:S6K1 interaction has not been shown to affect either CoAsy or S6K1 activity, indeed this interaction has yet to be validated at the endogenous level or without serum starvation. Therefore it is unlikely that the previously identified non-canonical functions of CoAsy are responsible for the increased HIF activity. Interactions

between CoAsy and proteins unrelated to CoA biosynthesis highlight a potential role for CoAsy to function as scaffold protein where a protein can bring together two interactors to focus enzymatic activity. Future experiments to identify binding partners of CoAsy may provide hints to the mechanism behind the role of CoAsy in HIF signaling. Preliminary experiments were performed to test if PHD2 or HIF-1α interacted with overexpressed CoAsy-EGFP.

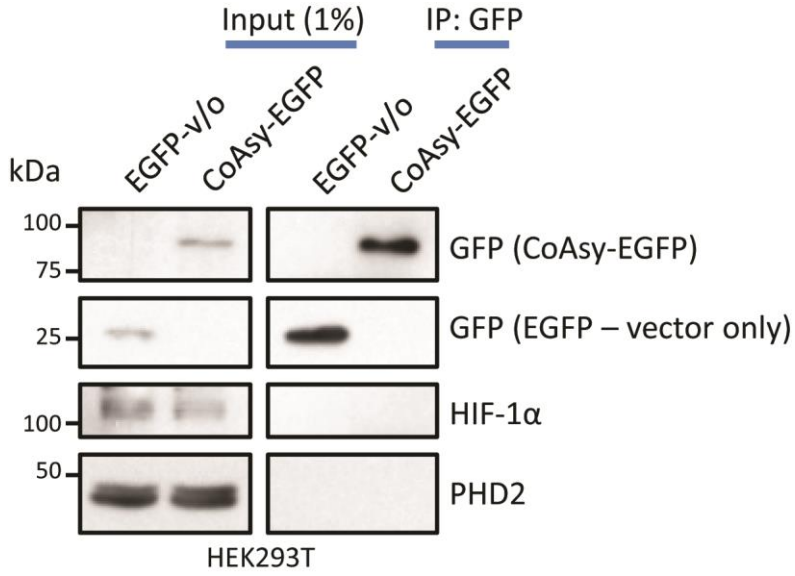

Figure 7.1: IP of CoAsy-EGFP and EGFP in HEK293T. HEK293T cells were transiently transfected with either EGFP-vector only or CoAsy-EGFP. 48 hours post transfection cells were lysed and immunoprecipitated with α-GFP prior to analysis by western blot. N=1.

This IP indicates that CoAsy does not interact with either HIF-1α or PHD2. Both the EGFP vector only and CoAsy-EGFP display an enrichment of protein during the IP that indicates the IP was successful. However in the co-IP, no HIF-1α or PHD2 protein was detected. It is possible that this result is a false negative, as no positive control was assayed. Therefore future experiments should include a previously identified interacting protein such as S6K1. Furthermore the co-IP panel should be expanded to encompass other proteins that are known to regulate HIF such as pVHL.

Alternative approaches to identify if CoAsy is acting as a scaffold can also be used such as immunofluorescence (IFA) to detect if proteins co-localise or alternatively proximity ligation assay (PLA) to detect if they directly interact (within 30-40 nm).

7.2 Coenzyme A or a Coenzyme A derivative negatively regulates HIFα protein stability

Overexpression of CoAsy had no effect on HIF-1α protein levels, however overexpression of Pank1β, an isoform of Pank1, did result in a significant decrease of both HIF-1α and HIF-2α protein levels with no changes observed in HIF-1β. RNAi mediated silencing of Pank1 resulted in stabilised HIF-1α regardless of oxygen tension, as was observed following knockdown of CoAsy. This suggests a role of the CoA biosynthesis pathway in regulating HIF, however it is unclear whether this is as a result of CoA or other derivatives. To address this a number of enzymes that utilize CoA as a cofactor were knocked down in both wild type and inducible shCoAsy A549 cells. This highlighted ACSS1 as a potential mediator of this pathway, which means that the conversion of acetate and CoA to acetyl-CoA in the mitochondria is the reaction required to negatively regulate HIF. However further experiments were required to test this further. This was repeated with a reporter assay to test if HIF activity was still increased following loss of ACSS1.

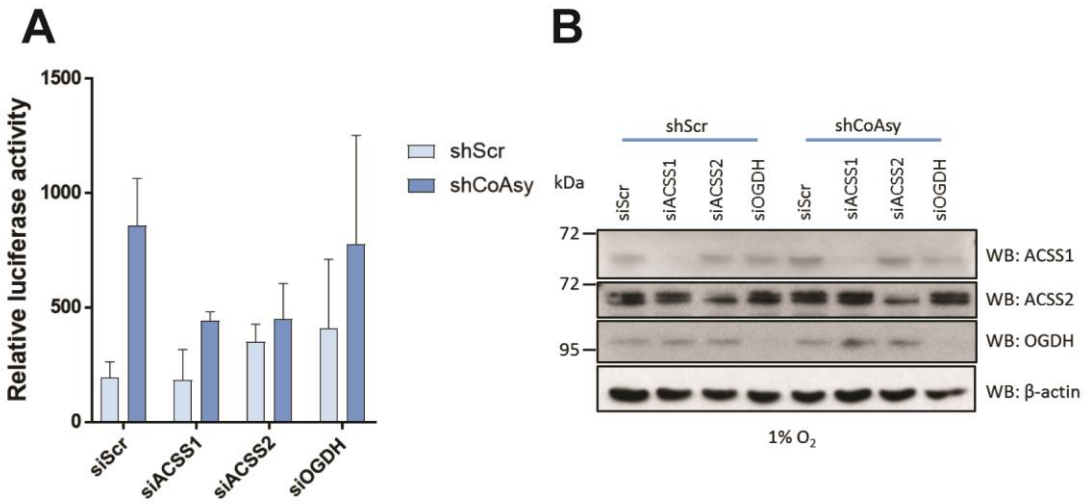

Figure 7.2.1: Reporter assay of HIF activity in A549-tet-shRNA cells following knockdown of ACSS1, ACSS2 and OGDH. Cells were plated out and treated with doxycycline (25 ng.mL^{-1}) before being treated with siRNA against *ACSS1*, *ACSS2, OGDH* and non-targeting control (40 nM). 48 hours post transfection cells were transfected with HRE driven nano-luciferase vector and *firefly* luciferase normalization vector before being placed into hypoxia overnight. Luciferase activity was measured (**A**) and knockdown was confirmed by western blot (**B**). Bar chart represents mean ± SD from 6 technical replicates. N=1.

The reporter shows that loss of CoAsy increases the HRE reporter activity as the shCoAsy line showed higher relative luciferase activity compared to the shScr line once treated with non-targeting control siRNA. The previous data indicated that loss of ACSS1 increased HIF-1α protein levels, which appeared to be in a CoAsy dependent manner. However the reporter results showed that this stabilised HIF does not activate the HRE reporter, as loss of *ACSS1* in the shScr line did not show increased luciferase activity. This result is in contrast to the reporter data following loss of CoAsy that shows an increase in reporter activity. Whilst further repeats are required to confirm this result, it suggests that loss of CoAsy may not regulate HIF through this enzyme.

CoA is not membrane permeable; therefore simply supplementing cell culture medium with CoA will not directly increase intracellular CoA. Instead CoA will

be converted to 4'phosphopantetheine and converted to CoA by CoAsy [196], which is important as this means CoA supplementation will not restore CoAsy deficiency. However a number of lipid based transfection reagents are capable of delivering small molecules to cells, therefore using this approach it is possible to transfect cells with CoA and other CoA derivatives and assess changes to HIF signaling. As a proof of concept experiment, this was performed with CoA in the A549-tet-shRNA cell lines.

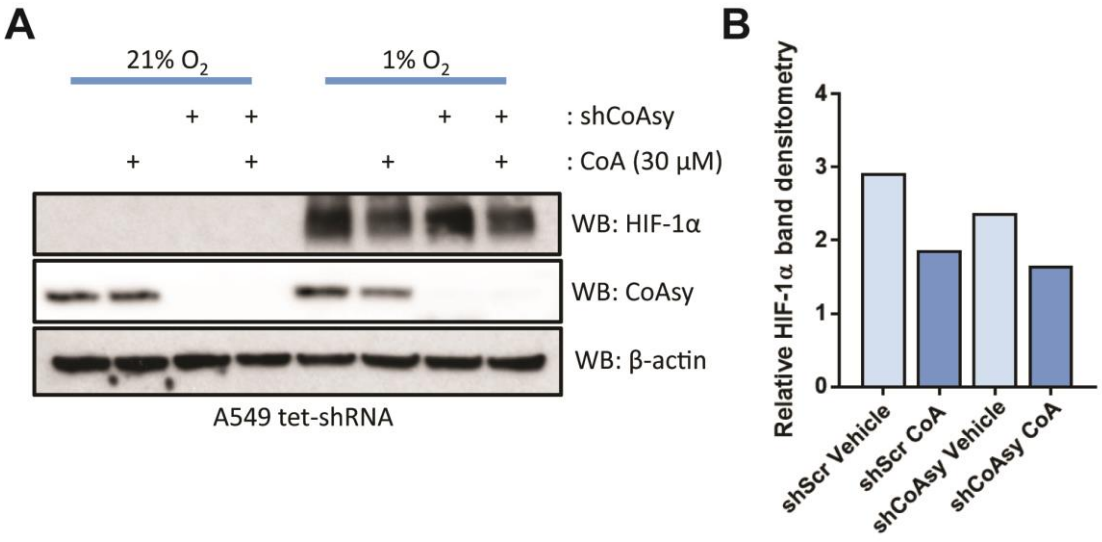

Figure 7.2.2: Transfection of A549-tet-shRNA cells with Coenzyme-A. A549-tet-shRNA cells were treated with doxycycline (25 ng.mL^{-1}) for 72 hours before being transfected with 30 µM CoA or equivalent volume of water using Lipofectamine transfection reagent. 2 hours post transfection cells were exposed to hypoxia for 4 hours before lysis and analysis by western blot (**A**). HIF-1α band intensity was calculated and normalized to β-actin and plotted in bar chart (**B**). N=1.

As can be seen in Figure 7.2.2 transfecting cells with CoA reduced HIF-1α protein expression in both the shScr and shCoAsy cell lines. The dose of 30 µM was used, as this is double the intracellular concentration of CoA in HeLa cells. No information was available as to the concentration of CoA in A549 cells at the time of this experiment. This suggests that it is possible to transfect CoA to cells, therefore future experiments will be performed with the addition of

acetyl-CoA as well as other precursors such as 4'pantetheine as a negative control. However in addition to this assay, a key future experiment is to develop a reliable method for determining CoA and CoA derivative concentrations in cell samples. This will confirm that the transfection reagent is successfully delivering the desired metabolite to cells.

7.2.1 Acetyl-CoA and HIF-1α

The main function of acetyl-CoA in cells is to act as an acetyl-carrier. The acetyl group is a labile subgroup that has been reported in many proteins. A number of acetylation events have been reported in HIF-1α. One such event is ARD1 mediated acetylation of HIF-1α at K532; this acetylation event was reported to destabilize HIF-1α through increased association with pVHL and subsequent increased turnover [226], therefore it stands to reason that loss of CoAsy may reduce this acetylation event and result in stabilised HIF-1α. However this result has been debated as further research has shown that only a specific splice variant of mouse ARD1 is able to acetylate HIF-1α whereas no such activity was observed with human ARD1 [227, 228]. HIF-1α is further acetylated at the N-terminus which acts to stabilize the protein post-translation [158]. This suggests that loss of CoAsy could regulate HIF through altered acetylation, however studies in A549 cells have shown that despite reduction of both CoA and acetyl-CoA following CoAsy knockdown, there is no significant changes in acetylation [204]. Instead certain proteins actually displayed increased acetylation, however HIF-1α was not reported to have differential acetylation in this dataset. Future experiments should directly assay HIF-1α acetylation following loss of CoAsy, as it is unclear whether this will increase or decrease

acetylation. This can be achieved through Immunoprecipitation of HIF-1α and western blot with an α-acetyl-lysine antibody.

7.3 The role of CoA and CoAsy in the TCA cycle and metabolic regulators of HIFs

CoA plays a major role in TCA cycle function as highlighted in figure 4.2.3.1. TCA cycle is impaired during low oxygen tension, indeed it is widely reported that not only is there a reduction of flux through the pathway, various metabolites accumulate during hypoxia such as succinate. Furthermore some of these metabolites have been reported to regulate HIF stability, often through inhibition of prolyl-hydroxylase function. This complex interplay between CoA, TCA cycle and HIF activity suggests an interesting biological relationship that may help explain how CoAsy regulates HIF. In addition to this, the glycolytic switch is a known occurrence in cancer; loss of CoAsy may also be a potential driver of this change in metabolism. Initial tracer analysis was performed with labeled glucose; this analysis involves growing cells with a metabolite labeled with a ‘heavy’ isotope, in this case all 6 carbons labeled with ^{13}C, followed by analysis of metabolites by mass spectrometry. Through this approach it is possible to quantify the total level of metabolites in cells as well as the contribution of the starting metabolite to that pool, which makes it possible to obtain an idea of how metabolites move through various pathways.

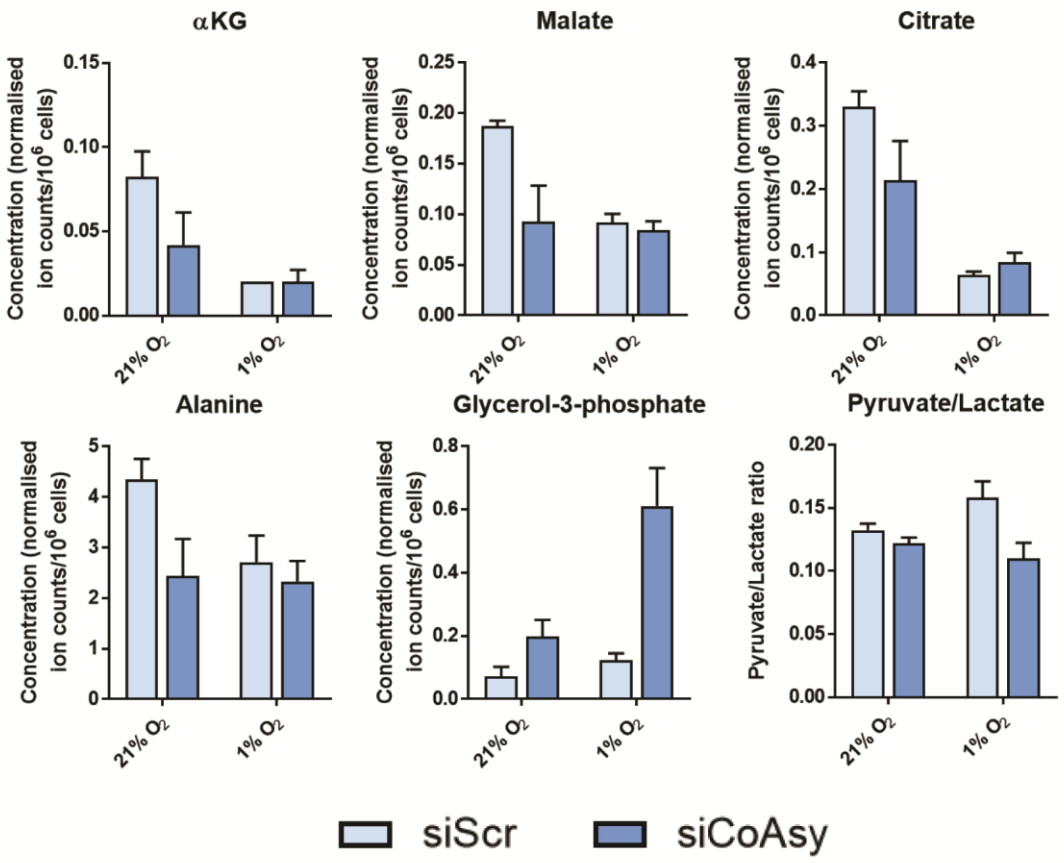

Figure 7.3.1: Steady state levels of metabolites from A549 cells. A549 cells were treated with siRNA targeting *COASY* or scrambled control for 24 hours before placing into hypoxia for 48 hours. 'Heavy' glucose media was added for final 24 hours before lysis and sent to Dr. Daniel Tennant for analysis. Full data set in appendix

The steady state levels of metabolites show a partial phenocopy of the hypoxia following loss of CoAsy in 21% O_2, this is highlighted in the levels of α-ketogluturate (αKG), malate and to a lesser extent citrate. Alanine also showed this trend, the majority of cellular alanine production occurs through transamination of pyruvate. Through analysis of the distribution of isotopomers, it is possible to determine the contribution of labeled glucose to each pool, which suggests how metabolic pathways are utilized following loss of CoAsy.

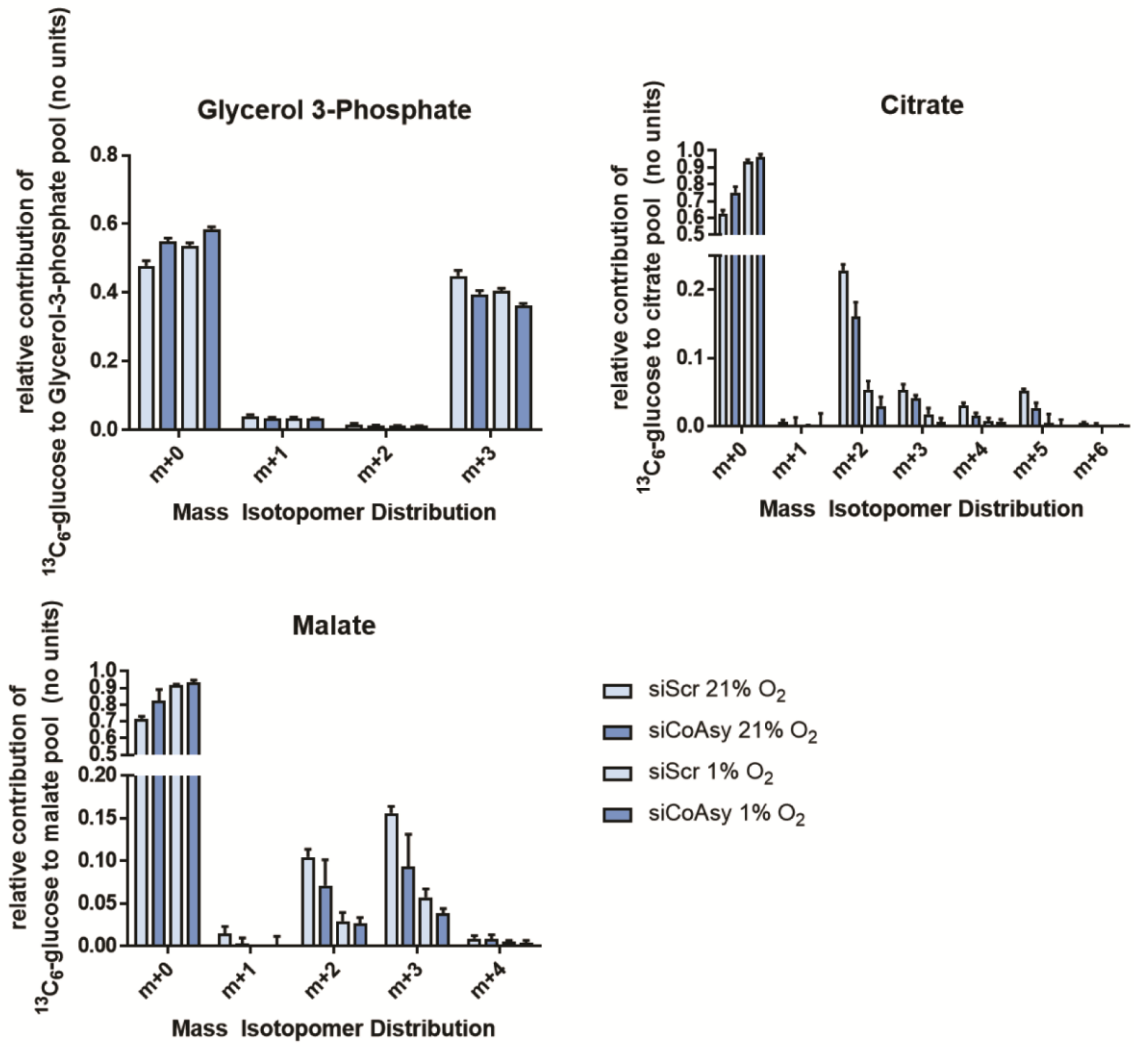

Figure 7.3.2: Mass isotopomer peaks for indicated metabolite as measured by mass spectrometry. Experiment was performed as previously described. Full dataset in appendix.

Through analysis of the labeled mass isotopomer ratio it can be seen that despite the increase in levels of glycerol 3-phosphate there is no significant change in the production, with the majority still being produced from glucose. However there is still a large proportion of unlabeled glycerol-3-phosphate from each condition (M+0 peak). Two metabolites in the TCA cycle have been highlighted here, analysis of citrate shows the M+2 peak shows a reduction in labeled glucose following treatment with siCoAsy, as this peak corresponds to citrate derived from acetyl-CoA feeding in from pyruvate dehydrogenase it

implies the 2 carbon metabolism is hindered. Comparison of the siScr conditions in normoxia and hypoxia reveals an even greater decrease in labeled glucose, this is to be expected as it has been well reported the HIF-mediated upregulation of PDK1 will result in increased phosphorylation of PDHA1 and subsequent inhibition of the dehydrogenase complex activity. In hypoxia the siRNA against CoAsy displays further reduction in labeling suggesting increased impairment of PDH complex activity beyond normally observed in hypoxia. Similar results were observed for malate. This leads to the question of what is the cellular fate of pyruvate?

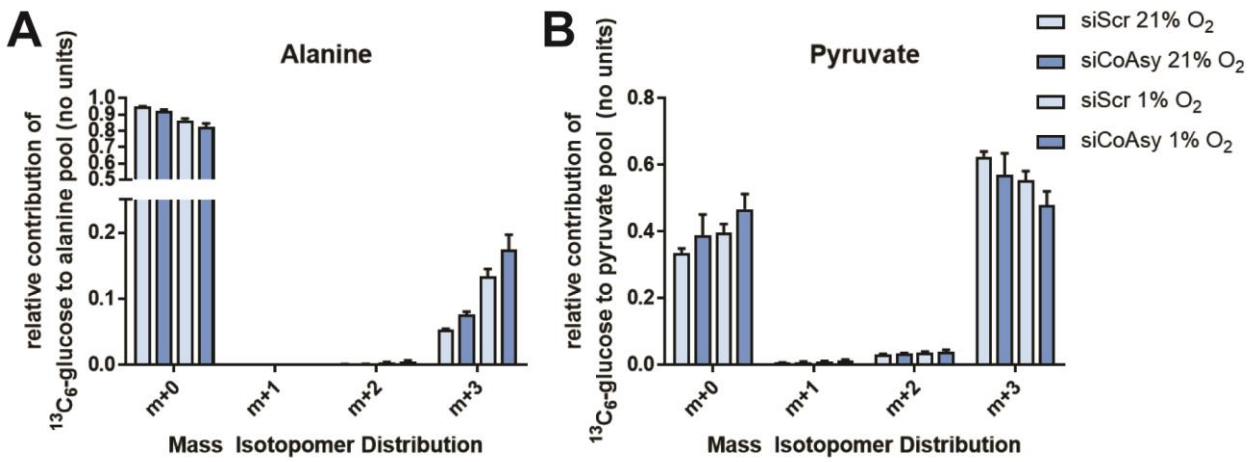

Figure 7.3.3: The contribution of glucose to alanine and pyruvate pools in A549 cells following loss of CoAsy. Mass isotopomer peaks for Pyruvate (**A**) and Alanine (**B**) as measured by mass spectrometry. Experiment was performed as previously described. Full dataset in appendix.

As can be seen in **Fig 7.3.3A** the majority of pyruvate comes from the labeled glucose. There is a small decrease in the glucose derived pyruvate pool following exposure to hypoxia, which is further increased with loss of CoA. The converse is true of alanine, where the majority of alanine remained unlabeled whereas the small labeled proportion indicates an increase of the M+3 population following loss of CoAsy, which is further increased following

exposure to hypoxia thereby suggesting an increased rate of transamination of pyruvate. It is important to note that the majority of TCA cycle intermediates displayed low levels of labeling with the majority of peaks from M+0 pool, which suggests that these cells rely heavily on glutamine as a carbon source. Whilst these results give a clue as to the metabolic flux following loss of CoAsy, further experiments should be repeated in an alternative cell line and with labeled glutamine experiments to compliment these findings. This is of particular importance due to the high levels of glutamine dependency observed in cultured cancer cells.

One interesting observation in this dataset is the reduction of steady-state levels of αKG. Prolyl-hydroxylase enzymes (PHDs) require αKG as well as O_2 for activity; therefore it stands to reason that this reduction of αKG may result in reduced PHD activity and subsequently stabilised HIFα. There is a commercially available antibody that specifically recognizes the hydroxylated proline residue in HIF-1α (P564), which acts as surrogate readout of PHD activity.

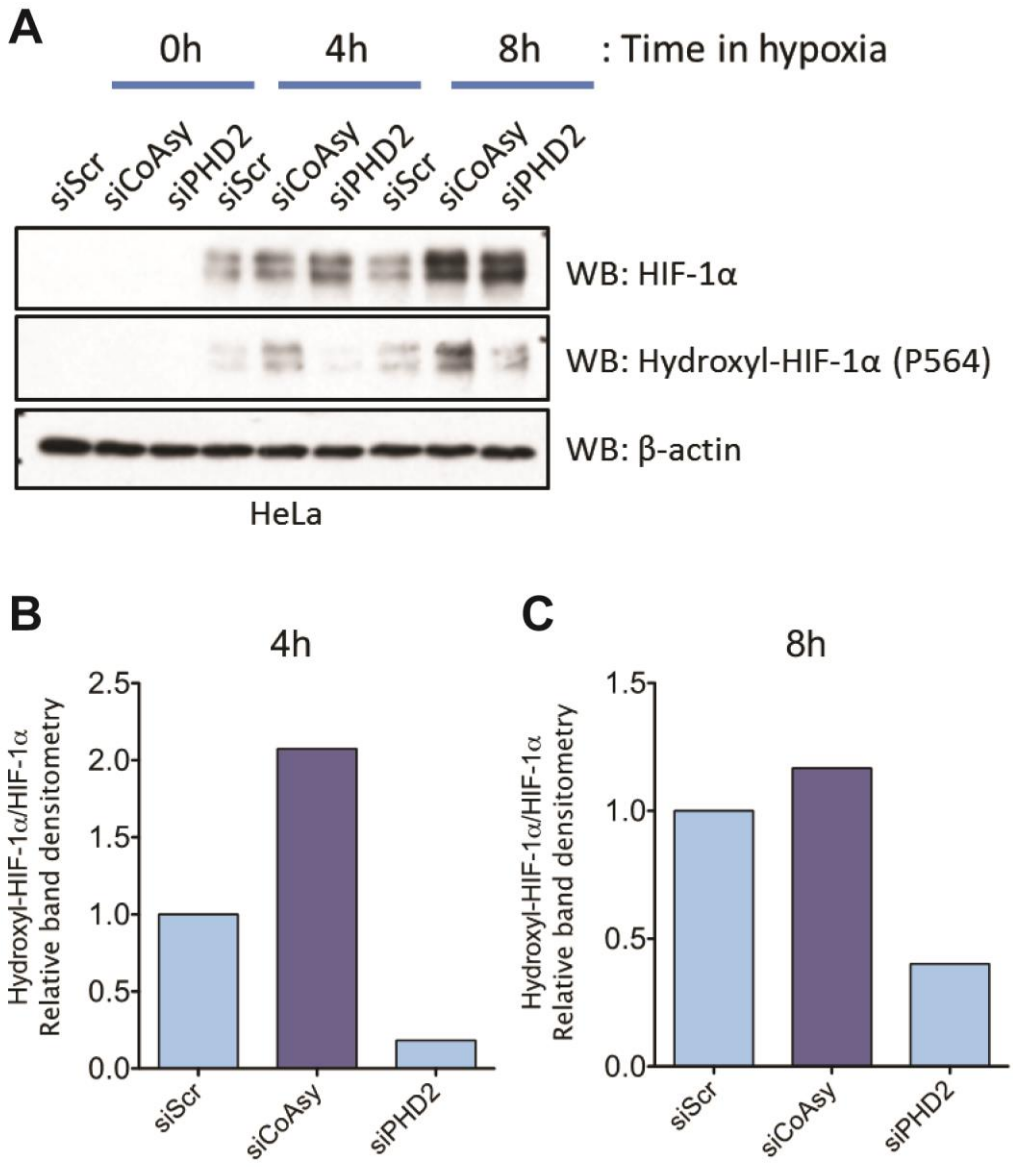

Figure 7.3.4: Loss of CoAsy does not alter HIF-1α hydroxylation. HeLa cells were treated with siRNA against *COASY*, *PHD2* and non-targeting control (40 nM). 72 hours post transfection cells were exposed to hypoxia (1% O_2) for 0, 4 and 8 hours before cell lysis and analysis by western blot (**A**). Densitometry of hydroxylated HIF-1α was quantified using ImageJ and normalysed to HIF-1α band densitometry. N=1.

In HeLa cells loss of CoAsy results in stabilised HIF-1α in both 4 and 8 hours of hypoxia as observed in other cell lines (**Fig. 7.3.4A**). Interestingly, the hydroxylated HIF-1α blot also shows increased in the siCoAsy treated cells in hypoxia, normalizing the hydroxylated HIF densitometry to total shows that in 4h (**B**) of hypoxia there is increased levels compared to scrambled control and

no change in 8 hours of hypoxia (**C**). For this assay the cells were lysed in RIPA buffer with EDTA free protease inhibitors, this buffer will completely lyse the cells and block protein degradation however some enzymatic activity may remain. Therefore the hydroxylation HIF is likely to have occurred post cell lysis and reoxygenation of samples whilst samples were being prepared for western blot. Despite this, it is still possible to determine whether hydroxylation is inhibited, as knockdown of PHD2 results in a large decrease of P564 hydroxylation (**Fig. 7.3.4B-C**). Therefore this datum suggests that loss of CoAsy does not impair prolyl hydroxylase activity, despite the reduction in αKG. Further experiments are required to test this such as MG132 chase and *in vitro* hydroxylation assays.

7.4 CoAsy regulates HIF-1α stability at the 30-389 and oxygen dependent degradation domain (ODDD)

Analysis of *HIF1A* and *HIF2A* mRNA did not show a significant increase following loss of CoAsy, therefore it was postulated that the increase in HIF protein occurs post transcription. Following this segments of HIF-1α were transfected in to A549 cells that had been treated with siRNA against *COASY*, *PHD2* and non-targeting control. Following loss of CoAsy there was a stabilization of the 30-389 and ODDD domains of HIF-1α with no change observed in the C-terminal domain (630-826). Little is known as to how the 30-389 domain is regulated, such novel findings could present different mechanisms of HIF degradation and alternative therapeutic options to target HIF signaling. The advantage of these overexpression segments of HIF is that they each contain the same promoter and 3' UTR, thereby ensuring the same

transcription and translation initiation occurs for each construct in conditions tested. The 30-389 domain contains a number of ubiquitinated residues that have been identified via unbiased screening for post-translational modifications. However no functional validation has been performed for these. Future experiments in determining whether these ubiquitination events are altered following loss of CoAsy are key to determining if these are the reason for the HIF regulation. The initial experiments to be performed will be immunoprecipitation of each segment in cell lines with CoAsy knocked down and western blot with α-ubiquitin antibody. Once changes have been characterized following loss of CoAsy mutation of each residue will allow for mapping of the specific residue or residues affected. This potential mechanism opens up potential for targeted therapies; as if there is an associated deubiquitinase (DUB) enzyme for these ubiquitination sites that is effected following loss of CoAsy, then this DUB poses an attractive candidate for drug inhibition.

7.5 Global CoAlation in hypoxia and specific CoAlation of HIF-1α

Protein CoAlation is a recently identified protein post-translational modification that is increased upon redox stress. Due to the previous literature surrounding hypoxia and this projects interest in CoA, the impact of hypoxia on CoAlation was analysed both basal levels and following redox stress. Treatment with menadione and H_2O_2 greatly increased protein CoAlation in normoxia, however exposure to hypoxia reduced protein CoAlation induced by menadione. This effect was not observed following treatment with H_2O_2, indicating that this decrease is perhaps a menadione specific effect. However the induction

observed following H_2O_2 treatment was not equal to that observed with menadione making cross comparisons difficult between these two treatments (see figures 4.4.1-2). Conversely basal levels of CoAlation increased following exposure to hypoxia, it has long been established that ROS levels increase following exposure to hypoxia therefore it stands to reason this could explain the increase in CoAlation. Attempts to identify direct CoAlation of HIF-1α were inconclusive. *In vitro* CoAlation assays showed reactivity with the α-CoA antibody, however this could be in part due to the GST tag. IP of endogenous HIF-1α from HEK293T cells did not show any signs of specific CoAlation, however the basal levels of CoAlation are low within these cells. IP of HIF-1α in HEK293-Pank1β cells showed a signal that potentially corresponds to CoAlated HIF-1α, however further validation is required. The functional consequence of CoAlation is yet to be determined, previous studies have shown recombinant enzymes show a reduction of activity following CoAlation in *in vitro* assays, however how this may alter HIF-1α is unclear. CoAlation occurs at free thiol groups of cysteine residues, of which a number have been identified in the PAS domains of mouse HIF-1α (which share near complete amino acid sequence homology) (**Fig. 7.5**). Therefore it stands to reason that HIF-1α could be subject to protein CoAlation, yet the biological significance of this is unclear.

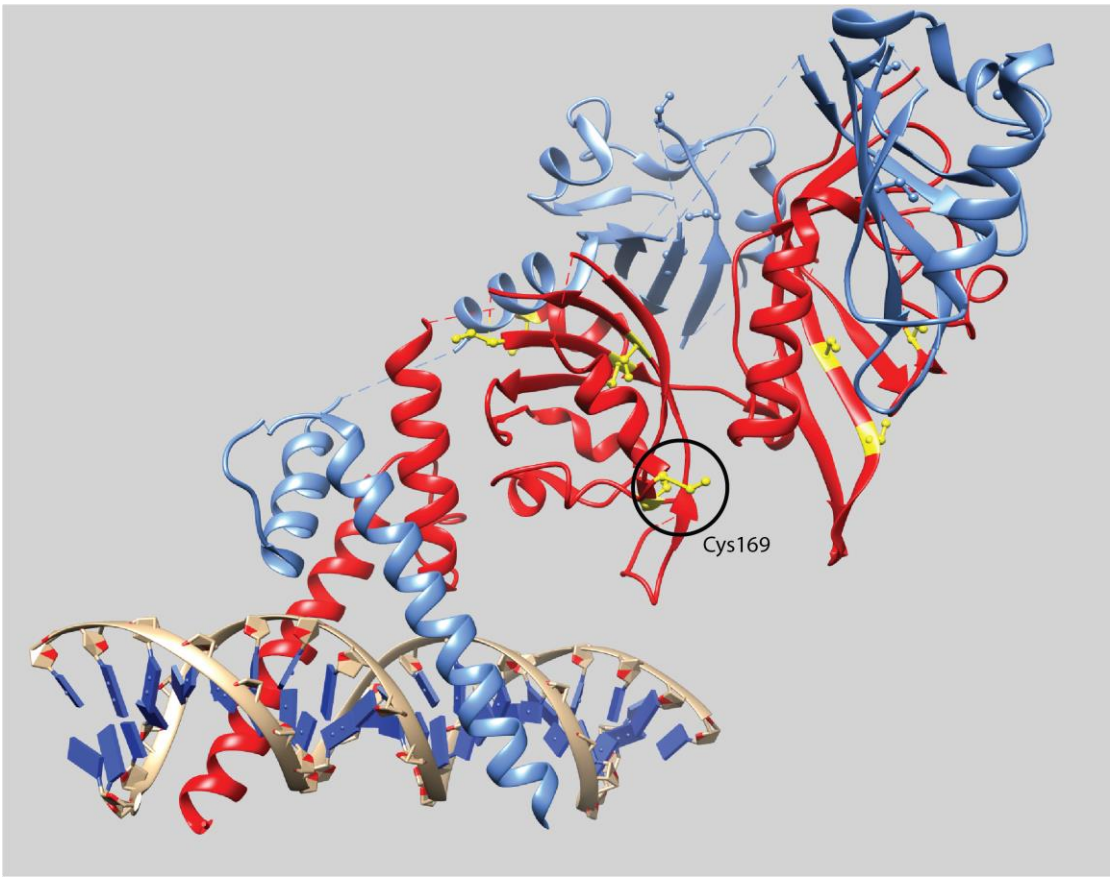

Figure 7.5: HIF-1α contains exposed cysteine residues in the 30-389 region. Crystal structure of mouse HIF-1α (red), HIF-1β (blue) and HRE sequence of DNA (brown and blue). Exposed free cysteine Cys169 is highlighted in black. Crystal structure PDB number: 4ZPR [229]. Image was prepared using Chimera.

7.6 The role of CoAsy in suppressing tumour aggressiveness

HIF signaling is a known driver of tumourigenesis across multiple cancer types and has been shown to increase tumour burden, cell proliferation, metastasis and drug resistance [230-232]. Therefore it stands to reason that increased HIF as a consequence of loss of CoAsy will recapitulate this phenotype. *In vitro* assays in A549-tet-shRNA inducible lines showed no difference between the shScr and the shCoAsy knockdown lines suggesting that loss of CoAsy and subsequent HIF stabilization did not affect tumourigenicity, however increased colony formation was observed in T47D cell inducible cell lines. It is unclear why this is the case, highlighting differences between both CoAsy and HIF

biology between in these cancer lines. In the A549-tet-shRNA there was only a modest increase in HIF target genes following loss of CoAsy suggesting that this stabilised HIF-1α, whilst this panel needs to be expanded and there was large variability in this assay, it indicates that in this cell line the increased HIF may not be as active on endogenous genes as on synthetic reporters. This could potentially explain why no changes were observed in proliferation or clonogenic potential following loss of CoAsy. However the increased clonogenic potential observed in T47D cells may not be through HIF activity, therefore the experiment should be repeated with knockdown of *HIF1A*, *HIF2A* or *ARNT* in order to determine if HIF activity is required and if there is any isoform specificity driving this phenotype. Furthermore qRT-PCR analysis of HIF target genes following loss of CoAsy in T47D cells should be performed, this will show if the stabilised HIF-1α is active in this cell line and if the *in vitro* data corroborates and implies causality to the breast cancer patient data where low *COASY* mRNA expression correlates with increased HIF target gene expression.

In addition to the proliferation based assays, wound healing assays were performed in the A549-tet-shRNA lines. Once again, no significant differences were observed between the two lines. This 2D wound closure assay can indicate differences in migration, however the coated plastic plates used for standard cell culture does not accurately mimic the extracellular matrix and poorly represents true metastasis. To address this transwell migration assays were performed whereby cells are plated on top of a thin layer of matrigel in a transwell insert (**Fig. 7.6A1**) and placing in high serum medium (**Fig. 7.6A2**).

Cells then migrate through matrigel (**Fig. 7.6A3**) before being stained with crystal violet and manually counted.

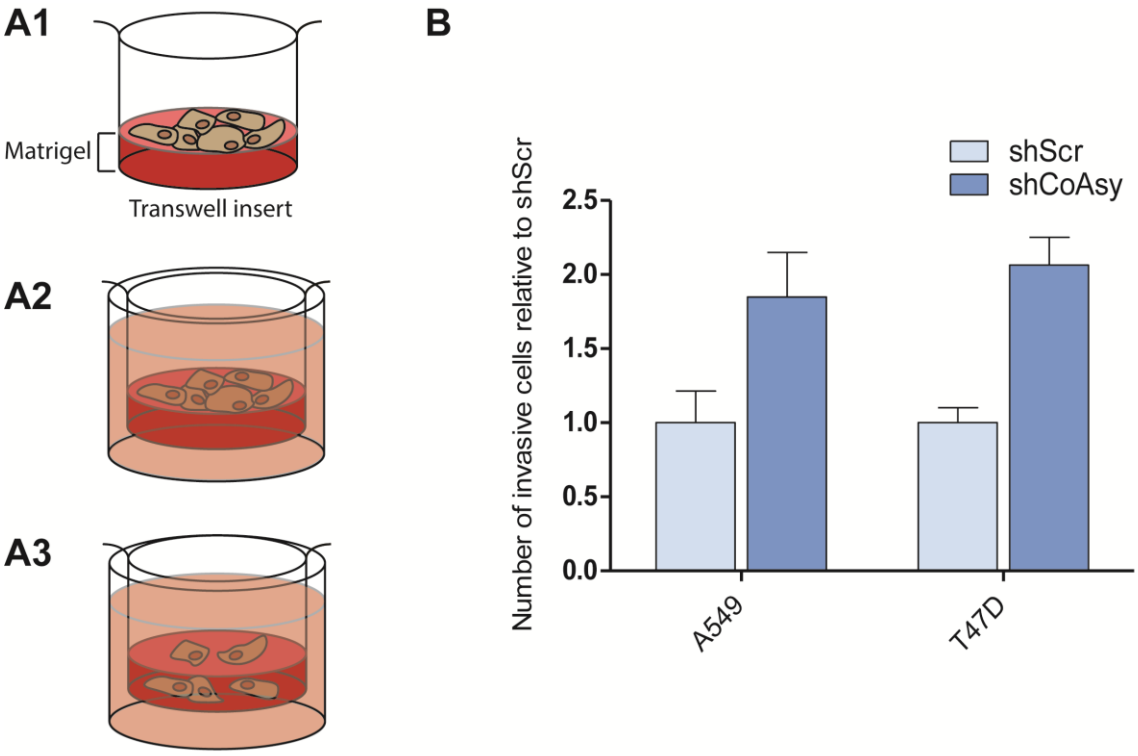

Figure 7.6: Loss of CoAsy increases cell migration through matrigel. A) Schematic diagram of transwell matrigel assay, cells are plated on top of a thin layer of matrigel (**A1**) before being placed in to high serum media (**A2**) to stimulate migration (**A3**). **B**) Transwell migration assay of A549 and T47D-tet-shRNA lines. Lines were pretreated with doxycycline (25 ng.mL-1) for 72 hours before plating and performing assay. Bar chart is mean of technical replicates ± SD. Experiment was performed by Dr. Miguel Hermida. N=1.

The matrigel invasion assay differs from the 2D assay in that before the cells invade through the matrigel the solid matrix must be degraded and space created for cells to invade through. In this preliminary experiment, loss of CoAsy increases cell invasion through matrigel in both the A549 and T47D lines. Whilst further repeats are required to confirm this result, this data indicates that CoAsy may curtail cell invasion and metastasis. It is unclear whether this is a result of increased HIF signaling; therefore this experiment should be repeated with knockdown of *HIF1A*, *HIF2A* and *ARNT*.

7.7 CoAsy expression in cancer

Through various bioinformatics approaches and analysis of CoAsy protein in lung tissue it was clear that high CoAsy expression correlated with poor patient outcome in lung cancer. There was a difference observed in overall survival between the lung adenocarcinoma (LUAD) cohort and lung squamous cell carcinoma (LUSC) cohort, whilst neither result was significant, when stratifying patients by *COASY* expression the hazard ratio was 0.79 for LUSC whereas it was 1.31 for LUAD. It is unclear why this may be the case; the cell type of origin for squamous cell carcinoma is still much debated with tumours postulated to arise from the squamous cells lining the proximal airway however LUSC arises from neuroendocrine cells. This highlights the importance of cellular context in considering CoAsy biology, indeed analysis of transcriptomes of adenocarcionmas and squamous cell carcinomas across multiple organ sites indicated that the histology represented gene expression variation more than organ site [233].

In breast cancer patients there was reduced *COASY* mRNA expression in primary tumour compared to adjacent and surrounding. Furthermore, stratifying patients by receptor patients revealed that CoAsy expression (both mRNA and protein) correlated with receptor status. In addition to this, low CoAsy expression correlated with poor patient outcome. Triple negative breast cancer (TNBC) remains an area of unmet need, with chemotherapy used as current standard first line treatment. Whilst a number of TNBC patients respond well to chemotherapy and appear to display increased sensitivity compared to other molecular subtypes of breast cancer, there is still a large subset of patients that

do not respond well and have limited therapeutic options [234]. Therefore identifying novel targets are of utmost importance. It has been reported that TNBC display an increased hypoxic signature, with elevated levels of HIF target gene expression [88]. Analysis of TCGA RNA-seq data displayed a significant negative correlation between *COASY* expression and a number of HIF target genes. It is unclear as to the relationship between CoAsy expression and HIF in TNBC as the only breast cancer cell line with CoAsy levels modified thus far has been T47D, which is an ER/PR positive cell line. As most of the TNBC cell lines assessed thus far have displayed low basal levels of CoAsy, future work should be performed to see if re-expression of CoAsy can reduce the HIF target gene expression and pseudo-hypoxic phenotype observed in these cell lines. In addition to this, the results show a reduction of *COASY* mRNA compared to adjacent tissue, however it is unclear whether this is observed at the protein level or not. The emerging role of protein translation in cancer is becoming increasingly well understood; therefore the levels of mRNA may not always reflect the protein levels. To address this future experiments should be performed to stain for CoAsy in breast TMA containing malignant tissue and matched normal tissue to determine if the RNA-seq data from the in-house cohort holds true for larger cohorts at the protein level.

So far this work has addressed CoAsy expression in lung and breast cancer, however targeting of hypoxic sensitive pathways is of significant interest in other cancers such as renal cell carcinoma. A defining event in clear cell renal cell carcinoma (ccRCC) is the early loss of chromosome 3p.2, in particular the *VHL* gene [235]; this results in stabilised HIF-1α and HIF-2 protein, interestingly

later stage disease also presents with loss of chromosome 14q and the subsequent deletion of *HIF1A* gene and it has been postulated that *HIF1A* acts as a tumour suppressor gene in this cancer [94, 235]. As CoAsy regulates HIF through the 30-389 region as well as the ODDD it is unlikely that this occurs in a VHL dependent manner as this is known to regulate ubiquitilyation at Lys674 therefore CoAsy may act as an alternative regulator of HIF in ccRCC.

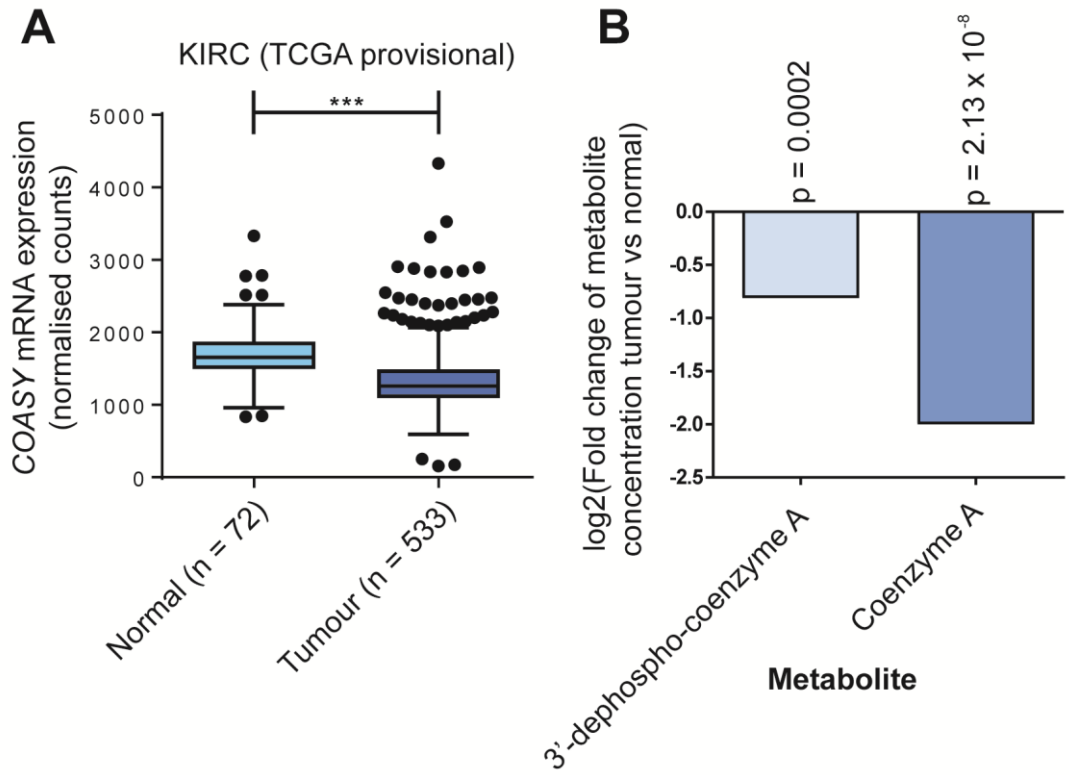

Figure 7.7: COASY and CoA is lost in ccRCC: A) *COASY* mRNA expression in clear cell renal cell carcinoma patients (ccRCC) taken from TCGA provisional data accessed via firebrowse server. **B**) Log2 of the fold change of concentration of the indicated metabolite in tumour vs normal adjacent tissue from clear cell renal cell carcinoma patients.

Analysis of RNA-seq data from TCGA provisional dataset from ccRCC patients displays a significant reduction of *COASY* expression in the tumour compared to adjacent normal tissue (**Fig. 7.7A**). Furthermore, published direct metabolomics analysis from 20 ccRCC patients and matched adjacent tissue displays a significant reduction of CoA levels (~75% reduction) in the tumour

samples, suggesting errors in CoA biosynthesis are impaired in tumour (**Fig. 7.7B**). Validation is required to test if CoAsy acts as a negative regulator of HIF in ccRCC cell lines however the patient data suggests that this disease is an interesting model with significant clinical potential for novel HIF-related targeted therapies.

7.8 Targeting loss of CoAsy in cancer cells

In order to identify an inhibitor that selectively targets CoAsy deficient cells, a library of 1170 FDA approved compounds was screened against A549, T47D and MCF10A inducible shRNA lines. The library encompasses a wide array of compounds, all of which contain a significant amount of preclinical data. One hit identified from the screen was the calcium channel blocker nicardipine HCl, which selectively targets the CaV1.2 isoform and is currently approved for treatment of hypertension. The first repeat showed ~3 fold selectivity for the CoAsy deficient A549 cells, the IC_{50} for this result was 3.26 µM, whilst the affinity of nicardipine HCl for the calcium channel receptor is in the sub micromolar range [236], furthermore the free available concentration in plasma achieved in patients following administration of 20 mg of nicardipine was ~100 nM [237], well below that required to kill A549 shCoAsy cells. Therefore nicardipine HCl would serve as a poor treatment option in targeting CoAsy deficient disease, however the high IC_{50} implies that the cell death observed is occurring by an off target mechanism and suggests that nicardipine may act as a tool compound in determining the off-target effect and a more appropriate inhibitor can be used. Whilst the subsequent data suggests this was a false positive, further cell lines with loss of CoAsy should be tested before fully

dismissing this result as false, particularly as selectivity was observed across each tested line in the primary drug screen.

7.9 The role of CoAsy in regulating immune checkpoint blockade

The field of immunotherapy has grown significantly over recent years with successful clinical trials performed across multiple cancer types. The bulk of current therapies target the PD-1/PD-L1 axis. Programmed death receptor 1 (PD-1) is a receptor expressed on activated T-cells which will initiate cell killing of neoplastic cells, however many cancers upregulate programmed death ligangd 1 (PD-L1) which renders these cells 'invisble' to the T-cells upon binding of the ligand to the receptor. Thereby inhibiting this interaction through either targeting of the receptor or ligand has proven to be successful in treating patients. There has been controversy regarding this as recent studies have shown that PD-L1 is a poor biomarker for anti-PD1 therapy suggesting alternative pathways are at play, however further understanding as to the mechanism behind the upregulation of these immune checkpoints is of significant interest. It has been reported that *CD274*, the gene that encodes PD-L1, is a hypoxic responsive gene. Therefore it stands to reason that loss of a negative regulator of HIF may induce increased PD-L1 expression. Analysis of TCGA (provisional) breast cancer dataset displays a significant negative correlation between *COASY* and *CD274* (Spearman's correlation = -0.1948, $p < 0.0001$), furthermore a significant correlation was also observed between *COASY* and *CTLA4* (Spearmean's correlation = -0.2279, $p < 0.0001$), an alternative immune checkpoint regulator (**Fig 7.9.1A-B**).

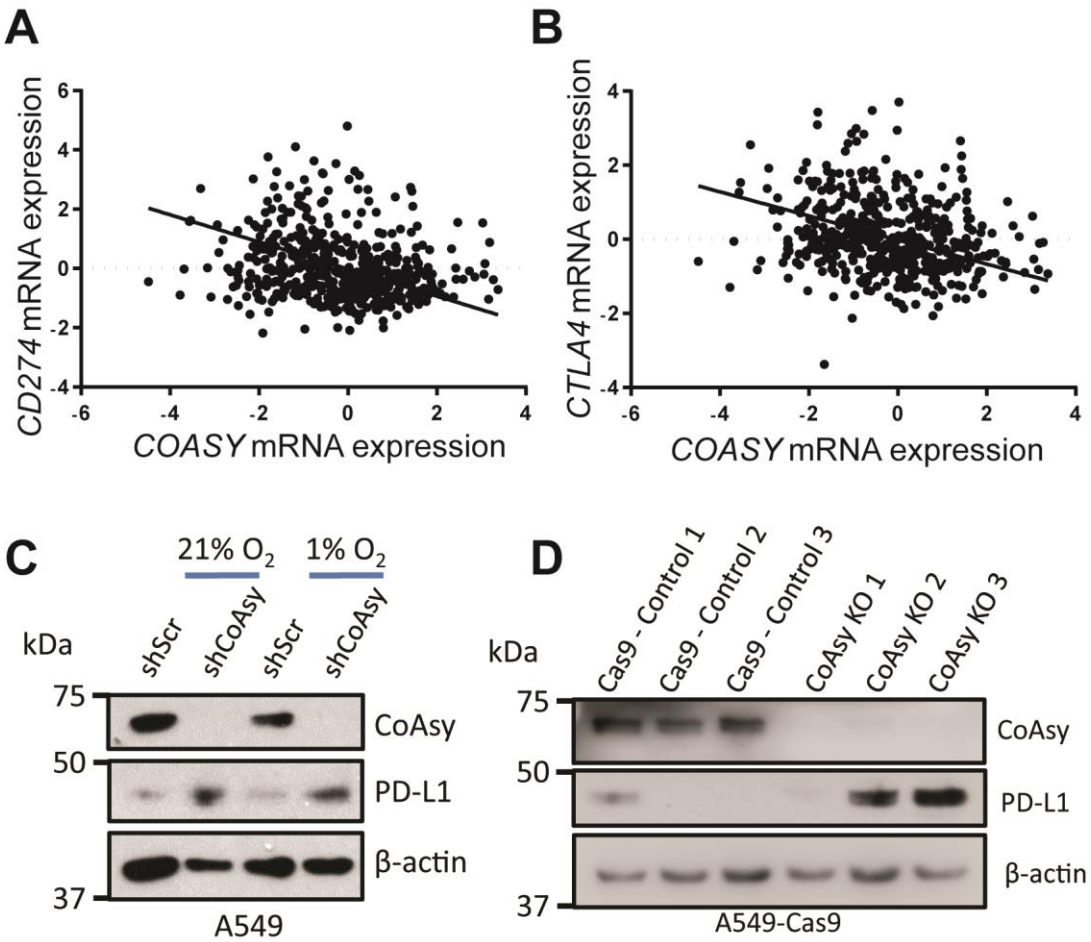

Figure 7.9.1: CoAsy may immune checkpoint blockade: A-B) Correlation of *COASY* with *CD274* (**A**) and *CTLA4* (**B**) mRNA levels. Data taken from TCGA provisional breast cancer dataset. **C**) A549-tet-shRNA cells were treated with doxycycline (25 ng.mL^{-1}) for 72 hours before being placed into hypoxia for 8 hours and cell lysis. N=1. **D**) A549 cells stably expressing Cas9 were transfected with crRNA against CoAsy or non-tareting control. Clones were selected and analysed by western blot. N=1.

To test directly if loss of CoAsy regulates PD-L1 protein expression, A549-tet-shRNA lines were treated with doxycycline to induce knockdown and cultured in normoxia or hypoxia (**Fig. 7.9.1A**). In addition to this a number of A549 lines that were edited with CRISPR/Cas9 to produce a hypermorphic form of CoAsy that is expressed at significantly lower levels were tested in normoxia (**Fig. 7.9.1B**). In both cases loss of CoAsy resulted in increased levels of PD-L1 protein. It is unclear if this is a HIF-dependent increase in protein. As patient data shows a negative correlation between *COASY* and *CD274* mRNA, the

upregulation is likely to occur at the transcriptional level and may be via HIF activity however direct validation is required to test this. Furthermore this requires validating in a wider range of cell types and an increased repertoire of immune checkpoint regulators such as CTLA-4 and IDO. Nevertheless, this initial finding offers up the exciting prospect of a novel regulator of immune checkpoint in tumour cells.

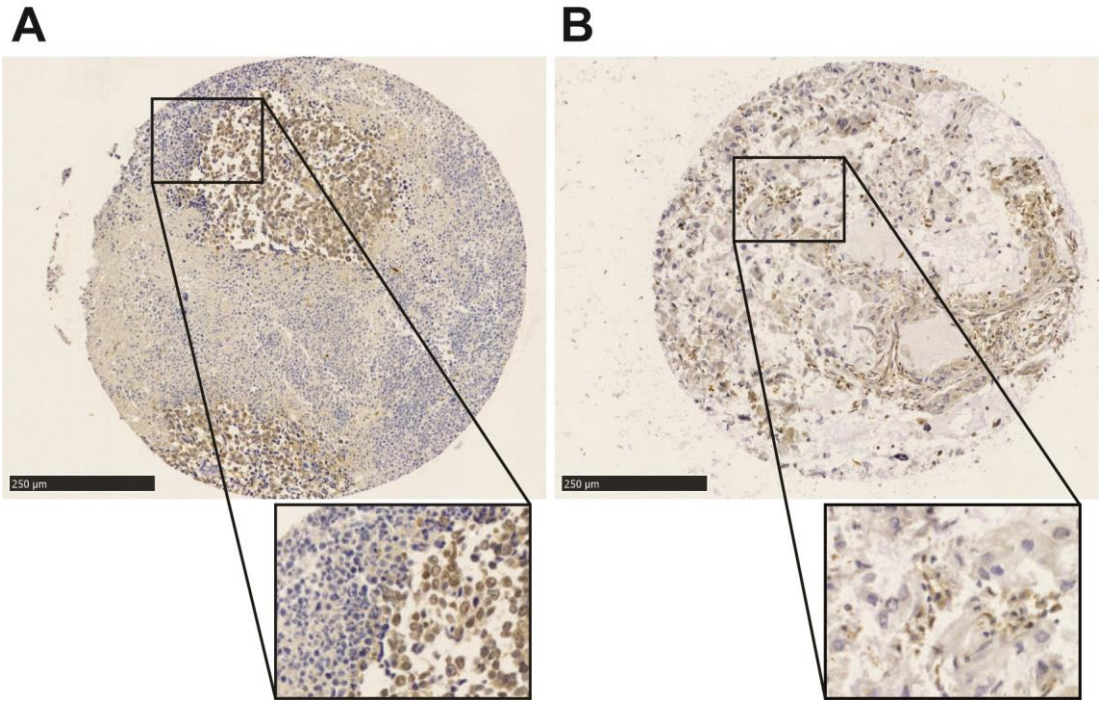

Figure 7.9.2: CoAsy expression is higher in infiltrating lymphocytes. Representative cores from lung TMA stained with anti-CoAsy pAb. **A**) Core shows weakly stained tumour cells surrounded by lymphocytes, highlighted region on the left and tumour cells on the right. **B**) Core shows weakly stained tumour cells from infiltrating lymphocytes displaying increased staining intensity. Scale bars indicate 250 µM.

Staining of the lung TMA showed increased CoAsy protein present in infiltrating lymphocytes (**Fig. 7.9.2A**). It was not possible to determine the lineage of these infiltrating cells as no counterstain was performed for specific markers, however in cores where the immune cells did not invade the tumour cells the staining was less intense (**Fig. 7.9.2B**). There are multiple possible explanations for this change. One possibility is the requirement for increased cellular CoA in

infiltrating and activated immune cells, as increased CoAsy may shift CoA homeostasis in these cells. Another possibility is the role of CoA in controlling macrophage polarization. Recent studies have identified that the cardiovascular drug etoxomir inhibits macrophage polarization (by IL-4) at high concentrations as a direct consequence of depleting intracellular CoA levels. The authors did not fully determine the molecular mechanism behind how CoA regulates macrophage polarization, however there is potential for this to occur through a HIF dependent pathway as HIF signaling has been shown to be crucial for both M1 and M2 macrophage activation.

7.10 Concluding remarks

Through this work we have identified CoAsy as a novel negative regulator of HIF-1α and HIF-2α at the post-translational stage. Whilst the mechanism behind this regulation is not known as of yet, the regions of HIF most affected have been identified, one of which contains a number of uncharacterized post-translational modifications. The datum further suggests that this occurs through depletion of CoA or CoA derivatives; whilst a number of metabolites have been identified as regulators of HIFs there has been no reports of CoA homeostasis being linked to hypoxic signaling. Analysis of patient samples highlighted loss of CoAsy in breast cancer, particularly in triple negative breast cancer. Furthermore, the *in vitro* experiments showed that CoAsy can regulate HIF in multiple cancer types which suggests that this biology may extend to other cancer types, indeed we have further shown that *COASY* is lost in ccRCC tumours compared to adjacent normal tissue. Furthermore we have performed a drug screen to identify an inhibitor that selectively targets CoAsy deficient

cells; whilst no specific inhibitor has been validated yet, a number show potential in developing a targeted therapy against CoAsy deficient cancers.

Appendix

8. Appendix

8.1 Alternative biological replicate for A549-tet-shRNA KD

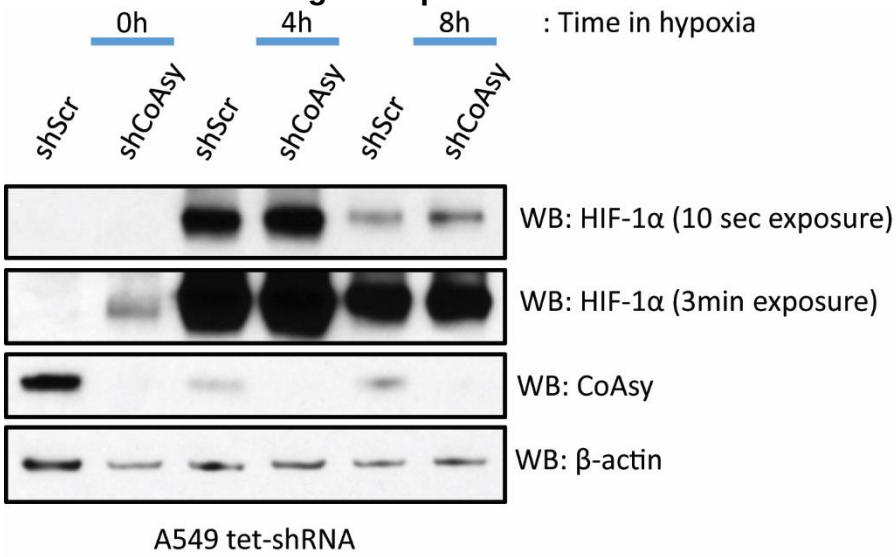

Figure 8.1: Knockdown of CoAsy in A549-tet-shRNA cells. A549-tet-shRNA inducible lines were plated before being treated with 25 ng.mL^{-1} doxycycline for 72 hours. Cells were exposed to hypoxia for 0, 4 or 8 hours hypoxia before cell lysis and analysis by western blot.

8.2 Alternative graphical representation of qRT-PCR data from figure 3.1.6.5

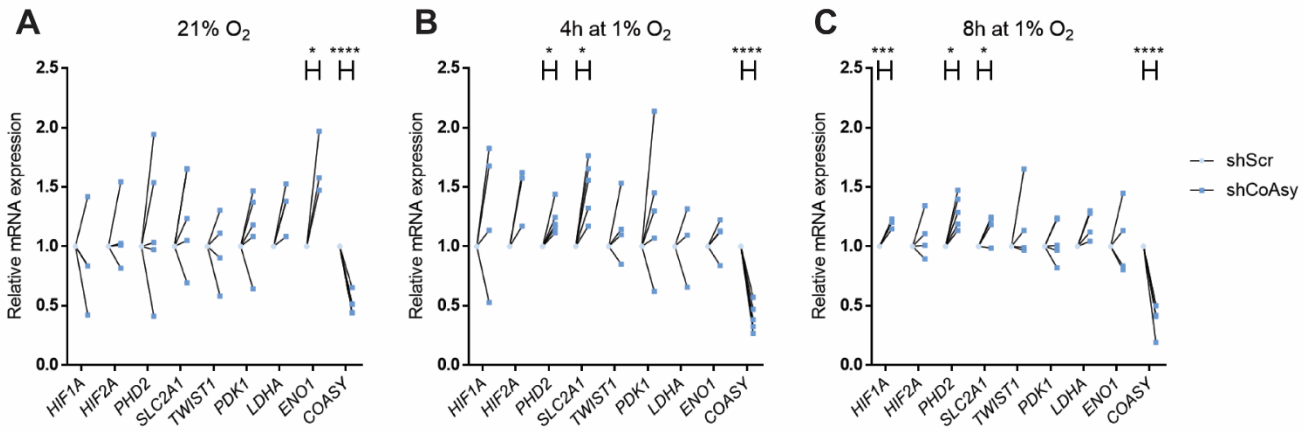

Figure 8.2: qRT-PCR analysis of HIF target genes and *HIF1A* and *HIF2A* mRNA levels. A549 cells were treated with doxycycline (25 ng.mL-1) for 72 hours before being placed in hypoxia for 0 (**A**), 4 (**B**) or 8 (**C**) hours before cell lysis and analysis by qRT-PCR. Results are mean ± SD. n=4. Statistical tests are multiple T-tests with Holm-Sidak method. * $p < 0.05$, ** $p < 0.01$, *** $p < 0.001$, **** $p < 0.0001$

8.3 Alternative biological replicate of HEK293-Pank1β treated with H_2O_2

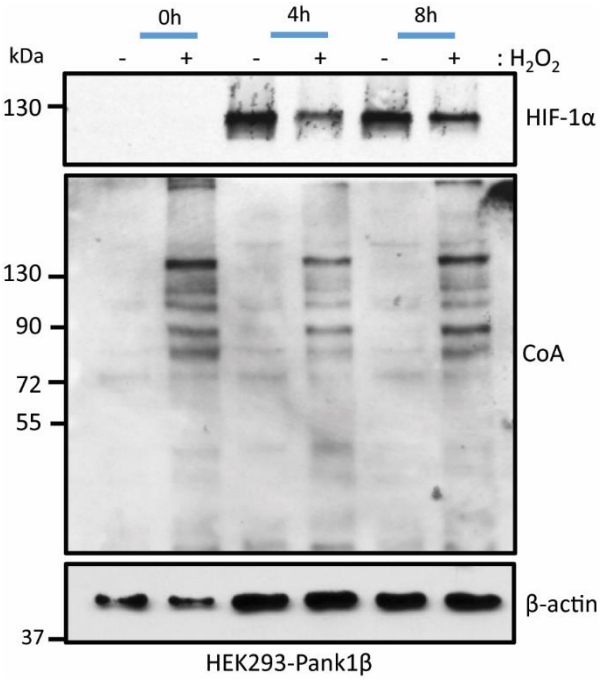

Figure 8.3: Alternative biological replicate of HEK293-Pank1β treated with H_2O_2. Non-reducing western blot analysis of Protein CoAlation in hypoxia following H_2O_2 treatment. HEK293-Pank1β cells were cultured in 1% O_2 for 0, 4 and 8 hours before treating with 500 µM of H_2O_2 for the final 30 minutes of incubation before cell lysis.

8.4 Remaining two biological replicates for T47D clonogenic assay

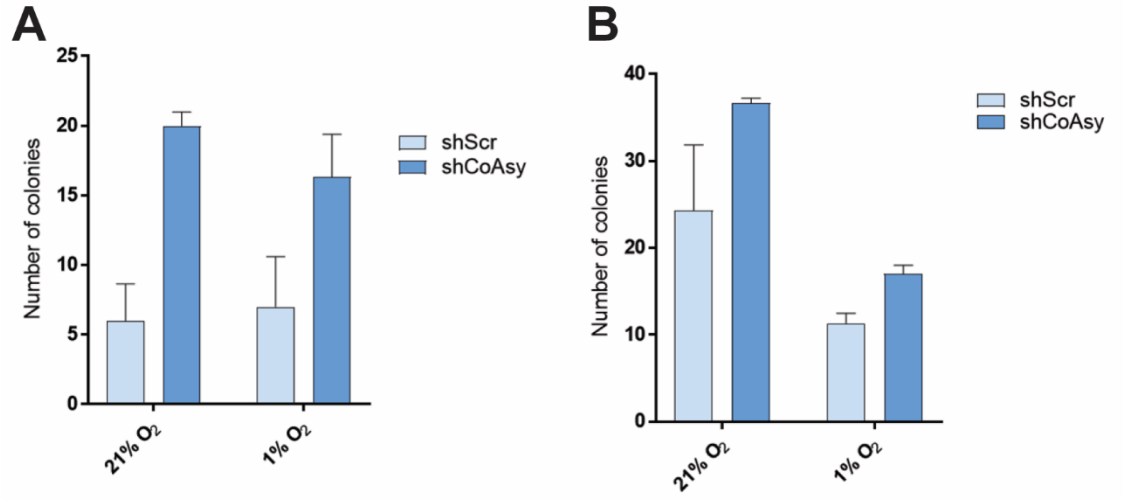

Figure 8.4: Colony assay of T47D-tet-shRNA cell lines. T47D-tet-shRNA cells were pretreated with doxycycline before replating at 100 cells per well in 6 well plates before culturing for 10 days in 21% O_2 or 1% O_2. Colonies were fixed stained and counted. **A** and **B** represent individual biological replicates to accompany figure 4.5.5

8.5 Full data set from ^{13}C Glucose tracer experiments

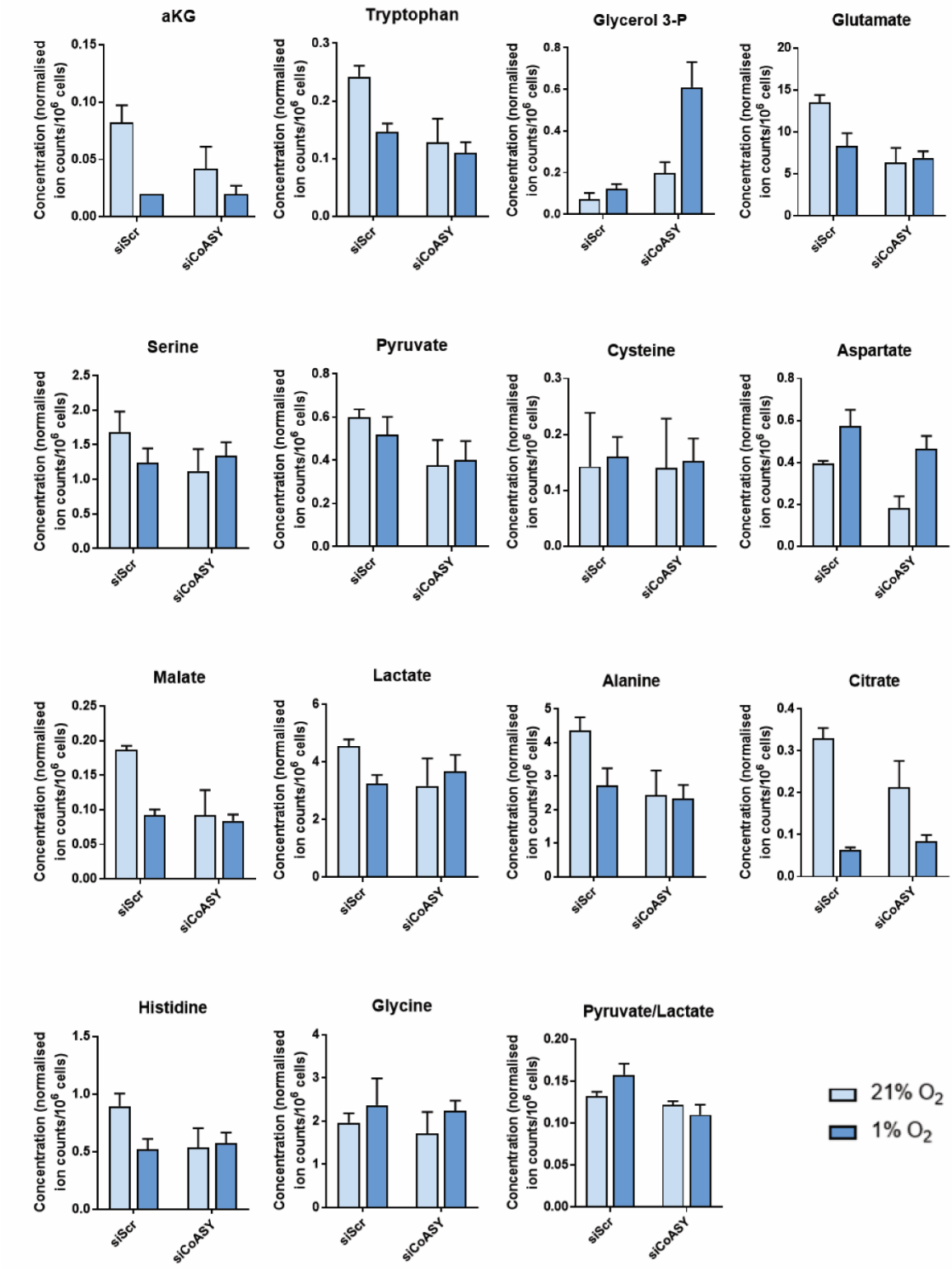

Figure 8.5.1: Steady state levels of metabolites from A549 cells. A549 cells were treated with siRNA targeting *COASY* or scrambled control for 24 hours before placing into hypoxia for 48 hours. 'Heavy' glucose media was added for final 24 hours before lysis and sent to Dr. Daniel Tennant for analysis

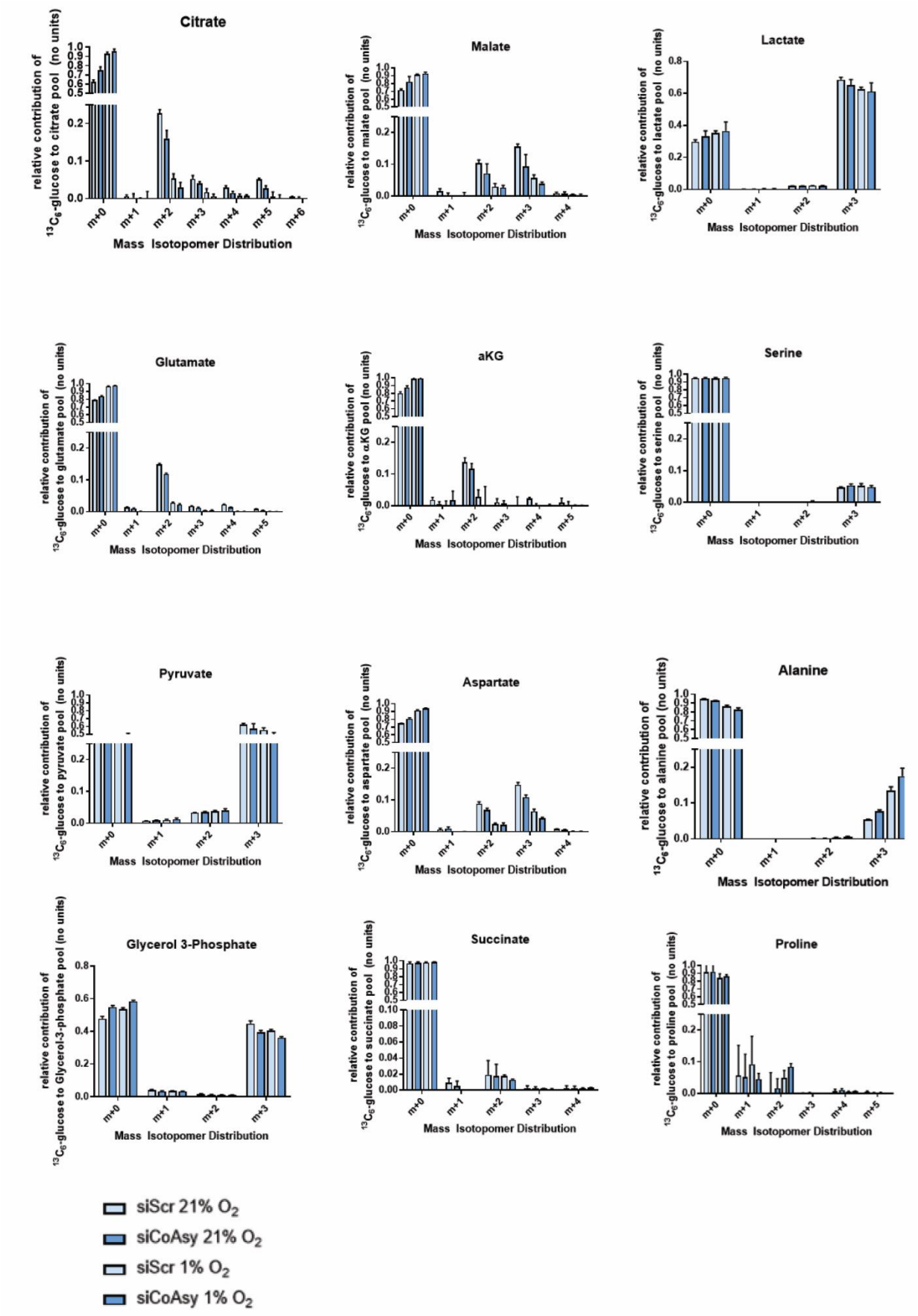

Figure 8.5.2: Mass isotopomer peaks for indicated metabolite as measured by mass spectrometry. Experiment was performed as previously described.

References:

1. UK, C.R. *Cancer incidence for common cancers*. Cancer Research UK 2016 [cited 2018 21/09/18]; Available from: http://www.cancerresearchuk.org/health-professional/cancer-statistics/incidence/common-cancers-compared.
2. WHO. *Cancer: Key facts*. 2018 [cited 2018 21/09/18]; Available from: http://www.who.int/news-room/fact-sheets/detail/cancer.
3. Weinberg, D.H.a.R., *The hallmarks of cancer.* Cell, 2000. **100**(1): p. 57-70.
4. Weinberg, D.H.a.R., *Hallmarks of Cancer: The Next Generation.* Cell, 2011. **144**: p. 646-674.
5. Gazdar, A.F., *Activating and resistance mutations of EGFR in non-small-cell lung cancer: role in clinical response to EGFR tyrosine kinase inhibitors.* Oncogene, 2009. **28**(Suppl 1): p. S24-S31.
6. Harbour, J.W. and D.C. Dean, *The Rb/E2F pathway: expanding roles and emerging paradigms.* Genes Dev, 2000. **14**(19): p. 2393-409.
7. Adams, J. and S. Cory, *The Bcl-2 apoptotic switch in cancer development and therapy.* Oncogene, 2007. **26**(9): p. 1324-37.
8. Jafri, M.A., et al., *Roles of telomeres and telomerase in cancer, and advances in telomerase-targeted therapies.* Genome Med, 2016. **8**.
9. Carmeliet, P., *VEGF as a key mediator of angiogenesis in cancer.* Oncology, 2005. **69 Suppl 3**: p. 4-10.
10. Kalluri, R., *The basics of epithelial-mesenchymal transition.* 2009. **119**(6): p. 1420-8.
11. UK, C.R. *www.cancerresearchuk.org/health-professional/cancer-statistics/statistics-by-cancer-type/lung-cancer*. 2016 21/09/18].
12. Simon, J.W.M., *Novel insights into the molecular origins and treatment of lung cancer.* Cell Cycle, 2010. **9**(20): p. 4098-4105.
13. Semenova, E.A., R. Nagel, and A. Berns, *Origins, genetic landscape, and emerging therapies of small cell lung cancer.* Genes & Development, 2015. **29**(14): p. 1447-1462.
14. Hanna, J.M. and M.W. Onaitis, *Cell of origin of lung cancer.* Journal of Carcinogenesis, 2013. **12**: p. 6.
15. Oser, M.G., et al., *Transformation from non-small-cell lung cancer to small-cell lung cancer: molecular drivers and cells of origin.* The Lancet. Oncology, 2015. **16**(4): p. e165-e172.
16. Chen, Z., et al., *Non-small-cell lung cancers: a heterogeneous set of diseases.* Nature Reviews Cancer, 2014. **14**: p. 535.
17. Lynch, T.J., et al., *Activating Mutations in the Epidermal Growth Factor Receptor Underlying Responsiveness of Non–Small-Cell Lung Cancer to Gefitinib.* New England Journal of Medicine, 2004. **350**(21): p. 2129-2139.
18. Shi, Y., et al., *A prospective, molecular epidemiology study of EGFR mutations in Asian patients with advanced non-small-cell lung cancer of adenocarcinoma histology (PIONEER).* J Thorac Oncol, 2014. **9**(2): p. 154-62.

19. Román, M., et al., *KRAS oncogene in non-small cell lung cancer: clinical perspectives on the treatment of an old target.* Molecular Cancer, 2018. **17**: p. 33.
20. Morgensztern, D., S. Devarakonda, and R. Govindan, *Genomic landscape of squamous cell carcinoma of the lung.* Am Soc Clin Oncol Educ Book, 2013: p. 348-53.
21. George, J., et al., *Comprehensive genomic profiles of small cell lung cancer.* Nature, 2015. **524**(7563): p. 47-53.
22. Campbell, J.D. and A. Alexandrov, *Distinct patterns of somatic genome alterations in lung adenocarcinomas and squamous cell carcinomas.* 2016. **48**(6): p. 607-16.
23. Solomon *et al.*, *First-line crizotinib versus chemotherapy in ALK-positive lung cancer.* N. Engl. J. Med, 2014. **371**: p. 2167-2177.
24. Forde, P.M., et al., *Neoadjuvant PD-1 Blockade in Resectable Lung Cancer.* New England Journal of Medicine, 2018. **378**(21): p. 1976-1986.
25. Gandhi, L., et al., *Pembrolizumab plus Chemotherapy in Metastatic Non–Small-Cell Lung Cancer.* New England Journal of Medicine, 2018. **378**(22): p. 2078-2092.
26. Reck, M., et al., *Pembrolizumab versus Chemotherapy for PD-L1–Positive Non–Small-Cell Lung Cancer.* New England Journal of Medicine, 2016. **375**(19): p. 1823-1833.
27. Capelletto, E., A. Mariniello, and S. Novello, *Targeted therapy in small cell lung cancer: A new era?* Lung Cancer, 2017. **108**: p. 252-253.
28. CRUK. *Breast Cancer statistics*. 21/09/18]; Available from: https://www.cancerresearchuk.org/health-professional/cancer-statistics/statistics-by-cancer-type/breast-cancer.
29. Polyak, K., *Breast cancer: origins and evolution.* The Journal of Clinical Investigation, 2007. **117**(11): p. 3155-3163.
30. Allen, M.D., et al., *Altered microenvironment promotes progression of preinvasive breast cancer: myoepithelial expression of alphavbeta6 integrin in DCIS identifies high-risk patients and predicts recurrence.* Clin Cancer Res, 2014. **20**(2): p. 344-57.
31. Hon, J.D.C., et al., *Breast cancer molecular subtypes: from TNBC to QNBC.* American Journal of Cancer Research, 2016. **6**(9): p. 1864-1872.
32. Jacquet, E., et al., *Endocrine therapy or chemotherapy as first-line therapy in hormone receptor-positive HER2-negative metastatic breast cancer patients.* Eur J Cancer, 2018. **95**: p. 93-101.
33. Inic, Z., et al., *Difference between Luminal A and Luminal B Subtypes According to Ki-67, Tumor Size, and Progesterone Receptor Negativity Providing Prognostic Information.* Clinical Medicine Insights. Oncology, 2014. **8**: p. 107-111.
34. Kallioniemi, O.P., et al., *ERBB2 amplification in breast cancer analyzed by fluorescence in situ hybridization.* Proceedings of the National Academy of Sciences, 1992. **89**(12): p. 5321-5325.
35. Alluri, P. and L. Newman, *Basal-like and Triple Negative Breast Cancers: Searching For Positives Among Many Negatives.* Surgical oncology clinics of North America, 2014. **23**(3): p. 567-577.
36. Perou, C.M., et al., *Molecular portraits of human breast tumours.* Nature, 2000. **406**(6797): p. 747-52.

37. Nik-Zainal, S., et al., *Landscape of somatic mutations in 560 breast cancer whole-genome sequences.* Nature, 2016. **534**: p. 47.
38. Mayer, P.V.a.A., *Hypoxia in cancer: significance and impact on clinical outcome.* Cancer Metastasis Rev., 2007. **26**(2): p. 225-239.
39. McKeown, S.R., *Defining normoxia, physoxia and hypoxia in tumours-implications for treatment response.* Br J Radiol, 2014. **87**(1035): p. 20130676.
40. Meijer, T.W., et al., *Targeting hypoxia, HIF-1, and tumor glucose metabolism to improve radiotherapy efficacy.* Clin Cancer Res, 2012. **18**(20): p. 5585-94.
41. Nordsmark, M., et al., *Prognostic value of tumor oxygenation in 397 head and neck tumors after primary radiation therapy. An international multi-center study.* Radiother Oncol, 2005. **77**(1): p. 18-24.
42. H. Lyng, K.S.a.K.R., *Changes in tumor oxygen tension during radiotherapy of uterine cervical cancer: relationships to changes in vascular density, cell density and frequeny of mitosis and apoptosis.* Int. J. Radiat. Oncol. , 2000. **98**: p. 139-142.
43. F. Dehdashti *et al.*, *In Vivo assessment of tumor hypoxia in lung cancer with ^{60}Cu-ATSM.* Eur. J. Nucl. Med. Mol. Imaging, 2003. **30**: p. 844-850.
44. L. Li, M.H., H. Zhu, W. Zhao, G. Yang and J. Yu, *Comparison of ^{18}F-Fluoroerythronitroimidazole and F-Fluorodeoxyglucose positron emission tomography and prognostic value in locally advanced non-small cell lung cancer.* Clinical Lung Cancer, 2010. **11**(5): p. 335-340.
45. G. Wang, B.J., E. Rue and G. Semenza, *Hypoxia-inducible factor 1 is a basic-helix-loop-helix-PAS heterodimer regulated by cellular O2 tension.* Proc. Natl. Acad. Sci. USA, 1995. **92**(12): p. 5510-5514.
46. B. Keith, R.J.a.M., Simon, *HIF-1a and HIF-2a: sibling rivalry in hypoxic tumour growth and progression.* Nat. Rev. Cancer, 2012. **12**: p. 9-23.
47. Tian, H., S.L. McKnight, and D.W. Russell, *Endothelial PAS domain protein 1 (EPAS1), a transcription factor selectively expressed in endothelial cells.* Genes Dev, 1997. **11**(1): p. 72-82.
48. Wiesener *et al.*, *Widespread, hypoxia-inducible expression of HIF-2a in distinct cell populations of different organs.* FASEB, 2002. **17**(2): p. 271-273.
49. M. Maynard, H., Qi. J. Chung, E, Lee. Y. Kondo, S. Hara, R. Conaway, J. Conaway and M. Ohh, *Multiple splice variants of the human HIF-3 alpha locus are targets of the von hippel-lindau E3 ubiquitin ligase complex.* J. Biol. Chem, 2003. **278**(13): p. 11032-11040.
50. Y. Makino, A.K., W. Wilson, H. Tanaka and L. Poellinger, *Inhibitory PAS domain protein (IPAS) is a hypoxia-inducible splicing variant of the hypoxia-inducible factor-3alpha locus.* J. Biol. Chem, 2002. **277**(36): p. 32405-32408.
51. P. Zhang, Q.Y., L. Lu, P. Chen and C. Duan, *Hypoxia-inducible factor 3 is an oxygen dependent transcription activator and reglates a distinct transcriptional response to hypoxia.* Cell Reports, 2014. **6**: p. 1110-1121.
52. Wenger, R.H., D.P. Stiehl, and G. Camenisch, *Integration of oxygen signaling at the consensus HRE.* Sci STKE, 2005. **2005**(306): p. re12.
53. J. Schodel, S.O., J. Ragoussis, C. Pugh, P. Ratcliffe and D. Mole, *High-resolution genome-wide mapping of HIF-binding sites by ChIP-seq.* Blood, 2011. **117**(23).

54. C. Hu, L.W., L. Chodosh, B. Keith and M. Simon, *Differential roles of Hypoxia inducible factor-1a (HIF-1a) and HIF-2a in hypoxic gene regulation.* Mol. Cell. Biology, 2003. **23**(24): p. 9361-9374.
55. R. Raval, K.L., M. Tran, H. Sowter, S. Mandriota, J. Li, C. Pugh, P. Maxwell, A. Harris and P. Ratcliffe, *Contrasting propterties of HIF-1 and HIF-2 in von hippel-lindau associated renal cell carcinoma.* Mol. Cell. Biology, 2005. **25**(13): p. 5675-5686.
56. Ivan, M., et al., *HIFalpha targeted for VHL-mediated destruction by proline hydroxylation: implications for O2 sensing.* Science, 2001. **292**(5516): p. 464-8.
57. Jaakkola, P., et al., *Targeting of HIF-alpha to the von Hippel-Lindau ubiquitylation complex by O2-regulated prolyl hydroxylation.* Science, 2001. **292**(5516): p. 468-72.
58. Epstein, A.C., et al., *C. elegans EGL-9 and mammalian homologs define a family of dioxygenases that regulate HIF by prolyl hydroxylation.* Cell, 2001. **107**(1): p. 43-54.
59. Masson, N., et al., *Independent function of two destruction domains in hypoxia-inducible factor-alpha chains activated by prolyl hydroxylation.* Embo j, 2001. **20**(18): p. 5197-206.
60. Berra, E., et al., *HIF prolyl-hydroxylase 2 is the key oxygen sensor setting low steady-state levels of HIF-1α in normoxia.* The EMBO Journal, 2003. **22**(16): p. 4082-4090.
61. Song, D., et al., *Defective Tibetan PHD2 binding to p23 links high altitude adaption to altered oxygen sensing.* J Biol Chem, 2014. **289**(21): p. 14656-65.
62. Hirsila, M., et al., *Characterization of the human prolyl 4-hydroxylases that modify the hypoxia-inducible factor.* J Biol Chem, 2003. **278**(33): p. 30772-80.
63. Ehrismann, D., et al., *Studies on the activity of the hypoxia-inducible-factor hydroxylases using an oxygen consumption assay.* Biochemical Journal, 2007. **401**(Pt 1): p. 227-234.
64. Iliopoulos, O., et al., *Negative regulation of hypoxia-inducible genes by the von Hippel-Lindau protein.* Proc Natl Acad Sci U S A, 1996. **93**(20): p. 10595-9.
65. Cockman, M.E., et al., *Hypoxia inducible factor-alpha binding and ubiquitylation by the von Hippel-Lindau tumor suppressor protein.* J Biol Chem, 2000. **275**(33): p. 25733-41.
66. Schoenfeld, A., E.J. Davidowitz, and R.D. Burk, *A second major native von Hippel–Lindau gene product, initiated from an internal translation start site, functions as a tumor suppressor.* Proceedings of the National Academy of Sciences of the United States of America, 1998. **95**(15): p. 8817-8822.
67. Min, J.H., et al., *Structure of an HIF-1alpha -pVHL complex: hydroxyproline recognition in signaling.* Science, 2002. **296**(5574): p. 1886-9.
68. Hon, W.C., et al., *Structural basis for the recognition of hydroxyproline in HIF-1 alpha by pVHL.* Nature, 2002. **417**(6892): p. 975-8.
69. Cardote, T.A.F., M.S. Gadd, and A. Ciulli, *Crystal Structure of the Cul2-Rbx1-EloBC-VHL Ubiquitin Ligase Complex.* Structure, 2017. **25**(6): p. 901-911.e3.

70. Pause, A., et al., *The von Hippel-Lindau tumor-suppressor gene product forms a stable complex with human CUL-2, a member of the Cdc53 family of proteins.* Proc Natl Acad Sci U S A, 1997. **94**(6): p. 2156-61.
71. Petroski, M.D. and R.J. Deshaies, *Function and regulation of cullin-RING ubiquitin ligases.* Nat Rev Mol Cell Biol, 2005. **6**(1): p. 9-20.
72. Salceda, S. and J. Caro, *Hypoxia-inducible factor 1alpha (HIF-1alpha) protein is rapidly degraded by the ubiquitin-proteasome system under normoxic conditions. Its stabilization by hypoxia depends on redox-induced changes.* J Biol Chem, 1997. **272**(36): p. 22642-7.
73. D. Foxler, K.B., V. James, T. Webb, M. Mee, S. Wong, Y. Feng, D. Constantin-Teodosiu, T. Petursdottir, J. Bjornsson, S. Ingvarsson, P. Ratcliffe, G. Longmore & T. Sharp *The LIMD1 protein bridges an association between the prolyl hydroxylases and VHL to repress HIF-1 activity.* Nature Cell Biology, 2012. **14**: p. 201-208.
74. D'Angelo, G., et al., *Hypoxia up-regulates prolyl hydroxylase activity: a feedback mechanism that limits HIF-1 responses during reoxygenation.* J Biol Chem, 2003. **278**(40): p. 38183-7.
75. Foxler, D.E., et al., *A HIF–LIMD1 negative feedback mechanism mitigates the pro‐tumorigenic effects of hypoxia.* EMBO Molecular Medicine, 2018. **10**(8): p. e8304.
76. Mahon, P.C., K. Hirota, and G.L. Semenza, *FIH-1: a novel protein that interacts with HIF-1α and VHL to mediate repression of HIF-1 transcriptional activity.* Genes & Development, 2001. **15**(20): p. 2675-2686.
77. McNeill, L.A., et al., *Hypoxia-inducible factor asparaginyl hydroxylase (FIH-1) catalyses hydroxylation at the beta-carbon of asparagine-803.* Biochemical Journal, 2002. **367**(Pt 3): p. 571-575.
78. Freedman, S.J., et al., *Structural basis for recruitment of CBP/p300 by hypoxia-inducible factor-1α.* Proceedings of the National Academy of Sciences of the United States of America, 2002. **99**(8): p. 5367-5372.
79. Dames, S.A., et al., *Structural basis for Hif-1 alpha /CBP recognition in the cellular hypoxic response.* Proc Natl Acad Sci U S A, 2002. **99**(8): p. 5271-6.
80. Koivunen, P., et al., *Catalytic properties of the asparaginyl hydroxylase (FIH) in the oxygen sensing pathway are distinct from those of its prolyl 4-hydroxylases.* J Biol Chem, 2004. **279**(11): p. 9899-904.
81. Dayan, F., et al., *The oxygen sensor factor-inhibiting hypoxia-inducible factor-1 controls expression of distinct genes through the bifunctional transcriptional character of hypoxia-inducible factor-1alpha.* Cancer Res, 2006. **66**(7): p. 3688-98.
82. Q. Wang, D.H., Y. Rui, A. Jiang, Z. Liu and L. Huang, *Prognosis value of HIF-1a expression in patients with non-small cell lung cancer.* Gene, 2014. **541**: p. 69-74.
83. Nanni, S., et al., *Endothelial NOS, estrogen receptor beta, and HIFs cooperate in the activation of a prognostic transcriptional pattern in aggressive human prostate cancer.* J Clin Invest, 2009. **119**(5): p. 1093-108.
84. Osada, R., et al., *Expression of hypoxia-inducible factor 1alpha, hypoxia-inducible factor 2alpha, and von Hippel-Lindau protein in epithelial ovarian neoplasms and allelic loss of von Hippel-Lindau gene:*

nuclear expression of hypoxia-inducible factor 1alpha is an independent prognostic factor in ovarian carcinoma. Hum Pathol, 2007. **38**(9): p. 1310-20.
85. Yoshimura, H., et al., *Prognostic impact of hypoxia-inducible factors 1alpha and 2alpha in colorectal cancer patients: correlation with tumor angiogenesis and cyclooxygenase-2 expression.* Clin Cancer Res, 2004. **10**(24): p. 8554-60.
86. Yamamoto, Y., et al., *Hypoxia-inducible factor 1alpha is closely linked to an aggressive phenotype in breast cancer.* Breast Cancer Res Treat, 2008. **110**(3): p. 465-75.
87. Helczynska, K., et al., *Hypoxia-inducible factor-2alpha correlates to distant recurrence and poor outcome in invasive breast cancer.* Cancer Res, 2008. **68**(22): p. 9212-20.
88. Briggs, K.J., et al., *Paracrine Induction of HIF by Glutamate in Breast Cancer: EglN1 Senses Cysteine.* Cell, 2016. **166**(1): p. 126-39.
89. Gerlinger, M., et al., *Genomic architecture and evolution of clear cell renal cell carcinomas defined by multiregion sequencing.* Nat Genet, 2014. **46**(3): p. 225-233.
90. Lidgren, A., et al., *The expression of hypoxia-inducible factor 1alpha is a favorable independent prognostic factor in renal cell carcinoma.* Clin Cancer Res, 2005. **11**(3): p. 1129-35.
91. Klatte, T., et al., *Hypoxia-inducible factor 1 alpha in clear cell renal cell carcinoma.* Clin Cancer Res, 2007. **13**(24): p. 7388-93.
92. Kondo, K., et al., *Inhibition of HIF2alpha is sufficient to suppress pVHL-defective tumor growth.* PLoS Biol, 2003. **1**(3): p. E83.
93. Maranchie, J.K., et al., *The contribution of VHL substrate binding and HIF1-alpha to the phenotype of VHL loss in renal cell carcinoma.* Cancer Cell, 2002. **1**(3): p. 247-55.
94. Shen, C., et al., *Genetic and Functional Studies Implicate HIF1α as a 14q Kidney Cancer Suppressor Gene.* Cancer discovery, 2011. **1**(3): p. 222-235.
95. Raval, R.R., et al., *Contrasting properties of hypoxia-inducible factor 1 (HIF-1) and HIF-2 in von Hippel-Lindau-associated renal cell carcinoma.* Mol Cell Biol, 2005. **25**(13): p. 5675-86.
96. Zhao, Y. and A.A. Adjei, *Targeting Angiogenesis in Cancer Therapy: Moving Beyond Vascular Endothelial Growth Factor.* Oncologist, 2015. **20**(6): p. 660-73.
97. Dvorak, H.F., *Vascular Permeability Factor/Vascular Endothelial Growth Factor: A Critical Cytokine in Tumor Angiogenesis and a Potential Target for Diagnosis and Therapy.* Journal of Clinical Oncology, 2002. **20**(21): p. 4368-4380.
98. Liu, Y., et al., *Hypoxia regulates vascular endothelial growth factor gene expression in endothelial cells. Identification of a 5' enhancer.* Circ Res, 1995. **77**(3): p. 638-43.
99. Maxwell, P.H., et al., *Hypoxia-inducible factor-1 modulates gene expression in solid tumors and influences both angiogenesis and tumor growth.* Proc Natl Acad Sci U S A, 1997. **94**(15): p. 8104-9.
100. Hellstrom, M., et al., *Dll4 signalling through Notch1 regulates formation of tip cells during angiogenesis.* Nature, 2007. **445**(7129): p. 776-80.

101. Lobov, I.B., P.C. Brooks, and R.A. Lang, *Angiopoietin-2 displays VEGF-dependent modulation of capillary structure and endothelial cell survival in vivo.* Proc Natl Acad Sci U S A, 2002. **99**(17): p. 11205-10.
102. Simon, M.P., R. Tournaire, and J. Pouyssegur, *The angiopoietin-2 gene of endothelial cells is up-regulated in hypoxia by a HIF binding site located in its first intron and by the central factors GATA-2 and Ets-1.* J Cell Physiol, 2008. **217**(3): p. 809-18.
103. Rossler, J., et al., *The selective VEGFR1-3 inhibitor axitinib (AG-013736) shows antitumor activity in human neuroblastoma xenografts.* Int J Cancer, 2011. **128**(11): p. 2748-58.
104. Bellesoeur, A., et al., *Axitinib in the treatment of renal cell carcinoma: design, development, and place in therapy.* Drug Design, Development and Therapy, 2017. **11**: p. 2801-2811.
105. Keating, G.M., *Axitinib: a review in advanced renal cell carcinoma.* Drugs, 2015. **75**(16): p. 1903-13.
106. Heldin, C.-H., *Targeting the PDGF signaling pathway in tumor treatment.* Cell Communication and Signaling : CCS, 2013. **11**: p. 97-97.
107. Chen, E.Y., et al., *Hypoxia Activates a Platelet-derived Growth Factor Receptor/Phosphatidylinositol 3-Kinase/Akt Pathway That Results in Glycogen Synthase Kinase-3 Inactivation.* Cancer Research, 2001. **61**(6): p. 2429.
108. Roots, R. and K.C. Smith, *On the nature of the oxygen effect on x-ray-induced DNA single-strand breaks in mammalian cells.* Int J Radiat Biol Relat Stud Phys Chem Med, 1974. **26**(5): p. 467-80.
109. Meijer, T.W.H., et al., *Targeting Hypoxia, HIF-1, and Tumor Glucose Metabolism to Improve Radiotherapy Efficacy.* Clinical Cancer Research, 2012. **18**(20): p. 5585-5594.
110. Coleman, M.C., et al., *2-deoxy-D-glucose causes cytotoxicity, oxidative stress, and radiosensitization in pancreatic cancer.* Free Radic Biol Med, 2008. **44**(3): p. 322-31.
111. Sattler, U.G. and W. Mueller-Klieser, *The anti-oxidant capacity of tumour glycolysis.* Int J Radiat Biol, 2009. **85**(11): p. 963-71.
112. Quennet, V., et al., *Tumor lactate content predicts for response to fractionated irradiation of human squamous cell carcinomas in nude mice.* Radiother Oncol, 2006. **81**(2): p. 130-5.
113. Groussard, C., et al., *Free radical scavenging and antioxidant effects of lactate ion: an in vitro study.* J Appl Physiol (1985), 2000. **89**(1): p. 169-75.
114. Zhang, M., et al., *HIF-1 Alpha Regulates the Response of Primary Sarcomas to Radiation Therapy through a Cell Autonomous Mechanism.* Radiat Res, 2015. **183**(6): p. 594-609.
115. Unruh, A., et al., *The hypoxia-inducible factor-1 alpha is a negative factor for tumor therapy.* Oncogene, 2003. **22**(21): p. 3213-20.
116. Chen, L., et al., *Effect of hypoxia-inducible factor-1alpha silencing on the sensitivity of human brain glioma cells to doxorubicin and etoposide.* Neurochem Res, 2009. **34**(5): p. 984-90.
117. Lv, Y., et al., *Hypoxia-inducible factor-1α induces multidrug resistance protein in colon cancer.* OncoTargets and therapy, 2015. **8**: p. 1941-1948.

118. Lu, J.F., D. Pokharel, and M. Bebawy, *MRP1 and its role in anticancer drug resistance.* Drug Metab Rev, 2015. **47**(4): p. 406-19.
119. Nardinocchi, L., et al., *Inhibition of HIF-1alpha activity by homeodomain-interacting protein kinase-2 correlates with sensitization of chemoresistant cells to undergo apoptosis.* Mol Cancer, 2009. **8**: p. 1.
120. Li, J., et al., *Knockdown of hypoxia-inducible factor-1alpha in breast carcinoma MCF-7 cells results in reduced tumor growth and increased sensitivity to methotrexate.* Biochem Biophys Res Commun, 2006. **342**(4): p. 1341-51.
121. Liu, L., et al., *Hypoxia-inducible factor-1 alpha contributes to hypoxia-induced chemoresistance in gastric cancer.* Cancer Sci, 2008. **99**(1): p. 121-8.
122. Shukla, S.K., et al., *MUC1 and HIF-1alpha Signaling Crosstalk Induces Anabolic Glucose Metabolism to Impart Gemcitabine Resistance to Pancreatic Cancer.* Cancer Cell, 2017. **32**(1): p. 71-87.e7.
123. Kalluri, R. and R.A. Weinberg, *The basics of epithelial-mesenchymal transition.* J Clin Invest, 2009. **119**(6): p. 1420-8.
124. Krishnamachary, B., et al., *Hypoxia-inducible factor-1-dependent repression of E-cadherin in von Hippel-Lindau tumor suppressor-null renal cell carcinoma mediated by TCF3, ZFHX1A, and ZFHX1B.* Cancer Res, 2006. **66**(5): p. 2725-31.
125. Zhu, Q.Q., et al., *The role of TWIST1 in epithelial-mesenchymal transition and cancers.* Tumour Biol, 2016. **37**(1): p. 185-97.
126. Gort, E.H., et al., *The TWIST1 oncogene is a direct target of hypoxia-inducible factor-2α.* Oncogene, 2007. **27**: p. 1501.
127. Yang, M.-H., et al., *Direct regulation of TWIST by HIF-1α promotes metastasis.* Nature Cell Biology, 2008. **10**: p. 295.
128. Duffy, M.J., et al., *Metalloproteinases: role in breast carcinogenesis, invasion and metastasis.* Breast Cancer Res, 2000. **2**(4): p. 252-7.
129. Choi, J.Y., et al., *Overexpression of MMP-9 and HIF-1α in Breast Cancer Cells under Hypoxic Conditions.* Journal of Breast Cancer, 2011. **14**(2): p. 88-95.
130. Lin, J.L., et al., *Hypoxia-inducible factor-1alpha regulates matrix metalloproteinase-1 activity in human bone marrow-derived mesenchymal stem cells.* FEBS Lett, 2008. **582**(17): p. 2615-9.
131. Jing, S.W., et al., *HIF-1alpha contributes to hypoxia-induced invasion and metastasis of esophageal carcinoma via inhibiting E-cadherin and promoting MMP-2 expression.* Acta Med Okayama, 2012. **66**(5): p. 399-407.
132. Warburg, O., *The Metabolism of Carcinoma Cells.* The Journal of Cancer Research, 1925. **9**(1): p. 148.
133. Liberti, M.V. and J.W. Locasale, *The Warburg Effect: How Does it Benefit Cancer Cells?* Trends in biochemical sciences, 2016. **41**(3): p. 211-218.
134. Kim, J.W., et al., *HIF-1-mediated expression of pyruvate dehydrogenase kinase: a metabolic switch required for cellular adaptation to hypoxia.* Cell Metab, 2006. **3**(3): p. 177-85.
135. Cui, X.G., et al., *HIF1/2alpha mediates hypoxia-induced LDHA expression in human pancreatic cancer cells.* Oncotarget, 2017. **8**(15): p. 24840-24852.

136. Hui, S., et al., *Glucose feeds the TCA cycle via circulating lactate.* Nature, 2017. **551**: p. 115.
137. Wise, D.R. and C.B. Thompson, *Glutamine addiction: a new therapeutic target in cancer.* Trends Biochem Sci, 2010. **35**(8): p. 427-33.
138. Metallo, C.M., et al., *Reductive glutamine metabolism by IDH1 mediates lipogenesis under hypoxia.* Nature, 2011. **481**: p. 380.
139. Wise, D.R., et al., *Hypoxia promotes isocitrate dehydrogenase-dependent carboxylation of alpha-ketoglutarate to citrate to support cell growth and viability.* Proc Natl Acad Sci U S A, 2011. **108**(49): p. 19611-6.
140. Gameiro, P.A., et al., *In vivo HIF-mediated reductive carboxylation is regulated by citrate levels and sensitizes VHL-deficient cells to glutamine deprivation.* Cell Metab, 2013. **17**(3): p. 372-85.
141. Masvidal, L., L. Hulea, and L. Furic, *mTOR-sensitive translation: Cleared fog reveals more trees.* 2017. **14**(10): p. 1299-1305.
142. Hudson, C.C., et al., *Regulation of hypoxia-inducible factor 1alpha expression and function by the mammalian target of rapamycin.* Mol Cell Biol, 2002. **22**(20): p. 7004-14.
143. Land, S.C. and A.R. Tee, *Hypoxia-inducible factor 1alpha is regulated by the mammalian target of rapamycin (mTOR) via an mTOR signaling motif.* J Biol Chem, 2007. **282**(28): p. 20534-43.
144. Toschi, A., et al., *Differential dependence of hypoxia-inducible factors 1 alpha and 2 alpha on mTORC1 and mTORC2.* J Biol Chem, 2008. **283**(50): p. 34495-9.
145. Luo, W., et al., *Hsp70 and CHIP selectively mediate ubiquitination and degradation of hypoxia-inducible factor (HIF)-1alpha but Not HIF-2alpha.* J Biol Chem, 2010. **285**(6): p. 3651-63.
146. Cesari, R., et al., *Parkin, a gene implicated in autosomal recessive juvenile parkinsonism, is a candidate tumor suppressor gene on chromosome 6q25-q27.* Proc Natl Acad Sci U S A, 2003. **100**(10): p. 5956-61.
147. Tay, S.P., et al., *Parkin enhances the expression of cyclin-dependent kinase 6 and negatively regulates the proliferation of breast cancer cells.* J Biol Chem, 2010. **285**(38): p. 29231-8.
148. Liu, J., et al., *Parkin targets HIF-1α for ubiquitination and degradation to inhibit breast tumor progression.* Nature Communications, 2017. **8**(1): p. 1823.
149. Montagner, M., et al., *SHARP1 suppresses breast cancer metastasis by promoting degradation of hypoxia-inducible factors.* Nature, 2012. **487**(7407): p. 380-4.
150. Fujimoto, K., et al., *Transcriptional repression by the basic helix-loop-helix protein Dec2: multiple mechanisms through E-box elements.* Int J Mol Med, 2007. **19**(6): p. 925-32.
151. Drazic, A., et al., *The world of protein acetylation.* Biochim Biophys Acta, 2016. **1864**(10): p. 1372-401.
152. Xenaki, G., et al., *PCAF is a HIF-1α cofactor that regulates p53 transcriptional activity in hypoxia.* Oncogene, 2008. **27**(44): p. 5785-5796.

153. Lim, J.H., et al., *Sirtuin 1 modulates cellular responses to hypoxia by deacetylating hypoxia-inducible factor 1alpha.* Mol Cell, 2010. **38**(6): p. 864-78.
154. Chen, R., et al., *The acetylase/deacetylase couple CREB-binding protein/Sirtuin 1 controls hypoxia-inducible factor 2 signaling.* J Biol Chem, 2012. **287**(36): p. 30800-11.
155. Xu, M., et al., *An acetate switch regulates stress erythropoiesis.* Nat Med, 2014. **20**(9): p. 1018-26.
156. Dioum, E.M., et al., *Regulation of hypoxia-inducible factor 2alpha signaling by the stress-responsive deacetylase sirtuin 1.* Science, 2009. **324**(5932): p. 1289-93.
157. Qian, D.Z., et al., *Class II histone deacetylases are associated with VHL-independent regulation of hypoxia-inducible factor 1 alpha.* Cancer Res, 2006. **66**(17): p. 8814-21.
158. Geng, H., et al., *HDAC4 protein regulates HIF1alpha protein lysine acetylation and cancer cell response to hypoxia.* J Biol Chem, 2011. **286**(44): p. 38095-102.
159. Wang, G.L., B.H. Jiang, and G.L. Semenza, *Effect of protein kinase and phosphatase inhibitors on expression of hypoxia-inducible factor 1.* Biochem Biophys Res Commun, 1995. **216**(2): p. 669-75.
160. Kietzmann, T., D. Mennerich, and E.Y. Dimova, *Hypoxia-Inducible Factors (HIFs) and Phosphorylation: Impact on Stability, Localization, and Transactivity.* Frontiers in Cell and Developmental Biology, 2016. **4**: p. 11.
161. Semenza, G.L., *A compendium of proteins that interact with HIF-1alpha.* Exp Cell Res, 2017. **356**(2): p. 128-135.
162. Chen, R.Q., et al., *Kinome siRNA screen identifies SMG-1 as a negative regulator of hypoxia-inducible factor-1alpha in hypoxia.* J Biol Chem, 2009. **284**(25): p. 16752-8.
163. Lasorella, A., et al., *Id2 mediates tumor initiation, proliferation, and angiogenesis in Rb mutant mice.* Mol Cell Biol, 2005. **25**(9): p. 3563-74.
164. Vandeputte, D.A., et al., *Expression and distribution of id helix-loop-helix proteins in human astrocytic tumors.* Glia, 2002. **38**(4): p. 329-38.
165. Lee, S.B., et al., *An ID2-dependent mechanism for VHL inactivation in cancer.* Nature, 2016. **529**(7585): p. 172-7.
166. Warfel, N.A., et al., *CDK1 stabilizes HIF-1α via direct phosphorylation of Ser668 to promote tumor growth.* Cell Cycle, 2013. **12**(23): p. 3689-3701.
167. Hubbi, M.E., et al., *Cyclin-dependent kinases regulate lysosomal degradation of hypoxia-inducible factor 1α to promote cell-cycle progression.* Proceedings of the National Academy of Sciences, 2014. **111**(32): p. E3325-E3334.
168. Pan, D., *The hippo signaling pathway in development and cancer.* Dev Cell, 2010. **19**(4): p. 491-505.
169. Huang, J., et al., *The Hippo signaling pathway coordinately regulates cell proliferation and apoptosis by inactivating Yorkie, the Drosophila Homolog of YAP.* Cell, 2005. **122**(3): p. 421-34.
170. Zhao, B., et al., *Inactivation of YAP oncoprotein by the Hippo pathway is involved in cell contact inhibition and tissue growth control.* Genes Dev, 2007. **21**(21): p. 2747-61.

171. Ma, B., et al., *Hypoxia regulates Hippo signalling through the SIAH2 ubiquitin E3 ligase.* Nature Cell Biology, 2014. **17**: p. 95.
172. Nakayama, K., et al., *Siah2 regulates stability of prolyl-hydroxylases, controls HIF1alpha abundance, and modulates physiological responses to hypoxia.* Cell, 2004. **117**(7): p. 941-52.
173. Chinopoulos, C., *Which way does the citric acid cycle turn during hypoxia? The critical role of alpha-ketoglutarate dehydrogenase complex.* J Neurosci Res, 2013. **91**(8): p. 1030-43.
174. Selak, M.A., et al., *Succinate links TCA cycle dysfunction to oncogenesis by inhibiting HIF-alpha prolyl hydroxylase.* Cancer Cell, 2005. **7**(1): p. 77-85.
175. Koivunen, P., et al., *Inhibition of hypoxia-inducible factor (HIF) hydroxylases by citric acid cycle intermediates: possible links between cell metabolism and stabilization of HIF.* J Biol Chem, 2007. **282**(7): p. 4524-32.
176. Ricketts, C., et al., *Germline SDHB mutations and familial renal cell carcinoma.* J Natl Cancer Inst, 2008. **100**(17): p. 1260-2.
177. Habano, W., et al., *Reduced expression and loss of heterozygosity of the SDHD gene in colorectal and gastric cancer.* Oncol Rep, 2003. **10**(5): p. 1375-80.
178. Toro, J.R., et al., *Mutations in the fumarate hydratase gene cause hereditary leiomyomatosis and renal cell cancer in families in North America.* Am J Hum Genet, 2003. **73**(1): p. 95-106.
179. Tomlinson, I.P., et al., *Germline mutations in FH predispose to dominantly inherited uterine fibroids, skin leiomyomata and papillary renal cell cancer.* Nat Genet, 2002. **30**(4): p. 406-10.
180. Isaacs, J.S., et al., *HIF overexpression correlates with biallelic loss of fumarate hydratase in renal cancer: novel role of fumarate in regulation of HIF stability.* Cancer Cell, 2005. **8**(2): p. 143-53.
181. Yang, M., et al., *The emerging role of fumarate as an oncometabolite.* Frontiers in Oncology, 2012. **2**: p. 85.
182. Yan, H., et al., *IDH1 and IDH2 mutations in gliomas.* N Engl J Med, 2009. **360**(8): p. 765-73.
183. Fathi, A.T., et al., *Isocitrate dehydrogenase 1 (IDH1) mutation in breast adenocarcinoma is associated with elevated levels of serum and urine 2-hydroxyglutarate.* Oncologist, 2014. **19**(6): p. 602-7.
184. Toth, L.N., F.B. de Abreu, and L.J. Tafe, *Non-small cell lung cancers with isocitrate dehydrogenase 1 or 2 (IDH1/2) mutations.* Hum Pathol, 2018. **78**: p. 138-143.
185. Dang, L., et al., *Cancer-associated IDH1 mutations produce 2-hydroxyglutarate.* Nature, 2009. **462**(7274): p. 739.
186. Losman, J.-A. and W.G. Kaelin, *What a difference a hydroxyl makes: mutant IDH, (R)-2-hydroxyglutarate, and cancer.* Genes & Development, 2013. **27**(8): p. 836-852.
187. Blouw, B., et al., *The hypoxic response of tumors is dependent on their microenvironment.* Cancer Cell, 2003. **4**(2): p. 133-46.
188. Acker, T., et al., *Genetic evidence for a tumor suppressor role of HIF-2alpha.* Cancer Cell, 2005. **8**(2): p. 131-41.

189. Koivunen, P., et al., *Transformation by the (R)-enantiomer of 2-hydroxyglutarate linked to EGLN activation.* Nature, 2012. **483**(7390): p. 484-8.
190. Zhang, D., et al., *Metabolic reprogramming of cancer-associated fibroblasts by IDH3alpha downregulation.* Cell Rep, 2015. **10**(8): p. 1335-48.
191. Burr, S.P., et al., *Mitochondrial Protein Lipoylation and the 2-Oxoglutarate Dehydrogenase Complex Controls HIF1alpha Stability in Aerobic Conditions.* Cell Metab, 2016. **24**(5): p. 740-752.
192. Baecker, V., *ImageJ macro tool sets for biological image analysis.* ImageJ user and Developer conference, 2012.
193. Rothwell, D.G., et al., *Functional expression of secreted proteins from a bicistronic retroviral cassette based on foot-and-mouth disease virus 2A can be position dependent.* Hum Gene Ther, 2010. **21**(11): p. 1631-7.
194. Szklarczyk, D., et al., *STRING v10: protein–protein interaction networks, integrated over the tree of life.* Nucleic Acids Research, 2015. **43**(Database issue): p. D447-D452.
195. Zhyvoloup, A., et al., *Molecular cloning of CoA Synthase. The missing link in CoA biosynthesis.* J Biol Chem, 2002. **277**(25): p. 22107-10.
196. Srinivasan, B., et al., *Extracellular 4'-phosphopantetheine is a source for intracellular coenzyme A synthesis.* 2015. **11**(10): p. 784-92.
197. Evers, C., et al., *Diagnosis of CoPAN by whole exome sequencing: Waking up a sleeping tiger's eye.* Am J Med Genet A, 2017.
198. Matarin, M.M., A.B. Singleton, and H. Houlden, *PANK2 gene analysis confirms genetic heterogeneity in neurodegeneration with brain iron accumulation (NBIA) but mutations are rare in other types of adult neurodegenerative disease.* Neurosci Lett, 2006. **407**(2): p. 162-5.
199. Zhyvoloup, A., et al., *Subcellular Localization and Regulation of Coenzyme A Synthase.* Journal of Biological Chemistry, 2003. **278**(50): p. 50316-50321.
200. Ahler, E., et al., *Doxycycline Alters Metabolism and Proliferation of Human Cell Lines.* PLoS ONE, 2013. **8**(5): p. e64561.
201. Yoshida, T., et al., *Transcriptional upregulation of HIF-1alpha by NF-kappaB/p65 and its associations with beta-catenin/p300 complexes in endometrial carcinoma cells.* Lab Invest, 2013. **93**(11): p. 1184-93.
202. Rock, C.O., et al., *Pantothenate kinase regulation of the intracellular concentration of coenzyme A.* J Biol Chem, 2000. **275**(2): p. 1377-83.
203. Chen, R., et al., *The Acetate/ACSS2 Switch Regulates HIF-2 Stress Signaling in the Tumor Cell Microenvironment.* PLoS ONE, 2015. **10**(2): p. e0116515.
204. Lin, C.-C., et al., *CoA synthase regulates mitotic fidelity via CBP-mediated acetylation.* Nature Communications, 2018. **9**(1): p. 1039.
205. Pietrocola, F., et al., *Acetyl coenzyme A: a central metabolite and second messenger.* Cell Metab, 2015. **21**(6): p. 805-21.
206. Bulusu, V., et al., *Acetate Recapturing by Nuclear Acetyl-CoA Synthetase 2 Prevents Loss of Histone Acetylation during Oxygen and Serum Limitation.* Cell Reports, 2017. **18**(3): p. 647-658.
207. Hornbeck, P.V., et al., *PhosphoSite: A bioinformatics resource dedicated to physiological protein phosphorylation.* Proteomics, 2004. **4**(6): p. 1551-61.

208. Kalousi, A., et al., *Casein kinase 1 regulates human hypoxia-inducible factor HIF-1.* J Cell Sci, 2010. **123**(Pt 17): p. 2976-86.
209. Bullen, J.W., et al., *Protein kinase A-dependent phosphorylation stimulates the transcriptional activity of hypoxia-inducible factor 1.* Sci Signal, 2016. **9**(430): p. ra56.
210. Tsuchiya, Y., et al., *Protein CoAlation: a redox-regulated protein modification by coenzyme A in mammalian cells.* Biochem J, 2017. **474**(14): p. 2489-2508.
211. Tsuchiya, Y., et al., *Protein CoAlation and antioxidant function of coenzyme A in prokaryotic cells.* Biochem J, 2018. **475**(11): p. 1909-1937.
212. Malanchuk, O.M., et al., *Generation and characterization of monoclonal antibodies specifi c to Coenzyme A.* Biopolymers & Cell, 2015. **31**(3): p. 187-192.
213. Guzy, R.D., et al., *Mitochondrial complex III is required for hypoxia-induced ROS production and cellular oxygen sensing.* Cell Metab, 2005. **1**(6): p. 401-8.
214. Klotz, L.O., et al., *2-Methyl-1,4-naphthoquinone, vitamin K(3), decreases gap-junctional intercellular communication via activation of the epidermal growth factor receptor/extracellular signal-regulated kinase cascade.* Cancer Res, 2002. **62**(17): p. 4922-8.
215. Lee, G., et al., *Oxidative Dimerization of PHD2 is Responsible for its Inactivation and Contributes to Metabolic Reprogramming via HIF-1α Activation.* Scientific Reports, 2016. **6**: p. 18928.
216. Lanczky, A., et al., *miRpower: a web-tool to validate survival-associated miRNAs utilizing expression data from 2178 breast cancer patients.* Breast Cancer Res Treat, 2016. **160**(3): p. 439-446.
217. Ruggero, D., *Translational Control in Cancer Etiology.* Cold Spring Harbor Perspectives in Biology, 2013. **5**(2): p. a012336.
218. Huang, W.Y., et al., *MethHC: a database of DNA methylation and gene expression in human cancer.* Nucleic Acids Res, 2015. **43**(Database issue): p. D856-61.
219. Cheol Kim, D., et al., *Quantitative DNA methylation and recurrence of breast cancer: a study of 30 candidate genes.* Cancer Biomark, 2012. **11**(2-3): p. 75-88.
220. Gort, E.H., et al., *Methylation of the TWIST1 promoter, TWIST1 mRNA levels, and immunohistochemical expression of TWIST1 in breast cancer.* Cancer Epidemiol Biomarkers Prev, 2008. **17**(12): p. 3325-30.
221. Shelton, R.S., M.G. Van Campen, and et al., *Quaternary ammonium salts as germicides; quaternary ammonium slats derived from cyclic amines.* J Am Chem Soc, 1946. **68**: p. 757-9.
222. Wallin, J.D., et al., *Intravenous nicardipine for the treatment of severe hypertension.* Am J Med, 1988. **85**(3): p. 331-8.
223. Roy, G. and G. Mugesh, *Bioinorganic Chemistry in Thyroid Gland: Effect of Antithyroid Drugs on Peroxidase-Catalyzed Oxidation and Iodination Reactions.* Bioinorganic Chemistry and Applications, 2006. **2006**: p. 23214.
224. Gudkova, D., et al., *EDC4 interacts with and regulates the dephospho-CoA kinase activity of CoA synthase.* FEBS Lett, 2012. **586**(20): p. 3590-5.

225. Nemazanyy, I., et al., *Specific interaction between S6K1 and CoA synthase: a potential link between the mTOR/S6K pathway, CoA biosynthesis and energy metabolism.* FEBS Lett, 2004. **578**(3): p. 357-62.
226. Jeong, J.W., et al., *Regulation and destabilization of HIF-1alpha by ARD1-mediated acetylation.* Cell, 2002. **111**(5): p. 709-20.
227. Bilton, R., et al., *Arrest-defective-1 protein, an acetyltransferase, does not alter stability of hypoxia-inducible factor (HIF)-1alpha and is not induced by hypoxia or HIF.* J Biol Chem, 2005. **280**(35): p. 31132-40.
228. Arnesen, T., et al., *Interaction between HIF-1 alpha (ODD) and hARD1 does not induce acetylation and destabilization of HIF-1 alpha.* FEBS Lett, 2005. **579**(28): p. 6428-32.
229. Wu, D., et al., *Structural integration in hypoxia-inducible factors.* Nature, 2015. **524**(7565): p. 303-8.
230. Liu, Z.J., G.L. Semenza, and H.F. Zhang, *Hypoxia-inducible factor 1 and breast cancer metastasis.* J Zhejiang Univ Sci B, 2015. **16**(1): p. 32-43.
231. Ajdukovic, J., *HIF-1--a big chapter in the cancer tale.* Exp Oncol, 2016. **38**(1): p. 9-12.
232. Balamurugan, K., *HIF-1 at the crossroads of hypoxia, inflammation, and cancer.* Int J Cancer, 2016. **138**(5): p. 1058-66.
233. Lin, E.W. and T.A. Karakasheva, *Comparative transcriptomes of adenocarcinomas and squamous cell carcinomas reveal molecular similarities that span classical anatomic boundaries.* 2017. **13**(8): p. e1006938.
234. Lips, E.H., et al., *Next generation sequencing of triple negative breast cancer to find predictors for chemotherapy response.* Breast Cancer Res, 2015. **17**(1): p. 134.
235. Mitchell, T.J., et al., *Timing the Landmark Events in the Evolution of Clear Cell Renal Cell Cancer: TRACERx Renal.* Cell, 2018. **173**(3): p. 611-623.e17.
236. Dahl, G.P., et al., *High affinity complexes of pannexin channels and L-type calcium channel splice-variants in human lung: Possible role in clevidipine-induced dyspnea relief in acute heart failure.* EBioMedicine, 2016. **10**: p. 291-297.
237. Graham, D.J.M., et al., *The metabolism and pharmacokinetics of nicardipine hydrochloride in man.* British Journal of Clinical Pharmacology, 1985. **20**(Suppl 1): p. 23S-28S.